

Electronic Thesis and Dissertation Repository

4-19-2011 12:00 AM

An Analytical and Numerical Treatment of Inclined Elliptical Orbits About a Kerr Black Hole

Peter G. Komorowski, *University of Western Ontario*

Supervisor: Martin Houde, *The University of Western Ontario*

Joint Supervisor: Sree Ram Valluri, *The University of Western Ontario*

A thesis submitted in partial fulfillment of the requirements for the Doctor of Philosophy degree in Physics

© Peter G. Komorowski 2011

Follow this and additional works at: <https://ir.lib.uwo.ca/etd>



Part of the [Cosmology, Relativity, and Gravity Commons](#)

Recommended Citation

Komorowski, Peter G., "An Analytical and Numerical Treatment of Inclined Elliptical Orbits About a Kerr Black Hole" (2011). *Electronic Thesis and Dissertation Repository*. 115.
<https://ir.lib.uwo.ca/etd/115>

This Dissertation/Thesis is brought to you for free and open access by Scholarship@Western. It has been accepted for inclusion in Electronic Thesis and Dissertation Repository by an authorized administrator of Scholarship@Western. For more information, please contact wlsadmin@uwo.ca.

AN ANALYTICAL AND NUMERICAL TREATMENT
OF
INCLINED ELLIPTICAL ORBITS ABOUT A KERR BLACK HOLE

(Spine title: Elliptical Orbits About a Kerr Black Hole)

(Thesis format: Integrated-Article)

by

Peter George Komorowski

Graduate Program in Physics and Astronomy

A thesis submitted in partial fulfillment
of the requirements for the degree of
Doctor of Philosophy

The School of Graduate and Postdoctoral Studies
The University of Western Ontario
London, Ontario, Canada

© Peter George Komorowski 2011

THE UNIVERSITY OF WESTERN ONTARIO
School of Graduate and Postdoctoral Studies

CERTIFICATE OF EXAMINATION

Supervisors

Dr. Martin Houde

Dr. Sree Ram Valluri

Supervisory Committee

Dr. Aaron Sigut

Dr. Paul Wiegert

Examiners

Dr. Jan Cami

Dr. Giovanni Fanchini

Dr. William L. Harper

Dr. Daniel Kennefick

This thesis by

Peter George Komorowski

entitled:

**AN ANALYTICAL AND NUMERICAL TREATMENT OF
INCLINED ELLIPTICAL ORBITS ABOUT A KERR BLACK HOLE**

is accepted in partial fulfilment of the
requirements for the degree of
Doctor of Philosophy

Date _____

Chair of the Thesis Examination Board

Abstract

Since its publication in 1915, Einstein's theory of general relativity has yielded significant results; they include: analytical solutions to the Einstein field equations; improved analysis of orbital dynamics; and the prediction of gravitational wave (GW) radiation. Gravitation is the weakest of the fundamental interactions; and theoretical models of GW generation and propagation show that its detection poses a significant technical challenge. Unlike the study of electromagnetic radiation, experiments within the laboratory are virtually impossible; so astronomical sources of GW, such as binary black hole systems, offer an alternative. But GW detection remains difficult. The matched filtering techniques used to discriminate a GW signal from background noise, require GW templates; thus a theoretical foreknowledge of binary black hole evolution is needed.

Extreme mass-ratio binary black hole systems may be modelled by a massive Kerr black hole (KBH) and a test-particle in an inclined elliptical orbit. The GW spectrum is determined by the latus rectum (\tilde{l}), eccentricity (e), and inclination (ι) of the orbit, which gradually change with loss of energy and angular momentum. The evolution of these orbital characteristics is described by equations widely available in the literature; so it is essential that corroborative techniques be found to assure accuracy. The last stable orbit (LSO) is an important end-point at which the zoom and whirl of the test-particle becomes pronounced; this also affects the GW spectrum.

An analytical and numerical study of the influence of KBH spin (\tilde{S}) on \tilde{l} and e of an equatorial LSO was performed first, followed by the derivation of a formula for the Carter constant (Q) of an inclined orbit in terms of \tilde{S} , \tilde{l} and e . This analysis drew attention to the abutment, a family of retrograde near-polar orbits, at which the consistency of evolution equations for Q with respect to those for \tilde{l} and e was tested. Further, the evolution of ι was also treated. To leading order in \tilde{S} , evolution equations for Q are consistent with those of \tilde{l} and e . The relationship between the evolution equation for ι with respect to \tilde{l} and e contains a second-order effect, which is yet to be fully characterised.

Keywords: relativity, general relativity, black hole, extreme mass-ratio binary black hole system, gravitational wave radiation, evolution equation, Carter constant, orbital angle of inclination, abutment, listing

Co-authorship

The general area of study, the evolution of the orbit of a compact object about a Kerr black hole, was introduced to me by Professor S. R. Valluri. For the duration of my research work, Professor S. R. Valluri and Professor M. Houde were joint-supervisors. The detailed analytical calculation of the last stable orbits about Schwarzschild and Kerr black holes, and the development and use of the concept of the abutment for near-polar orbits about a Kerr black hole, were solely my work. The three articles in which the details of this work were published, were composed by me in my capacity as the primary author.

to Laurie

Acknowledgements

I gratefully acknowledge the help, guidance, and support of my thesis supervisors, Professor Martin Houde and Professor Sreeram Valluri. And I acknowledge the financial support given to me, during my time at Western, under the Western Graduate Research Scholarship.

It was my pleasure and privilege to have enjoyed countless pots of tea and countless hours of theoretical physics discussion at the home of Doctors Natalia Kiriushcheva & Sergei V. Kuzmin.

My fellow graduate student, Iftekhar-Ul Haque, is a true friend with whom I share a love of mathematics, physics, language, and philosophy.

Contents

| | |
|---|--------------|
| Certificate of Examination | ii |
| Abstract | iii |
| Co-authorship | v |
| Acknowledgements | vii |
| List of Tables | xiv |
| List of Figures | xvi |
| List of Initialisms, Acronyms, & Abbreviations | xviii |
| List of Symbols | xix |
| 1 Introduction | 1 |
| 1.1 Theories and Principles of Relativity | 1 |
| 1.1.1 Galileo’s Law of Inertia | 2 |
| 1.1.2 The Restricted Principle of Relativity | 4 |
| 1.2 Special Relativity | 6 |
| 1.2.1 Introduction | 6 |
| 1.2.2 Lorentz Boost | 7 |
| 1.2.3 Minkowski Space | 8 |
| 1.2.4 Relativistic Velocity Composition Law | 10 |

| | | |
|----------|--|-----------|
| 1.3 | General Relativity | 12 |
| 1.3.1 | Introduction | 12 |
| 1.3.2 | The Principle of Equivalence | 12 |
| 1.3.3 | The Principle of General Covariance | 13 |
| 1.3.4 | The Einstein Equations | 14 |
| 1.3.5 | Exact Solutions to the Einstein Equations | 16 |
| 1.4 | Gravitational Wave Radiation | 21 |
| 1.4.1 | The Gravitational Wave Propagation Region | 21 |
| 1.4.2 | The Gravitational Wave Generation Region | 23 |
| 1.5 | Extreme Binary Black Hole Systems | 24 |
| 1.5.1 | Introduction | 24 |
| 1.5.2 | Post-Newtonian Approximation | 26 |
| 1.5.3 | Four-Momentum of Orbiting Test-Particles | 28 |
| 1.5.4 | Constants of Motion | 30 |
| 1.6 | Thesis Outline | 32 |
| 1.6.1 | Chapter 2 | 33 |
| 1.6.2 | Chapter 3 | 33 |
| 1.6.3 | Chapter 4 | 34 |
| 1.7 | References | 35 |
| 2 | A Study of Elliptical Last Stable Orbits About a Massive Kerr Black Hole | 44 |
| | Abstract | 45 |
| 2.1 | Introduction | 46 |
| 2.2 | Understanding the Last Stable Orbit About a Rotating Massive Black Hole | 48 |
| 2.2.1 | Kerr Metric | 48 |
| 2.2.2 | Effective Potential | 50 |
| 2.2.3 | Last Stable Orbit (LSO) for a CO in the Equatorial Plane of the Kerr Black Hole | 53 |

| | | |
|----------|---|-----------|
| 2.2.4 | Calculating the LSO Properties | 66 |
| 2.2.5 | Calculations | 71 |
| 2.3 | Conclusions | 83 |
| 2.A | The Kerr metric and its Inverse | 85 |
| 2.B | Use of the Companion Matrix to Solve a Quartic Equation | 86 |
| 2.C | Use of the Companion Matrix to Find the Analytical Solution for \tilde{l}_{LSO} for a General Elliptical Orbit | 87 |
| 2.4 | References | 90 |
| 3 | The Carter Constant for Inclined Orbits About a Massive Kerr Black Hole: circular orbits | 94 |
| | Abstract | 95 |
| 3.1 | Introduction | 96 |
| 3.2 | The Motion of a Test-Particle in an Inclined Orbit | 98 |
| 3.2.1 | Basic Orbital Equations | 98 |
| 3.2.2 | Effective Radial Potential | 100 |
| 3.2.3 | Orbital Angular Momentum at the Last Stable Orbit | 101 |
| 3.3 | Analysis of the Trajectory Equations | 105 |
| 3.3.1 | Introduction | 105 |
| 3.3.2 | Roots of the Radial Equation | 107 |
| 3.3.3 | Roots of the Polar-Angle Equation | 110 |
| 3.3.4 | Orbital Energy and an Analytical Expression for X^2 | 111 |
| 3.3.5 | Prograde and Retrograde Descriptions of X^2 | 113 |
| 3.4 | The Characteristics of the Carter Constant Equations and the Domain of the Orbital Parameters | 116 |
| 3.4.1 | Introduction | 116 |
| 3.4.2 | Last Stable Orbit | 118 |

| | | |
|----------|---|------------|
| 3.4.3 | The Abutment | 120 |
| 3.4.4 | Polar Orbit | 122 |
| 3.4.5 | Some Characteristics of the Carter Constant Formulae | 124 |
| 3.5 | The Analysis of the Carter Constant for an Evolving Orbit | 128 |
| 3.5.1 | Introduction | 128 |
| 3.5.2 | The Evolutionary Path in the $Q - \tilde{l}$ Plane | 129 |
| 3.5.3 | The Analysis of ι on the Abutment | 131 |
| 3.6 | Conclusions | 141 |
| 3.A | Terms | 143 |
| 3.B | Ancillary Equations | 143 |
| 3.B.1 | The Kerr metric and its Inverse | 143 |
| 3.B.2 | Effective Potentials | 144 |
| 3.B.3 | Ninth Order Polynomial in \tilde{l} for calculating \tilde{l}_{LSO} | 145 |
| 3.B.4 | The First and Second Derivatives of Q_X | 146 |
| 3.B.5 | The 2PN flux for Q | 147 |
| 3.B.6 | Tables associated with figures 3-1, 3-2, and 3-3 | 148 |
| 3.C | An Explicit Treatment of $d\theta/d\tau$ in the Effective Potential | 149 |
| 3.4 | References | 152 |
| 4 | The Carter Constant for Inclined Elliptical Orbits About a Massive Kerr Black Hole: near-polar, near-circular orbits | 157 |
| | Abstract | 158 |
| 4.1 | Introduction | 159 |
| 4.2 | An Analytical Formula for the Angle of Inclination of an Elliptical Orbit on the Abutment | 161 |
| 4.2.1 | Introduction | 161 |
| 4.2.2 | Review of Analytical Formulae | 162 |

| | | |
|-------|--|-----|
| 4.2.3 | Analytical Formula for $\iota(e, \tilde{l})$ on the Abutment | 169 |
| 4.2.4 | Derivatives of $\iota(e, \tilde{l})$ on the Abutment | 171 |
| 4.2.5 | Directional Derivatives in the $\tilde{l} - e$ Plane | 171 |
| 4.3 | Correction of $\partial\iota/\partial\tilde{l}$ and $\partial\iota/\partial e$ for Second-order Effects | 174 |
| 4.3.1 | Introduction | 174 |
| 4.3.2 | Second-order Effects in Q_{path} | 174 |
| 4.3.3 | Application of the Reductive Ansätze to the Analytical Derivation of $\partial\iota/\partial\tilde{l}$ and $\partial\iota/\partial e$ | 179 |
| 4.3.4 | Analytical Derivation of the Common Primitive, $\wp(e, \tilde{l})$ | 181 |
| 4.4 | The Treatment of dQ/dt and dt/dt on the Abutment | 182 |
| 4.4.1 | The dQ/dt Evolution Equations | 182 |
| 4.4.2 | The Second-order Calculation of dt/dt for the Leading Order of \tilde{S} (weak-field regime) | 187 |
| 4.4.3 | The Independence of the Abutment of Radiation Back-reaction Models | 189 |
| 4.5 | Conclusions | 190 |
| 4.A | Ancillary Equations | 191 |
| 4.A.1 | Maclaurin Series Expansions of Various Functions | 191 |
| 4.A.2 | Selected Trigonometric Identities | 191 |
| 4.A.3 | Taylor Series for two Variables | 191 |
| 4.A.4 | Treatment of the Taylor Series Under Partial Differentiation | 192 |
| 4.A.5 | Treatment of Q_X as a Series in \tilde{l} | 193 |
| 4.A.6 | The 2PN Flux for Q | 194 |
| 4.A.7 | Evolution Equations for \tilde{l} , e , and ι | 195 |
| 4.B | Series Expansions of Critical Values in Terms of \tilde{S} and \tilde{l} | 197 |
| 4.B.1 | First-order Calculations | 197 |

| | | |
|----------|------------------------------------|------------|
| 4.B.2 | Third-order Calculations | 198 |
| 4.B.3 | Fifth-order Calculations | 199 |
| 4.3 | References | 201 |
| 5 | Summary and Future Work | 205 |
| 5.1 | Summary | 205 |
| 5.2 | Future work | 207 |
| 5.3 | References | 209 |
| | Curriculum Vitae | 211 |

List of Tables

| | | |
|-----|---|-----|
| 1.1 | Schwarzschild radii for spherically symmetrical bodies of various masses. | 18 |
| 1.2 | The representation of metres and kg in units of time. | 19 |
| 2.1 | A summary of the factors found in equation (2.25) for $\tilde{S} = 0.0, 0.5,$ and 1.0. | 59 |
| 2.2 | LSO parameters calculated for both circular and elliptical orbits where $\tilde{S} = 0.5 (ret), 0.0,$ and 0.5 | 67 |
| 2.3 | Retrograde LSO data from [10, 2] and results calculated using the nu- merical and analytical methods presented in this work | 73 |
| 2.4 | Prograde LSO data from [10, 2] and results calculated using the numer- ical and analytical methods presented in this work | 74 |
| 2.5 | Results of polynomial fit applied to the retrograde numerical data plotted in figure 2-5. | 81 |
| 2.6 | Results of polynomial fit applied to the prograde numerical data plotted in figure 2-4. | 82 |
| 3.1 | Parameters calculated for the tangential intersection of the Q_X and Q_{LSO} curves for an elliptical orbit about a KBH of spin $\tilde{S} = 0.5$ and $\tilde{S} = 0.99$. | 126 |
| 3.2 | An estimate of $(M^2/m) \partial \tilde{l} / \partial t$, based on equation (3.83), for circular orbits. | 130 |
| 3.3 | The values of $\partial \iota / \partial \tilde{l}$ (in radians) obtained by a linear extrapolation by $\delta \tilde{l} = 10^{-32}$ | 134 |
| 3.4 | The coefficients and powers of the series that describes $\left(\partial \iota / \partial \tilde{l} \right)_{min}$. . . | 137 |

| | | |
|-------|--|-----|
| 3.5 | An estimate of $(M^2/m) \partial v/\partial t$, based on equation (3.94), for circular orbits. | 138 |
| 3.A.1 | Orbital Parameters | 143 |
| 3.B.1 | Numerical values of R_{LSO} estimated from figure 3-1 for a circular LSO around an SBH. | 148 |
| 3.B.2 | Numerical values of R_{LSO} estimated from figure 3-1 for a circular LSO around an SBH. | 148 |
| 3.B.3 | Numerical values of R_{LSO} estimated from figure 3-3 for a circular orbit around a KBH of spin $\tilde{S} = 0.99$ | 148 |
| 4.1 | The coefficients of $-5/64 M^2/m \tilde{l}^3 dQ/dt$ up to \tilde{l}^{-3} | 185 |

List of Figures

| | | |
|-----|---|-----|
| 2-1 | Effective Potentials for various values of \tilde{L} where $\tilde{S} = 0$ | 53 |
| 2-2 | A plot of R_{LSO} vs. \tilde{L} for the first and second derivatives of \tilde{V} with respect to R | 54 |
| 2-3 | The relationship between the orbital angular momentum, \tilde{L} , and radius R for a prograde and retrograde orbit. | 57 |
| 2-4 | The LSO latus rectum, \tilde{l} , calculated for KBH systems in which the test-particle is in a prograde orbit. | 77 |
| 2-5 | The LSO latus rectum, \tilde{l} , calculated for KBH systems in which the test-particle is in a retrograde orbit. | 78 |
| 2-6 | A comparison of orbits in BL and spherical coordinates for a KBH of spin, $\tilde{S} = 0.5$ (prograde and retrograde). | 79 |
| 2-7 | A comparison of orbits in BL and spherical coordinates for a KBH of spin, $\tilde{S} = 0.99$ (prograde and retrograde). | 80 |
| 3-1 | The relationship between \tilde{L}_z and pericentre, R , for an SBH. Various values of Q are depicted. | 102 |
| 3-2 | The relationship between \tilde{L}_z and pericentre, R , for a KBH with $\tilde{S} = 0.50$.103 | |
| 3-3 | The relationship between \tilde{L}_z and pericentre, R , for a KBH with $\tilde{S} = 0.99$.104 | |
| 3-4 | A plot of X_-^2 with respect to Q for a circular orbit ($\tilde{l} = 6.25$) about a KBH of spin $\tilde{S} = 0.5$ | 114 |
| 3-5 | A sequence of $Q - \tilde{l}$ maps for various values of e for a KBH system with $\tilde{S} = 0.99$ | 117 |

| | | |
|-----|--|-----|
| 3-6 | The three Q formulae derived in Section 3.4 define a map. | 125 |
| 3-7 | The values of $\left \left(\partial \iota / \partial \tilde{l} \right)_{min} \right $ plotted for various values of \tilde{S} for circular orbits, where $\tilde{S} = 0.99$ and $10^2 \leq \tilde{l} \leq 10^{12}$ | 139 |
| 3-8 | Contours of constant Q in the $\tilde{l} - \iota$ plane for a circular ($e = 0$) orbit about a KBH with spin $\tilde{S} = 0.99$ | 140 |
| 4-1 | A schematic presentation of the $\tilde{l} - e$ plane in which Q_{path} is depicted making contact of the first order at a point (\tilde{l}_o, e_o) on the Q_X surface. | 177 |

List of Initialisms, Acronyms, & Abbreviations

| | |
|-------|---|
| BL | Boyer-Lindquist |
| CO | Compact object $\sim 1 \rightarrow 10$ solar masses |
| EMRI | Extreme mass ratio inspirals |
| GW | Gravitational wave radiation |
| KBH | Kerr black hole |
| LIGO | Earth-based laser interferometer gravitational wave observatory |
| LISA | Laser interferometer space antenna |
| LSO | Last stable orbit |
| MBH | Massive black hole $\sim 10^6 \rightarrow 10^7$ solar masses |
| PN | Post-Newtonian |
| 2PN | Post-Newtonian to second order |
| 2.5PN | Post-Newtonian to 2.5 order (includes GW losses) |
| 3PN | Post-Newtonian to third order |
| 4PN | Post-Newtonian to fourth order |
| PPN | Parameterised Post-Newtonian |
| pro. | Prograde |
| ret. | Retrograde |
| SBH | Schwarzschild black hole |

List of Symbols

- Greek indicies represent numbers in the set $\{0, 1, 2, 3\}$
- Latin indicies represent numbers in the set $\{1, 2, 3\}$

| | |
|--------------|---|
| m | Test-particle rest mass |
| M_{\odot} | One solar mass |
| M | Mass of MBH (typically $\sim 10^6 \rightarrow 10^7 M_{\odot}$) |
| a | Semi-major axis of an elliptical orbit |
| a_i, b_i | Functions of e used in the reductive ansätze |
| A | aM^{-1} |
| dt | Coordinate time |
| $d\tilde{t}$ | dtM^{-1} |
| e | Eccentricity |
| E | Orbital energy |
| \tilde{E} | Em^{-1} |
| $g_{\mu\nu}$ | General metric in curved space |
| G | Gravitational constant |
| G | Einstein tensor |
| \mathbf{J} | Spin angular momentum (KBH) |
| l | Latus rectum |

| | |
|----------------------|--|
| \tilde{l} | lM^{-1} |
| L | Orbital angular momentum (equatorial orbit) |
| \tilde{L} | $L(mM)^{-1}$ |
| L_θ | Orbital angular momentum (θ component) |
| \tilde{L}_θ | $L_\theta(mM)^{-1}$ |
| L_z | Orbital angular momentum (z component) |
| \tilde{L}_z | $L_z(mM)^{-1}$ |
| m_{rest} | Test-particle rest mass |
| m_{rel} | Relativistic mass of a test-particle |
| $p(x)$ | A given polynomial in terms of some variable x . |
| \mathbf{P} | Momentum vector in three space |
| \vec{P} | Four-momentum |
| P | Orbital period of secondary object |
| Q | Carter constant (already normalised by dividing by $(mM)^2$) |
| Q_{path} | Instantaneous Carter constant of an evolving orbit |
| Q_X | Carter constant of an orbit at the abutment |
| r | Orbital radius |
| \tilde{r} | rM^{-1} (Normalised with respect to MBH mass, only used in the Introduction) |
| r_1, r_2, r_3, r_4 | Roots of a polynomial |
| r_a | Root pertaining to the apocentre |
| r_p | Root pertaining to the pericentre |
| R | rM^{-1} (normalised with respect to MBH mass) |
| R | Ricci scalar |
| R_a | Apocentre (normalised) |
| R_p | Pericentre (normalised) |
| $R_z(\theta)$ | A rotation matrix for a rotation, θ , about the z -axis. |
| \mathbf{s} | $\mathbf{J}M^{-1}$ |
| \tilde{S} | $ \mathbf{J} M^{-2}$ |

| | |
|---------------------|--|
| u | Velocity parameter |
| \vec{U} | Four-velocity |
| \mathbf{v} | Velocity vector in three space |
| V | Effective potential |
| \tilde{V} | Vm^{-1} |
| \tilde{V}_+ | Normalised effective potential for prograde orbits |
| \tilde{V}_- | Normalised effective potential for retrograde orbits |
| V | Velocity difference between two inertial frames |
| W | $2\pi M\nu$ |
| X^2 | $(\tilde{L}_z - \tilde{S}\tilde{E})^2$ |
| X_-^2 | Governs prograde, polar and retrograde orbits up to the abutment |
| X_+^2 | Governs retrograde orbits beyond the abutment |
| β | v/c |
| γ | $1/\sqrt{1 - \beta^2}$ |
| Δ | $r^2 - 2Mr + \mathbf{s} ^2$ |
| $\tilde{\Delta}$ | ΔM^{-2} |
| $\eta_{\mu\nu}$ | Minkowski metric |
| θ | Polar angle |
| ι | Orbital angle of inclination |
| λ | An affine parameter |
| $\Lambda_{\alpha'}$ | Lorentz transform metric. |
| μ | The ratio mM^{-1} |
| ν | Radial frequency of secondary object |
| ρ | Scalar mass density |
| ρ | $M\sqrt{r^2 + \mathbf{s} ^2 \cos^2(\theta)}$ |
| Σ | ρ^2 |
| $\tilde{\Sigma}$ | ΣM^{-2} |

| | |
|----------------|-----------------|
| τ | Proper time |
| $\tilde{\tau}$ | τM^{-1} |
| ϕ | Azimuthal angle |

Chapter 1

Introduction

1.1 Theories and Principles of Relativity

A sequence of developments in theoretical and experimental physics, mathematics, and astronomical observation have brought us to Einstein's theory of general relativity [1–3]. The approach taken to develop and test dynamical theories required that particular natural phenomena behave in a consistent manner regardless of one's frame of reference. In Galilean relativity, the dynamical behaviour of material bodies within an inertial frame of reference was found to be independent of the frame's speed of travel [4]. Further, the investigation of the influence of gravity on material bodies of various compositions and masses gained importance and proceeded in earnest [4, 5].

When the empirical laws of electricity and magnetism were augmented and summarised into a concise set of equations by Maxwell, the theoretical understanding of electromagnetism deepened [6]. This development helped theorists to better understand electrodynamics and the propagation of light as part of a relativity theory. The interferometer experiments of Michelson and Morley, which were designed to measure changes in the propagation time of light caused by the motion of the Earth through the aether, yielded one of the most important null results in science. The aether, an absolute frame of reference, was discredited.

At first, dynamical behaviour in an inertial frame of reference was considered. But in modern general relativity, all natural phenomena are required to behave consistently, in all frames, inertial and non-inertial. Indeed, relativity has become a metaprinciple, a pattern to be followed by all laws of physics [7–9]. And thus far, the experimental testing of Einstein’s theory has not contradicted its validity (see Chapter 4 (page 101) in French [10], Chapters 6 and 7 in Ohanian [11], Chapter 10 in Hartle [12], and Will [13]).

To quote Richard Feynman¹ (Chapter 11, first page in Kennefick [14]),

"...the discovery of what is true is helped by experiments."

But Feynman expressed concern that for want of experimental results it is hard to perform a rigorous treatment of advanced hypotheses in relativistic gravitation. Although mathematical rigor offers guidance, without the benefit of experimental results, progress remains difficult. So Feynman exhorted theoreticians to create and test ideas through mathematical calculation, as a substitute for experimentation. In his words [14],

"...since we are not pushed by experiment, we must be pulled by imagination."

Imagination is no feint breeze; one is easily blown off course. So the theoretician must maintain a footing in the realm of the observable and the verifiable, yet not become tethered by old comforts. The history and growth of scientific principles in general, and the principles of relativity in particular, confirm this necessity.

1.1.1 Galileo’s Law of Inertia

The concept of inertial frames, frames of reference of uniform velocity amongst themselves, was introduced by Galileo to be more than a philosophical abstraction; it was a way to construct, to understand, and to interpret dynamical experiments in the real world;

¹From an address Feynman delivered at Chapel Hill in 1957.

and that was the revolution that transformed the natural sciences. Galileo performed and repeated many experimental tests of his hypotheses, which ultimately brought him to the law of inertia: *There is no dynamical test that reveals if one is in a state of constant motion or at rest.*

One's inability to perform a dynamical experiment to elucidate the state of motion of one's inertial frame leads one to conjecture the following (see Chapter 11 in Einstein [2]):

Conjecture 1 *Time is absolute; its progression is independent of the motion of an inertial frame.*

Conjecture 2 *Distance is independent of the state of motion of the inertial frame.*

These conjectures form the foundation of classical mechanics; together, they lead to the following corollary:

Corollary 3 *Time and space are independent and exclusive of one another.*

Eventually, Newton built upon this concept and developed the Galilean transformation equations:

$$t' = t, \tag{1.1}$$

by virtue of time (t) being global and absolute;

$$x' = x - Vt, \tag{1.2}$$

where V is a constant difference in velocity, as measured along the x -axis, between the inertial frames; and

$$y' = y \tag{1.3}$$

$$z' = z, \tag{1.4}$$

since the relative motion occurs only along the x -axis. Upon differentiating equation (1.2) with respect to time, t , one obtains the Galilean velocity addition law:

$$\begin{aligned} V &= \frac{dx}{dt} - \frac{dx'}{dt} \\ &= v - v'. \end{aligned} \tag{1.5}$$

One observes that V is determined by a linear relationship of v and v' , with no physical limitation placed on their values; consequently the relationship between a moving frame of reference and a beam of light became an important topic of concern.

1.1.2 The Restricted Principle of Relativity

The aether served the sole and singular purpose of explaining the propagation of light. And by conjecture, it gave light, and electromagnetic radiation in general, an absolute and global frame of reference. But the concept is untenable since it implies that one can propose an optical experiment to distinguish one's state of uniform motion from that of being at rest, an insight that cannot be achieved by the use of any dynamical experiment (Chapter 6 in Bondi [15]). Indeed, some have described the aether concept as absurd; yet it would be natural for such confusion to arise from such a conventional wisdom [15].

The expectation that there be an underlying uniformity to the physical universe led to the restricted principle of relativity: *no experiment can be performed, which will detect uniform motion with respect to the aether* [16, 17]. But to confirm this principle, new experimental observations were essential.

In 1881, Michelson made the first attempts to detect the absolute aether frame by using an instrument of his own invention, the Michelson interferometer. This device is composed of two rigid beam pathways of equal optical length, set at right angles to one another. A monochromatic light source (lasers had not yet been invented) supplies a single beam of light, which is split between the two paths; thus an interference pattern can be created, permitting an accurate measurement of any relative time delay between the

two beams of light. By rotating the entire apparatus in the laboratory, and by extension the aether wind, it was expected that a difference in travel time would be observed as a shift in the fringes of the interference pattern. In 1887 Michelson and Morley began their collaboration. Using a larger scale version of the Michelson interferometer, the observed shift in the fringes was significantly smaller (by a factor of forty) than what had been expected; this was a null result (see Chapter 2 in [10]).

The null result of the Michelson-Morley experiment was explained by a new physical phenomenon, the FitzGerald contraction: a mechanism by which the aether wind, a result of the Earth's motion, causes a contraction of matter, including the interferometer itself, exclusively in the direction of travel (see Chapter 8 [6]). In a letter to the editor of *Science*, published in 1889 [18], FitzGerald reasoned that because the structure of physical matter is fundamentally based on the electromagnetic force between the atoms and molecules, it is natural to expect the aether wind to affect such a compressive strain. H. A. Lorentz undertook his own analysis of the Michelson-Morley experiment in 1892; and without prior knowledge of FitzGerald's work, derived a similar result [19].

In 1932, Kennedy and Thorndike performed an adaptation of the Michelson-Morley experiment in which the two arms of the interferometer differed in length. They obtained a null result that could not be explained by the FitzGerald contraction alone²; it confirmed that a time dilation effect, as described in special relativity is required [10]. It is interesting to note that when Larmor (1898) [20] published the results of his treatment of the invariance of the Maxwell's equations, he stated:

"... the individual electrons describe corresponding parts of their orbits in times shorter for the latter system in the ratio ... $(1 - 1/2 v^2/c^2)$, while those less advanced in the direction of v are also relatively very slightly further on in their orbits on account of the difference of time-reckoning."

Although tantalisingly close to describing time dilation, like FitzGerald, he insisted

²And yet, one ought not to hastily dismiss the intuitive brilliance of FitzGerald's suggestion [6].

upon an electromechanical explanation. Lorentz undertook a similar study of the invariance of Maxwell's equations (1904) and proposed a "local time" [21]. It was Einstein's own treatment of Maxwell's equations, and his effort to make the laws of dynamics consistent with them, that produced special relativity [1].

1.2 Special Relativity

1.2.1 Introduction

Maxwell's equations lead to an important result (see section 9.2.1 in Griffiths [22]): the speed of light can be calculated directly from the permittivity of free space, $\epsilon_o \cong 8.854187817 \dots \times 10^{-12} \text{ C}^2 \text{ m}^{-2} \text{ N}^{-1}$ (2006 CODATA recommended values [23]), and the permeability of free space, $\mu_o \equiv 4\pi \times 10^{-7} \text{ N s}^2 \text{ C}^{-2}$ (2006 CODATA recommended values [24]), *viz.* $c \equiv 1/\sqrt{\epsilon_o \mu_o}$. (By modern convention the metre is defined as an exact quantity (CGPM [25]); correspondingly, the speed of light, c , is defined to be exactly 299,792,458 m/s (2006 CODATA recommended values [26]).)

Corollary 3 (section 1.1.1), and conjectures 1 and 2 from which it arose, imply that space and time may each be taken as invariant quantities regardless of the inertial frame of the observer. Einstein rejected Conjecture 1, but he did not do so capriciously; he reasoned that without the means to transmit information instantaneously, it is impossible to impose the simultaneity required for a true universal time to exist. Indeed, simultaneity is relative, not absolute (Chapter 3 in [10]).

Einstein postulated the following:

Postulate 1: *All of the laws of physics are uniform and unvariable, regardless of the particular inertial frame in which they are tested.*

Postulate 2: *In free space, the speed of light is of the same value, $c = 299,792,458$ m/s, regardless of the particular frame of reference in which it is measured, and regardless of the placement of the light source in another inertial frame of reference.*

In one respect, Postulate 2 may be inferred from Postulate 1; but Postulate 2 expresses

a new idea: the speed of light will be consistently measured to be, $c = 299,792,458$ m/s, in free space from any inertial frame of reference (see Chapter 3 [10]), regardless of the relative motion of the inertial frame in which the light originates. This postulate was confirmed through the astronomical observations of de Sitter [27].

It is not certain if Einstein knew of the null result of the Michelson-Morley experiment while composing his famous 1905 paper [1]. But in his 1921 address at King's College, London, England, Einstein described the Michelson-Morley experiment as an incisive demonstration of the restricted and special principles of relativity [28]. Further, Eddington observed that although the Michelson-Morley experiment is intrinsically disadvantaged by the use of a narrow range of non-relativistic velocities, the invariance of Maxwell's equations offers conclusive theoretical support for the null result of the Michelson-Morley experiment (Chapter 1 [17]).

1.2.2 Lorentz Boost

The derivation of the Lorentz transformation or boost, presented in Appendix 1 of Einstein's book [2], elucidates the physical arguments that underlie the theory of special relativity. But this is not unexpected since the quality of Einstein's genius was such that he could see into the heart of a problem.

The instantaneous time and position of an object, photon, or observation is called an event in spacetime; and these events can be plotted on a space-time³ or Minkowski diagram, which is merely a graph with a vertical t -axis and a horizontal x -axis. The locus of events associated with a moving object is called a world-line; and for a beam of light it is independent of the speed of travel of one inertial frame with respect to another. Therefore, the transformation that describes the mapping of spacetime coordinates, or events, in one inertial frame to another can be algebraically derived. The result, which

³Spacetime refers to the 1+3 dimensional time and space described by the Einstein equations; while space-time refers to the two dimensional $x - t$ plots (Minkowski diagrams) of the type used by Bondi in [15] to plot world-lines.

is associated with an inertial frame moving along the x -axis at a velocity $\beta = v/c$ with respect to the observer's rest frame, was found to be:

$$t' = \gamma t - \gamma\beta x \quad (1.6)$$

$$x' = \gamma x - \gamma\beta t \quad (1.7)$$

$$y' = y \quad (1.8)$$

$$z' = z \quad (1.9)$$

where $\gamma = 1/\sqrt{1 - \beta^2}$ [29]. This coordinate transformation is conveniently represented by the following tensorial equation:

$$x_{\alpha'} = \Lambda_{\alpha'}^{\alpha} x_{\alpha}, \quad (1.10)$$

where $\Lambda_{\alpha'}^{\alpha}$ is the Lorentz boost, which can be written in matrix form:

$$\Lambda_{\alpha'}^{\alpha} = \begin{bmatrix} \gamma & -\gamma\beta & 0 & 0 \\ -\gamma\beta & \gamma & 0 & 0 \\ 0 & 0 & 1 & 0 \\ 0 & 0 & 0 & 1 \end{bmatrix}. \quad (1.11)$$

The Lorentz boost not only describes the FitzGerald contraction, but also time dilation. Further, no electromechanical mechanism is invoked, nor the existence of an aether wind. The Lorentz transformation or boost, which describes a coordinate transformation between two inertial frames of reference, is consistent with the notion of relativity as a metaprinciple.

1.2.3 Minkowski Space

It is a seminal result of Einstein's theory of special relativity that if two frames of reference are in relative motion, then a measurement of space and time in one will be a linear

combination of space and time in the other. This property is expressed mathematically by equations (1.10) and (1.11), which are consequences of Postulate 2 in section 1.1.1 (see Chapter 2 in Thorne [7]).

In 1908, Hermann Minkowski [8] contributed to Einstein's work by treating the invariance of the speed of light in four-dimensional spacetime. By so doing, Minkowski introduced the concept of proper time, τ , and the invariant interval, $d\tau$; in Einstein's own words [28],

"... the four-dimensional continuum formed by the union of space and time retains the absolute character which according to the earlier theory, belonged to both space and time separately."

The formula for $d\tau^2$ in flat space is:

$$-c^2 d\tau^2 = -c^2 dt^2 + dx^2 + dy^2 + dz^2. \quad (1.12)$$

Because $d\tau$ is invariant, it does not change its value under a coordinate transformation.

Therefore,

$$-c^2 d\tau^2 = -c^2 d\bar{\tau}^2 \quad (1.13)$$

\Rightarrow

$$-c^2 dt^2 + dx^2 + dy^2 + dz^2 = -c^2 d\bar{t}^2 + d\bar{x}^2 + d\bar{y}^2 + d\bar{z}^2, \quad (1.14)$$

where

$$\bar{t} = \bar{t}(t, x, y, z)$$

$$\bar{x} = \bar{x}(t, x, y, z)$$

$$\bar{y} = \bar{y}(t, x, y, z)$$

$$\bar{z} = \bar{z}(t, x, y, z)$$

represent the coordinate transformation. The signs of the terms in equations (1.12)

and (1.14) suggest a 1+3 spacetime signature⁴ (i.e. $(-, +, +, +)$). The introduction of tensorial notation (an aspect of differential geometry) improved the treatment of invariant quantities in flat spacetime

$$-c^2 d\tau^2 = \eta_{\alpha\beta} dx^\alpha dx^\beta, \quad (1.15)$$

where $dx^\alpha = (cdt, dx, dy, dz)$ and the Minkowski metric is,

$$\eta_{\alpha\beta} = \text{diag}(-1, 1, 1, 1); \quad (1.16)$$

$\eta_{\alpha\beta}$ represents a pseudo-euclidian geometry [30].

The form taken by the formulae in equation (1.14) demonstrates the principle that the laws of physics must be expressed and described mathematically in a manner that is independent of the frame of reference. Indeed, it is this approach that enabled Einstein to undertake a detailed treatment of electrodynamics in the second part of his 1905 paper [1]. The expressions for the interval, $d\tau$, in curved spacetime are important to know; and differential geometry facilitates such a treatment.

1.2.4 Relativistic Velocity Composition Law

The Lorentz boost, which can be treated as a rotation in spacetime by making the substitution $\beta = \tanh(u)$, may be written in a new form:

$$\Lambda_{\alpha'}^\alpha = \begin{bmatrix} \cosh(u) & -\sinh(u) & 0 & 0 \\ -\sinh(u) & \cosh(u) & 0 & 0 \\ 0 & 0 & 1 & 0 \\ 0 & 0 & 0 & 1 \end{bmatrix}, \quad (1.17)$$

⁴The designation of 1+3 spacetime is not to be confused with the breaking of spacetime into a collection of three-dimensional, space-like foliations.

where $\{u \in \mathbb{R} | -\infty \leq u \leq \infty\}$ is the velocity parameter (section 3.6 in Carmeli [31] and section 1.4 in Hobson et al. [30]). Such a construct resembles a rotation matrix such as:

$$R_z(\theta) = \begin{bmatrix} \cos(\theta) & \sin(\theta) & 0 \\ -\sin(\theta) & \cos(\theta) & 0 \\ 0 & 0 & 1 \end{bmatrix}, \quad (1.18)$$

where θ defines the angle of rotation about the z -axis, in three-dimensional space. Therefore, the parameter u may be interpreted as a rotation in spacetime, an interpretation originally developed by Minkowski (see section 2.1 in Weber [32]). The benefit of this analogy, and the form depicted in equation (1.17), lies in the simplified derivation of a relativistic velocity-composition law:

$$\frac{V}{c} = \frac{\beta - \beta'}{1 - \beta\beta'}, \quad (1.19)$$

viz.

$$\frac{V}{c} = \tanh(u - u') \quad (1.20)$$

where

$$\begin{aligned} u &= \tanh^{-1}(\beta) \\ u' &= \tanh^{-1}(\beta'); \end{aligned}$$

and β and β' correspond to v/c and v'/c in their respective frames of reference. The relativistic velocity-composition law approaches the Galilean velocity-addition law (equation (1.5)) in the classical limit, as required. Further, equation (1.20) places an upper limit of c (the speed of light) on the value of $|V|$.

1.3 General Relativity

1.3.1 Introduction

Special relativity applies exclusively to inertial frames of reference; but such frames exclude gravitational effects. The path that led to a generalised theory of relativity followed a new line of reasoning; Einstein sought a fundamental understanding of the principle of equivalence: the observed equality of inertial mass (inertia) and gravitational mass (weight), regardless of the composition of the bodies in question (see Appendix Five in [2]).

Einstein had initially balked at treating special relativity as a four-dimensional mathematical construct (see pg 643 in Gribbin [33]); but in 1912 he recognised it as an indispensable tool for developing a generalised principle of relativity that included gravity (see Chapter 2 in Thorne [7] and Chapter 11 (last page) in [33]). Indeed, Einstein would come to attribute his success in developing general relativity to Minkowski's four-dimensional representation of spacetime⁵ (see Chapter 17 in [2]), which facilitated the tensorial treatment of spacetime curvature. Thus both general invariance, and covariant quantities could be represented rigorously. The theory of general relativity rests upon two formal and complementary principles: the principle of equivalence and the principle of general covariance.

1.3.2 The Principle of Equivalence

The equivalence of weight and inertia was confirmed, to increasingly high experimental accuracy, by such luminaries as Galileo (*c.* 1610), Newton (1680, 1686-87), and Eötvös

⁵The remark Minkowski made about Albert Einstein, his former student was: "Das ist für mich eine große Überraschung, denn Einstein war ein großer Faulpelz, und für Mathematik interessierte er sich überhaupt nicht [34]." In English it is: "This is a big surprise for me, as Einstein was a real lazybones, and he was not interested in math whatsoever [35]." The word, Faulpelz, means lazybones not lazy dog; it was translated incorrectly. It is a colloquial term one might use to describe the laziness of a person for whom one has great fondness.

(1890, 1922) (see table 1.3.1 in [31] and table 2.2 in [13]). But Einstein carried this empirical result to the inspired conclusion that a non-inertial frame in free-fall appears to be absent of gravity, and in the converse case, a frame that experiences a constant acceleration is indistinguishable from one in which a gravitational field is present.

To carry the principle of equivalence forward to a generalisation of special relativity, one must revisit the concept of the invariance of the speed of light [36]. In a non-inertial frame, subject to a constant acceleration, light will follow a particular curvilinear path. Certainly, the speed of light as measured in any frame must equal one; but now one finds that a gravitational field must cause a beam of light to change its direction, to bend (see section 6.2 in [12]). Further, the equivalence principle demonstrates that in such a non-inertial frame, in which a source of light pulses (e.g. a strobe light with a steady emission rate) has been installed in the floor, a detector in the ceiling will record a slower pulse rate; thus one may infer that time elapses more slowly in a stronger gravitational field. These effects were incorporated into a generalised metric representation of spacetime through pseudo-Riemann geometry (section 6.3 in [12]).

The principle of equivalence is intended to be applied locally. Indeed, a free-falling and non-rotating frame above the surface of the Earth still experiences tidal forces. And there are important consequences regarding a free-falling mass or charge; no electromagnetic [37, 38] or GW energy is emitted by a charged particle that experiences a constant acceleration (see Lecture 9 in [39]).

1.3.3 The Principle of General Covariance

In Einstein's 1905 paper [1], the analysis of the Maxwell equations proceeded by requiring their governing formulae be of a consistent form, regardless of the inertial frame in which they might be put to paper and used to analyse electrodynamic phenomena. Further, a frame of reference may be characterised as a four-dimensional spacetime, so that the treatment of different frames of reference is reduced to the mathematical treatment of coordinate systems. But when analysing physical phenomena, a special subclass of

coordinate systems, such as inertial frames, is insufficient [40]; the principle of general covariance requires that the mathematical expressions that describe physical phenomena and predict the behaviour of natural systems, be of the same form in all coordinate systems [40].

The departure from the idealisation of an inertial frame, leads one to consider coordinate systems in which spacetime is curved by virtue of the presence of a gravitational field. The principle of general covariance offers a criterion for extending the domain of physical formulae to general coordinate systems. Further, physically significant quantities will be invariant under a general coordinate transformation (see sections 1.5 and 2.1 in Carmeli [31]). General coordinate transformations can be represented by

$$\bar{x}^\alpha = \bar{f}^\alpha(x^0, x^1, x^2, x^3), \quad (1.21)$$

where \bar{f}^α is a set of four real-valued continuous functions of x^α . The coordinate transform, \bar{f}^α , must be differentiable and invertible, therefore, its Jacobian,

$$\left| \frac{\partial \bar{f}^\alpha}{\partial x^\beta} \right|, \quad (1.22)$$

must be non-zero [31].

Equation (1.21) resembles equation (1.10) in form, therefore, the Lorentz boost, as a transformation between inertial frames, is a special case of the general coordinate transformation in equation (1.21).

1.3.4 The Einstein Equations

1.3.4.1 Absence of Matter

Riemann geometry facilitates the treatment of curvature in a 1+3 spacetime. The nature and characteristics of the intrinsic curvature of spacetime (one does not discuss a four-dimensional manifold embedded within a five-dimensional manifold) is built upon the

extension of the Minkowski metric, $\eta_{\alpha\beta}$, to include the more general metric quantity, $g_{\alpha\beta}$. The elements of $g_{\alpha\beta}$ are not constants (as in the case of $\eta_{\alpha\beta}$), but functions of the variables x^α . The general metric, $g_{\alpha\beta}$, represents a solution to the Einstein equations; but to develop the Einstein equations themselves, one must consider the Riemann geometry of $g_{\alpha\beta}$.

The Riemann-Christoffel tensor, $R_{\mu\nu\sigma}^\lambda$, is derived by analytically treating the absolute change of a vector carried around a loop of infinitesimal size. The use of the covariant derivative is essential in the case where spacetime is curved; and the connection coefficients, $\Gamma_{\mu\nu}^\lambda$ (functions of $g_{\alpha\beta}$), present themselves in the result,

$$(\nabla_\nu \nabla_\sigma - \nabla_\sigma \nabla_\nu) v_\mu = R_{\mu\nu\sigma}^\epsilon v_\epsilon \quad (1.23)$$

where

$$R_{\mu\nu\sigma}^\epsilon = \Gamma_{\mu\sigma}^\alpha \Gamma_{\alpha\nu}^\epsilon - \Gamma_{\mu\nu}^\alpha \Gamma_{\alpha\sigma}^\epsilon + \Gamma_{\mu\sigma,\nu}^\epsilon - \Gamma_{\mu\nu,\sigma}^\epsilon$$

(see sections 33 and 34 in Eddington [41] or Chapter 1 in Bona [42]). It is a necessary and sufficient condition that $R_{\mu\nu\sigma}^\lambda = 0$ for spacetime to be flat (see Chapter 3 in Eddington [41]). The vanishing of the Ricci scalar, $R = g^{\mu\sigma} g_{\lambda\alpha} g^{\nu\alpha} R_{\mu\nu\sigma}^\lambda$, is not a sufficient condition for flat spacetime. And a zero value for the Ricci tensor ($R^{\mu\nu} = 0$) indicates that the corresponding curved spacetime has no sources; that is, the region of space contains no matter.

Einstein derived the equations for gravitational potential in free space in 1915 [43, 44]:

$$G^{\mu\nu} = 0, \quad (1.24)$$

where

$$G^{\mu\nu} = R^{\mu\nu} - \frac{1}{2} g^{\mu\nu} R \quad (1.25)$$

is the Einstein tensor. In the general case, where matter is present, the Einstein equation

is:

$$G^{\mu\nu} = 8\pi T^{\mu\nu}, \quad (1.26)$$

where $T^{\mu\nu}$ is the stress-energy tensor [45]:

$$T^{\mu\nu} = \rho \frac{dx^\mu}{d\tau} \frac{dx^\nu}{d\tau} \quad (1.27)$$

where ρ , a scalar, is the mass density. As is the case of $G^{\mu\nu}$, $T^{\mu\nu}$ also satisfies the Bianchi identities.

1.3.5 Exact Solutions to the Einstein Equations

1.3.5.1 Flat Space

The Minkowski metric, $\eta_{\alpha\beta} = \text{diag}(-1, 1, 1, 1)$, is an exact solution to $G_{\alpha\beta} = 0$; but by virtue of its corresponding Riemann-Christoffel tensor, $R_{\mu\nu\sigma}^\lambda \equiv 0$, it may be considered to be the trivial solution. It is Lorentz invariant and applies to spacetime without sources. Flat spacetime is an idealisation, which finds use in the construction of a linearised model for gravitation [46, 45].

1.3.5.2 The Schwarzschild Metric - a spherically symmetric solution

In 1915, Karl Schwarzschild, inspired by Einstein's theory of general relativity, sought a solution to the Einstein equations that described the curvature of spacetime outside a spherically symmetric star with no angular rotation [7]. His result:

$$d\tilde{\tau}^2 = - \left(1 - \frac{2}{\tilde{r}}\right) dt^2 + \left(1 - \frac{2}{\tilde{r}}\right)^{-1} d\tilde{r}^2 + \tilde{r}^2 d\Omega^2, \quad (1.28)$$

where

$$d\Omega^2 = d\theta^2 + \sin^2(\theta) d\phi^2,$$

was presented on his behalf by Einstein in January, 1916. The parameters in equation (1.28) have been normalised with respect to the mass, M , of the gravitation body (i.e. $\tilde{r} = r/M$, $\tilde{t} = t/M$, and $\tilde{\tau} = \tau/M$); no normalisation is required for the angles θ and ϕ . It is important to recognise that although in modern times the Schwarzschild geometry is associated with non-rotating black holes, it was originally derived as a solution for stars; indeed, any non-rotating object has the Schwarzschild geometry as its external solution. Later, in 1916, Schwarzschild derived a solution for the interior of a star. Such solutions are complicated [29], and lie beyond the scope of this work.

The exterior Schwarzschild solution describes the gravitational field of an isolated particle of mass, M , in a region of free space, therefore, $R^{\mu\nu} = 0$. The metric is autonomous (not explicitly dependent on time) and it is unchanged under time reversal (see sections 10.1 and 10.2 in [29]).

In the Schwarzschild line element (equation (1.28)) there is a term, $(1 - 2/\tilde{r})$, common to the $d\tilde{t}^2$ and $d\tilde{r}^2$ elements, which offers an insight into some of the important properties of the Schwarzschild geometry. As $\tilde{r} \rightarrow \infty$, (i.e. the properties of the line element are considered at locations far distant from the gravitating body), the Schwarzschild line element asymptotically approaches that of Minkowski space (equation (1.16)). For decreasing values of \tilde{r} , the spacetime curvature becomes more pronounced; and a coordinate singularity exists at $\tilde{r} = 2$. The quantity, $\tilde{t} = t/M$, which appears in the Schwarzschild metric through the term, $d\tilde{t}^2$, corresponds to the Schwarzschild or coordinate time (normalised by dividing by the mass of the black hole, M) as it would be measured in a stationary frame at an infinite distance away (see Susskind and Lindesay [47]).

At the radius $\tilde{r} = 2$, the coefficient of $d\tilde{r}^2$ is at a coordinate singularity. This radial position, the Schwarzschild radius, defines the event horizon of a Schwarzschild black hole (SBH). As an exercise in visualising the scale of this coordinate singularity, one may neglect any rotational angular momentum and calculate the Schwarzschild radius of a given body, whether it is massive or not.

Table 1.1: Schwarzschild radii for spherically symmetrical bodies of various masses. The data is presented in MKS units; but geometrised units, for which $c = 1$ and $G = 1$ will be used henceforth, see table 1.2.

| Category | Object | Mass [kg] | True Radius [m] | Schwarzschild Radius [m] |
|--------------------|------------------|------------------------|-----------------------|--------------------------|
| lepton | electron | 9.11×10^{-31} | $< 10^{-22}$ [48] | 1.4×10^{-57} |
| hadron | proton | 1.67×10^{-27} | 5.0×10^{-16} | 2.5×10^{-54} |
| sports | bocce ball | 1.00 | 5.5×10^{-2} | 1.5×10^{-27} |
| large satellite | Moon | 7.35×10^{22} | 1.7×10^6 | 1.1×10^{-4} |
| planet | Earth | 5.97×10^{24} | 6.4×10^6 | 8.9×10^{-3} |
| white dwarf | Sirius B | 1.95×10^{30} | 5.7×10^6 | 2.9×10^3 |
| star | Sun | 1.99×10^{30} | 7.0×10^8 | 3.0×10^3 |
| neutron star | PSR 1913+16 | 2.87×10^{30} | 1.0×10^4 | 4.3×10^3 |
| M supergiant | α Orionis | 3.78×10^{31} | 8.2×10^{11} | 5.6×10^4 |
| massive black hole | $10^7 M_{\odot}$ | 1.99×10^{37} | 3.0×10^{10} | 3.0×10^{10} |

The values tabulated in table 1.1⁶ demonstrate that the Schwarzschild radius is so small as to be beyond the realm of our everyday experience; MKS units, which are familiar to the general reader, are used at this point. The Schwarzschild radius of a bocce ball is five orders of magnitude smaller than the estimated upper limit of the electron radius. The Schwarzschild radius of the Earth is less than 1 cm in size. Consequently, virtually all the of mass of these bodies lies outside the Schwarzschild radius. This circumstance is even true for an object as massive as the Sun, which has a Schwarzschild radius of 3 km. But this work focuses on black holes and extreme mass-ratio binary black hole systems, for which the event horizon is no longer an abstraction.

Henceforth in this work, geometrised units will be used. By setting the speed of light, $c = 1$, distance can be expressed in units of seconds. In addition, by setting the gravitational constant, $G = 1$, it is also possible to express mass and energy, as well as momentum, in units of seconds. An important result can be calculated for the Sun: one solar mass $\cong 5 \mu s$.

⁶The calculations of the Schwarzschild radius given here are for illustrative purposes; they are based on the external Schwarzschild geometry.

Table 1.2: The representation of metres and kg in units of time.

| Parameter | Symbol | Geometrised Units |
|------------------------|----------|--|
| speed of light | c [26] | $299,795,458 \text{ m/s} = 1$ $\Rightarrow 1 \text{ m} = 1/299795458 \text{ s}$ |
| gravitational constant | G [49] | $6.67428 \dots \times 10^{-11} \text{ m}^3 \text{ kg}^{-1} \text{ s}^{-2} = 1$ $\Rightarrow 1 \text{ kg} = 2.47702 \times 10^{-36} \text{ s}$ |

1.3.5.3 Kerr Black Hole - an axisymmetric solution

Because an SBH does not rotate, it possesses spherical symmetry and serves as a useful idealisation. But one expects most black holes to possess some spin angular momentum (\mathbf{J}), therefore, the spherical symmetry associated with an SBH is broken, becoming an axisymmetric spacetime, orientated parallel to the axis of rotation. In 1963, Roy Kerr derived the analytical solution to the Einstein field equations for a spinning black hole [50]. This result was the culmination of an effort made by many researchers over a period of several years; hence a black hole with spin angular momentum is called a Kerr black hole (KBH).

The form of the Kerr spacetime line element used today [50]:

$$d\tilde{\tau}^2 = -\frac{\tilde{\Delta} - \tilde{S}^2 \sin^2(\theta)}{\tilde{\Sigma}} d\tilde{t}^2 + \frac{\tilde{\Sigma}}{\tilde{\Delta}} d\tilde{r}^2 + \tilde{\Sigma} d\theta^2 - 4\frac{\tilde{S}\tilde{r} \sin^2(\theta)}{\tilde{\Sigma}} d\tilde{t}d\phi + \frac{(\tilde{r}^2 + \tilde{S}^2)^2 - \tilde{S}^2\tilde{\Delta} \sin^2(\theta)}{\tilde{\Sigma}} \sin^2(\theta) d\phi^2, \quad (1.29)$$

where

$$\tilde{S} = \frac{|\mathbf{J}|}{M^2}$$

$$\Delta = M^2 (\tilde{r}^2 - 2\tilde{r} + \tilde{S}^2) \Rightarrow \tilde{\Delta} = \tilde{r}^2 - 2\tilde{r} + \tilde{S}^2$$

and

$$\Sigma = \rho^2 = M^2 (\tilde{r}^2 + \tilde{S}^2 \cos^2(\theta)) \Rightarrow \tilde{\Sigma} = \tilde{r}^2 + \tilde{S}^2 \cos^2(\theta),$$

differs from the form originally published by Kerr. As before (i.e. equation (1.28))

the parameters in the equation are normalised with respect to the mass, M , of the Kerr black hole (KBH). The use of Boyer-Lindquist coordinates simplifies the metric to a form with a single off-diagonal element⁷ for $d\tilde{t}d\phi$ (see Appendix 3.B.1). Further, in the limit as $\tilde{S} \rightarrow 0$, equation (1.29) approaches the Schwarzschild geometry. As in the case of the Schwarzschild geometry the Kerr metric is also stationary, and $R^{\mu\nu} = 0$ throughout the region of free space outside the rotating body [51, 52]. The terms are autonomous. But under time reversal, the off-diagonal elements (those that contain $d\phi dt$) change sign, therefore, the Kerr spacetime geometry is stationary, but not static.

The free space surrounding the Kerr black hole contains some important regions. The event horizon for a KBH corresponds to the singularity of the coefficient for $d\tilde{r}^2$, hence

$$\tilde{r}_H = 1 \pm \sqrt{1 - \tilde{S}^2}, \quad (1.30)$$

where the positive root corresponds to the event horizon of an SBH ($\tilde{S} = 0$). Interestingly, the value of \tilde{r}_H is independent of the polar angle θ . But this does not mean the event horizon of a KBH is spherically symmetrical; it only appears so when represented in Boyer-Lindquist coordinates.

By solving for the roots of the coefficient of $d\tilde{t}^2$ one finds the definition of the ergosphere of the KBH:

$$\tilde{r}_{Ergo} = 1 \pm \sqrt{1 - \tilde{S}^2 \cos^2(\theta)}, \quad (1.31)$$

which describes another null surface (positive root) that extends farther into space than the event horizon.

⁷There are two, symmetrically placed off-diagonal elements, both of which correspond to $d\tilde{t}d\phi$. Because they are equal, one may consider their combination to be a single element.

1.4 Gravitational Wave Radiation

Gravitational wave (GW) radiation is a singularly intriguing concept, not only because the question of whether or not it exists remains unanswered (see an historical account by Kennefick [14]), but because the study of GW offers a fundamental insight into Einstein's theory of general relativity. One might give the search for experimental evidence of GW a status equal to that of the Michelson-Morley experiment; the consequences will be equally profound.

Einstein laid the foundation of the prediction of GW in his expositional work of 1916 [45]. Using the gauge invariance of the equations of linearised gravity, he transformed them into a set of wave equations whilst preserving their covariance amongst Lorentz coordinate transformations. Therefore, in the context of linearised gravity, GW might be detected far from its source in the propagation region, in regions of spacetime with vanishingly small curvature and perturbation.

1.4.1 The Gravitational Wave Propagation Region

Although this aspect of GW study lies outside the scope of this work, it will be described here in a cursory manner. In the propagation region, far from the GW source, GW radiation is of minuscule amplitude; hence, in 1916 Einstein explored a new treatment of special problems in gravitational theory by working to a first-order approximation of $g_{\mu\nu}$ about $\eta_{\mu\nu}$:

$$g_{\mu\nu} = \eta_{\mu\nu} + h_{\mu\nu} \tag{1.32}$$

where

$$|h_{\mu\nu}| \ll 1.$$

Einstein specified that the perturbation, $h_{\mu\nu}$, exhibits tensor-like behaviour only amongst linear, orthogonal coordinate transformations (i.e. Lorentz transformations).

Consider the Einstein field equation with matter present (equation (1.26)); Einstein

substituted the expression in equation (1.32) into a modified, yet mathematically equivalent field equation (see Chapter 6 in [53]):

$$R_{\mu\nu} = 8\pi \left(T_{\mu\nu} - \frac{1}{2}g_{\mu\nu}T \right) \quad (1.33)$$

where

$$T = T^\alpha{}_\alpha, \quad (1.34)$$

to obtain:

$$h_{\mu\alpha}^{\nu\alpha} + h_{\nu\alpha}^{\mu\alpha} - h_{\mu\nu,\alpha}^\alpha - h_{\alpha,\mu\nu}^\alpha = 16\pi \left(T_{\mu\nu} - \frac{1}{2}g_{\mu\nu}T \right). \quad (1.35)$$

He then performed an initial simplification of equation (1.35) through the field redefinition,

$$\bar{h}_{\mu\nu} = h_{\mu\nu} - \frac{1}{2}\eta_{\mu\nu}h, \quad (1.36)$$

where

$$h = h^\alpha{}_\alpha.$$

The final form of the wave equation was derived by using the condition [46, 45],

$$\bar{h}_{\mu\nu}^{\nu\mu} = 0. \quad (1.37)$$

Because

$$T_{\mu\nu}^{\nu\mu} = 0 \quad (1.38)$$

one obtains:

$$\eta^{\alpha\beta}\partial_\alpha\partial_\beta\bar{h}_{\mu\nu} = -16\pi T_{\mu\nu}. \quad (1.39)$$

Equation (1.39) yields two important results: first, the propagation speed of GW radiation equals one; and second, a general solution, which incorporates retarded potentials, may be used

$$\bar{h}_{\mu\nu} = -4 \int \frac{T_{\mu\nu}(x', t-r)}{r} d^3x' \quad (1.40)$$

where

$$r = +\sqrt{(x_i x^i - 2x_i x'^i + x'^i x'_i)}. \quad (1.41)$$

Because one is concerned with the propagation region, equation (1.40) can be simplified to:

$$\bar{h}_{\mu\nu} = -\frac{4}{R} \int T_{\mu\nu}(x', t - r) d^3x' \quad (1.42)$$

where

$$R = +\sqrt{x_i x^i}.$$

One may proceed by inserting a simplified expression for $T_{\mu\nu}$, which approximates some physical GW source such as a binary black hole system.

1.4.2 The Gravitational Wave Generation Region

The emission and detection of high frequency GW radiation within the laboratory is virtually impossible since there are structural limitations in mechanical GW generation systems and because the GW wavelength is inordinately long (perhaps 10^6 times greater than the characteristic length of the emitter; see section 8.5 in Weber [32]). Weber also described an alternative method in which piezoelectric crystals are driven at a point close to fracture; but the number of crystals needed (perhaps 10^6 small crystals) and the crystal size (50 cm a side) make the scheme impractical. The suggestion that quantum mechanical experiments be constructed is interesting [54]; but it is well outside the scope of this work, in which classical general relativity theory is treated.

Because of their extraordinarily strong gravitational fields, black holes and particles in orbit around black holes have gained attention as feasible sources of GW (Detweiler in [55]). Preliminary analysis has shown that the resonance of the event horizon of an isolated black hole, although scientifically interesting, is insufficiently large in amplitude for detection to be practical far away. Further, the mechanism for GW generation based upon the radial free-fall of a test-particle has been numerically estimated and found to

be weak. Such a result might be inferred from the principle of equivalence (see section 1.3.2).

It is predicted that an infalling particle that possesses some orbital angular momentum, even an amount sufficient for only one full orbit before crossing the event horizon of the massive black hole (MBH), will emit substantially more GW energy than would be produced during a radial free-fall (see table 1 [55]). The energy emitted by orbiting particles that have greater orbital angular momentum, and thus stay aloft for a longer time, are calculated to produce even greater amounts of GW energy. An improved understanding of the orbital evolution of extreme mass-ratio binary black hole systems is beneficial, especially if they become the primary source of GW radiation.

Although the treatments of GW propagation and GW generation are separate, there is an important practical connexion between the two regimes. The raw signals, which are expected to contain significant quantities of noise, will be filtered by a correlation technique; therefore, good estimates of the most reasonable GW waveforms are needed for use as templates. An understanding of the evolution of the extreme binary black hole systems over time is essential for this purpose.

1.5 Extreme Binary Black Hole Systems

1.5.1 Introduction

As stated above, extreme binary systems are expected to emit a GW spectrum most suitable for detection [56–58]. Such systems contain a compact object (CO) of 1 to 10 solar masses in a bound orbit about an MBH of 10^6 solar masses (or more). As the CO revolves in an inspiral motion about the MBH its acceleration causes GW radiation to be emitted [59, 60]. Because the GW radiation carries energy and angular momentum away from the binary system, the radiation reaction causes the orbit of the CO to become progressively less eccentric and smaller in radius until the CO plunges into the MBH [61, 62]. In turn the changing eccentricity and period of the CO orbit affects the frequency

distribution of the GW spectrum and its energy content.

In the work of Peters and Mathews [59], a binary system composed of a massive SBH and a CO was modelled as a time-dependent quadrupole inertia tensor where the bodies were assumed to be point masses governed by Keplerian motion, their motion causing GW emission in analogy to electromagnetic systems. The average rate of energy loss was calculated by integrating the GW power density over a period of time (i.e. a period of a single CO orbit) and over the entire sphere of solid angle 4π steradians. Those authors were able to derive a power loss formula, expressed in terms of orbit eccentricity, e , semi-major axis, a , and the respective masses of the bodies in the system (CO mass, m , and MBH mass, M).

In subsequent work, Peters [60] expanded and augmented these concepts to calculate both the energy content and momentum flux of the gravitational radiation. The difficulty that lay in finding analytical wave solutions to Einstein's field equations inspired the development and use of series solutions composed of expansions of the CO velocity and \tilde{r} ($\tilde{r} = r/M$). Although Peters made no direct reference to the Post Newtonian (PN) approximation (originally used by Einstein [45]), he provided an example of how it can be used to develop approximate evolution equations of PN order for a binary system. The mass-energy tensor was used to calculate the energy and angular momentum loss of the system.

1.5.1.1 The Parameterised Post-Newtonian Formalism

Before describing the post-Newtonian approximation, it is advantageous to avoid confusion by briefly defining the Parameterised post-Newtonian formalism. In addition to Einstein's theory of general relativity, many alternate metric theories of relativistic gravitation have been proposed [12]. The parameterised post-Newtonian (PPN) formalism offers a structured system to categorise these theories by introducing ten independently adjustable parameters ($\gamma, \beta, \xi, \alpha_1, \alpha_2, \alpha_3, \zeta_1, \zeta_2, \zeta_3, \zeta_4$) [13]. Einstein gravitation is represented in a particularly simple way with $\gamma = \beta = 1$; the eight remaining parameters

equal zero. The work undertaken here excludes non-metric gravitational theories and uses Einstein's theory of general relativity exclusively.

1.5.2 Post-Newtonian Approximation

The details of the derivation and application of the Post-Newtonian (PN) approximation to problems of relativistic motion and GW emission are outside the scope of this work. Some highly detailed and technical outlines are available to the interested reader (Chapter 9 in Weinberg [63] or see Asada et al. [64]) and a detailed analysis of relativistic celestial mechanics is presented by Brumberg [65]. A pedagogical introduction of the PN approximation method in both an historical context and with respect to GW emission is presented by Kennefick (Chapter 3 in [14]). Further, a cautionary analysis of PN approximation methods is provided by Damour [66].

The change with respect to time of the characteristics of an inspiraling orbit may be described by a set of evolution equations that have been derived to the necessary PN order. The PN approximation can be traced back to Einstein's first attempts (in 1915) to calculate the apsidal precession of Mercury [14]. In the case of the planet Mercury, the observed precession differs slightly from the value calculated using the Newtonian mechanics of the solar system by an amount $\sim 43.03''/100\text{y}$ (see table 8.3 in [63]). General relativity provided Einstein with a clear and direct estimate of this difference, without the need to take into account the contributions of the other planets in the solar system. But without the benefit of an exact solution to the Einstein field equations in the vicinity of the Sun, this task would be difficult.

To perform a second-order perturbation of the planet's Newtonian behaviour, the quantity v^2/c^2 (where v is the orbital speed of Mercury) was used to make a small correction to the Newtonian equations of motion for spacetime curvature arising from the Sun's mass. Given the expression for the lowest order of gravitational field strength

in a spherically symmetrical system,

$$\begin{aligned} U &= \left(\frac{M}{r} \right) \\ &= \frac{1}{\tilde{r}}, \end{aligned} \tag{1.43}$$

one may apply the virial theorem to approximate the lowest order of the test-particle orbital speed:

$$v = \sqrt{\frac{1}{\tilde{r}}}.$$

The use of expansion series of $1/\sqrt{\tilde{r}}$ serves to model the motions of particles in their orbits. This technique has been used to order $1/\tilde{r}$ to model the motions of planets in the solar system.

In cases where greater precision is needed, higher orders of $v^2 \sim 1/\tilde{r}$ are demanded. Expressions that include v^2 terms are called first-post-Newtonian, and those that contain v^4 terms are called second-post-Newtonian. The terms of v to even power describe a conservative system. The inclusion of a v^5 term introduces an energy loss by GW emission.

The detailed treatment of the orbital motion of a CO, in conjunction with the quadrupole (and perhaps higher multipole [67]) formalism to describe energy and angular momentum loss, provide models to describe orbital evolution. The rotation of an MBH (i.e. a Kerr black hole, KBH) complicates the evolution of the CO orbit; the Lense-Thirring precession [68–70] causes the coupling of the KBH spin to the orbital angular momentum of the CO, which contributes an additional energy term to the Lagrangian and Hamiltonian action integrals [71, 72]. But this behaviour is contained in the Kerr spacetime solution. In the analysis to follow, exact solutions are used.

The Teukolsky equations [73–75] represent an improvement in modelling the GW emission and the evolution of CO and test-particle orbits. And like the PN approximation, the details of this method lie outside the scope of this work. To reiterate, the emphasis of this work is to introduce a new method of testing or validating sets of

evolution equations from sources in the literature.

1.5.3 Four-Momentum of Orbiting Test-Particles

To begin, consider the three-momentum (\mathbf{P}) of a particle of rest-mass (m_{rest}) that travels at a velocity (\mathbf{v}) in an inertial frame. According to the Newtonian definition of \mathbf{P} :

$$\begin{aligned}\mathbf{P} &= m_{rest}\mathbf{v} \\ &= m_{rest}\frac{dx^i}{dt},\end{aligned}\tag{1.44}$$

where m_{rest} is postulated to be constant. But one must explore the true relationship between mass and velocity of the particle.

In special relativity, one can derive the relativistic four-momentum (\vec{P}):

$$\vec{P} = m_{rest} \left(\frac{dx^\alpha}{d\tau} \right),\tag{1.45}$$

where m_{rest} is truly invariant, and the derivative is performed with respect to proper time, τ .

The invariance of m_{rest} is an important aspect of the treatment to follow. But the conventional wisdom that mass increases with increasing particle speed is not in contradiction because m_{rest} is a distinct quantity from the relativistic mass (m_{rel}). Consider the following derivation (see Chapter 9, pages 144-145, in Eddington [17]) in which the old definition of momentum is used:

$$\begin{aligned}\vec{P} &= m_{rest} \left(\frac{dx^\alpha}{d\tau} \right) \\ &= m_{rest} \left(\frac{dt}{d\tau} \right) \left[1, \frac{dx^i}{dt} \right] \\ &= m_{rel} \left[1, \frac{dx^i}{dt} \right].\end{aligned}\tag{1.46}$$

Using the Minkowski metric,

$$\begin{aligned}
 -d\tau^2 &= -dt^2 + dx^2 + dy^2 + dz^2 \\
 &= -dt^2 (1 - \mathbf{v} \cdot \mathbf{v}) \\
 &= -dt^2 (1 - \beta^2),
 \end{aligned} \tag{1.47}$$

which yields:

$$\frac{dt}{d\tau} = \frac{1}{\sqrt{1 - \beta^2}}. \tag{1.48}$$

From equations (1.46) and (1.48) one finds:

$$\begin{aligned}
 m_{rel} &= m_{rest} \left(\frac{dt}{d\tau} \right) \\
 &= \frac{m_{rest}}{\sqrt{1 - \beta^2}},
 \end{aligned} \tag{1.49}$$

as required.

Consider the dot product:

$$\begin{aligned}
 \vec{P} \cdot \vec{P} &= m_{rest}^2 \eta_{\alpha\beta} \frac{dx^\alpha}{d\tau} \frac{dx^\beta}{d\tau} \\
 &= -m_{rest}^2 \left(\frac{dt}{d\tau} \right)^2 (1 - \mathbf{v} \cdot \mathbf{v}) \\
 &= -m_{rest}^2,
 \end{aligned} \tag{1.50}$$

where $\vec{P} \cdot \vec{P}$ is confirmed to be an invariant quantity. This invariance property also applies to curved space, therefore, one may specify the following generally covariant expression:

$$\begin{aligned}
 \vec{P} \cdot \vec{P} &= m_{rest}^2 g_{\alpha\beta} \frac{dx^\alpha}{d\tau} \frac{dx^\beta}{d\tau} \\
 &= -m_{rest}^2.
 \end{aligned} \tag{1.51}$$

Given an extreme mass-ratio binary black hole system, one may use the metric of an

SBH or KBH as a reasonable approximation of $g_{\alpha\beta}$. Equation (1.51) may be used to calculate the properties of the test-particle orbit. The use of an orbiting test-particle to model the behaviour of a CO is an important approach, which will be presented in the next section and the chapters to follow.

1.5.4 Constants of Motion

The quantity m_{rest} (henceforth m) is invariant, and may be regarded as a constant of motion. But the remaining constants of motion are yet to be revealed. Consider the Lagrangian of a test-particle,

$$\mathfrak{L} = \frac{1}{2} g_{\alpha\beta} \frac{dx^\alpha}{d\tau} \frac{dx^\beta}{d\tau}. \quad (1.52)$$

It is defined in terms of the metric and velocities, where the exact solutions to the Einstein field equations (i.e. Minkowski, Schwarzschild, or Kerr) described in section 1.3.5 can be incorporated into the equation through the term $g_{\alpha\beta}$.

1.5.4.1 Case I: Flat spacetime (Minkowski)

In this case, only the derivatives of the spacetime variables are found in \mathfrak{L} since the Minkowski metric consists of constants (see equation (1.16)). Therefore, by evaluating the Euler-Lagrange equation,

$$\frac{\partial}{\partial\tau} \frac{\partial\mathfrak{L}}{\partial\dot{x}^\lambda} - \frac{\partial\mathfrak{L}}{\partial x^\lambda} = 0, \quad (1.53)$$

one finds,

$$\frac{\partial}{\partial\tau} \frac{\partial\mathfrak{L}}{\partial\dot{x}^\lambda} = 0, \quad (1.54)$$

\Rightarrow

$$\begin{aligned} \frac{\partial\mathfrak{L}}{\partial\dot{x}^\lambda} &= \text{constant} \\ &= P_\lambda, \end{aligned} \quad (1.55)$$

from which one may infer that each component of \vec{P} , that is the canonical momentum, P_λ , is a constant of motion in flat spacetime. This result is expected.

1.5.4.2 Case II: Curved spacetime due to a gravitating mass

Consider a gravitating point mass. In the most general case, the geometry of the surrounding spacetime is described by an oblate spherical symmetry that arises from the spin angular momentum of the point mass.

a) Schwarzschild ($\tilde{S} = 0$) In this special case, the resulting spacetime is spherically symmetrical and described by the Schwarzschild metric (equation (1.28)). Examination of the Schwarzschild metric reveals an explicit dependence on both \tilde{r} and θ . By virtue of the spherical symmetry, one may set $\theta = \pi/2$ (and $\dot{\theta} = 0$) without loss of generality.

By inspection, one can identify two additional constants of motion for a test-particle in orbit around the point mass: $E = -P_t$ and $L_z = P_\phi$. The first constant of motion, E , corresponds to the orbital energy of the test-particle; the second, L_z , corresponds to the z -component of orbital angular momentum. All four canonical momenta may be calculated *viz.* $\partial\mathcal{L}/\partial\dot{x}^\lambda$.

b) Kerr ($0 < \tilde{S} < 1.0$) The Kerr metric (see equation (1.29)) does not describe a spherical symmetry, therefore, θ cannot be set to $\pi/2$ without loss of generality. By inspection, the Kerr line element has the same two symmetries that were found in the Schwarzschild metric; thus, the two constants of motion, E and L_z , are easily identified. The remaining constant of motion, associated with the general case of an inclined orbit, is harder to find (Carter [76]).

Carter, in his paper of 1968 [76] performed an analysis of the Hamilton-Jacobi equation (obtained for the Kerr metric) in which he discovered a constant of motion, the Carter constant,

$$Q = \frac{\cos^2(\theta) L_z^2}{\sin^2(\theta)} + L_\theta^2 + \cos^2(\theta) S^2 (m^2 - E^2), \quad (1.56)$$

where θ is the polar angle and L_θ is the instantaneous value of the test-particle's angular momentum in the polar direction. The parameter, L_θ , is not a constant of motion.

Because GW emission causes a loss of energy and orbital angular momentum, the constants of motion (with the exception of m) are expected to change in value, which is a contradiction in terms, therefore, it is assumed that their values change by an infinitesimal amount over one orbital period.

1.6 Thesis Outline

One of the most important goals in experimental gravitation today is the detection of gravitational wave (GW) radiation [56, 58]. For this effort to succeed one requires a precise theoretical understanding of the GW emission process [59, 60, 77, 71]. In principle, by modelling the dynamics and evolution of GW radiating systems, one can improve the probability of detecting a very weak GW spectrum against a noisy background.

In this Thesis I present my studies of extreme mass-ratio binary black hole systems⁸. These systems are composed of a massive Kerr black hole (KBH), about which a much less massive compact object (CO) travels in an inspiraling orbit. In Chapter 2, an emphasis is placed on understanding the last stable orbit (LSO) of a CO travelling in an elliptical orbit on the KBH equatorial plane. In Chapter 3, the treatment of the LSO is extended to include inclined orbits; and an analysis of the Carter constant (Q) of the LSO, is performed for near-polar retrograde orbits. The novel idea of the abutment, which is the family of near-polar retrograde orbits at which Q is a maximum (for given latus rectum \tilde{l} and eccentricity e), is introduced. In Chapter 4, the abutment is used to test the consistency of the evolution equation for Q with respect to those for \tilde{l} and e .

⁸Chapters 2 and 3 correspond to two papers that have been published in Classical and Quantum Gravity (CQG) ([78] and [79]). Chapter 4 contains the manuscript of a paper, available on arXiv [80], which has also been submitted to CQG.

1.6.1 Chapter 2

The event horizon is a fundamentally important boundary when analysing the behaviour of a radially infalling test-particle; but the introduction of a bound test-particle in an orbit about a KBH gives rise to a new boundary condition, the LSO, which is encountered before the event horizon can be reached. At the LSO, the test-particle begins its plunge towards the event horizon [81, 82]. Unlike the precipitous drop of a radially infalling test-particle, the orbiting test-particle approaches the LSO gradually, in an orbit that evolves by emitting a GW energy and angular momentum flux. Further, the onset of pronounced orbital zoom and whirl behaviour is expected to impart a unique signature on the GW signal [57, 83].

A test-particle in an elliptical, equatorial orbit about a KBH was treated by calculating its effective potential. This method made it possible to investigate the properties of two constants of motion, E and L_z . Further, an analytical expression for \tilde{l} at the LSO was derived as a function of e and the normalised spin (\tilde{S}) of the KBH. This expression was confirmed by comparing analytically calculated values with those obtained by numerical techniques, and with those already published in the literature.

1.6.2 Chapter 3

The treatment of the LSO is continued, but in the case of inclined orbits about a KBH, for which the third constant of motion (Q) is greater than zero. Although an analytical expression for \tilde{l} was not derived in this case, numerical techniques yielded reliable results. Further, an analytical expression for Q at the LSO, in terms of \tilde{l} , e , and \tilde{S} , was derived. And an expression for the angle of orbital inclination, ι , to be applied to orbits in general, was derived in terms of Q , \tilde{l} , e , and \tilde{S} .

An analytical treatment of Q for the general case of elliptical, inclined orbits revealed a new feature, the abutment. The abutment describes a set of near-polar, retrograde orbits in which Q is at its maximum value for given \tilde{l} and e . An analytical expression was

derived for Q on the abutment. And this offered a mathematical method to calculate an expression for $dQ/d\tilde{l}$. It was also possible to use numerical methods to estimate an expansion formula for $d\iota/d\tilde{l}$ for application to circular orbits. Second-order behaviour of $d\iota/d\tilde{l}$ was also revealed.

1.6.3 Chapter 4

The focus of this work widened to include near-polar, retrograde orbits that were slightly elliptical. The reason for concentrating on this type of orbit is two-fold: one, the abutment is comprised of near-polar, retrograde orbits; and two, pathological behaviour is observed in the way in which polar orbits evolve [84] if the evolution of Q is ignored and set to zero [85]. In their study, Gair and Glampedakis [84], made use of higher order PN approximations and the Teukolsky formalism to improve the behaviour of the model. In this work, the abutment was used to test the consistency of the dQ/dt equations with respect to the evolution equations for $d\tilde{l}/dt$ and de/dt . Although such evolution equations were not provided in [84], the required sets of expressions were available in Barausse et al. [86] and Ganz et al. [87]. Hence an analytical comparison could be made.

A detailed analysis of the second-order behaviour of $d\iota/dt$ was also performed. Although no analytical characterisation of the relationship between the second-order behaviour and radiation back-reaction could be made at this time, the equations for $d\iota/dt$ were found to be consistent with the PN back-reaction models in the literature.

1.7 References

- [1] A. Einstein. Zur Elektrodynamik bewegter Körper. *Annalen der Physik*, 17:891, 1905. URL <http://www.fourmilab.ch/etexts/einstein/specrel/www/>.
- [2] A. Einstein. *Relativity: the Special and General Theory; translated by Robert W. Lawson*. Three Rivers Press, New York, New York, 1961.
- [3] A. Einstein. The Principle of Relativity; Original Papers by A. Einstein and H. Minkowski. Translated into English by M.N. Saha and S.N. Bose; with a historical introduction by P.C. Mahalanobis, 01 2011. URL <http://www.archive.org/details/theprincipleofre00einsuoft>.
- [4] G. Galilei. *Dialogue Concerning the Two Chief World Systems*. University of California Press Berkley, 1967.
- [5] I. Newton. *Principia Mathematica: Mathematical Principles of Natural Philosophy*. The Folio Society, London, England, 2008.
- [6] B. J. Hunt. *The Maxwellians*. Cornell University Press, 1994.
- [7] K. S. Thorne. *Black Holes and Time Warps: Einstein's outrageous legacy*. W. W. Norton and Company, Inc. New York, 1994.
- [8] H. Minkowski. Mechanics and the Relativity Postulate. In M. Janssen, J. D. Norton, J. Renn, T. Sauer, and J. Stachel, editors, *The Genesis of General Relativity*, volume 250 of *Boston Studies in the Philosophy of Science*, pages 1199–1212. Springer Netherlands, 2007.
- [9] A. Einstein. *Einstein's Essays in Science*, chapter What is the Theory of Relativity?, pages 48–52. Dover Publications Inc. Mineola, New York, 2009.
- [10] A. P. French. *Special Relativity*. Thomas Nelson and Sons Ltd, 1968.

- [11] H. Ohanian and R. Ruffini. *Gravitation and Spacetime*. W. W. Norton and Company, Inc. Fifth Avenue, New York, N. Y. 10110, 2nd edition, 1994.
- [12] J. B. Hartle. *Gravity: an introduction to Einstein's general relativity*. Addison Wesley, 2003.
- [13] C. M. Will. *Theory and Experiment in Gravitational Physics*. Cambridge University Press, 1993.
- [14] D. Kennefick. *Traveling at the Speed of Thought: Einstein and the Quest for Gravitational Waves*. Princeton University Press, Princeton, NJ USA, 2007.
- [15] H Bondi. *Relativity and Common Sense: a new approach to Einstein*. Heinemann Educational Books Ltd. London UK, 1978.
- [16] A. S. Eddington. *Report on the Relativity Theory of Gravitation*. Dover Phoenix editions. Dover Publications Inc. Mineola, New York, 2006.
- [17] A. S. Eddington. *Space, Time, and Gravitation: an outline of the General Relativity Theory*. Cambridge science classics. Cambridge, 1987. Reprint of 1920 edition.
- [18] G. F. FitzGerald. The Ether and the Earth's Atmosphere. *Science*, 13:390, 1889.
- [19] H. A. Lorentz. *The Principle of Relativity*, chapter Michelson's Interference Experiment. Dover Publications Inc. Mineola, New York, 1952.
- [20] J. Larmor. A Dynamical Theory of the Electric and Luminiferous Medium. Part III. Relations with Material Media. *Philosophical Transactions of the Royal Society of London. Series A, Containing Papers of a Mathematical or Physical Character*, 190:pp. 205–300+493, 1897. URL <http://www.jstor.org/stable/90729>.
- [21] H. A. Lorentz. *The Principle of Relativity*, chapter Electromagnetic Phenomona in a System Moving with Any Velocity Less Than Light. Dover Publications Inc. Mineola, New York, 1952.

- [22] D. J. Griffiths. *Introduction to Electrodynamics*. Addison Wesley, 3rd edition, 1999.
- [23] Electric constant, 2006. URL <http://physics.nist.gov/cgi-bin/cuu/Value?ep0>.
- [24] Magnetic constant, 2006. URL <http://physics.nist.gov/cgi-bin/cuu/Value?mu0>.
- [25] Standard metre, 1983. URL <http://physics.nist.gov/cuu/Units/current.html>.
- [26] Speed of light, 2006. URL <http://physics.nist.gov/cgi-bin/cuu/Value?c>.
- [27] W. de Sitter. Ein astronomischer Beweis für die Konstanz der Lichtgeschwindigkeit. *Physik. Zeitschr.*, 14:429, 1913.
- [28] A. Einstein. *Einstein's Essays in Science*, chapter On the Theory of Relativity, pages 48–52. Dover Publications Inc. Mineola, New York, 2009.
- [29] B. F. Schutz. *A First Course in General Relativity*. Cambridge University Press, 17 edition, 2005.
- [30] M. P. Hobson, G. Efstathiou, A. N. Lasenby, and L. H. Ford. *General Relativity: An Introduction for Physicists*. Cambridge University Press, 2007.
- [31] M. Carmeli. *Classical fields: general relativity and gauge theory*. World Scientific, 2001.
- [32] J. Weber. *General Relativity and Gravitational Waves*. Interscience Tracts on Physics and Astronomy, New York: Interscience, 1961, 1961.
- [33] J. Gribbin. *History of Western Science*. The Folio Society, London, England, 2006.
- [34] D. Truhović-Gjurić, D. Durić-Truhović, and W. G. Zimmermann. *Im Schatten Albert Einsteins*. P. Haupt, 4th edition, 1988.
- [35] S. Mittler and M. Zinke-Allmang. Private Communication, March 2011.
- [36] A. Einstein. *The Principle of Relativity*, chapter The Foundation of the General Theory of Relativity. Dover Publications Inc. Mineola, New York, 1952.

- [37] A. K. Singal. The Equivalence Principle and an Electric Charge in a Gravitational Field. *General Relativity and Gravitation*, 27(9):953–967, 1995.
- [38] A. K. Singal. The Equivalence Principle and an Electric Charge in a Gravitational Field II. A Uniformly Accelerated Charge Does Not Radiate. *General Relativity and Gravitation*, 29(11):1371–1390, 1997.
- [39] R. P. Feynman, F. B. Morinigo, and W. G. Wagner. *Feynman Lectures on Gravitation*. Westview Press, 2003.
- [40] P. G. Bergmann. *The Riddle of Gravitation*. Dover Publications Inc. New York, 1992.
- [41] A. S. Eddington. *The Mathematical Theory of Relativity*. Cambridge, 1923.
- [42] C. Bona and C. Palenzuela-Luque, editors. *Elements of Numerical Relativity*, volume 673 of *Lecture Notes in Physics*, Berlin Springer Verlag, 2005. Springer Verlag.
- [43] A. Einstein. Die Feldgleichungen der Gravitation. *Sitzungsberichte der Königlich Preußischen Akademie der Wissenschaften (Berlin)*, pages 844–847, 1915.
- [44] A. Einstein. *The Collected Papers of Albert Einstein, Volume 6: The Berlin Years: Writings, 1914-1917.*, chapter The Field Equations of Gravitation, page 117. Princeton University Press (Princeton, New Jersey), 1997.
- [45] A. Einstein. *The Collected Papers of Albert Einstein, Volume 6: The Berlin Years: Writings, 1914-1917.*, chapter Approximative Integration of the Field Equations of Gravitation. Princeton University Press (Princeton, New Jersey), 1997.
- [46] A. Einstein. Näherungsweise Integration der Feldgleichungen der Gravitation. *Sitzungsberichte der Königlich Preußischen Akademie der Wissenschaften (Berlin)*, pages 688–696, 1916.

- [47] L. Susskind and J. Lindesay. *An Introduction to Black Holes, Information and the String Theory Revolution: The Holographic Universe*. World Scientific Publishing Company, Singapore, 2005.
- [48] H. Dehmelt. A Single Atomic Particle Forever Floating at Rest in Free Space: New Value for Electron Radius. *Physica Scripta Volume T*, 22:102–110, 1988.
- [49] Gravitational constant, 2006. URL <http://physics.nist.gov/cgi-bin/cuu/Value?bg>.
- [50] M. Visser. *The Kerr Spacetime*, chapter The Kerr spacetime - a brief introduction. Cambridge University Press, 2009.
- [51] E. Poisson. *A Relativist's Toolkit: the mathematics of black-hole mechanics*. Cambridge University Press, 2004.
- [52] N. Sago, T. Tanaka, W. Hikida, K. Ganz, and H. Nakano. Adiabatic Evolution of Orbital Parameters in Kerr Spacetime. *Progress of Theoretical Physics*, 115(5): 873–907, 2006.
- [53] F. de Felice and C. J. S. Clarke. *Relativity on Curved Manifolds*. Cambridge University Press, 1990.
- [54] G. Papini and S. R. Valluri. Gravitons in Minkowski Space-time. Interactions and Results of Astrophysical Interest. *Physics Reports (Section C of Physics Letters)*, 33(2):51–125, 1977.
- [55] S. L. Detweiler. Black Holes and Gravitational Waves: Perturbation Analysis. In L. L. Smarr, editor, *Sources of gravitational radiation; Proceedings of the Workshop, Seattle, Wash., July 24-August 4, 1978*, 1979.
- [56] K. S. Thorne. *300 Years of Gravitation*, chapter Gravitational Radiation. Cambridge University Press, 1987.

- [57] K. Glampedakis and D. Kennefick. Zoom and Whirl: Eccentric equatorial orbits around spinning black holes and their evolution under gravitational radiation reaction. *Phys. Rev. D*, 66(4):044002, 2002.
- [58] F. A. Chishtie, S. R. Valluri, K. M. Rao, D. Sikorski, and T. Williams. The Analysis of Large Order Bessel Functions in Gravitational Wave Signals from Pulsars. *Inter. J. Mod. Phys. D*, 17(8):1197–1212, 2008.
- [59] P. C. Peters and J. Mathews. Gravitational Radiation from Point Masses in a Keplerian Orbit. *Phys. Rev.*, 131(1):435–440, 1963.
- [60] P. C. Peters. Gravitational Radiation and the Motion of Two Point Masses. *Phys. Rev.*, 136(4B):B1224–B1232, 1964.
- [61] É. É. Flanagan and T. Hinderer. Evolution of the Carter Constant for Inspirals into a Black Hole: Effect of the black hole quadrupole. *Phys. Rev. D*, 75(12):124007, 2007.
- [62] S. A. Hughes. Evolution of Circular, Nonequatorial Orbits of Kerr Black Holes due to Gravitational-Wave Emission. *Phys. Rev. D*, 61(8):084004, 2000.
- [63] S. Weinberg. *Gravitation and Cosmology: principles and applications of the general theory of relativity*. John Wiley and Sons Inc., 1972.
- [64] H. Asada, T. Futamase, and P. A. Hogan. *Equations of Motion in General Relativity*. Oxford University Press, 2011.
- [65] V. A. Brumberg. *Essential Relativistic Celestial Mechanics*. IOP Publishing Bristol, UK, 1991.
- [66] T. Damour. *300 Years of Gravitation*, chapter The Problem of Motion in Newtonian and Einsteinian Gravity. Cambridge University Press, 1978.

- [67] K. S. Thorne. Multipole Expansions of Gravitational Radiation. *Reviews of Modern Physics*, 52:299–339, 1980.
- [68] B. Mashhoon, F. W. Hehl, and D. S. Theiss. On the Gravitational Effects of Rotating Masses - The Thirring-Lense Papers. *General Relativity and Gravitation*, 16:711–750, 1984.
- [69] I. Ciufolini. The 1995 - 99 Measurements of the Lense-Thirring Effect Using Laser-Ranged Satellites. *Class. Quantum Grav.*, 17(12):2369–2380, 2000.
- [70] I. Ciufolini and E. C. Pavlis. A Confirmation of the General Relativistic Prediction of the Lense-Thirring Effect. *Nature*, 431:958–960, 2004.
- [71] F. D. Ryan. Effect of Gravitational Radiation Reaction on Circular Orbits Around a Spinning Black Hole. *Phys. Rev. D*, 52:3159, 1995.
- [72] F. D. Ryan. Effect of Gravitational Radiation Reaction on Nonequatorial Orbits Around a Kerr Black Hole. *Phys. Rev. D*, 53:3064–3069, 1996.
- [73] W. H. Press and S. A. Teukolsky. On the Evolution of the Secularly Unstable, Viscous Maclaurian Spheroids. *Astrophys. J.*, 181:513–518, 1973.
- [74] S. A. Teukolsky. Perturbations of a Rotating Black Hole. I. Fundamental Equations for Gravitational, Electromagnetic, and Neutrino-Field Perturbations. *Astrophys. J.*, 185:635–648, 1973.
- [75] W. H. Press and S. A. Teukolsky. Perturbations of a Rotating Black Hole. II. Dynamical Stability of the Kerr Metric. *Astrophys. J.*, 185:649–674, 1973.
- [76] B. Carter. Global Structure of the Kerr Family of Gravitational Fields. *Physical Review*, 174:1559–1571, 1968.
- [77] L. E. Kidder, C. M. Will, and A. G. Wiseman. Spin Effects in the Inspiral of Coalescing Compact Binaries. *Phys. Rev. D*, 47:4183, 1993.

- [78] P. G. Komorowski, S. R. Valluri, and M. Houde. A Study of Elliptical Last Stable Orbits About a Massive Kerr Black Hole. *Class. Quantum Grav.*, 26(8):085001, 2009.
- [79] P. G. Komorowski, S. R. Valluri, and M. Houde. The Carter Constant for Inclined Orbits About a Massive Kerr Black Hole: I. circular orbits. *Class. Quantum Grav.*, 27(22):225023, 2010.
- [80] P. G. Komorowski, S. R. Valluri, and M. Houde. The Carter Constant for Inclined Orbits About a Massive Kerr Black Hole: II. near-circular, near-polar orbits. *ArXiv e-prints*, arXiv:1101.0996v1 [gr-qc], 2011.
- [81] A. Ori and K. S. Thorne. Transition from Inspiral to Plunge for a Compact Body in a Circular Equatorial Orbit Around a Massive, Spinning Black Hole. *Phys. Rev. D*, 62(12):124022, 2000.
- [82] P. A. Sundararajan. Transition from Adiabatic Inspiral to Geodesic Plunge for a Compact Object Around a Massive Kerr Black Hole: Generic orbits. *Phys. Rev. D*, 77(12):124050, 2008.
- [83] J. Healy, J. Levin, and D. Shoemaker. Zoom-Whirl Orbits in Black Hole Binaries. *Physical Review Letters*, 103(13):131101, 2009.
- [84] J. R. Gair and K. Glampedakis. Improved Approximate Inspirals of Test Bodies into Kerr Black Holes. *Phys. Rev. D*, 73(6):064037, 2006.
- [85] K. Glampedakis, S. A. Hughes, and D. Kennefick. Approximating the Inspiral of Test Bodies into Kerr Black Holes. *Phys. Rev. D*, 66(6):064005, 2002.
- [86] E. Barausse, S. A. Hughes, and L. Rezzolla. Circular and Noncircular Nearly Horizon-Skimming Orbits in Kerr Spacetimes. *Phys. Rev. D*, 76(4):044007, 2007.

- [87] K. Ganz, W. Hikida, H. Nakano, N. Sago, and T. Tanaka. Adiabatic Evolution of Three ‘Constants’ of Motion for Greatly Inclined Orbits in Kerr Spacetime. *Progress of Theoretical Physics*, 117:1041–1066, 2007.

Chapter 2

A Study of Elliptical Last Stable Orbits About a Massive Kerr Black Hole

Abstract

The last stable orbit (LSO) of a compact object (CO) is an important boundary condition when performing numerical analysis of orbit evolution. Although the LSO is already well understood for the case where a test-particle is in an elliptical orbit around a Schwarzschild black hole (SBH) and for the case of a circular orbit about a Kerr black hole (KBH) of normalised spin, \tilde{S} ($|\mathbf{J}|/M^2$, where \mathbf{J} is the spin angular momentum of the KBH); it is worthwhile to extend our knowledge to include elliptical orbits about a KBH. This extension helps to lay the foundation for a better understanding of gravitational wave (GW) emission.

The mathematical developments described in this work sprang from the use of an effective potential (\tilde{V}) derived from the Kerr metric, which encapsulates the Lense-Thirring precession. That allowed us to develop a new form of analytical expression to calculate the LSO Radius for circular orbits (R_{LSO}) of arbitrary KBH spin. We were then able to construct a numerical method to calculate the latus rectum (\tilde{l}_{LSO}) for an elliptical LSO.

Formulae for \tilde{E}^2 (square of normalised orbital energy) and \tilde{L}^2 (square of normalised orbital angular momentum) in terms of eccentricity, e , and latus rectum, \tilde{l} , were previously developed by others for elliptical orbits around an SBH and then extended to the KBH case; we used these results to generalise our analytical \tilde{l}_{LSO} equations to elliptical orbits. LSO data calculated from our analytical equations and numerical procedures, and those previously published, are then compared and found to be in excellent agreement.

2.1 Introduction

One of the most important goals in experimental gravitation today is the detection of gravitational wave (GW) radiation [1–3]. To achieve this goal, considerable effort has been made to improve the theoretical understanding of the evolution of compact object (CO) orbits in extreme black hole systems [4–9]. In this paper, we assume a point-like test-particle since the ratio of CO mass to the mass of the massive black hole (MBH) will be small (i.e. $\leq 10^{-5}$ [10]); and the effect of the CO mass upon the post-Newtonian (PN) equations that we will use in our subsequent modelling of the CO orbits is negligible [11, 2, 4]. In this paper, we shall then assume the behaviour of the CO to be closely approximated by that of a test-particle. If reference is made to the orbital evolution of a true CO, as described by the PN evolution equations, then we will use the term, CO. The treatment of CO orbital evolution we will present in a forthcoming paper will be based on the work of [4, 5, 12, 11, 6–8, 13] in which PN equations for a rotating MBH, also called a Kerr black hole (KBH), are considered.

The objective of this study is to lay the foundation for our subsequent work that will include the numerical calculation of the GW energy emission by extreme KBH systems where the CO is in an elliptical orbit in the equatorial plane of the KBH. The most basic quadrupole model [4, 5] admitted solutions in closed form [5, 14]; but because the more comprehensive evolution equations now used are too complicated to admit an analytical solution, numerical integration of orbital parameters is required [8]. Therefore the last stable orbit (LSO) becomes an important boundary condition. Such an analysis requires an understanding of how \tilde{V} depends on \tilde{L} and on the inclination of the CO orbit. To undertake future work for inclined orbits it is important to know the minimum physically meaningful value of \tilde{L} .

Previous research has demonstrated how the effective potential (\tilde{V}) of a test-particle in an equatorial orbit around a Schwarzschild black hole (SBH) [15–17] can be calculated from the Schwarzschild metric and used to determine the latus rectum of the LSO (\tilde{l}_{LSO}).

A treatment of \tilde{V} for a KBH system, where the test-particle follows a circular LSO (section 12.7 of [18]) yields an analytical expression for the value R_{LSO} in terms of normalised spin, \tilde{S} , (equation 12.7.24 in [18], [19]) ($\tilde{S} = |\mathbf{s}|/M$ where $\mathbf{s} = \mathbf{J}/M$ and \mathbf{J} represents the spin angular momentum of the KBH). Such treatment of \tilde{V} also gives rise to expressions (equations 12.7.17 and 12.7.18 in [18]) for the orbital energy, \tilde{E} , and orbital angular momentum, \tilde{L} . In [16] the energy and orbital angular momentum equations were also derived for an SBH system with the test-particle in an elliptical orbit. In the significant work by Glampedakis and Kennefick [2], their treatment of \tilde{E} and the quantity, $(\tilde{L} - \tilde{S}\tilde{E})$, enabled us to derive generalised R_{LSO} formulae for elliptical orbits. Analytical expressions have a clear usefulness in the development of new theoretical concepts and numerical methods [10, 20].

The Lense-Thirring effect, an apodeictic [21] prediction of general relativity, is the means by which the rotation of the KBH imparts important changes on the test-particle orbit [22, 23, 21, 24] that are distinct from those associated with the SBH. The swirling of spacetime in the vicinity of the KBH applies a torsion to the orbiting test-particle; therefore, the orbit evolution will be altered, thus causing changes in the point at which the test-particle reaches its LSO. We shall develop an analytical and numerical methodology to calculate the LSO of a test-particle in elliptical orbit about a KBH. Numerical estimates of the latus rectum of the elliptical LSO orbits with respect to KBH spin are available in the literature (table I in [2], based upon the work of Schmidt [25], and table I in [10]); and they will provide a means to validate our results.

In section 2.2.1, the Kerr metric is introduced and used in section 2.2.2 as the basis of developing some essential analytical formulae to calculate the orbital angular momentum of test-particles in circular paths around a KBH (section 2.2.3). A formula for R_{LSO} (prograde and retrograde) is then developed analytically and the general formula for the \tilde{l}_{LSO} of elliptical orbits is also presented. In section 2.2.4 the development and demonstration of a numerical algorithm to determine the latus rectum and eccentricity of test-particles of higher orbital angular momentum then follows. The results of this

analysis (section 2.2.5), as well as results obtained from the general analytical formulae for LSO *latus rectum*, are compared with results obtained from the literature. In section 2.3 we shall draw conclusions.

2.2 Understanding the Last Stable Orbit About a Rotating Massive Black Hole

2.2.1 Kerr Metric

The Kerr metric (see equation 13.12 in [26]) represents the solution to the Einstein Field Equations in the case where the MBH possesses spin angular momentum,

$$g_{\alpha\beta} \Big|_{Kerr} = \begin{bmatrix} -\frac{\Delta - M^2 \tilde{S}^2 \sin^2(\theta)}{\rho^2} & 0 & 0 & -2M \frac{M^2 \tilde{S} R \sin^2(\theta)}{\rho^2} \\ 0 & \frac{\rho^2}{\Delta} & 0 & 0 \\ 0 & 0 & \rho^2 & 0 \\ -2M \frac{M^2 \tilde{S} R \sin^2(\theta)}{\rho^2} & 0 & 0 & \frac{M^4 (R^2 + \tilde{S}^2)^2 - M^2 \tilde{S}^2 \Delta \sin^2(\theta)}{\rho^2} \sin^2(\theta) \end{bmatrix}, \quad (2.1)$$

where $\rho = M \sqrt{R^2 + \cos^2(\theta) \tilde{S}^2}$ and $\Delta = M^2 (R^2 - 2R + \tilde{S}^2)$ in which the factors, $R = r/M$ and $\tilde{S} = |\mathbf{J}|/M^2$, are used to express the metric in dimensionless terms. The symmetric off-diagonal elements, $-2M^3 \tilde{S} R \sin^2(\theta) / \rho^2$, correspond to the Lense-Thirring precession that arises from the spin of a central KBH of mass, M . Observe that when, $\tilde{S} = 0$, the Kerr metric equals the Schwarzschild Metric.

Although the Schwarzschild Metric is expressed in spherical coordinates, when the central black hole rotates it is appropriate to use the Kerr metric expressed in Boyer-Lindquist (BL) coordinates. The conversion of the BL coordinate system variables to Cartesian coordinate variables is represented by these equations (see equation 11.4.7 in

[27] and see also [28]) :

$$\begin{aligned} x &= \sqrt{R_{BL}^2 + \tilde{S}^2} \sin(\theta) \cos(\phi - f), \\ y &= \sqrt{R_{BL}^2 + \tilde{S}^2} \sin(\theta) \sin(\phi - f), \\ z &= R_{BL} \cos(\theta), \end{aligned} \tag{2.2}$$

where

$$f = \pm \arctan\left(\frac{\tilde{S}}{R_{BL}}\right). \tag{2.3}$$

Because $0 \leq \tilde{S} < 1.0$, a prograde or retrograde orbit is represented by the respective use of a plus or minus sign in equation (2.3). The BL coordinate system will be used throughout this treatment. The conversion of LSO radius from BL to spherical coordinates is required whenever one performs a simulation of the evolution equations reported in [29, 7, 30, 31, 8]. This conversion is uncomplicated in the current application (in which the angle, ι , between the orbital angular momentum vector and the spin axis of the KBH is zero), and proceeds by adding the squares of x , y , and z as shown in equation (2.2) to obtain,

$$R_{Spherical}^2 = x^2 + y^2 + z^2. \tag{2.4}$$

By substituting the relationships in equation (2.2) into equation (2.4), one obtains the mathematical relationship,

$$R_{Spherical}^2 = R_{BL}^2 + \tilde{S}^2 \sin^2(\theta). \tag{2.5}$$

Recall that \tilde{S} is the normalised spin of the KBH and θ is the polar angle of the test-particle in its orbit. In this study, we work with orbits that are exclusively in the equatorial plane of the KBH. Therefore one sets $\theta = \frac{\pi}{2}$ to obtain

$$R_{Spherical}^2 = R_{BL}^2 + \tilde{S}^2. \tag{2.6}$$

Such a relationship is required for transforming LSO radii (BL coordinates) into the spherical coordinate system.

2.2.2 Effective Potential

We shall develop a formulation of the effective potential of a test-particle in orbit about a KBH. By so doing, the location of the LSO can be estimated. In the following equations and calculations the radius, R , is represented in BL coordinates. For simplicity of notation, the BL subscript will be suppressed (except in section 2.2.5.2).

The four-momentum can be expressed as:

$$P_\gamma = \left[-E, m \frac{\rho^2}{\Delta} \left(\frac{dR}{d\tau} \right), 0, mM\tilde{L} \right] \quad (2.7)$$

for a particle of mass m and,

$$P_\gamma = \left[-E, \frac{\rho^2}{\Delta} \left(\frac{dR}{d\lambda} \right), 0, L \right], \quad (2.8)$$

for zero mass, where E is the energy of the orbital element and \tilde{L} is the orbital angular momentum of the particle in orbit normalised with respect to its mass, m , and the KBH mass, M . The $(dR/d\tau)$ is the derivative of the radial component of the compact object with respect to the proper time, τ . For the zero-mass particle (which has no rest mass), L is its total linear momentum (*viz.* $L = E_{photon}/c$). The factor, $dR/d\lambda$, is the derivative of the radial component of the zero-mass particle with respect to an affine parameter, λ , which is used in place of proper time, τ , since a zero-mass particle always follows a null path.

The invariant quantity of mass-energy can be calculated for each case of a test-particle of infinitesimal mass

$$\vec{P} \cdot \vec{P} = P_\gamma P_\delta g^{\delta\gamma} \Big|_{Kerr} = -m^2, \quad (2.9)$$

and a zero-mass particle

$$\vec{P} \cdot \vec{P} = P_\gamma P_\delta g^{\delta\gamma} \Big|_{Kerr} = 0. \quad (2.10)$$

In that respect, the expected behaviour of a test mass will differ from that of a zero-mass orbital element. From these equations, the effective potential can be calculated by making a few assumptions about the path taken by the orbiting zero-mass particle. The inverse Kerr metric ($g^{\delta\gamma}$) is shown in Appendix 3.B.1 (equations (3.B2) and (3.B3)).

2.2.2.1 Test-particle

We restrict our work to the case of a test-particle of mass, m , in orbit about a KBH with $\theta = \frac{\pi}{2}$. By evaluating $\vec{P} \cdot \vec{P}$ (see equation (2.9)) using the test mass four-momentum (see equation (2.7)) one obtains,

$$\begin{aligned} \vec{P} \cdot \vec{P} &= - \left(R^4 E^2 - R^4 m^2 \left(\frac{dR}{d\tau} \right)^2 - R^2 m^2 \tilde{L}^2 + R^2 E^2 \tilde{S}^2 \right. \\ &\quad \left. + 2 R E^2 \tilde{S}^2 + 2 R m^2 \tilde{L}^2 + 4 R E \tilde{S} m \tilde{L} \right) \\ &\quad \times \left(R^4 - 2 R^3 + R^2 \tilde{S}^2 \right)^{-1} \\ &= -m^2. \end{aligned} \quad (2.11)$$

To develop a relationship between the effective potential and the orbital parameters several sequential steps must be followed. First, all terms in equation (2.11) are collected and equated to zero, then divided by m^2 ; the $(dR/d\tau)^2$ terms are then collected on the right hand side of the equation. Noting that $E/m = \tilde{E}$ represents the specific energy content of the orbiting test-particle, one then obtains,

$$\begin{aligned} &\left(R^2 \tilde{S}^2 + 2 R \tilde{S}^2 + R^4 \right) \tilde{E}^2 - \left(4 R \tilde{S} \tilde{L} \right) \tilde{E} \\ &- \left(\tilde{L}^2 R^2 - 2 \tilde{L}^2 R + R^2 \left(R^2 - 2 R + \tilde{S}^2 \right) \right) \\ &= R^4 \left(\frac{dR}{d\tau} \right)^2. \end{aligned} \quad (2.12)$$

At the points of closest (pericentre) and farthest (apocentre) approach the derivative of R with respect to τ is zero. By performing that simplification, one obtains a quadratic equation in \tilde{E} , i.e.

$$\begin{aligned}
& - \left(R^2 \tilde{S}^2 + 2R\tilde{S}^2 + R^4 \right) \tilde{E}^2 + \left(4R\tilde{S}\tilde{L} \right) \tilde{E} \\
& + \left(\tilde{L}^2 R^2 - 2\tilde{L}^2 R + R^2 \left(R^2 - 2R + \tilde{S}^2 \right) \right) \\
& = 0.
\end{aligned} \tag{2.13}$$

The factored form of equation (2.13) corresponds to the following equation [17]:

$$\left(\tilde{E} - \tilde{V}_+ \right) \left(\tilde{E} - \tilde{V}_- \right) = 0. \tag{2.14}$$

Therefore two solutions for the effective potential can be calculated:

$$\begin{aligned}
\tilde{V}_\pm &= \frac{-b \mp \sqrt{b^2 - 4ac}}{2a} \\
a &= - \left(R^4 + R^2 \tilde{S}^2 + 2\tilde{S}^2 R \right) \\
b &= 4R\tilde{S}\tilde{L} \\
c &= \left(\tilde{L}^2 R^2 - 2\tilde{L}^2 R + R^2 \left(R^2 - 2R + \tilde{S}^2 \right) \right).
\end{aligned} \tag{2.15}$$

For the SBH (i.e. $\tilde{S} = 0$), the value of \tilde{V}_\pm^2 (from equation (2.15)) becomes:

$$\tilde{V}_\pm^2 = \frac{(R - 2) \left(R^2 + \tilde{L}^2 \right)}{R^3}, \tag{2.16}$$

which depends only on the values of R and \tilde{L} , as expected (as shown in figure 2-1).

The effective potential contains important information. In the case of the SBH, the relationship between V_\pm and R describes the test-particle orbit and leads us to a calculation of the values of \tilde{L} and R at which the test-particle can no longer sustain a stable orbit. The LSO is an important characteristic of the binary system that is identified as the point at which the \tilde{V}_+ curve (figure 2-1) has a slope of zero and the second derivative

with respect to R is not positive. The effective potential, \tilde{V}_- , corresponds to particles and photons for which their orbital angular momentum has an opposite sense to the KBH spin (section 11.3 in [17]). The mathematical treatment of \tilde{V}_+ , which is presented in the sections that follow, preserves its prograde and retrograde properties; indeed, we have found that the use of \tilde{V}_- in the calculations that follow yield the same results.

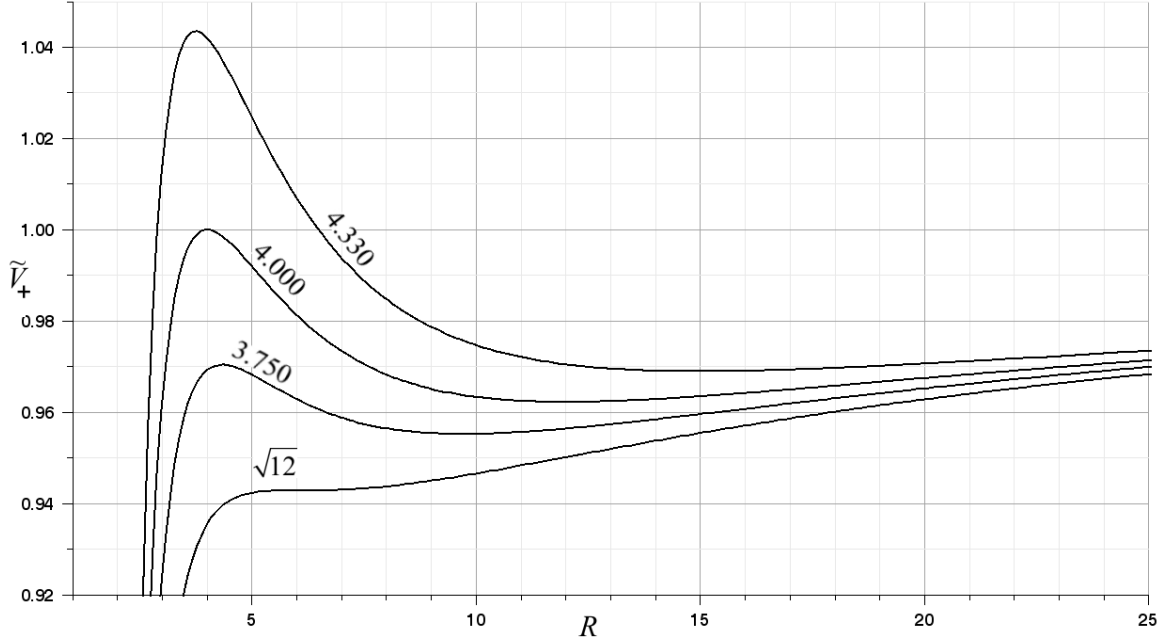


Figure 2-1: Effective Potentials for various values of \tilde{L} where $\tilde{S} = 0$.

2.2.3 Last Stable Orbit (LSO) for a CO in the Equatorial Plane of the Kerr Black Hole

The equations for the radius of a circular or elliptical LSO can be calculated through a mathematical treatment of the following two equations:

$$\frac{d\tilde{V}_+}{dR} = 0 \quad (2.17)$$

and

$$\frac{d^2\tilde{V}_+}{dR^2} \leq 0, \quad (2.18)$$

where the point of inflection (which corresponds to a circular LSO) can be found by evaluating the intersection points of equations (2.17) and (2.18).

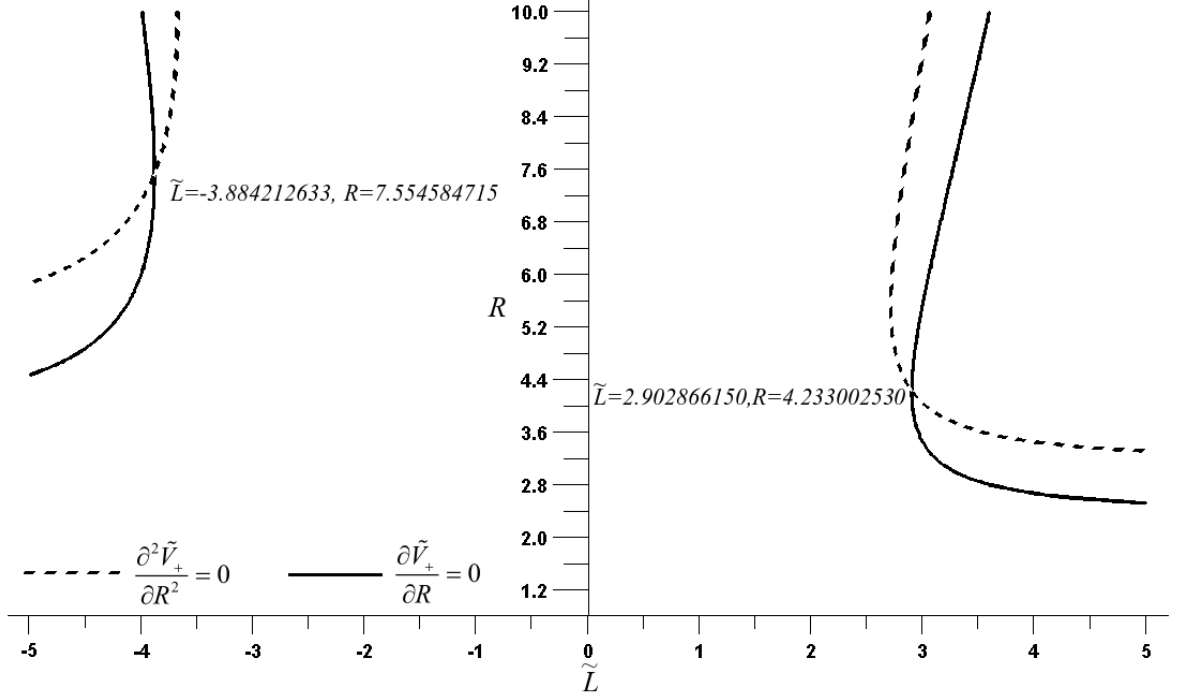


Figure 2-2: A plot of R_{LSO} vs. \tilde{L} for the first and second derivatives of \tilde{V} with respect to R .

The loci of these two equations is depicted in the (R, \tilde{L}) plane for a KBH with a spin value of $\tilde{S} = 0.5$ (see figure 2-2). Their intersection points (derived numerically with Maple 11), $[R = 7.554584715, \tilde{L} = -3.884212633]$ and $[R = 4.233002530, \tilde{L} = 2.902866150]$, correspond to the radial position of the LSO, R , of a test-particle with an orbital angular momentum of \tilde{L} . These points differ from $[R = 6.0, \tilde{L} = \pm\sqrt{12}]$, which is the solution for an SBH. The existence of an intersection point on the graphical plot notwithstanding (see figure 2-2), on frequent occasions no result was returned by Maple. On other occasions a correct value of R was returned, while the value calculated for \tilde{L} deviated by at least a factor of two from the graphical result. Such inconsistent

behaviour was attributed to the great complexity of the expressions being treated and the associated floating point round off error; therefore, an analytic method was sought.

2.2.3.1 Orbital Angular Momentum

The derivative of \tilde{V}_+ , equated to zero, can be used to determine an analytical expression for \tilde{L}^2 in terms of R and \tilde{S} for circular or elliptical orbits. From equations (2.15) and (2.17) one obtains,

$$\begin{aligned}
\frac{d\tilde{V}_+}{dR} &= \left(-3 \tilde{S}^2 R^4 \tilde{L}^2 + 6 \tilde{S}^2 R^3 \tilde{L}^2 - 2 R^2 \tilde{S}^4 \tilde{L}^2 \right. \\
&\quad + R^5 \tilde{L}^2 \tilde{S}^2 + 2 \tilde{S}^2 R^5 - 3 R^6 \tilde{S}^2 - 3 R^6 \tilde{L}^2 \\
&\quad - 3 \tilde{S}^4 R^4 - \tilde{S}^6 R^2 - 2 R \tilde{S}^6 + 8 \tilde{S}^4 R^2 - R^8 + R^7 \tilde{L}^2 \\
&\quad \left. + \left(6 R^2 \tilde{S} \tilde{L} + 2 \tilde{S}^3 \tilde{L} \right) \sqrt{R^3 \left(R^2 - 2 R + \tilde{S}^2 \right) \left(R^3 + \tilde{L}^2 R + \tilde{S}^2 R + 2 \tilde{S}^2 \right)} \right) \\
&\div \left(\sqrt{R^3 \left(R^2 - 2 R + \tilde{S}^2 \right) \left(R^3 + \tilde{L}^2 R + \tilde{S}^2 R + 2 \tilde{S}^2 \right)} \right. \\
&\quad \left. \left(R^3 + \tilde{S}^2 R + 2 \tilde{S}^2 \right)^2 \right) \\
&= 0.
\end{aligned} \tag{2.19}$$

The denominator of equation (2.19) can be disregarded because the quotient is equated to zero; it is also required that the roots of the factors present in the denominator lie outside the range of physically attainable R values. To be specific, the roots of $\left(R^2 - 2 R + \tilde{S}^2 \right)$ correspond to the event horizon for massless particles, those of R^3 are zero and beyond the LSO, and the roots of $\left(R^3 + \tilde{L}^2 R + \tilde{S}^2 R + 2 \tilde{S}^2 \right)$ and $\left(R^3 + \tilde{S}^2 R + 2 \tilde{S}^2 \right)$ are complex and thus also physically unattainable for real values of R .

The simplified power series is thus derived from the numerator of equation (2.19) after

eliminating the square root,

$$\begin{aligned}
& R^3 \left(9R - 6R^2 + R^3 - 4\tilde{S}^2 \right) \tilde{L}^4 \\
& - 2R^2 \left(-3R^4 + R^5 - 12\tilde{S}^2 R + 6R^2\tilde{S}^2 + 2R^3\tilde{S}^2 + 5\tilde{S}^4 + \tilde{S}^4 R \right) \tilde{L}^2 \\
& + \left(R^4 + 2R^2\tilde{S}^2 - 4\tilde{S}^2 R + \tilde{S}^4 \right)^2 \\
& = 0.
\end{aligned} \tag{2.20}$$

Therefore \tilde{L}^2 can be obtained directly by using the quadratic formula,

$$\tilde{L}^2 = \frac{-b \pm \sqrt{b^2 - 4ac}}{2a}, \tag{2.21}$$

where we have redefined:

$$\begin{aligned}
a &= R^3 \left(9R - 6R^2 + R^3 - 4\tilde{S}^2 \right) \\
b &= -2R^2 \left(-3R^4 + R^5 - 12\tilde{S}^2 R + 6R^2\tilde{S}^2 + 2R^3\tilde{S}^2 + 5\tilde{S}^4 + \tilde{S}^4 R \right) \\
c &= \left(R^4 + 2R^2\tilde{S}^2 - 4\tilde{S}^2 R + \tilde{S}^4 \right)^2.
\end{aligned}$$

Two solutions are found that correspond to the orbital angular momenta of a test-particle in a prograde orbit,

$$\begin{aligned}
\tilde{L}_{Pro}^2 &= \left(-3R^6 + R^7 - 12R^3\tilde{S}^2 + 6R^4\tilde{S}^2 \right. \\
&\quad \left. + 2R^5\tilde{S}^2 + 5\tilde{S}^4 R^2 + \tilde{S}^4 R^3 \right. \\
&\quad \left. - 2\tilde{S} \left(3R^2 + \tilde{S}^2 \right) \left(R^2 - 2R + \tilde{S}^2 \right) \sqrt{R^3} \right) \\
&\quad \left(R^3 \left(9R - 6R^2 + R^3 - 4\tilde{S}^2 \right) \right)^{-1},
\end{aligned} \tag{2.22}$$

and in a retrograde orbit,

$$\begin{aligned}
\tilde{L}_{Ret}^2 = & \left(-3R^6 + R^7 - 12R^3\tilde{S}^2 + 6R^4\tilde{S}^2 \right. \\
& + 2R^5\tilde{S}^2 + 5\tilde{S}^4R^2 + \tilde{S}^4R^3 \\
& + 2\tilde{S} \left(3R^2 + \tilde{S}^2 \right) \left(R^2 - 2R + \tilde{S}^2 \right) \sqrt{R^3} \Big) \\
& \left(R^3 \left(9R - 6R^2 + R^3 - 4\tilde{S}^2 \right) \right)^{-1}. \tag{2.23}
\end{aligned}$$

An analytical expression for \tilde{L}^2 with respect to R and \tilde{S} has been derived. But one must consider that the formula is limited to providing a value of \tilde{L}^2 that corresponds to a test-particle in its LSO (BL coordinates) about a KBH of spin \tilde{S} . These formulae (equations (2.22) and (2.23)) do not provide a relationship between R and \tilde{L}^2 for a general orbit.

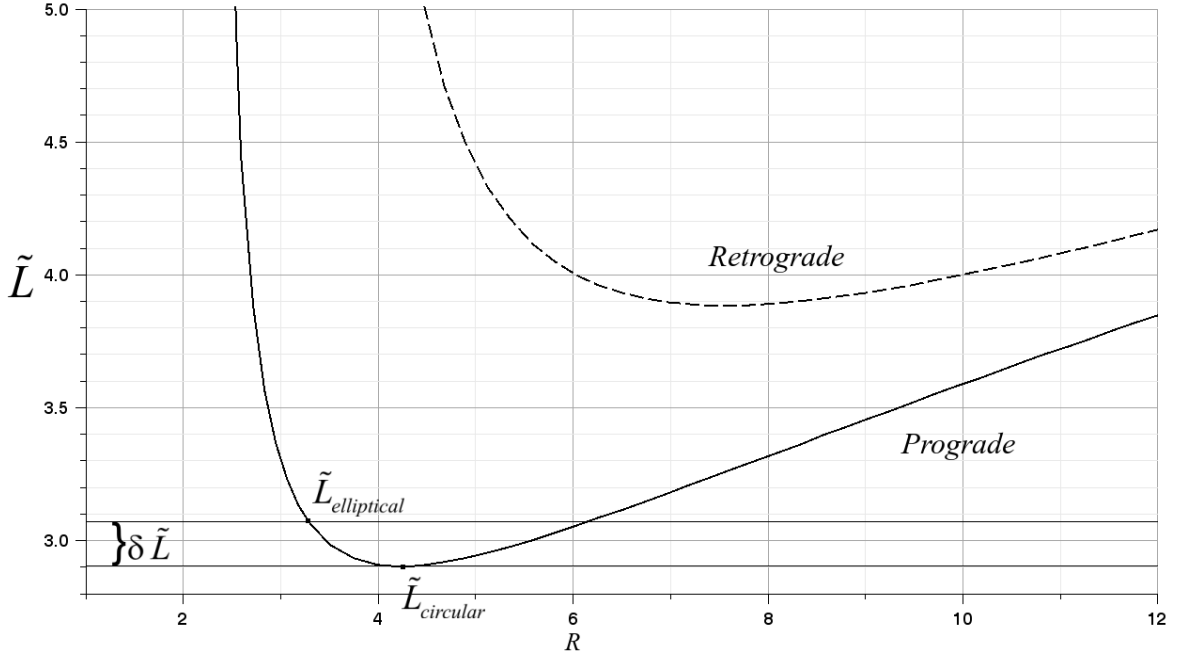


Figure 2-3: The relationship between the orbital angular momentum, \tilde{L} , and radius R for a prograde and retrograde orbit.

Consider an example where $\tilde{S} = 0.5$. The relationship between the value of \tilde{L} and the radius $R \in [1.0, 6.0]$ is plotted in figure 2-3. One observes a power series for which

the values of R and \tilde{L} for a circular orbit (at the point of inflection) occur at the local minimum. Therefore it is possible to derive an expression for the radius of the LSO, R_{LSO} , at that point of inflection for an arbitrary spin, \tilde{S} , where $0 \leq \tilde{S} < 1$.

2.2.3.2 Circular LSO Radius

The calculation of such an analytical relationship proceeds as follows. The derivative of \tilde{L}^2 with respect to R is set equal to zero. From equation (2.21) we obtain:

$$\begin{aligned} \frac{d(\tilde{L}^2)}{dR} = & \left[\tilde{S}\sqrt{R}/R \left(3R^7 - 45R^5 + 20\tilde{S}^2R^5 + 54R^4 - 26\tilde{S}^2R^4 \right. \right. \\ & \left. \left. + 9\tilde{S}^4R^3 + 24\tilde{S}^2R^3 - 26\tilde{S}^4R^2 - 54\tilde{S}^2R^2 + 53\tilde{S}^4R - 12\tilde{S}^6 \right) \right. \\ & \pm \left(R^8 - 2R^6\tilde{S}^2 - 3R^4\tilde{S}^4 - 12R^7 - 28\tilde{S}^2R^5 - 24\tilde{S}^4R^3 \right. \\ & \left. + 45R^6 + 126\tilde{S}^2R^4 + 57\tilde{S}^4R^2 + 20\tilde{S}^6 \right. \\ & \left. \left. - 54R^5 - 144\tilde{S}^2R^3 - 90\tilde{S}^4R + 108\tilde{S}^2R^2 \right) \right] \\ & \times \left[R^2 \left(-R^3 + 4\tilde{S}^2 + 6R^2 - 9R \right)^2 \right]^{-1} = 0. \end{aligned} \quad (2.24)$$

Where the plus sign corresponds to a prograde orbit and the minus sign corresponds to a retrograde orbit. The denominator contains a factor (i.e. $(-R^3 + 4\tilde{S}^2 + 6R^2 - 9R)$) with roots that correspond to the photon LSO, and a factor R^2 with roots equal to zero, which lie beyond the event horizon and are thus unattainable.

Table 2.1: A summary of the factors found in equation (2.25) for $\tilde{S} = 0.0$, 0.5 , and 1.0 .

| Factor | $\tilde{S} = 0.0$ | $\tilde{S} = 0.5$ | $\tilde{S} = 1.0$ | Comments |
|---|--|--|---|----------|
| $(\tilde{S}^2 - R^3)$ | $\begin{Bmatrix} 0 \\ 0 \\ 0 \end{Bmatrix}$ | $\begin{Bmatrix} 0.630 \\ -0.315 (1 \pm i\sqrt{3}) \end{Bmatrix}$ | $\begin{Bmatrix} 1.0 \\ -0.5 (1 \pm i\sqrt{3}) \end{Bmatrix}$ | |
| $(9\tilde{S}^4 - 28\tilde{S}^2R - 6\tilde{S}^2R^2 + 36R^2 - 12R^3 + R^4)$ | $\begin{Bmatrix} 0 \\ 0 \\ 6 \\ 6 \end{Bmatrix}$ | $\begin{Bmatrix} 0.106 \pm i0.079 \\ 4.233 \\ 7.555 \end{Bmatrix}$ | $\begin{Bmatrix} 1 \\ 1 \\ 1 \\ 9 \end{Bmatrix}$ | (a) |
| $(\tilde{S}^4 + 2\tilde{S}^2R^2 - 4\tilde{S}^2R + R^4)$ | $\begin{Bmatrix} 0 \\ 0 \\ 0 \\ 0 \end{Bmatrix}$ | $\begin{Bmatrix} 0.0646 \\ 0.804 \\ -0.434 \pm i1.007 \end{Bmatrix}$ | $\begin{Bmatrix} 0.296 \\ 1 \\ -0.648 \pm i1.721 \end{Bmatrix}$ | |
| $(R^3 - 4\tilde{S}^2 - 6R^2 + 9R)$ | $\begin{Bmatrix} 0 \\ 3 \\ 3 \end{Bmatrix}$ | $\begin{Bmatrix} 0.121 \\ 2.347 \\ 3.532 \end{Bmatrix}$ | $\begin{Bmatrix} 1 \\ 1 \\ 4 \end{Bmatrix}$ | (b) |

(a) Corresponds to radius of LSO for test-particles.
(b) Corresponds to radius of LSO for massless particles (e.g. photons or gravitons).

The simplification of the equation by taking only the numerator and eliminating the square root, can proceed to yield the following result:

$$\begin{aligned}
& R^3 \left(\tilde{S}^2 - R^3 \right) \left(9 \tilde{S}^4 - 28 \tilde{S}^2 R - 6 \tilde{S}^2 R^2 + 36 R^2 - 12 R^3 + R^4 \right) \\
& \times \left(\tilde{S}^4 + 2 \tilde{S}^2 R^2 - 4 \tilde{S}^2 R + R^4 \right) \left(R^3 - 4 \tilde{S}^2 - 6 R^2 + 9 R \right)^2 \\
& = 0.
\end{aligned} \tag{2.25}$$

Fortunately, the polynomial that expresses the relationship between \tilde{S} and R_{LSO} , is already simplified into a product of some binomials, trinomials, and quartics (see table 2.1). Each one can be assessed by considering the examples of an SBH with no spin ($\tilde{S} = 0.0$) and a KBH with $\tilde{S} = 0.5$. For the former case, the solution, $\left[R = 6.0, \tilde{L} = \sqrt{12} \right]$, is known; for the second case, it has been calculated numerically, $\left[R = 4.233002530, \tilde{L} = 2.902866150 \right]$. These cases help one to identify the relevant factor. It is interesting to observe that some of the radii in table 2.1 have complex values.

The factor that yields the values of the LSO radii (one for each of the possible prograde and retrograde orbits of the CO) is:

$$\left(9 \tilde{S}^4 - 28 \tilde{S}^2 R - 6 \tilde{S}^2 R^2 + 36 R^2 - 12 R^3 + R^4 \right) = 0. \tag{2.26}$$

This quartic equation (2.26) can be converted to a companion matrix which is solved for its eigenvalues to yield the analytical solutions for R_{LSO} for the prograde and retrograde orbits (see Appendix 2.B). These solutions are:

$$R_{pro} = 3 + \sqrt{Z} - \sqrt{\frac{16\tilde{S}^2}{\sqrt{Z}} - Z + 3 \left(3 + \tilde{S}^2 \right)} \tag{2.27}$$

and

$$R_{ret} = 3 + \sqrt{Z} + \sqrt{\frac{16\tilde{S}^2}{\sqrt{Z}} - Z + 3 \left(3 + \tilde{S}^2 \right)} \tag{2.28}$$

where:

$$Z = 3 + \tilde{S}^2 + (3 + \tilde{S}) \left((1 + \tilde{S})(1 - \tilde{S})^2 \right)^{\frac{1}{3}} + (3 - \tilde{S}) \left((1 - \tilde{S})(1 + \tilde{S})^2 \right)^{\frac{1}{3}}.$$

Although formulae that are analytically the same as ours have already been developed by Bardeen et al. [19], our formulae were derived by independent means and are simpler. The numerical results of each equation differ insignificantly over the physically valid range of $0 \leq \tilde{S} < 1.0$. And our formulae are more robust with respect to round-off error when evaluated numerically; and they are roborant of the preexisting calculations.

2.2.3.3 Orbital Energy and Angular Momentum at the LSO

One can derive new formulae for the test-particle orbital energy, \tilde{E} , and angular momentum, \tilde{L} , in terms of parameters \tilde{S} , e , and latus rectum, \tilde{l} , by using equation (2.15) as a starting point. We know that,

$$\tilde{V}_+ = \tilde{E}, \tag{2.29}$$

\Rightarrow

$$\tilde{E} = \frac{\left[2R\tilde{S}\tilde{L} + \sqrt{R \left(R^2 - 2R + \tilde{S}^2 \right) \left(R^5 + R^3\tilde{L}^2 + R^3\tilde{S}^2 + 2R^2\tilde{S}^2 \right)} \right]}{\left[R \left(R^3 + \tilde{S}^2 R + 2\tilde{S}^2 \right) \right]^{-1}} \tag{2.30}$$

when the test-particle is in its LSO. Although the roots in R are readily found by Maple, they are inordinately long and not useful. A more effective derivation method, similar to the one used in [2], shall be outlined.

By manipulating the formula in equation (2.30) we obtain:

$$R^3 - \left(\frac{2}{1 - \tilde{E}^2} \right) R^2 + \left(\frac{\tilde{L}^2 + \tilde{S}^2 - \tilde{E}^2 \tilde{S}^2}{1 - \tilde{E}^2} \right) R - \left(\frac{2 (\tilde{L} - \tilde{E} \tilde{S})^2}{1 - \tilde{E}^2} \right) = 0 \quad (2.31)$$

from which we can obtain the expressions for the sum and the product of the roots in R directly from the coefficients of the polynomial, *viz.*

$$(R - r_1)(R - r_2)(R - r_3) = 0 \quad (2.32)$$

which implies,

$$R^3 - (r_1 + r_2 + r_3) R^2 + (r_1 r_3 + r_1 r_2 + r_2 r_3) R - r_1 r_2 r_3 = 0. \quad (2.33)$$

Where $\{r_1, r_2, r_3\}$ are the roots in (2.32) and (2.33). We find the following equations for the sum of the R roots (i.e. $R_{sum} = r_1 + r_2 + r_3$):

$$R_{sum} = 2 \left(1 - \tilde{E}^2 \right)^{-1}, \quad (2.34)$$

and for their product (i.e. $R_{prod} = r_1 r_2 r_3$),

$$R_{prod} = R_{sum} \left(\tilde{L} - \tilde{E} \tilde{S} \right)^2. \quad (2.35)$$

The corresponding formulae for \tilde{E} and \tilde{L} are as follows:

$$\tilde{E} = \pm \frac{\sqrt{R_{sum} (R_{sum} - 2)}}{R_{sum}}, \quad (2.36)$$

and,

$$\tilde{L} = \frac{\sqrt{R_{sum} (R_{sum} - 2)} \tilde{S} \pm \sqrt{R_{sum} R_{prod}}}{R_{sum}}. \quad (2.37)$$

For the LSO, the roots, $\{r_1, r_3\}$, correspond to the LSO radius; therefore, we make the

following substitutions:

$$r_1 = r_3 = R_{Min} = \frac{\tilde{l}}{1+e}, \quad (2.38)$$

and

$$r_2 = R_{Max} = \frac{\tilde{l}}{1-e}, \quad (2.39)$$

where \tilde{l} is the latus rectum of the elliptical LSO. We can now set:

$$\begin{aligned} R_{sum} &= 2R_{Min} + R_{Max} \\ &= 2\frac{\tilde{l}}{1+e} + \frac{\tilde{l}}{1-e} \end{aligned} \quad (2.40)$$

and

$$\begin{aligned} R_{Prod} &= \frac{R_{Min}^2 R_{Max}}{\tilde{l}^3} \\ &= \frac{1}{(1+e)^2 (1-e)}. \end{aligned} \quad (2.41)$$

By substituting equations (2.40) and (2.41) into equations (2.36) and (2.37) the following formulae are obtained:

$$\tilde{E}^2 = 1 - 2(1-e^2) \left(\tilde{l}(3-e) \right)^{-1} \quad (2.42)$$

and,

$$\tilde{L}^2 = \left(\tilde{S}\tilde{E} \pm \tilde{l} \sqrt{\frac{1}{(1+e)(3-e)}} \right)^2 \quad (2.43)$$

\Rightarrow

$$\left(\tilde{L} - \tilde{S}\tilde{E} \right)^2 (1+e)(3-e) = \tilde{l}^2. \quad (2.44)$$

They express the square of the orbital energy and the orbital angular momentum in terms of the eccentricity, e , and latus rectum, \tilde{l} , of a test-particle in its LSO about a KBH of spin, \tilde{S} . In equation (2.43), the prograde orbit takes the minus sign and the retrograde orbit takes the plus sign. The modified form of equation (2.43) shown in equation (2.44)

corresponds to equation (23) in [2].

Similar equations derived by Cutler, Kennefick, and Poisson [16],

$$\tilde{E}^2 = \left((\tilde{l} - 2(1+e))(\tilde{l} - 2(1-e)) \right) \tilde{l}^{-1} (\tilde{l} - 3 - e^2)^{-1} \quad (2.45)$$

and

$$\tilde{L}^2 = \tilde{l}^2 (\tilde{l} - 3 - e^2)^{-1}, \quad (2.46)$$

are only valid for SBH systems. Equation (2.43) reduces to equation (2.46) when $\tilde{S} = 0$ and the relationship $\tilde{l} = 6 + 2e$ is used.

Glampedakis and Kennefick [2] present a similar treatment which has the advantage of yielding more general results since it is not assumed that the test-particle has reached the LSO (i.e. $r_1 > r_3$). Therefore

$$r_3 = 2 \left(\tilde{L} - \tilde{S}\tilde{E} \right)^2 (1 - e^2) \left[\tilde{l}^2 \left(1 - \tilde{E}^2 \right) \right]^{-1}, \quad (2.47)$$

with, $r_1 = R_{Min}$ and $r_2 = R_{Max}$, as before. Their formula for energy,

$$\tilde{E} = \sqrt{1 - \tilde{l}^{-1} (1 - e^2) \left\{ 1 - \tilde{l}^{-2} \left(\tilde{L} - \tilde{S}\tilde{E} \right)^2 (1 - e^2) \right\}}, \quad (2.48)$$

proves to be ideal for generalising our formulae for circular LSOs, R_{LSO} , to one for elliptical orbits, \tilde{l}_{LSO} (See Appendix 2.C).

2.2.3.4 Elliptical LSO Radius

The evaluation of $X^2 = \left(\tilde{L} - \tilde{S}\tilde{E} \right)^2$ in [2] provides a means to extend equations (2.27) and (2.28) beyond their use with circular LSOs to more general elliptical LSOs by direct substitution of X^2 into equation (2.44). Although a leading order Taylor expansion (see equation (24) in [2]) is available from a slow rotation approximation of equation (2.44) (i.e. $\tilde{S} \approx 0$), we present our analytical results.

The general form of the \tilde{l}_{LSO} equations for elliptical orbits are:

$$\begin{aligned} \tilde{l}_{pro} &= (3 + e) + \sqrt{Z_o} \\ &- \sqrt{16 \frac{\tilde{S}^2 (1 + e)}{\sqrt{Z_o}} - Z_o + (3 + e)^2 + \tilde{S}^2 (1 + e) (3 - e)} \end{aligned} \quad (2.49)$$

and

$$\begin{aligned} \tilde{l}_{ret} &= (3 + e) + \sqrt{Z_o} \\ &+ \sqrt{16 \frac{\tilde{S}^2 (1 + e)}{\sqrt{Z_o}} - Z_o + (3 + e)^2 + \tilde{S}^2 (1 + e) (3 - e)} \end{aligned} \quad (2.50)$$

where:

$$\begin{aligned} Z_o &= 1/3 \tilde{S}^2 (1 + e) (3 - e) + 1/3 (3 + e)^2 \\ &+ 1/3 \frac{\tilde{S}^4 (1 + e)^2 (3 - e)^2 - 2 \tilde{S}^2 (3 + e) (1 + e) (e^2 + 15) + (3 + e)^4}{(Z_i)^{(\frac{1}{3})}} \\ &+ 1/3 (Z_i)^{\frac{1}{3}}, \end{aligned}$$

$$\begin{aligned} Z_i &= (3 + e)^6 \\ &+ \tilde{S}^2 (1 + e) \left(\tilde{S}^2 (1 + e) \left(\tilde{S}^2 (1 + e) (3 - e)^3 + 3e^4 + 18e^2 + 459 \right) - 3 (e^2 + 15) (3 + e)^3 \right) \\ &+ 24 \sqrt{3} \sqrt{Z_{ii}}, \end{aligned}$$

and

$$Z_{ii} = (1 + e)^4 \tilde{S}^6 \left(1 - \tilde{S}^2 \right) \left((1 - e) (e + 3)^3 - \tilde{S}^2 (1 + e) (3 - e)^3 \right).$$

As required, equations (2.49) and (2.50) reduce to equations (2.27) and (2.28) when $e = 0$. By setting $\tilde{S} = 0$, both equations reduce to $\tilde{l} = 6 + 2e$. And in the extreme cases, where $\tilde{S} = 1$ (retrograde and prograde), equation (2.49) reduces to $\tilde{l} = 1 + e$ and equation (2.50) reduces to $5 + e + 4\sqrt{1 + e}$, as required. A detailed treatment of equations (2.49)

and (2.50) will be outlined in a forthcoming paper.

2.2.4 Calculating the LSO Properties

2.2.4.1 Introduction

The elements have now been found to perform general calculations of the LSO for arbitrary values of KBH spin, \tilde{S} , orbital angular momentum, \tilde{L} , and total energy, \tilde{E} . Although we have analytical formulae that give us \tilde{l}_{LSO} for general elliptical orbits, it is important to construct and outline our methodology in preparation for future work on test-particle orbits that are inclined with respect to the equatorial plane of the KBH. We must quantify the relationship between the value of \tilde{L} for the test-particle orbit and the shape of its effective potential surface.

Here we outline, in detail, our numerical method for calculating the latus rectum, \tilde{l} , and eccentricity, e , of LSO orbits. These values will help us to appraise the usefulness of our new, generalised \tilde{l}_{LSO} equations in (2.49) and (2.50).

2.2.4.2 Algorithm

For clarity, an example where $\tilde{S} = 0.5$ and the test-particle is in a prograde orbit is demonstrated. In table 2.2, the calculations for a retrograde orbit, and an SBH are included for comparison.

Such an algorithm proceeds as follows:

Specify the KBH spin - A given problem will most likely have a prior specification of a fixed value of \tilde{S} , where $0 \leq \tilde{S} < 1$ for either a prograde or retrograde orbit (if a retrograde orbit is used, *(ret)*, will follow the value assigned to \tilde{S}). In this example we shall use $\tilde{S} = 0.5$ and a prograde orbit since it has already been used in the calculation of R_{LSO} and \tilde{L} for prograde and retrograde LSOs previously in this paper (see 2.2.3 and figure 2-2). Similar calculations were performed for the $\tilde{S} = 0.5(\text{ret})$ case, and for an SBH (See table 2.2).

Table 2.2: LSO parameters calculated for both circular and elliptical orbits where $\tilde{S} = 0.5$ (*ret*), 0.0, and 0.5 to four decimal places; these values may be carried to greater precision.

| KBH Spin (\tilde{S}) | Circular Orbit | | | | Elliptical Orbit | | |
|--------------------------|-------------------|---------|---------|------------|-------------------|----------|---------|
| | 0.5(<i>ret</i>) | 0.00 | +0.5 | | 0.5(<i>ret</i>) | 0.00 | +0.5 |
| $\delta\tilde{L}$ | | 0.00 | | | | 0.01 | |
| R_{LSO} | 7.5546 | 6.0000 | 4.2330 | R_{\min} | 7.3576 | 5.8317 | 4.1033 |
| \tilde{L}^2 | 15.0871 | 12.0000 | 8.4266 | | 15.0971 | 12.0100 | 8.4266 |
| \tilde{E}_{LSO} | 0.9728 | 0.9428 | 0.9179 | | 0.9549 | 0.9429 | 0.9181 |
| R_{\max} | 7.5546 | 6.0000 | 4.2330 | | 7.9806 | 6.3675 | 4.5210 |
| A_{BL} | 7.5546 | 6.0000 | 4.2330 | | 7.66912 | 6.0996 | 4.31215 |
| e_{BL} | 0.0000 | 0.0000 | 0.0000 | | 0.04062 | 0.04392 | 0.0484 |
| \tilde{l}_{BL} | 7.5546 | 6.0000 | 4.2330 | | 7.6565 | 6.0880 | 4.3020 |
| W_{BL} | 0.04935 | 0.06804 | 0.10856 | | 0.04822 | 0.06638 | 0.10577 |
| $A_{spherical}$ | 7.57111 | 6.0000 | 4.2624 | | 7.68512 | 6.09960 | 4.34110 |
| $e_{spherical}$ | 0.0000 | 0.0000 | 0.0000 | | 0.04045 | 0.0439 | 0.0478 |
| $\tilde{l}_{spherical}$ | 7.57111 | 6.0000 | 4.26243 | | 7.67284 | 6.087834 | 4.3312 |
| $W_{spherical}$ | 0.04919 | 0.06804 | 0.10753 | | 0.04806 | 0.06638 | 0.10477 |

We use either equation (2.27) for a prograde orbit or equation (2.28) for a retrograde orbit to directly calculate R_{LSO} (BL coordinates) thus,

$$\tilde{S} = 0.5 \Rightarrow R_{LSO} = 4.23300, \quad (2.51)$$

which gives us the LSO radius of a circular orbit, R_{LSO} .

Find \tilde{L} - The values of \tilde{S} and R_{LSO} can now be used to calculate the value of \tilde{L}^2 assuming the LSO is at a point of inflection (i.e. a circular orbit) *viz.* equations (2.22) or (2.23) depending on the direction of the orbit. The result for $\tilde{S} = 0.5$ and $R_{LSO} = 4.23300$ is found to be,

$$\tilde{L}^2 = 8.4266319. \quad (2.52)$$

This value is necessarily a positive quantity, hence the need to ensure that the correct prograde or retrograde orbital angular momentum equation has been used.

Calculate \tilde{E} - Because the values of \tilde{S} , R_{LSO} , and \tilde{L} are known at the point of inflection, we can use \tilde{V}_+ (see equation (2.15)) to directly calculate the energy, \tilde{E} , of the test-particle in a circular orbit, i.e.

$$\tilde{E} = 0.91788201. \quad (2.53)$$

The value of $\tilde{E} < 1.0$, hence the orbit is bound. Whenever $\tilde{E} \geq 1.0$, the orbit is not bound.

Expand to include elliptical orbits - By careful examination of figure 2-3 one sees that the local minimum of \tilde{L} corresponds to the case where the LSO is circular; the values of R_{LSO} and the radius of the local minimum of the potential, \tilde{V}_+ , (figure 2-1) coincide, as expected. The angular momentum, \tilde{L} , that corresponds to an elliptical LSO is then higher than that for a circular LSO.

The algorithm shall be broadened to include the case of an elliptical orbit. For the orbit to be elliptical, the orbital angular momentum, ($\tilde{L} = \sqrt{\tilde{L}^2} \Rightarrow \tilde{L} = \sqrt{8.4266319}$) must be increased by an arbitrary factor $\delta\tilde{L}$ (where $\delta\tilde{L} > 0$, see figure 2-3); the slight increase in \tilde{L} above its minimum value changes the LSO from a circular orbit, to one that is elliptical. Accordingly the value of \tilde{E} will increase and the value of R_{Min} will be reduced. A similar treatment of elliptical orbits, based upon increments of \tilde{L} , can be found in [10].

Find R_{Min} for the elliptical orbit - By working with a larger value of orbital angular momentum in the form ($\tilde{L}_{Elliptical} = \tilde{L}_{Circular} + \delta\tilde{L}$) we can calculate the value of R_{Min} without requiring the new value of the orbital energy, \tilde{E} (see figure 2-3). If $\delta\tilde{L} = 0.01$, then $\tilde{L} = 2.904588078$; therefore, (*viz.* equations (2.22) or (2.23)) the new value of R_{Min} can be calculated numerically to yield:

$$R_{Min} = 4.10329200. \quad (2.54)$$

Correspondingly, the total orbital energy can be calculated (*viz.* equation (2.15)):

$$\tilde{E}_{LSO}^{Elliptical} = 0.9180746, \quad (2.55)$$

cf.,

$$\tilde{E}_{LSO}^{Circular} = 0.91788201. \quad (2.56)$$

As required: $\tilde{E}_{LSO}^{Elliptical} > \tilde{E}_{LSO}^{Circular}$.

Find the maximum radius for an elliptical orbit - In calculating a data set, the various values of $\delta\tilde{L}$ are selected and the corresponding values of e and \tilde{l} are found. Now that the value of $\tilde{E}_{LSO}^{Elliptical}$ is known, the maximum radius of the elliptical orbit (R_{Max}) can be calculated numerically, *viz.* $\tilde{V}_+ = \tilde{E}_{LSO}^{Elliptical}$, because the effective potential of the test-particle has the same value at R_{Min} and R_{Max} . The result is:

$$R_{Max} = 4.520999771. \quad (2.57)$$

Determine the elliptical orbit parameters - We now have the information necessary to calculate the latus rectum, \tilde{l} , and the eccentricity, e , of the orbit. The dimensionless semi-major axis, A , of the elliptical orbit can be calculated from the values of R_{LSO} and R_{Max} :

$$\begin{aligned} A &= \frac{(R_{Min} + R_{Max})}{2}, \\ &= 4.3121. \end{aligned} \quad (2.58)$$

$$\begin{aligned} e &= 1 - \frac{R_{Min}}{A}, \\ &= 0.0484. \end{aligned} \quad (2.59)$$

The latus rectum, \tilde{l} , may now be calculated,

$$\begin{aligned}\tilde{l} &= A(1 - e^2), \\ &= 4.3020.\end{aligned}\tag{2.60}$$

Note: the values of A , \tilde{l} , R_{LSO} (for circular LSO), R_{Min} and R_{Max} are expressed in terms of BL coordinates.

2.2.4.3 Calculation of the normalised orbital frequency

According to the relativistic form of Kepler's third law (see problem 17.4 in [32] or exercise 12.7 in [18]), the orbital period of a closed orbit, P , can be expressed in terms of the semi-major axis of the orbit, a , and the mass, M of the central body about which the test-particle orbits. This equation applies to elliptical orbits in general. If the orbit is subject to precession, then the value, ν , represents the orbital frequency of the test-particle in an open orbit. Hence,

$$P = 2\pi \left| \frac{a^{3/2} \pm |\mathbf{s}| \sqrt{M}}{\sqrt{M}} \right|,\tag{2.61}$$

where $\mathbf{s} = \mathbf{J}/M$; and the plus sign corresponds to the prograde orbit and the minus sign corresponds to the retrograde orbit. The corresponding orbital frequency is:

$$\nu = P^{-1};\tag{2.62}$$

therefore,

$$\nu = \frac{1}{2\pi} \left| \frac{\sqrt{M}}{\left(a^{3/2} \pm |\mathbf{s}| \sqrt{M} \right)} \right|,\tag{2.63}$$

which leads to,

$$\begin{aligned} W &= 2\pi M\nu \\ &= \left| \frac{M^{3/2}}{\left(a^{3/2} \pm |\mathbf{s}| \sqrt{M}\right)} \right|, \end{aligned} \quad (2.64)$$

(in equation (2.64) the parameter, a , refers to the length of the semi-major axis). When variables normalised with respect to the KBH mass, M , are used:

$$A = \frac{a}{M}, \quad (2.65)$$

and

$$\tilde{S} = |\mathbf{s}|/M; \quad (2.66)$$

one obtains,

$$W = \left| \frac{1}{A^{3/2} \pm \tilde{S}} \right|. \quad (2.67)$$

If equation (2.60) is then used to represent equation (2.67) in terms of the dimensionless latus rectum, \tilde{l} :

$$W = \left| (1 - e^2)^{\frac{3}{2}} / \left(\tilde{l}^{\frac{3}{2}} \pm \tilde{S} (1 - e^2)^{\frac{3}{2}} \right) \right|. \quad (2.68)$$

2.2.5 Calculations

2.2.5.1 LSO and orbit characteristics

Three methods were used to calculate \tilde{l}_{LSO} for orbits of various eccentricity ($0 \leq e \leq 1.0$) and KBH spin ($\tilde{S} = 0.5, 0.99$; prograde and retrograde). The values obtained here are shown alongside those found in the literature [10, 2] in tables 2.3 and 2.4. The \tilde{l}_{LSO} values we obtained by following the algorithm described in 2.2.4.2 are listed in the Numerical column. The general formulae described in 2.2.3.4 were used to generate the values in the Analytical column. A third method was used to numerically estimate the \tilde{l}_{LSO} values

directly from the companion matrix (Appendix 2.C) by first substituting the \tilde{S} and e values into the matrix before calculating its eigenvalues.

The agreement between our various calculation methods, and with the results published previously in [10, 2] is excellent (i.e. error $< 0.1\%$). Therefore the algorithmic method we have outlined in 2.2.4.2 may be considered reliable. And the use of the companion matrix (see Appendices 2.B and 2.C) in performing numerical calculations of the LSO parameters has been successfully demonstrated.

Table 2.3: Retrograde LSO data from [10, 2] and results calculated using the numerical and analytical methods presented in this work (our results were rounded off to four decimal places).

| e | Ret. Limit $\tilde{l} = 5 + e$ $+4\sqrt{1+e}$ | \tilde{l} for $\tilde{S} = 0.99$ (ret.) | | | | \tilde{l} for $\tilde{S} = 0.5$ (ret.) | | | | $\tilde{l} = 6 + 2e$ | |
|-----|---|---|-----------|------------|---------------------|--|------------|---------------------|-----------|----------------------|------------|
| | | [2] *[10] | Numerical | Analytical | Companion Matrix | Numerical | Analytical | Companion Matrix | Numerical | | Analytical |
| 0.0 | 9.0000 | 8.972* | 8.9719 | 8.9719 | 8.9719 | 8.9719 | 8.9719 | 7.5549 | 7.5546 | 7.5546 | 6.00 |
| 0.1 | 9.2952 | 9.266 | 9.2662 | 9.2662 | 9.2662 | 9.2662 | 9.2662 | 7.8040 | 7.8039 | 7.8039 | 6.20 |
| 0.2 | 9.5818 | 9.552 | 9.5519 | 9.5519 | 9.5519 | 9.5519 | 9.5519 | 8.0489 | 8.0488 | 8.0488 | 6.40 |
| 0.3 | 9.8607 | 9.83 | 9.8301 | 9.8301 | 9.8301 | 9.8301 | 9.8301 | 8.2922 | 8.2899 | 8.2899 | 6.60 |
| 0.4 | 10.1329 | 10.102 | 10.1017 | 10.1016 | 10.1016 | 10.1016 | 10.1016 | 8.5275 | 8.5274 | 8.5275 | 6.80 |
| 0.5 | 10.3990 | 10.367 | 10.3671 | 10.3671 | 10.3671 | 10.3671 | 10.3671 | 8.7620 | 8.7620 | 8.7620 | 7.00 |
| 0.6 | 10.6596 | 10.627 | 10.6272 | 10.6272 | 10.6272 | 10.6272 | 10.6272 | 8.9940 | 8.9939 | 8.9939 | 7.20 |
| 0.7 | 10.9154 | 10.882 | 10.8824 | 10.8824 | 10.8824 | 10.8824 | 10.8824 | 9.2233 | 9.2233 | 9.2233 | 7.40 |
| 0.8 | 11.1666 | 11.133 | 11.1332 | 11.1332 | 11.1332 | 11.1332 | 11.1332 | 9.4506 | 9.4505 | 9.4505 | 7.60 |
| 0.9 | 11.4136 | 11.38 | 11.3798 | 11.3798 | 11.3798 | 11.3798 | 11.3798 | 9.6756 | 9.6756 | 9.6756 | 7.80 |
| 1.0 | 11.6569 | 11.623 | 11.6226 | 11.6227 | 11.6227 | 11.6227 | 11.6227 | 9.8988 | 9.8990 | 9.8990 | 8.00 |

Table 2.4: Prograde LSO data from [10, 2] and results calculated using the numerical and analytical methods presented in this work (our results were rounded off to four decimal places).

| e | $\tilde{l} =$ $6 + 2e$ | \tilde{l} for $\tilde{S} = 0.5$ | | | | \tilde{l} for $\tilde{S} = 0.99$ | | | | Pro. Limit $\tilde{l} =$ $1 + e$ |
|-----|---------------------------|-----------------------------------|-----------|------------|---------------------|------------------------------------|-----------|------------|---------------------|--|
| | | $\frac{[2]}{*[10]}$ | Numerical | Analytical | Companion Matrix | $\frac{[2]}{*[10]}$ | Numerical | Analytical | Companion Matrix | |
| 0.0 | 6.00 | 4.233* | 4.2330 | 4.2330 | 4.2330 | 1.454* | 1.4545 | 1.4545 | 1.4545 | 1.00 |
| 0.1 | 6.20 | 4.377 | 4.3769 | 4.3769 | 4.3769 | 1.516 | 1.5156 | 1.5156 | 1.5156 | 1.10 |
| 0.2 | 6.40 | 4.526 | 4.5259 | 4.5259 | 4.5259 | 1.595 | 1.5950 | 1.5950 | 1.5950 | 1.20 |
| 0.3 | 6.60 | 4.679 | 4.6792 | 4.6792 | 4.6792 | 1.685 | 1.6852 | 1.6852 | 1.6852 | 1.30 |
| 0.4 | 6.80 | 4.836 | 4.8360 | 4.8360 | 4.8360 | 1.782 | 1.7822 | 1.7822 | 1.7822 | 1.40 |
| 0.5 | 7.00 | 4.996 | 4.9959 | 4.9959 | 4.9959 | 1.883 | 1.8835 | 1.8835 | 1.8835 | 1.50 |
| 0.6 | 7.20 | 5.158 | 5.1584 | 5.1584 | 5.1584 | 1.988 | 1.9876 | 1.9876 | 1.9876 | 1.60 |
| 0.7 | 7.40 | 5.323 | 5.3232 | 5.3233 | 5.3232 | 2.094 | 2.0954 | 2.0939 | 2.0939 | 1.70 |
| 0.8 | 7.60 | 5.49 | 5.4899 | 5.4901 | 5.4900 | 2.201 | 2.2016 | 2.2016 | 2.2016 | 1.80 |
| 0.9 | 7.80 | 5.658 | 5.6584 | 5.6586 | 5.6584 | 2.31 | 2.3104 | 2.3104 | 2.3104 | 1.90 |
| 1.0 | 8.00 | 5.828 | 5.8284 | 5.8287 | 5.8284 | 2.42 | 2.4199 | 2.4200 | 2.4200 | 2.00 |

2.2.5.2 Conversion from the BL to the spherical coordinate system

The foregoing analysis was performed in the BL coordinate system in which we suppressed the use of the, BL, subscript. To apply these estimates of the LSO parameters in the problem of setting the boundary conditions needed in modelling the evolution equations, it is necessary to convert them to the spherical coordinate system. We shall describe this conversion process, and state the appropriate caveats.

Equation (2.6) provides the means to convert any radial distance on an elliptical orbit (that lies in the equatorial plane of the KBH) expressed in BL coordinates into a radial distance in spherical (or cylindrical) coordinates. But one cannot proceed precipitously; an elliptical orbit in the BL coordinate system, will be only a good approximation of an ellipse once expressed in the spherical coordinate system. In addition, careful consideration must be given to the values of ϕ in their respective coordinate systems as there will be some important differences that will demand a more profound understanding and a more cautious interpretation.

Consider the case of a test-particle in an elliptical orbit about a KBH. The absence of the parameter, ϕ , from equation (2.6) notwithstanding; the angle,

$$\phi_{spherical} = \phi_{BL} \mp \arctan \left(\frac{\tilde{S}}{R_{BL}} \right) \quad (2.69)$$

viz. equations (2.2) and (2.3), will force the points on the orbit that correspond to $R_{Min(spherical)}$, $R_{Max(spherical)}$, and the position of the MBH at the focus of the ellipse, to be no longer collinear. Therefore the use of the values of $R_{Min(spherical)}$ and $R_{Max(spherical)}$ to calculate $e_{spherical}$ (*viz.* equation (2.59)) is potentially a source of error, especially for KBHs of large spin.

We calculate:

$$R_{Min(spherical)} = \sqrt{R_{Min(BL)}^2 + \tilde{S}^2} \quad (2.70)$$

and

$$R_{Max(spherical)} = \sqrt{R_{Max(BL)}^2 + \tilde{S}^2}. \quad (2.71)$$

These two values are used to calculate the semi-major axis:

$$A_{Spherical} = \frac{R_{Min(spherical)} + R_{Max(spherical)}}{2}, \quad (2.72)$$

from which one can obtain

$$e_{spherical} = 1 - \frac{R_{Min(spherical)}}{A_{LSO(spherical)}}. \quad (2.73)$$

The latus rectum can be calculated using,

$$\tilde{l}_{spherical} = A_{spherical} (1 - e_{spherical}^2), \quad (2.74)$$

which is analogous to equation (2.60). The orbital frequency, $W_{spherical}$, is obtained from equation (2.67). The values of these parameters expressed in spherical coordinates are reported in table 2.2.

The behaviour of $\phi_{spherical}$ is not part of this study; but further investigation will be undertaken since an understanding of $\phi_{spherical}$ is essential for properly characterising the zoom and whirl of the test-particle in its orbit. A diagrammatic comparison of test-particle orbits in the BL and spherical coordinate systems is shown in figures 2-6 and 2-7 for a KBH of spins of $\tilde{S} = 0.5$ and $\tilde{S} = 0.99$ respectively. The orbit parameters are taken from tables 2.3 and 2.4 for $e = 0.7$. One can view the shift in the value of $\phi_{spherical}$ as arising from the Lense-Thirring precession [33]; the orbit has a shape that can be approximated as an ellipse that is precessing. The orbit diagrams shown in figures 2-6 and 2-7 exclude this orbital precession.

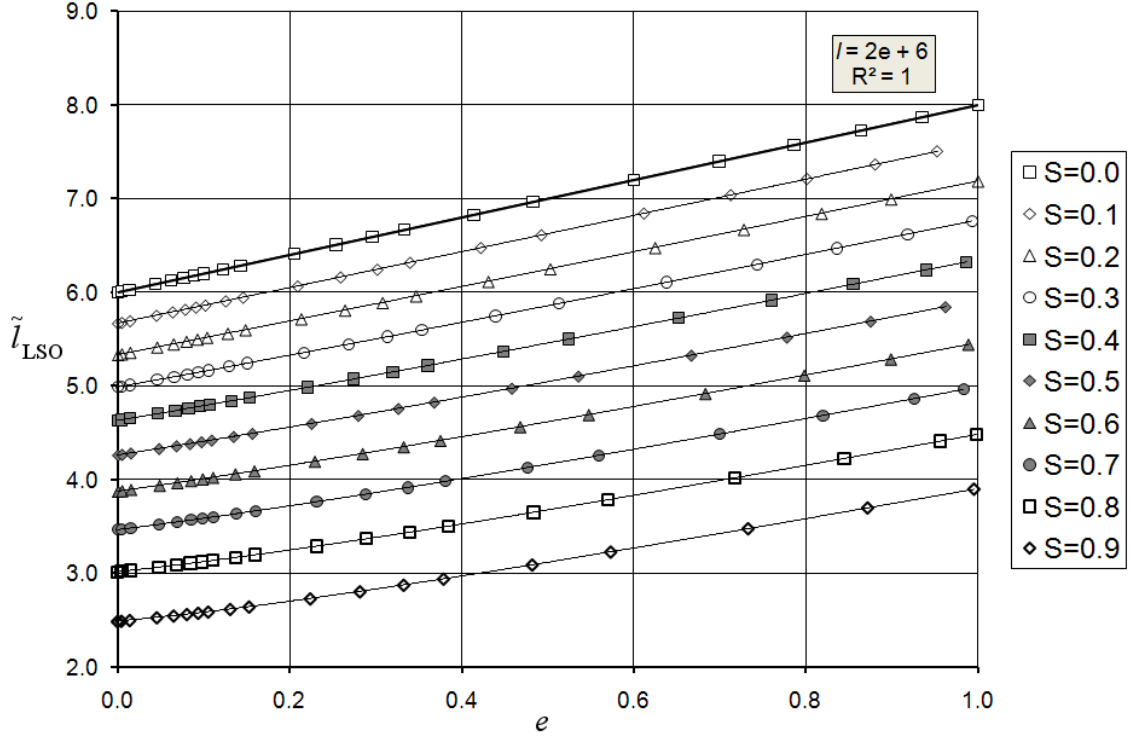


Figure 2-4: The LSO latus rectum, \tilde{l} , calculated for KBH systems in which the test-particle is in a prograde orbit.

2.2.5.3 LSO formulae

The LSO formulae we seek will be used in future work to calculate the test-particle orbital frequency, W , in terms of the eccentricity of the orbit, e , and KBH spin, \tilde{S} . One such relationship is already known for the SBH, i.e.

$$\tilde{l} = 6 + 2e \quad (2.75)$$

[16, 8]. But we require additional formulae for KBH systems of various values of spin, and for the prograde and retrograde orbits. To this end, the algorithm outlined in section 2.2.4.2 was used to calculate a sequence of latus rectum values, \tilde{l} , for LSOs of differing eccentricity, e , in spherical coordinates. These results are plotted in figures 2-4 and 2-5, for prograde and retrograde orbits respectively, and each set was fit to a sixth order

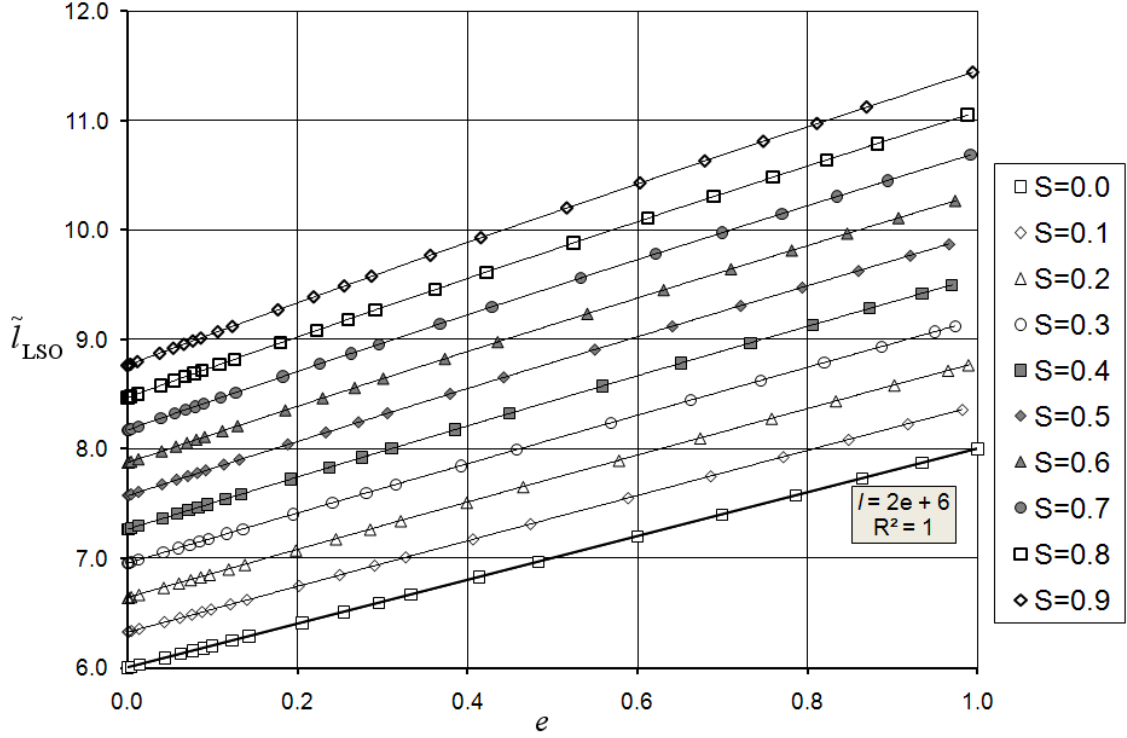
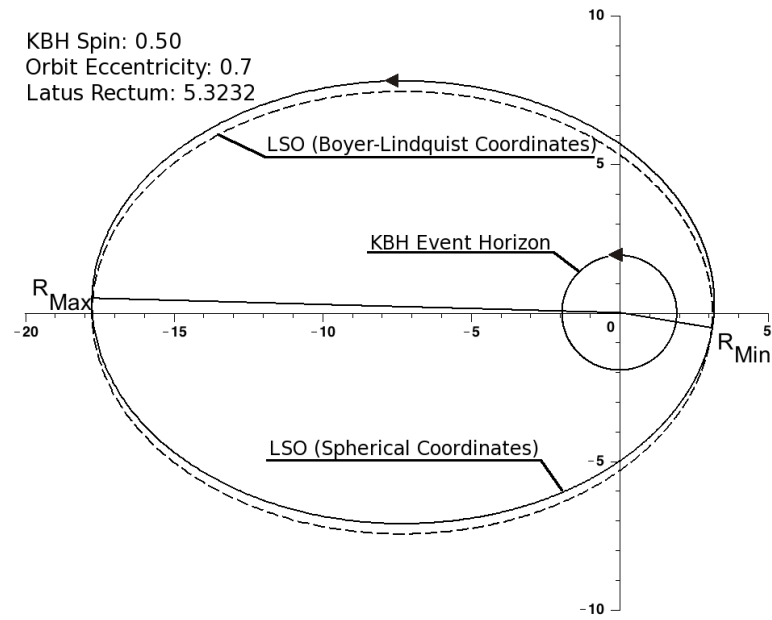


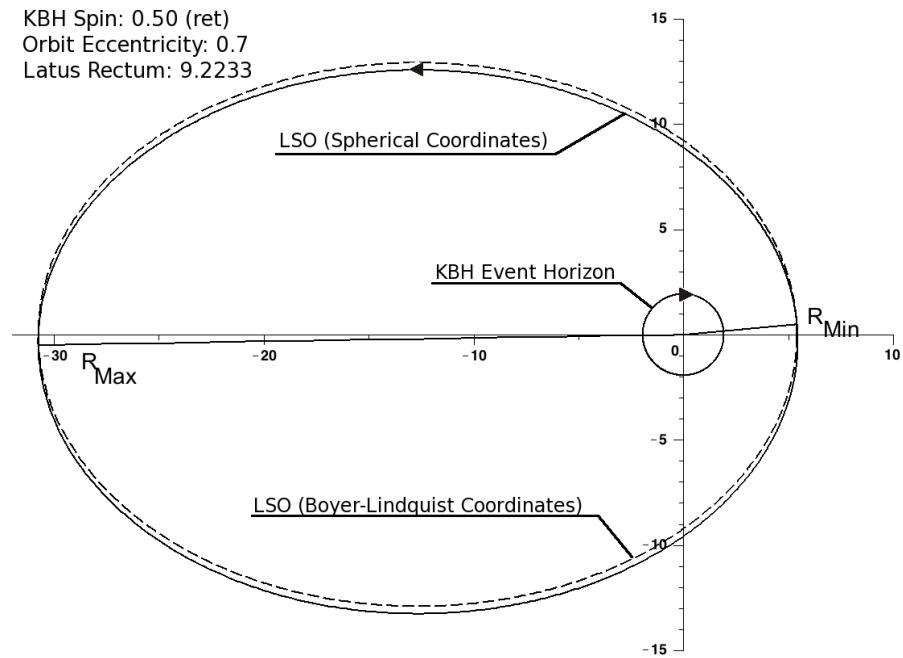
Figure 2-5: The LSO latus rectum, \tilde{l} , calculated for KBH systems in which the test-particle is in a retrograde orbit.

polynomial equation of the form, $\tilde{l} = \sum c_k e^k$, where c_k corresponds to the coefficients to be calculated (see tables 2.5 and 2.6). The result for the SBH system is shown in each of the two figures where the least squares fit yielded a linear result, $\tilde{l} = 6.00 + 2.00 e$, which is consistent with equation (2.75). Such agreement is noteworthy because the least squares fit, based upon results previously known through the analytical and numerical analysis described in section 2.2.4.2, corroborate the LSO relationship for the SBH.

The linear approximations obtained for the KBH systems were used to calculate the LSO radii which are essential for determining the point at which an inspiraling CO will plunge. Although the data point pairs, (e, \tilde{l}) , derived for a particular spin became slightly nonlinear with increasing spin, the square of the correlation coefficient equals 1.

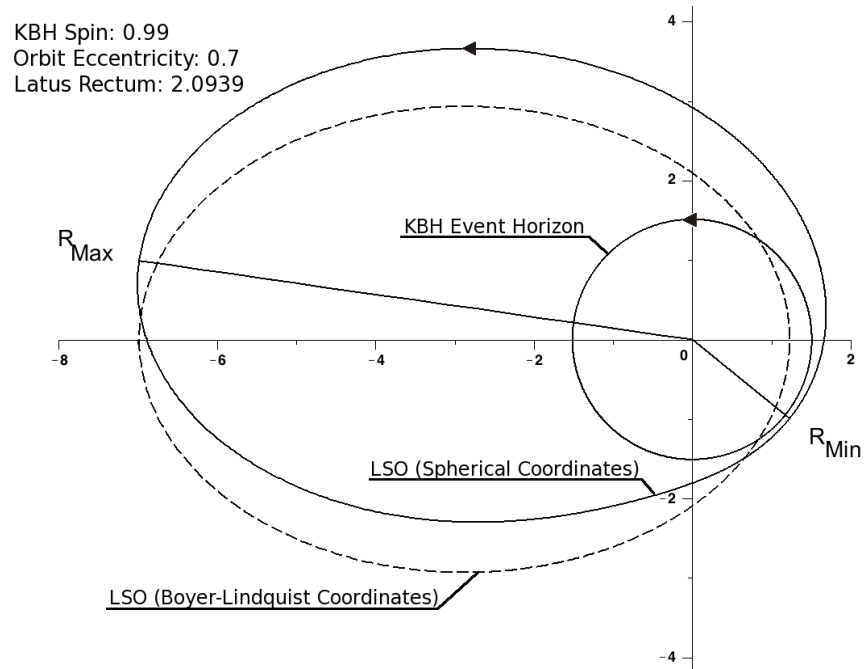


(a) Prograde

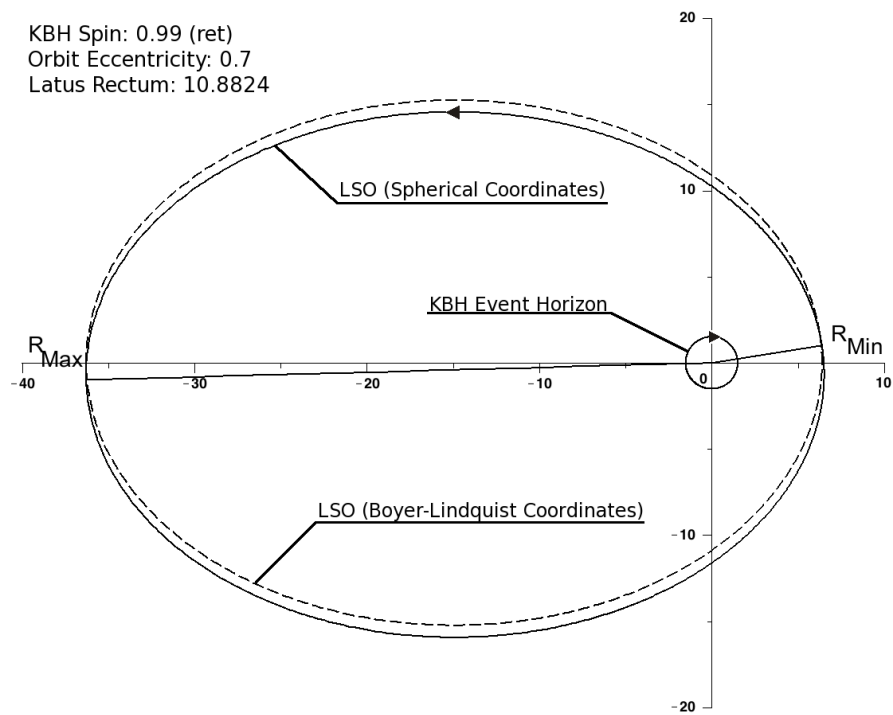


(b) Retrograde

Figure 2-6: A comparison of orbits in BL and spherical coordinates for a KBH of spin, $\tilde{S} = 0.5$ (prograde and retrograde). The view is taken from above the KBH equatorial plane. Orbital precession is not included.



(a) Prograde



(b) Retrograde

Figure 2-7: A comparison of orbits in BL and spherical coordinates for a KBH of spin, $\tilde{S} = 0.99$ (prograde and retrograde). The view is taken from above the KBH equatorial plane. Orbital precession is not included.

Table 2.5: Results of polynomial fit applied to the retrograde numerical data plotted in figure 2-5.

| BH Spin \tilde{S} | Linear formula for \tilde{l} | | | | | | Higher order elements | | | | | |
|---------------------|--------------------------------|------------|-------------|------------|-------------|-------------|-----------------------|-------|-------|-------|----------|----------|
| | e^0 | e^1 | e^2 | e^3 | e^4 | e^5 | e^6 | e^7 | e^8 | e^9 | e^{10} | e^{11} |
| 0.9 (ret) | 8.76368819 | 2.92119702 | 0.33453310 | 0.16602960 | -0.09065641 | 0.03831375 | | | | | | |
| 0.8 (ret) | 8.46962456 | 2.82317780 | 0.30786011 | 0.15360882 | -0.08371386 | 0.03530157 | | | | | | |
| 0.7 (ret) | 8.17299740 | 2.72430368 | -0.27924670 | 0.14009690 | -0.07604155 | 0.03187198 | | | | | | |
| 0.6 (ret) | 7.87358073 | 2.62450180 | -0.24852313 | 0.12560249 | -0.06816165 | 0.02862914 | | | | | | |
| 0.4 (ret) | 7.26528803 | 2.42174450 | -0.17955312 | 0.09226403 | -0.04980520 | 0.02082535 | | | | | | |
| 0.3 (ret) | 6.95574501 | 2.31856739 | -0.14063185 | 0.07298940 | -0.03924209 | 0.01633534 | | | | | | |
| 0.2 (ret) | 6.64205200 | 2.21400672 | -0.09814800 | 0.05147560 | -0.02743187 | 0.011263294 | | | | | | |
| 0.1 (ret) | 6.32368545 | 2.10788976 | -0.05153641 | 0.02741063 | -0.01455267 | 0.005952846 | | | | | | |
| 0.0* | 6.0 | 2.00000040 | -0.00000483 | 0.00001992 | -0.00003693 | 0.000031685 | 0.00193952 | | | | | |

*Consistent with [16]; the nonlinear elements for $\tilde{S} = 0.0$ were probably caused by round-off error.

Table 2.6: Results of polynomial fit applied to the prograde numerical data plotted in figure 2-4.

| BH Spin \tilde{S} | Linear formula for \tilde{l} | | | | | | Higher order elements | | | | | |
|---------------------|--------------------------------|-------------|-------------|---------------|-------------|--------------|-----------------------|-------|-------|-------|----------|----------|
| | e^0 | e^1 | e^2 | e^3 | e^4 | e^5 | e^6 | e^7 | e^8 | e^9 | e^{10} | e^{11} |
| 0.0* | 6.0 | 2.00000040 | -0.00000483 | 0.00001992 | -0.00003693 | 0.000031685 | 0.00193952 | | | | | |
| 0.1 | 5.67018444 | 1.89006614 | 0.05750384 | -0.03176865 | 0.01680801 | -0.006864538 | | | | | | |
| 0.3 | 4.98764730 | 1.66256737 | 0.19655943 | -0.1141250883 | 0.05877986 | -0.022595600 | 0.00446315 | | | | | |
| 0.4 | 4.63164012 | 1.54390266 | 0.28322003 | -0.1707514543 | 0.08749217 | -0.032784703 | | | | | | |
| 0.5 | 4.26243011 | 1.42082938 | 0.38722646 | -0.2455511898 | 0.126235551 | -0.046174540 | | | | | | |
| 0.6 | 3.87579316 | 1.29193960 | 0.51696785 | -0.350625042 | 0.181780713 | -0.063577889 | | | | | | |
| 0.7 | 3.46458090 | 1.15481823 | 0.68958146 | -0.516713627 | 0.279766279 | -0.096357483 | | | | | | |
| 0.8 | 3.01472694 | 1.004702210 | 0.94648977 | -0.8316991247 | 0.505649851 | -0.187007189 | | | | | | |
| 0.9 | 2.48927662 | 0.829143989 | 1.43455997 | -1.6864540901 | 1.335128043 | -0.627997923 | 0.13242755 | | | | | |

*Consistent with [16]; the nonlinear elements for $\tilde{S} = 0.0$ were probably caused by round-off error.

2.3 Conclusions

A knowledge of the relationship between the latus rectum, \tilde{l} , of a last stable orbit (LSO) and the Kerr black hole (KBH) spin, \tilde{S} , where $\tilde{S} = |\mathbf{J}|/M^2$, is essential for the calculation of the compact object (CO) orbit evolution in extreme black hole systems, and thus the gravitational wave energy emission. The Kerr metric provides the basis for the derivation of analytical relationships between orbital angular momentum squared (\tilde{L}^2) and the apogee of the last stable orbit (R_{Min}) for the prograde and retrograde elliptical orbits of test-particles about a KBH. These formulae lead directly to new and simplified representations of R_{LSO} with respect to KBH spin for circular orbits, which in turn are used as a starting point in performing numerical analysis of elliptical LSOs. By using the prograde and retrograde relationships between the values of \tilde{L}^2 and R_{Min} that we have derived from the effective potential, an elliptical LSO can be analysed numerically to yield values for R_{Min} . The algorithm provides a foundation that will be generalised to include inclined orbits for which the effective potential is more complicated than that for the case where the orbit lies in the equatorial plane of the KBH. Therefore finding the relationship between R_{Min} and orbital angular momentum becomes paramount as it allow for the methodical treatment of orbits of successively greater eccentricity and orbital angular momentum.

Formulae for orbital energy, \tilde{E} , and the quantity, $(\tilde{L} - \tilde{S}\tilde{E})$, have led us to the derivation of analytical expressions for \tilde{l} in terms of \tilde{S} and orbit eccentricity. The LSO values obtained by using these formulae were in excellent agreement with those in the literature, therefore, demonstrating their validity. The usefulness of these analytical expressions may be found in the advantage gained in future theoretical and numerical investigations. These equations and the others we have derived here also demonstrate the importance of using parameters that are normalised with respect to the KBH mass, M .

The values of R_{Min} and R_{Max} , in Boyer-Lindquist (BL) coordinates, must be trans-

formed to spherical coordinates. The $\tilde{l}_{LSO(spherical)}$ and LSO eccentricity ($e_{Spherical}$) can then be estimated and used in the integration of the post-Newtonian orbital evolution equations. Because we can now calculate analytically the $e_{Spherical}$ and $\tilde{l}_{LSO(spherical)}$ values for a range of KBH spins, ($0 \leq \tilde{S} < 1$; retrograde and prograde), it would facilitate the modelling of CO orbit evolution about a massive KBH.

The companion matrix (CM) has been shown to be of great use in finding the roots of complicated polynomials in an analytical form. The use of the CM in numerical work is also encouraging, especially because one can perform various linear operations on the CM in order to transform the final results.

Further investigation will be performed using the results of this work as a foundation. The methodologies that underlie our numerical algorithm will be extended to the case of inclined orbits. The radial frequency behaviour will also be treated by performing analytical integration of the radial path of the test-particle between the orbit pericentre and apocentre. The post-Newtonian evolution equations that describe the inspiral of COs in extreme binary black hole systems will then be modelled.

Appendix 2.A The Kerr metric and its Inverse

$$g_{\alpha\beta} \Big|_{Kerr} = \begin{bmatrix} -\frac{\Delta - M^2 \tilde{S}^2 \sin^2(\theta)}{\rho^2} & 0 & 0 & -2M \frac{M^2 \tilde{S} R \sin^2(\theta)}{\rho^2} \\ 0 & \frac{\rho^2}{\Delta} & 0 & 0 \\ 0 & 0 & \rho^2 & 0 \\ -2M \frac{M^2 \tilde{S} R \sin^2(\theta)}{\rho^2} & 0 & 0 & \frac{M^4 (R^2 + \tilde{S}^2)^2 - M^2 \tilde{S}^2 \Delta \sin^2(\theta)}{\rho^2} \sin^2(\theta) \end{bmatrix}, \quad (2.A1)$$

The inverse Kerr metric expressed in the Boyer-Lindquist coordinate system. To simplify the presentation of the metric, we define the parameter:

$$\Sigma = \rho^2 = M^2 (R^2 + \tilde{S}^2 \cos^2(\theta)).$$

The inverse Kerr metric is:

$$g^{\delta\gamma} \Big|_{Kerr} = (\Sigma)^{-1} \begin{bmatrix} -\frac{\Sigma(R^2 + \tilde{S}^2) + 2\tilde{S}^2 R - 2\cos^2(\theta)\tilde{S}^2 R}{(R^2 - 2R + \tilde{S}^2)} & 0 & 0 & -2\frac{\tilde{S}R}{M(R^2 - 2R + \tilde{S}^2)} \\ 0 & \Delta & 0 & 0 \\ 0 & 0 & 1 & 0 \\ -2\frac{\tilde{S}R}{M(R^2 - 2R + \tilde{S}^2)} & 0 & 0 & \frac{R^2 - 2R + \tilde{S}^2 \cos^2(\theta)}{(R^2 - 2R + \tilde{S}^2)\sin^2(\theta)} \end{bmatrix}. \quad (2.A2)$$

For equatorial orbits, $\theta = \frac{\pi}{2}$, therefore, the inverse Kerr metric simplifies to the form:

$$g^{\delta\gamma} \Big|_{Kerr} = \begin{bmatrix} -\frac{R^4 + R^2 \tilde{S}^2 + 2\tilde{S}^2 R}{(R^2 - 2R + \tilde{S}^2)R^2} & 0 & 0 & -2\frac{\tilde{S}}{M(R^2 - 2R + \tilde{S}^2)R} \\ 0 & \frac{R^2 - 2R + \tilde{S}^2}{R^2} & 0 & 0 \\ 0 & 0 & \frac{1}{M^2 R^2} & 0 \\ -2\frac{\tilde{S}}{M(R^2 - 2R + \tilde{S}^2)R} & 0 & 0 & \frac{R^2 - 2R}{(R^2 - 2R + \tilde{S}^2)M^2 R^2} \end{bmatrix}. \quad (2.A3)$$

The determinant of the Kerr metric was calculated to be, $Det = -\Sigma^2 \sin^2(\theta)$.

Appendix 2.B Use of the Companion Matrix to Solve a Quartic Equation

Given the task of finding the roots of a polynomial, ($p(R) = 0$), one might proceed by regarding it to be the characteristic polynomial of a matrix for which the eigenvalues are sought (i.e. the companion matrix) (see chapter 7 in [34]).

$$\begin{aligned} p(R) &= \left(R^4 - 12 R^3 - 6 \tilde{S}^2 R^2 + 36 R^2 - 28 \tilde{S}^2 R + 9 \tilde{S}^4 \right) \\ &= 0. \end{aligned} \tag{2.B1}$$

The creation of said matrix proceeds trivially to produce the companion matrix, M (see section 7.4.6 in [34]):

$$M = \begin{bmatrix} 0 & 0 & 0 & -9 \tilde{S}^4 \\ 1 & 0 & 0 & 28 \tilde{S}^2 \\ 0 & 1 & 0 & 6 \tilde{S}^2 - 36 \\ 0 & 0 & 1 & 12 \end{bmatrix}, \tag{2.B2}$$

from which one may calculate the eigenvalues. These eigenvalues represent the solutions of equation (2.B1). There are four solutions, which are (in simplified form):

$$R = 3 \pm \sqrt{Z} \pm \sqrt{\frac{16 \tilde{S}^2}{\sqrt{Z}} - Z + 3(3 + \tilde{S}^2)} \tag{2.B3}$$

where

$$\begin{aligned}
Z &= 3 + \tilde{S}^2 \\
&+ (3 + \tilde{S}) \left((1 + \tilde{S}) (1 - \tilde{S})^2 \right)^{\frac{1}{3}} \\
&+ (3 - \tilde{S}) \left((1 - \tilde{S}) (1 + \tilde{S})^2 \right)^{\frac{1}{3}}
\end{aligned} \tag{2.B4}$$

We know by evaluating the solutions at $\tilde{S} = 0$ (the Schwarzschild case) which two of the four solutions ought to be retained. They are:

$$R = 3 + \sqrt{Z} \pm \sqrt{\frac{16\tilde{S}^2}{\sqrt{Z}} - Z + 3(3 + \tilde{S}^2)}. \tag{2.B5}$$

Appendix 2.C Use of the Companion Matrix to Find the Analytical Solution for \tilde{l}_{LSO} for a General Elliptical Orbit

Treatment of the orbital energy, \tilde{E} , and the quantity, $(X = \tilde{L} - \tilde{S}\tilde{E})$, leads to an analytical expression for the latus rectum, \tilde{l} , of the last stable orbit (LSO) of a test-particle. An analytical form of \tilde{E} (see [2]) is:

$$\tilde{E} = \sqrt{1 - (1 - e^2) \left(1 - \frac{X^2(1 - e^2)}{\tilde{l}^2} \right)} \tilde{l}^{-1}. \tag{2.C1}$$

In Appendix A of [2] the term X^2 has been calculated to be,

$$X^2 = \frac{-n \mp \sqrt{d}}{2f}, \tag{2.C2}$$

for which the negative sign corresponds to a prograde orbit and the positive sign corresponds to a retrograde orbit. The functions in equation (2.C2) are:

$$f = \frac{\tilde{l}(\tilde{l} - 3 - e^2)^2 - 4\tilde{S}^2(1 - e)^2(1 + e)^2}{\tilde{l}^3} \quad (2.C3)$$

and

$$n = -2 \frac{\tilde{l}(\tilde{l} - 3 - e^2) + \tilde{S}^2(\tilde{l} + 1 + 3e^2)}{\tilde{l}}; \quad (2.C4)$$

and the discriminator ($d = n^2 - 4fc$):

$$d = \frac{16\tilde{S}^2}{\tilde{l}^3} \left(\tilde{l}(\tilde{l} - 2 - 2e) + \tilde{S}^2(1 + e)^2 \right) \left(\tilde{l}(\tilde{l} - 2 + 2e) + \tilde{S}^2(1 - e)^2 \right) \quad (2.C5)$$

where

$$c = \left(\tilde{l} - \tilde{S}^2 \right)^2. \quad (2.C6)$$

The analytical relationship between \tilde{l}_{LSO} of the LSO orbit and \tilde{S} and e can be found by solving either of the following equalities:

$$X_{Prograde}^2(1 + e)(3 - e) = \tilde{l}^2 \quad (2.C7)$$

and

$$X_{Retrograde}^2(1 + e)(3 - e) = \tilde{l}^2. \quad (2.C8)$$

By manipulating either of the equations (2.C7) or (2.C8) and removing the square root, one obtains the characteristic polynomial:

$$\begin{aligned} p(\tilde{l}) &= \tilde{l}^4 + (-4e - 12)\tilde{l}^3 \\ &\quad + \left(-4\tilde{S}^2e + 2\tilde{S}^2e^2 - 6\tilde{S}^2 + 4e^2 + 24e + 36 \right) \tilde{l}^2 \\ &\quad - 4\tilde{S}^2(1 + e)(e^2 + 7)\tilde{l} + (1 + e)^2(-3 + e)^2\tilde{S}^4 \\ &= 0. \end{aligned} \quad (2.C9)$$

Converting the characteristic polynomial (equation (2.C9)) into a companion matrix yields (see section 7.4.6 in [34]):

$$M = \begin{bmatrix} 0 & 0 & 0 & -\tilde{S}^4 (1+e)^2 (3-e)^2 \\ 1 & 0 & 0 & 4\tilde{S}^2 (1+e) (e^2+7) \\ 0 & 1 & 0 & -2\tilde{S}^2 e^2 + 4e\tilde{S}^2 + 6\tilde{S}^2 - 4e^2 - 24e - 36 \\ 0 & 0 & 1 & 4(3+e) \end{bmatrix}. \quad (2.C10)$$

The eigenvalues of equation (2.C10) can be evaluated analytically and they correspond to the roots of equation (2.C9). Two of those roots correspond to the latus rectum (\tilde{l}) of each of the prograde and retrograde test-particle orbits. One can also substitute the KBH spin, \tilde{S} , and the eccentricity of the orbit, e , into the companion matrix and then calculate its eigenvalues to numerically calculate the values of \tilde{l} .

The analytical form of the eigenvalues is complicated; but a factorised form is presented here to illustrate how the solutions for \tilde{l} were identified. The four eigenvalues, λ_i ($i = 1..4$), are:

$$\begin{aligned} \lambda_i &= (3+e) \pm \sqrt{Z_o} \\ &\pm \sqrt{16 \frac{\tilde{S}^2 (1+e)}{\sqrt{Z_o}} - Z_o + (3+e)^2 + \tilde{S}^2 (1+e) (3-e)}. \end{aligned} \quad (2.C11)$$

By following the same reasoning as in Appendix 2.B, we know that the solutions sought will each correspond to $6+2e$ when $\tilde{S} = 0$. In that case, $Z_o = (3+e)^2$, therefore, equation (2.C11) simplifies to:

$$\lambda_i = (3+e) \pm (3+e) \pm (0). \quad (2.C12)$$

Therefore two of the eigenvalues, where $\lambda_i = 0$, are excluded.

2.4 References

- [1] K. S. Thorne. *300 Years of Gravitation*, chapter Gravitational Radiation. Cambridge University Press, 1987.
- [2] K. Glampedakis and D. Kennefick. Zoom and Whirl: Eccentric equatorial orbits around spinning black holes and their evolution under gravitational radiation reaction. *Phys. Rev. D*, 66(4):044002, 2002.
- [3] F. A. Chishtie, S. R. Valluri, K. M. Rao, D. Sikorski, and T. Williams. The Analysis of Large Order Bessel Functions in Gravitational Wave Signals from Pulsars. *Inter. J. Mod. Phys. D*, 17(8):1197–1212, 2008.
- [4] P. C. Peters and J. Mathews. Gravitational Radiation from Point Masses in a Keplerian Orbit. *Phys. Rev.*, 131(1):435–440, 1963.
- [5] P. C. Peters. Gravitational Radiation and the Motion of Two Point Masses. *Phys. Rev.*, 136(4B):B1224–B1232, 1964.
- [6] L. S. Finn. Detection, Measurement, and Gravitational Radiation. *Phys. Rev. D*, 46:5236–5249, 1992.
- [7] F. D. Ryan. Effect of Gravitational Radiation Reaction on Circular Orbits Around a Spinning Black Hole. *Phys. Rev. D*, 52:3159, 1995.
- [8] L. Barack and C. Cutler. Lisa Capture Sources: Approximate waveforms, signal-to-noise ratios, and parameter estimation accuracy. *Phys. Rev. D*, 69:082005, 2004.
- [9] É. É. Flanagan and T. Hinderer. Evolution of the Carter Constant for Inspirals into a Black Hole: Effect of the black hole quadrupole. *Phys. Rev. D*, 75(12):124007, 2007.

- [10] A. Ori and K. S. Thorne. Transition from Inspiral to Plunge for a Compact Body in a Circular Equatorial Orbit Around a Massive, Spinning Black Hole. *Phys. Rev. D*, 62(12):124022, 2000.
- [11] W. Junker and G. Schaefer. Binary Systems - Higher Order Gravitational Radiation Damping and Wave Emission. *Mon. Not. R. astr. Soc.*, 254:146–164, 1992.
- [12] V. A. Brumberg. *Essential Relativistic Celestial Mechanics*. IOP Publishing Bristol, UK, 1991.
- [13] S. A. Hughes, S. Drasco, É. É. Flanagan, and J. Franklin. Gravitational Radiation Reaction and Inspiral Waveforms in the Adiabatic Limit. *Physical Review Letters*, 94(22):221101, 2005.
- [14] V. Pierro and I. M. Pinto. Exact Solution of Peters-Mathews Equations for any Orbital Eccentricity. *Nuovo Cimento B Serie*, 111(5):631–644, 1996.
- [15] S. Chandrasekhar. *The Mathematical Theory of Black Holes*. Oxford University Press, 1983.
- [16] C Cutler, D. Kennefick, and E Poisson. Gravitational Radiation Reaction for Bound Motion Around a Schwarzschild Black Hole. *Phys. Rev. D*, 50(6):3816–3835, 1994.
- [17] B. F. Schutz. *A First Course in General Relativity*. Cambridge University Press, 17 edition, 2005.
- [18] S. L. Shapiro and S. A. Teukolsky. *Black Holes, White Dwarfs, and Neutron Stars: The physics of compact objects*. Wiley-Interscience, New York,, 1983.
- [19] J. M. Bardeen, W. H. Press, and S. A. Teukolsky. Rotating Black Holes: Locally nonrotating frames, energy extraction, and scalar synchrotron radiation. *Astrophys. J.*, 178:347, 1972.

- [20] P. A. Sundararajan. Transition from Adiabatic Inspiral to Geodesic Plunge for a Compact Object Around a Massive Kerr Black Hole: Generic orbits. *Phys. Rev. D*, 77(12):124050, 2008.
- [21] I. Ciufolini and E. C. Pavlis. A Confirmation of the General Relativistic Prediction of the Lense-Thirring Effect. *Nature*, 431:958–960, 2004.
- [22] B. Mashhoon, F. W. Hehl, and D. S. Theiss. On the Gravitational Effects of Rotating Masses - The Thirring-Lense Papers. *General Relativity and Gravitation*, 16:711–750, 1984.
- [23] I. Ciufolini. The 1995 - 99 Measurements of the Lense-Thirring Effect Using Laser-Ranged Satellites. *Class. Quantum Grav.*, 17(12):2369–2380, 2000.
- [24] I. Ciufolini. Dragging of Inertial Frames. *Nature*, 449:41–47, 2007.
- [25] W. Schmidt. Celestial Mechanics in Kerr Spacetime. *Class. Quantum Grav.*, 19(10):2743–2764, 2002.
- [26] M. P. Hobson, G. Efstathiou, A. N. Lasenby, and L. H. Ford. *General Relativity: An Introduction for Physicists*. Cambridge University Press, 2007.
- [27] F. de Felice and C. J. S. Clarke. *Relativity on Curved Manifolds*. Cambridge University Press, 1990.
- [28] F. de Felice and G. Preti. On the Meaning of the Separation Constant in the Kerr Metric. *Class. Quantum Grav.*, 16:2929–2935, 1999.
- [29] L. E. Kidder, C. M. Will, and A. G. Wiseman. Spin Effects in the Inspiral of Coalescing Compact Binaries. *Phys. Rev. D*, 47:4183, 1993.
- [30] F. D. Ryan. Effect of Gravitational Radiation Reaction on Nonequatorial Orbits Around a Kerr Black Hole. *Phys. Rev. D*, 53:3064–3069, 1996.

- [31] S. A. Hughes. Evolution of Circular, Nonequatorial Orbits of Kerr Black Holes due to Gravitational-Wave Emission. *Phys. Rev. D*, 61(8):084004, 2000.
- [32] A. P. Lightman, W. H. Press, R. H. Price, and S. A. Teukolsky. *Problem Book in Relativity and Gravitation*. Princeton University Press (Princeton, New Jersey), 1975.
- [33] W. Rindler. The Case Against Space Dragging. *Physics Letters A*, 233(1-2):25–29, 1997.
- [34] G. H. Golub and C. F. van Loan. *Matrix Computations*. Baltimore : Johns Hopkins University Press, 1996. (Johns Hopkins studies in the mathematical sciences), 1996.

Chapter 3

The Carter Constant for Inclined Orbits About a Massive Kerr Black Hole: circular orbits

Abstract

In an extreme binary black hole system, an orbit will increase its angle of inclination (ι) as it evolves in Kerr spacetime. We focus our attention on the behaviour of the Carter constant (Q) for near-polar orbits and develop an analysis that is independent of and complements radiation reaction models. For a Schwarzschild black hole, the polar orbits represent the abutment between the prograde and retrograde orbits at which Q is at its maximum value for given values of latus rectum (\tilde{l}) and eccentricity (e). The introduction of spin ($\tilde{S} = |\mathbf{J}|/M^2$) to the massive black hole causes this boundary, or abutment, to be moved towards greater orbital inclination; thus it no longer cleanly separates prograde and retrograde orbits.

To characterise the abutment of a Kerr black hole (KBH), we first investigated the last stable orbit (LSO) of a test-particle about a KBH, and then extended this work to general orbits. To develop a better understanding of the evolution of Q we developed analytical formulae for Q in terms of \tilde{l} , e , and \tilde{S} to describe elliptical orbits at the abutment, polar orbits, and last stable orbits (LSO). By knowing the analytical form of $\partial Q/\partial \tilde{l}$ at the abutment, we were able to test a 2PN flux equation for Q . We also used these formulae to numerically calculate the $\partial \iota/\partial \tilde{l}$ of hypothetical circular orbits that evolve along the abutment. From these values we have determined that $\partial \iota/\partial \tilde{l} = -\left(122.7\tilde{S} - 36\tilde{S}^3\right)\tilde{l}^{-11/2} - \left(63/2\tilde{S} + 35/4\tilde{S}^3\right)\tilde{l}^{-9/2} - 15/2\tilde{S}\tilde{l}^{-7/2} - 9/2\tilde{S}\tilde{l}^{-5/2}$. By taking the limit of this equation for $\tilde{l} \rightarrow \infty$, and comparing it with the published result for the weak-field radiation-reaction, we found the upper limit on $\left|\partial \iota/\partial \tilde{l}\right|$ for the full range of \tilde{l} up to the LSO. Although we know the value of $\partial Q/\partial \tilde{l}$ at the abutment, we find that the second and higher derivatives of Q with respect to \tilde{l} exert an influence on $\partial \iota/\partial \tilde{l}$. Thus the abutment becomes an important analytical and numerical laboratory for studying the evolution of Q and ι in Kerr spacetime and for testing current and future radiation back-reaction models for near-polar retrograde orbits.

3.1 Introduction

In his landmark work of 1968, Brandon Carter derived a new constant of motion that pertained to orbital motion in the gravitational field of a Kerr black hole (KBH) [1]. In due course, this constant became known as the Carter constant, which joins the set of important constants of motion: orbital angular momentum (L_z , z -axis projection), orbital energy (E), and finally the Carter constant (Q). These constants of motion can be developed rigorously from the Hamilton-Jacobi equation [1–3].

An extreme mass ratio binary black hole system is composed of a secondary object (which may be a compact object (CO) of several solar masses) in orbit around a primary object (which is a massive black hole (MBH) of several million solar masses). Extreme mass ratio inspirals (EMRIs) are expected to emit gravitational wave radiation (GW) of sufficiently high energy and in the appropriate frequency band for detection by the Laser Interferometer Space Antenna (LISA) to be feasible [4–7]. The emission of GW causes the constants of motion to evolve, which in turn affects the GW power spectrum. Therefore some useful methods have been developed to describe this evolution. For example, the quadrupole formalism [8–11] and the Teukolsky equation [12–14] have yielded important results. The analytical description of the evolution of Q has been more difficult to achieve than it has for the other two constants of motion [15], although the use of the Teukolsky equation has shown great promise [16, 15, 4, 5, 7] in this endeavour.

As the CO inspirals, the gravitational radiation reaction causes the value of Q to change [16–18, 15, 4, 19–21, 5, 22, 7]. Therefore a non-equatorial orbit lists as its angle of inclination, ι , increases with respect to time; a near-polar prograde orbit becomes polar, and ultimately retrograde [23, 17]. Such listing behaviour of an inclined orbit has been studied and confirmed using the most current Teukolsky-based fluxes [22]. It is our goal to develop an analytical and numerical methodology for testing and improving radiation reaction models for predicting orbit listing and inspirals for near-polar orbits.

Our interest lies in studying KBH systems; yet, the Schwarzschild black hole (SBH)

is an important datum. An infinitesimal amount of spin angular momentum ($\delta\tilde{S} \ll 1$) may be imparted to an MBH such that, for practical purposes, it can be regarded as an SBH (by virtue of its minuscule effect on the surrounding spacetime); and yet, the spherical symmetry of the system has been broken and a z -axis defined. Then an SBH can be considered to have a prograde or retrograde inclined orbit. And the set of polar orbits define the abutment, at which Q will be at its maximum value (Q is non-negative for any bound orbit), for given values of \tilde{l} , e , and \tilde{S} (*ceteris paribus*).

In section 3.2 the motion of a test-particle in an inclined orbit is analysed from first principles [24–27] to yield the effective radial potential and an analytical expression of \tilde{L}_z for a last stable orbit (LSO). In section 3.3 we continue our analysis to find the roots of the effective radial and polar-angle potentials and use them to derive analytical expressions for \tilde{E} and X^2 (where $X = \tilde{L}_z - \tilde{S}\tilde{E}$). The concept of the abutment is then refined. In section 3.4, we derive a set of critical formulae that express Q at the LSO, along the abutment, and for the set of polar orbits. The interrelationships between these formulae are examined and a map of admissible values of Q , with respect to \tilde{l} and e is drawn. In section 3.5, this map is used to better understand the path in the Q - \tilde{l} plane that is followed by an evolving circular orbit. We demonstrate the importance of the first and second derivatives of Q (on the abutment) with respect to \tilde{l} for understanding the rate of change of ι as the orbit lists.

We shall use geometrical units by setting the speed of light and gravitational constant to unity (i.e. $c = 1$ and $G = 1$); therefore, mass-energy is in units of time (seconds). In addition, many of the parameters we use will be normalised with respect to the mass of the black hole (M) or with respect to the test-particle mass (m). In Appendix 3.A, the symbols used in this paper are tabulated. By emphasising normalised variables, the analytical equations and numerical formalism are much better handled.

3.2 The Motion of a Test-Particle in an Inclined Orbit

A sound mathematical analysis can be made on the assumption that the secondary body is of infinitesimal mass (i.e. a test-particle). In such a case, the background metric of the MBH dominates. In the case of EMRIs, the small ratio of the CO mass to the MBH mass ($\eta \lesssim 10^{-5}$) warrants our use of idealised test-particle calculations [4, 28, 5, 7].

3.2.1 Basic Orbital Equations

We begin by considering a test-particle in orbit about a KBH of arbitrary spin, \tilde{S} , for which the four-momentum can be given the general definition [29],

$$P_\gamma = \left[-m\tilde{E}, m\frac{\tilde{\Sigma}}{\tilde{\Delta}} \left(\frac{dR}{d\tilde{\tau}} \right), mM\tilde{L}_\theta, mM\tilde{L}_z, \right] \quad (3.1)$$

where

$$\tilde{\Delta} = \left(R^2 - 2R + \tilde{S}^2 \right) \quad (3.2)$$

and

$$\tilde{\Sigma} = \left(R^2 + \tilde{S}^2 \cos^2(\theta) \right). \quad (3.3)$$

Unlike the analysis in Komorowski et al. [29], we shall use normalised variables at the outset and offer a more thorough treatment. Because we are now considering inclined elliptical orbits, one cannot simplify the four-momentum by setting $\tilde{L}_\theta = 0$. But by knowing the Carter constant in terms of normalised variables (i.e. obtained by dividing through by mM),

$$Q = \frac{\cos^2(\theta) \tilde{L}_z^2}{\sin^2(\theta)} + \tilde{L}_\theta^2 + \cos^2(\theta) \tilde{S}^2 (1 - \tilde{E}^2), \quad (3.4)$$

one can obtain the component of orbital angular momentum, \mathbf{L} , projected upon the

equatorial plane of the KBH,

$$\tilde{L}_\theta = \sqrt{Q - \frac{\cos^2(\theta) \tilde{L}_z^2}{\sin^2(\theta)} - \cos^2(\theta) \tilde{S}^2 (1 - \tilde{E}^2)}, \quad (3.5)$$

and substitute it into the expression for the four-momentum:

$$P_\gamma = \left[-m\tilde{E}, m \frac{\tilde{\Sigma}}{\tilde{\Delta}} \left(\frac{dR}{d\tilde{\tau}} \right), mM \sqrt{Q - \frac{\cos^2(\theta) \tilde{L}_z^2}{\sin^2(\theta)} - \cos^2(\theta) \tilde{S}^2 (1 - \tilde{E}^2)}, mM \tilde{L}_z \right]. \quad (3.6)$$

The invariant quantity,

$$\vec{P} \cdot \vec{P} = P_\gamma P_\delta g^{\delta\gamma} \Big|_{Kerr} = -m^2, \quad (3.7)$$

is calculated tensorially using the inverse Kerr metric (see Appendix 3.B.1) and used to develop the radial orbital equation for a test-particle:

$$\begin{aligned} \tilde{\Sigma}^2 \left(\frac{dR}{d\tilde{\tau}} \right)^2 &= - (1 - \tilde{E}^2) R^4 + 2 R^3 \\ &\quad - \left(\tilde{L}_z^2 + \tilde{S}^2 (1 - \tilde{E}^2) + Q \right) R^2 \\ &\quad + 2 \left(\left(\tilde{L}_z - \tilde{S} \tilde{E} \right)^2 + Q \right) R - Q \tilde{S}^2. \end{aligned} \quad (3.8)$$

By setting $Q = 0$, equation (3.8) reduces to the equation for an equatorial orbit (see [20]).

At the radial turning points, $dR/d\tilde{\tau} = 0$. Equation (3.8) becomes:

$$\begin{aligned} 0 &= R^4 - 2 \frac{R^3}{1 - \tilde{E}^2} \\ &\quad + \frac{\left(\tilde{L}_z^2 + \tilde{S}^2 (1 - \tilde{E}^2) + Q \right) R^2}{1 - \tilde{E}^2} \\ &\quad - 2 \frac{\left(\left(\tilde{L}_z - \tilde{S} \tilde{E} \right)^2 + Q \right) R}{1 - \tilde{E}^2} + \frac{Q \tilde{S}^2}{1 - \tilde{E}^2}. \end{aligned} \quad (3.9)$$

In the limit $\tilde{S} \rightarrow 0$ (set $\tilde{S} = 0$ while retaining a non-zero value for Q) equation (3.9)

becomes

$$0 = R^4 - 2 \frac{R^3}{1 - \tilde{E}^2} + \frac{(\tilde{L}_z^2 + Q) R^2}{1 - \tilde{E}^2} - 2 \frac{(\tilde{L}_z^2 + Q) R}{1 - \tilde{E}^2}. \quad (3.10)$$

Thus, the square of the total orbital angular momentum, $\tilde{L}^2 = \tilde{L}_z^2 + Q$, confirms that, for the specific case of an SBH, Q represents the square of the component of angular momentum projected on $x-y$ plane of the coordinate system (see Appendix B in Schmidt [30] and Appendix 3.C in this paper for a more detailed treatment).

Some important research [21, 31] has been performed by working with the orbital inclination angle, ι , instead of Q ; but in our study, the value of Q will be taken as a system parameter. If Q is chosen to be zero, then the orbital plane coincides with the equatorial plane of the KBH (i.e. $\iota = 0$ and $\theta \equiv \pi/2$) and for a test-particle in a polar orbit (i.e. $\iota = \frac{\pi}{2}$ and $0 \leq \theta \leq \pi$) \tilde{L}_z must vanish. The choice of working directly with the Carter constant, Q , as a system parameter is consistent with the approach taken by Carter [1] and more recently emphasised by others [32, 5, 22]

3.2.2 Effective Radial Potential

To proceed, we use a version of equation (3.8), which is quadratic in \tilde{E}

$$\begin{aligned} & -R \left(R^3 + R\tilde{S}^2 + 2\tilde{S}^2 \right) \tilde{E}^2 + 4R\tilde{L}_z\tilde{S}\tilde{E} \\ & + R(R-2) \left(Q + \tilde{L}_z^2 \right) + R^2 \left(R^2 - 2R + \tilde{S}^2 \right) + Q\tilde{S}^2 \\ & = 0. \end{aligned} \quad (3.11)$$

The roots of this equation can be used to determine the effective potential of the test-particle (\tilde{V}_\pm):

$$\begin{aligned} \tilde{V}_\pm &= \left(2R\tilde{L}_z\tilde{S} \pm \sqrt{RZ\tilde{\Delta}} \right) \\ &\times \left(R \left(R^3 + \tilde{S}^2 R + 2\tilde{S}^2 \right) \right)^{-1} \end{aligned} \quad (3.12)$$

where

$$Z = R^5 + \left(Q + \tilde{S}^2 + \tilde{L}_z^2\right) R^3 + 2 R^2 \tilde{S}^2 + \tilde{S}^2 R Q + 2 Q \tilde{S}^2.$$

When the last stable orbit (LSO) is reached, \tilde{E} corresponds to a local maximum of \tilde{V}_+ closest to the event horizon. Therefore one calculates the derivative of \tilde{V}_+ with respect to R and equates it to zero, i.e.

$$\begin{aligned} \frac{d\tilde{V}_+}{dR} &= - \left(2R\tilde{S}\tilde{L}_z \left(3R^2 + \tilde{S}^2 \right) \sqrt{RZ\tilde{\Delta}} + R^3 Z_1 \tilde{L}_z^2 \right. \\ &\quad \left. + \left(R^3 + \tilde{S}^2 R + 2\tilde{S}^2 \right) Z_2 \right) \\ &\quad \times \left(R\sqrt{RZ\tilde{\Delta}} \left(R^3 + \tilde{S}^2 R + 2\tilde{S}^2 \right)^2 \right)^{-1} \\ &= 0 \end{aligned} \tag{3.13}$$

where

$$Z_1 = R^5 - 3R^4 + \tilde{S}^2 R^3 - 3R^2 \tilde{S}^2 + 6\tilde{S}^2 R - 2\tilde{S}^4,$$

and

$$\begin{aligned} Z_2 &= -R^6 + R^5 Q - \left(2\tilde{S}^2 + 3Q \right) R^4 + \left(2Q\tilde{S}^2 + 4\tilde{S}^2 \right) R^3 \\ &\quad - \left(\tilde{S}^4 + 2Q\tilde{S}^2 \right) R^2 + \tilde{S}^4 Q R + \tilde{S}^4 Q. \end{aligned}$$

3.2.3 Orbital Angular Momentum at the Last Stable Orbit

We can now develop an equation for the \tilde{L}_z of a test-particle in an inclined orbit about a KBH (in a manner similar to that described in [29]) and extend the concept to general orbits. It should be noted, the value of \tilde{L}_z considered here is not valid for general orbits, but pertains to the LSO. After eliminating the square root in equation (3.13) to yield a

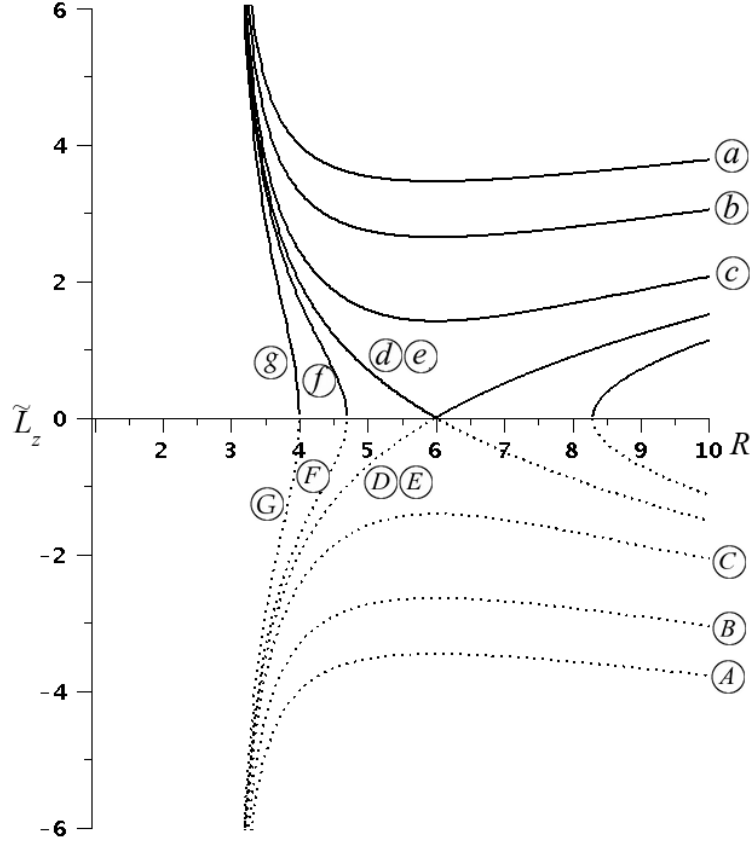


Figure 3-1: The relationship between \tilde{L}_z and pericentre, R , for an SBH. Various values of Q are depicted. The polar LSO and abutment are superimposed (d, e). In table 3.B.1 some values of R_{LSO} for this SBH system are listed.

new equation that is quadratic in \tilde{L}_z^2 the solution is found to be:

$$\begin{aligned}
 \tilde{L}_z^2 = & \left\{ -R^8 + (3 + Q)R^7 + (-2\tilde{S}^2 - 6Q)R^6 \right. \\
 & + \left((-6 + 2Q)\tilde{S}^2 + 9Q \right)R^5 + \left(-\tilde{S}^4 + (-10Q + 12)\tilde{S}^2 \right)R^4 \\
 & + \left((-5 + Q)\tilde{S}^4 + 6Q\tilde{S}^2 \right)R^3 - 6\tilde{S}^4R^2Q \\
 & + 5\tilde{S}^4RQ - 2\tilde{S}^6Q \\
 & \left. \pm 2\tilde{S} \left(3R^2 + \tilde{S}^2 \right) \tilde{\Delta} \sqrt{\left(R^5 - R^4Q + 3R^3Q + Q^2\tilde{S}^2 \right)} \right\} \\
 & \left(R^4 \left(R^3 + 9R - 4\tilde{S}^2 - 6R^2 \right) \right)^{-1}, \tag{3.14}
 \end{aligned}$$

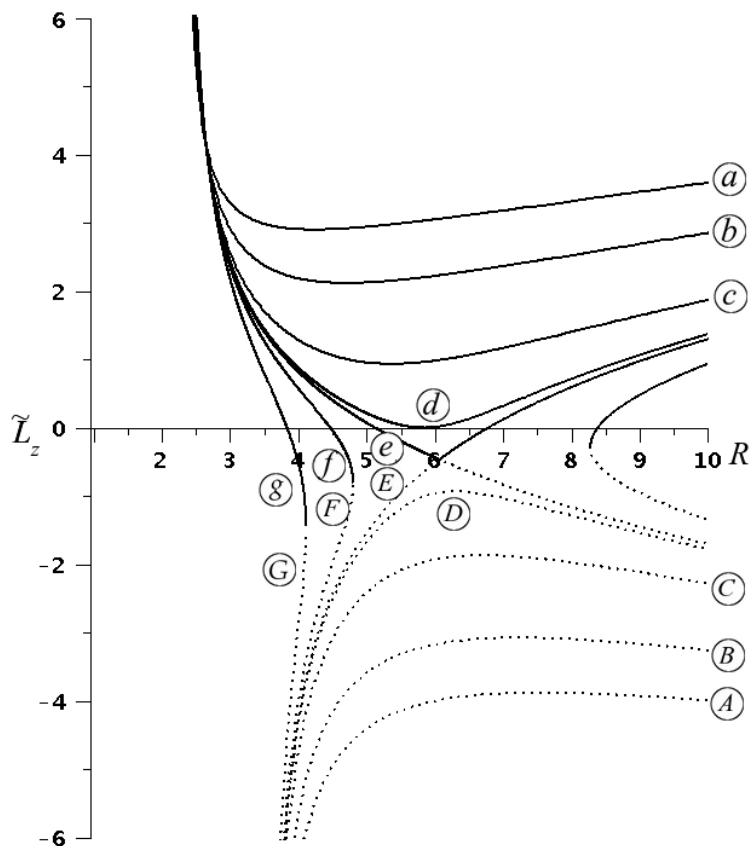


Figure 3-2: The relationship between \tilde{L}_z and pericentre, R , for a KBH with $\tilde{S} = 0.50$. Various values of Q are depicted. The polar LSO (d) and the LSO at the abutment (e) are distinct. In table 3.B.2 some values of R_{LSO} for this KBH system are listed.

which provides a relationship between \tilde{L}_z and R (which here, represents the pericentre radius) of the test-particle LSO. This result is independent of whether one begins the calculation with \tilde{V}_+ or \tilde{V}_- .

One can now plot \tilde{L}_z with respect to the value of the pericentre (the point of closest approach, R_p) for an LSO for the cases where $\tilde{S} = 0.0$ (figure 3-1), $\tilde{S} = 0.5$ (figure 3-2) and $\tilde{S} = 0.99$ (figure 3-3). The values of \tilde{L}_z calculated for an SBH are plotted in figure 3-1 for the range of Q values 0.0 to 16.0.

For an SBH, the prograde (plus) and retrograde (minus) formulae for \tilde{L}_z^2 (equation (3.14)) are reflections of one another about the R axis (figure 3-1). But when $\tilde{S} > 0$, the plus equations are pulled below the R axis and this symmetry is lost (figures 3-2 and

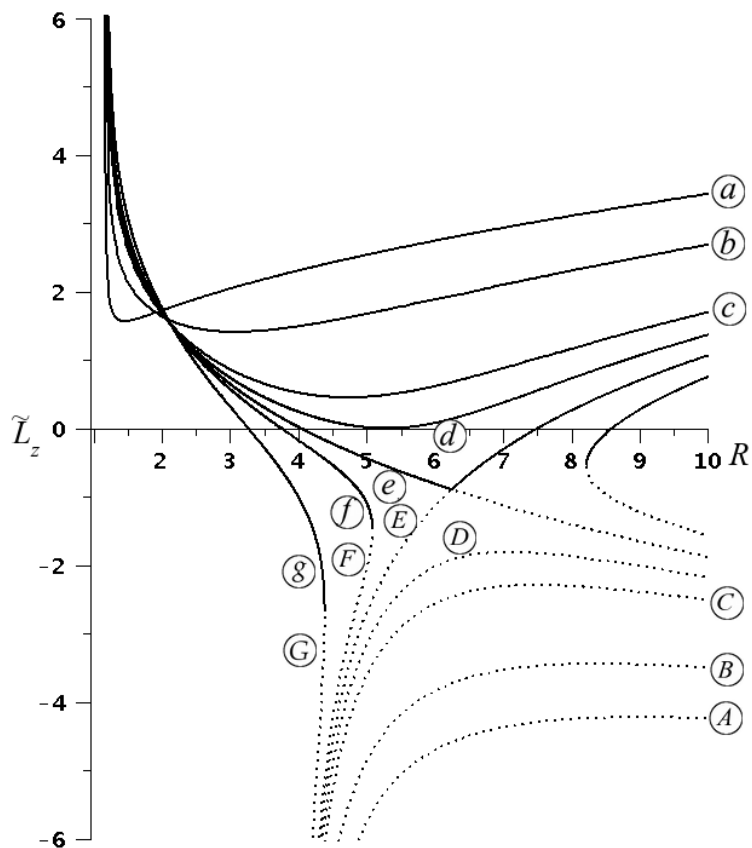


Figure 3-3: The relationship between \tilde{L}_z and pericentre, R , for a KBH with $\tilde{S} = 0.99$. Various values of Q are depicted. The separation of the polar LSO (d) and the LSO at the abutment (e) is increased with the higher value of \tilde{S} . In table 3.B.3 some values of R_{LSO} for this KBH system are listed.

3-3). There now exists a set of retrograde LSOs which are governed by the plus form of equation (3.14). The importance of this fact is revealed when we set the quantity beneath the square root in equation (3.14) to zero; i.e.

$$R^5 - QR^4 + 3QR^3 + Q^2\tilde{S}^2 = 0. \quad (3.15)$$

The polynomial describes the boundary at which the plus and minus equations for \tilde{L}_z^2 are equal and it offers an insight into the behaviour of Q for LSOs that are nearly polar

($\iota \simeq \pi/2$). If $\tilde{S} = 0$, then for an elliptical LSO [33, 11, 29],

$$R_p = 2(3 + e)/(1 + e). \quad (3.16)$$

By substituting equation (3.16) into equation (3.15) and solving for Q , one obtains:

$$Q = 4(3 + e)^2 [(1 + e)(3 - e)]^{-1}. \quad (3.17)$$

This result applies to LSOs at the boundary and specifies an upper limit on Q for orbits around an SBH. Now we must develop these ideas for general orbits about a KBH that have not yet reached their LSO.

3.3 Analysis of the Trajectory Equations

3.3.1 Introduction

There exist four trajectory equations [1, 34, 30] in two categories:

category (a)

(those that are periodic in radius, R , or polar angle, θ)

$$\tilde{\Sigma} \frac{dR}{d\tilde{\tau}} = \pm \sqrt{\tilde{V}_R(R)} \quad (3.18)$$

$$\tilde{\Sigma} \frac{d\theta}{d\tilde{\tau}} = \pm \sqrt{\tilde{V}_\theta(\theta)} \quad (3.19)$$

category (b)

(those that are monotonically increasing in azimuthal angle, φ , or coordinate time, t)

$$\tilde{\Sigma} \frac{d\phi}{d\tilde{\tau}} = \tilde{V}_\phi \quad (3.20)$$

$$\tilde{\Sigma} \frac{d\tilde{t}}{d\tilde{\tau}} = \tilde{V}_t. \quad (3.21)$$

See Appendix 3.B.2 to see equations for functions $\tilde{V}_R(R)$, \tilde{V}_θ , \tilde{V}_ϕ , and \tilde{V}_t . We have already developed equation (3.18) in section 3.2.1 (equation (3.8)). And equation (3.19) can also be developed by a similar method (see Appendix 3.C).

One obtains, *viz.* equations (3.18) and (3.19), the following condition

$$\frac{dR}{\sqrt{\tilde{V}_R(R)}} = \frac{d\theta}{\sqrt{\tilde{V}_\theta(\theta)}}, \quad (3.22)$$

on the geodesic of the test-particle, which is a general form of the equation specified by Schmidt (equation (16) in [30]). Given equation (3.19) [34], one can find the proper time of the orbit:

$$\begin{aligned} \tilde{\tau} &= \int_{\theta_1}^{\theta_2} \frac{\tilde{\Sigma} d\theta}{\sqrt{\tilde{V}_\theta}} \\ &= \int_{r_1}^{r_2} \frac{R^2 dR}{\sqrt{\tilde{V}_R}} + \tilde{S}^2 \int_{\theta_1}^{\theta_2} \frac{\cos^2(\theta)}{\sqrt{\tilde{V}_\theta}} d\theta, \end{aligned} \quad (3.23)$$

where the integral has been split into its separate R and θ integral terms *viz.* equation (3.22). The same result is found when starting with equation (3.18) instead. Two other important integrals that can be calculated for coordinate time and azimuthal angle are given in Schmidt (equations (14) and (15) [30]) in which a detailed analysis is made on the basis of the Hamiltonian. Equation (3.23) can be solved to yield elliptic functions [20]; therefore, the roots of \tilde{V}_R and V_θ contain information necessary for deriving analytical formulae for Q in terms of \tilde{l} and e (for given \tilde{S}) and ι as a function of Q . This will be shown in sections 3.3.3 and 3.4.

3.3.2 Roots of the Radial Equation

We introduce $X = \tilde{L}_z - \tilde{S}\tilde{E}$ and convert equation (3.9) to the form:

$$\begin{aligned}
0 &= R^4 - 2 \frac{R^3}{(1 - \tilde{E}^2)} \\
&+ \frac{(X^2 + \tilde{S}^2 + 2\tilde{S}\tilde{E}X + Q) R^2}{(1 - \tilde{E}^2)} \\
&- \frac{2(X^2 + Q)R}{(1 - \tilde{E}^2)} + \frac{Q\tilde{S}^2}{(1 - \tilde{E}^2)}. \tag{3.24}
\end{aligned}$$

This substitution is consistent with the approach in [29] and that undertaken by Glampedakis and Kennefick [20], and it will help us derive the latus rectum of the LSO. Analytically, the use of X^2 in this case offers an advantage over the use of L_z^2 .

3.3.2.1 Elliptical Orbits

By finding the four roots of equation (3.24) one can derive analytical formulae for X and \tilde{E} , in terms of e , \tilde{l} , Q , and \tilde{S} , which apply to general orbits (and are not limited to the LSO). The roots are easily obtained in terms of the constants of motion: \tilde{L}_z , \tilde{E} , and Q ; but they are complicated and as such not helpful. To simplify the analysis, we assume *a priori* that an inclined orbit can be characterised by an eccentricity, e [35]. Therefore the radius of the orbit at its pericentre is described by

$$r_p = \frac{\tilde{l}}{1 + e}, \tag{3.25}$$

and correspondingly, at its apocentre

$$r_a = \frac{\tilde{l}}{1 - e}. \tag{3.26}$$

To proceed, consider an expansion of the four possible roots $\{r_4 < r_3 \leq r_p \leq r_a\}$:

$$\begin{aligned}
& R^4 - (r_3 + r_4 + r_a + r_p) R^3 \\
& + (r_4 r_3 + r_3 r_a + r_3 r_p + r_4 r_a + r_4 r_p + r_p r_a) R^2 \\
& - (r_4 r_3 r_a + r_4 r_3 r_p + r_3 r_p r_a + r_4 r_p r_a) R + r_4 r_3 r_p r_a \\
& = 0.
\end{aligned} \tag{3.27}$$

By equating the coefficients of the two polynomials in equations (3.24) and (3.27) one obtains the two independent equations:

$$\frac{\tilde{l} (2 r_4 r_3 + r_3 \tilde{l} + r_4 \tilde{l})}{(1 - e^2)} = 2 \frac{X^2 + Q}{1 - \tilde{E}^2}, \tag{3.28}$$

and

$$\frac{r_4 r_3 \tilde{l}^2}{1 - e^2} = \frac{Q \tilde{S}^2}{1 - \tilde{E}^2}, \tag{3.29}$$

which have been simplified *viz.* equations (3.25) and (3.26). Let us solve equations (3.28) and (3.29) to obtain:

$$r_3 = \frac{(1 - e^2)}{\tilde{l}^3 (1 - \tilde{E}^2)} \left[\left(Q (\tilde{l} - \tilde{S}^2) + X^2 \tilde{l} \right) \pm \sqrt{Z_3} \right] \tag{3.30}$$

and

$$r_4 = \frac{Q \tilde{S}^2 (1 - e^2)}{r_3 \tilde{l}^2 (1 - \tilde{E}^2)} \tag{3.31}$$

where

$$\begin{aligned}
Z_3 & = (\tilde{l} - \tilde{S}^2)^2 Q^2 \\
& - \tilde{l} \left(\frac{(1 - \tilde{E}^2) \tilde{S}^2 \tilde{l}^3}{1 - e^2} - 2 X^2 \tilde{l} + 2 X^2 \tilde{S}^2 \right) Q + X^4 \tilde{l}^2.
\end{aligned}$$

If $Q = 0$ then selecting the minus sign in equation (3.30) yields $r_3 = 0$; therefore, the plus sign is the one taken as physically meaningful. For $Q = 0$, equation (3.30) reduces to

$$r_3 = 2 \frac{X^2 (1 - e^2)}{\tilde{l}^2 (1 - \tilde{E}^2)}, \quad (3.32)$$

which applies to an equatorial orbit. The value of r_4 equals zero when $Q = 0$ as can be seen in equation (3.31).

3.3.2.2 Parabolic Orbits

Parabolic orbits have importance to the empirical study of the interaction of stars with massive black holes (MBHs) [36, 37]. For parabolic orbits both $e = 1$ and $\tilde{E} = 1$. We refer back to equation (3.24); and set $\tilde{E} = 1$:

$$\begin{aligned} 0 &= R^3 \\ &- \frac{1}{2} \left(X^2 + \tilde{S}^2 + 2\tilde{S}X + Q \right) R^2 \\ &+ (X^2 + Q) R - \frac{1}{2} Q \tilde{S}^2. \end{aligned} \quad (3.33)$$

There are now three possible finite roots $\{r_4 < r_3 \leq r_p\}$, which can be used in a new general equation (r_a is infinite in the case of a parabolic orbit):

$$R^3 - (r_3 + r_4 + r_p) R^2 + (r_4 r_3 + r_3 r_p + r_4 r_p) R - r_4 r_3 r_p = 0. \quad (3.34)$$

The pericentre simplifies (*viz.* $e = 1$) to become,

$$r_p = \frac{\tilde{l}}{2}; \quad (3.35)$$

and correspondingly, at its apocentre,

$$r_a \rightarrow \infty. \quad (3.36)$$

We obtain the solutions for the additional roots:

$$r_3 = \frac{1}{\tilde{l}^2} \left[\left(Q \left(\tilde{l} - \tilde{S}^2 \right) + X^2 \tilde{l} \right) \pm \sqrt{Z_4} \right] \quad (3.37)$$

and

$$r_4 = \frac{Q \tilde{S}^2}{r_3 \tilde{l}} \quad (3.38)$$

where

$$Z_4 = \left(\tilde{l} - \tilde{S}^2 \right)^2 Q^2 - \tilde{l} \left(\tilde{S}^2 \tilde{l}^2 - 2 X^2 \tilde{l} + 2 X^2 \tilde{S}^2 \right) Q + X^4 \tilde{l}^2.$$

3.3.3 Roots of the Polar-Angle Equation

Let us focus on the denominator of the second term in equation (3.23), i.e. $\sqrt{\tilde{V}_\theta}$, to derive an analytical relationship for the limits of integration, θ_1 and θ_2 , from which one may determine ι . We shall work with \tilde{V}_θ in terms of \tilde{L}_z , i.e.

$$\mathcal{I} = \tilde{S}^2 \int_{\theta_1}^{\theta_2} \frac{\sin(\theta) \cos^2(\theta) d\theta}{\sqrt{Q \sin^2(\theta) - \sin^2(\theta) \cos^2(\theta) \tilde{S}^2 \left(1 - \tilde{E}^2 \right) - \cos^2(\theta) \tilde{L}_z^2}}. \quad (3.39)$$

Equation (3.23) is an elliptic integral; thus the limits of integration correspond to the zeros of the denominator. By making the substitution

$$u = \cos(\theta), \quad (3.40)$$

the integral, \mathcal{I} , becomes

$$\begin{aligned} \mathcal{I} &= \tilde{S}^2 \int_{u_1}^{u_2} \frac{-u^2 du}{\sqrt{\tilde{S}^2 \left(1 - \tilde{E}^2 \right) u^4 - \left(Q + \tilde{L}_z^2 + \tilde{S}^2 \left(1 - \tilde{E}^2 \right) \right) u^2 + Q}} \\ &= \tilde{S}^2 \int_{u_1}^{u_2} \frac{-u^2 du}{\tilde{S} \sqrt{1 - \tilde{E}^2} \sqrt{(u^2 - \beta_+) (u^2 - \beta_-)}}, \end{aligned} \quad (3.41)$$

for which the roots, $\beta_{\pm} = \cos^2(\theta_{\pm})$, can be calculated and used to determine (*viz.* $\cos(\theta) = \cos(\frac{\pi}{2} - \iota) = \sin(\iota)$) the exact angle of inclination of an orbit for which the values of \tilde{S} , Q , and \tilde{L}_z are known, when working in Boyer-Lindquist coordinates. We will calculate ι using

$$\sin^2(\iota) = \frac{1}{2} \frac{Q + \tilde{L}_z^2 + \tilde{S}^2(1 - \tilde{E}^2) - \sqrt{(Q + \tilde{L}_z^2 + \tilde{S}^2(1 - \tilde{E}^2))^2 - 4Q\tilde{S}^2(1 - \tilde{E}^2)}}{\tilde{S}^2(1 - \tilde{E}^2)}, \quad (3.42)$$

which differs from the approximation in [21, 5]. In dealing with results that are first-order and third-order in \tilde{S} , one may consider the approximation to ι to be reasonably close to equation (3.42) [38].

3.3.4 Orbital Energy and an Analytical Expression for X^2

As outlined in [20], the next step will be to develop a formula for orbital energy, \tilde{E} , in terms of e , \tilde{l} , and X^2 . By referring to equations (3.24) and (3.27), this derivation proceeds by solving

$$r_4 + r_3 + r_p + r_a = 2(1 - \tilde{E}^2)^{-1} \quad (3.43)$$

to yield

$$\tilde{E} = \pm \frac{1 - e^2}{\tilde{l}^2} \sqrt{Q(\tilde{l} - \tilde{S}^2) + X^2\tilde{l} + \tilde{l}^3(e^2 + \tilde{l} - 1)(1 - e^2)^{-2}}, \quad (3.44)$$

for which we use the positive case. For $Q = 0$, equation (3.44) simplifies to

$$\tilde{E} = \sqrt{1 - \frac{(1 - e^2)}{\tilde{l}} \left(1 - \frac{X^2(1 - e^2)}{\tilde{l}^2}\right)}, \quad (3.45)$$

which is the expression for \tilde{E} in an equatorial orbit.

It is interesting to observe that for an inclined orbit around an SBH ($\tilde{S} = 0$), the

equation for \tilde{E} (equation (3.44)) reduces to

$$\tilde{E} = \sqrt{\frac{(\tilde{l} - 2(1 + e))(\tilde{l} - 2(1 - e))}{\tilde{l}(\tilde{l} - 3 - e^2)}}, \quad (3.46)$$

which is the expression for orbital energy of a test-particle in orbit around an SBH, (Cutler, Kennefick, and Poisson (see equation (2.5) in [33])). Further, this equation for \tilde{E} shows no dependence on Q . This property is expected since the orbital energy must be independent of orientation in the spherically symmetric coordinate system of an SBH.

In the general case, we observe that \tilde{E} is a function of X^2 (see equation (3.44)); and thus it is not in explicit form because $X = \tilde{L}_z - \tilde{S}\tilde{E}$. Therefore the use of X^2 in place of $(\tilde{L}_z - \tilde{S}\tilde{E})^2$ simplifies the analysis by avoiding an unending recursive substitution of \tilde{E} into the equation. Although one may derive a formula for \tilde{E} in explicit form, it is better to perform the analysis using equation (3.44).

To calculate an analytical expression for X^2 , we substitute equation (3.44) into our original quartic (equation (3.9)) and evaluate it at either r_p or r_a (the two simplest choices of the four roots) to yield:

$$\begin{aligned} & (1 + e)^{-2} \left(\tilde{l}^2 (\tilde{S}^2 - \tilde{l}) + 2QS^2(1 + e^2) + \tilde{l}(X^2 + Q)(\tilde{l} - 3 - e^2) \right) \quad (3.47) \\ & + 2\tilde{S}X \sqrt{\tilde{l}(X^2 + Q)(1 - e^2)^2 - Q\tilde{S}^2(1 - e^2)^2 + \tilde{l}^3(\tilde{l} + e^2 - 1)} \\ & = 0. \end{aligned}$$

By eliminating the square root, and solving for X^2 in the resulting quadratic, one obtains:

$$X_{\pm}^2 = \frac{Z_5 + Z_6Q \pm 2\tilde{S}\sqrt{Z_7Z_8Z_9}}{\tilde{l}\left(\tilde{l}(3 - \tilde{l} + e^2)^2 - 4\tilde{S}^2(1 - e^2)^2\right)}, \quad (3.48)$$

where

$$Z_5 = \tilde{l}^3 \left\{ (\tilde{l} + 3e^2 + 1)\tilde{S}^2 - \tilde{l}(3 - \tilde{l} + e^2) \right\},$$

$$Z_6 = -2(1 - e^2)^2 \tilde{S}^4 + 2\tilde{l} \left(2e^4 + (2 - \tilde{l})e^2 + 4 - \tilde{l} \right) \tilde{S}^2 - \tilde{l}^2 (3 - \tilde{l} + e^2)^2,$$

$$Z_7 = \tilde{S}^2 (1 + e)^2 + \tilde{l} (\tilde{l} - 2(1 + e)),$$

$$Z_8 = \tilde{S}^2 (1 - e)^2 + \tilde{l} (\tilde{l} - 2(1 - e)),$$

and

$$Z_9 = \left(\tilde{l}^5 + \tilde{S}^2 Q^2 (1 - e^2)^2 + Q \tilde{l}^3 (3 - \tilde{l} + e^2) \right). \quad (3.49)$$

X_{\pm}^2 has a minus and a plus solution, which we will carefully describe in the next section. We have avoided the analytical difficulties that would arise by working with \tilde{L}_z directly. Indeed, the advantage of using $X = \tilde{L}_z - \tilde{S}\tilde{E}$ is more than a simple change of variables, but rather an essential step in solving these equations.

3.3.5 Prograde and Retrograde Descriptions of X^2

The expression for X_{\pm}^2 (see equation (3.48)) contains the square root, $\pm 2\tilde{S} \sqrt{Z_7 Z_8 Z_9}$, for which, Q is found only in Z_9 as a quadratic. Therefore it is easy to derive an expression for Q for which $Z_9 = 0$ and thus determine where the minus and plus equations for X_{\pm}^2 meet or abut (*viz.* $Z_9 = 0$). This information is important for determining which form of equation (3.48) to use. We will call the set of general orbits for which $Z_9 = 0$, the abutment, to avoid confusing it with the result for the boundary between the plus and minus forms of \tilde{L}_z at the LSO.

A prograde orbit has an $\tilde{L}_z > 0$. Correspondingly, when $\tilde{L}_z < 0$ the orbit is retrograde. If $\tilde{L}_z = 0$, then the orbit is polar. When using the minus and plus forms of the equation

for X_{\pm}^2 (equation (3.48)), one must recognise that X_-^2 governs all of the prograde orbits, the polar orbits, and the near-polar retrograde orbits up to the abutment; and X_+^2 governs the remaining retrograde orbits. If one considers an SBH system then the abutment will be comprised only of polar orbits (and it is only then that X_{\pm}^2 cleanly separates the prograde and retrograde orbits). If $\tilde{S} > 0$, the abutment will always consist of retrograde orbits.

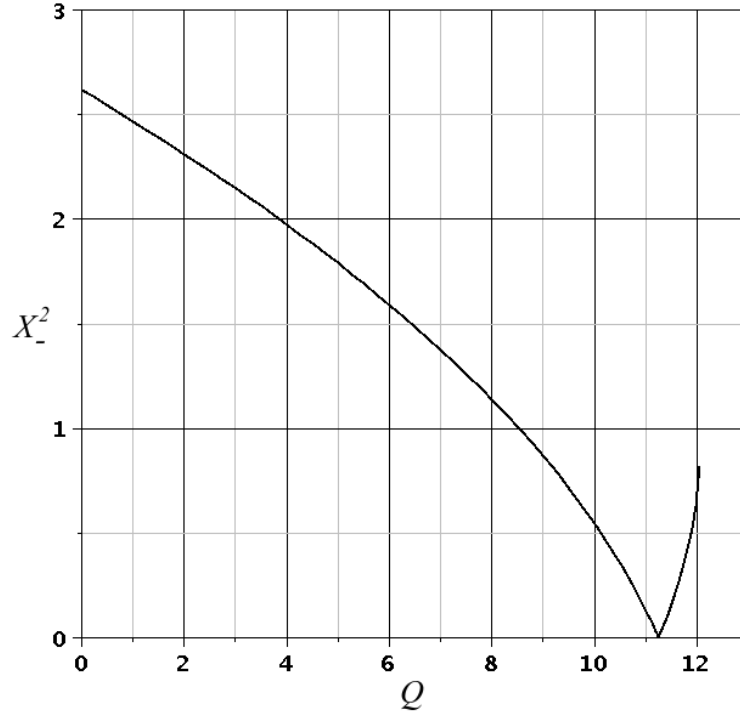


Figure 3-4: A plot of X_-^2 with respect to Q for a circular orbit ($\tilde{l} = 6.25$) about a KBH of spin $\tilde{S} = 0.5$. The slope of X_- can be assumed to have no discontinuities; therefore, the point at $Q_{switch} = 11.26$ indicates that if $Q > Q_{switch}$ then $X_- = -\sqrt{X_-^2}$.

For orbits governed by X_+^2 , $X_+ = -\sqrt{X_+^2}$; but for those governed by X_-^2 , the choice of sign depends on the value of Q . The plot of X_-^2 with respect to Q for a circular orbit with $\tilde{l} = 6.25$ about a KBH of $\tilde{S} = 0.5$ (figure 3-4) shows that for $\partial X_-/\partial Q$ to remain continuous over the range of real values of Q , the minus sign must be chosen when evaluating X_- for $Q > Q_{switch}$. An analytical formula for Q_{switch} can be found by

solving $X_-^2 = 0$ for Q . The general solution is

$$Q_{switch} = \tilde{l}^2 \left(\tilde{l} - \tilde{S}^2 \right) \left(\tilde{l} \left(\tilde{l} - e^2 - 3 \right) + 2 \left(1 + e^2 \right) \tilde{S}^2 \right)^{-1}, \quad (3.50)$$

and for an SBH

$$Q_{switch} = \tilde{l}^2 \left(\tilde{l} - e^2 - 3 \right)^{-1}. \quad (3.51)$$

For large orbits ($\tilde{l} \rightarrow \infty$) equation (3.50) can be converted to its asymptotic form by first factoring out \tilde{l} from each term to obtain,

$$Q = \tilde{l} \left(1 - \frac{\tilde{S}^2}{\tilde{l}} \right) \left(1 - \frac{3 + e^2}{\tilde{l}} + \frac{2(1 + e^2)\tilde{S}^2}{\tilde{l}^2} \right)^{-1}, \quad (3.52)$$

for which the denominator may be brought up to the numerator to yield

$$Q \cong \tilde{l} \left(1 - \frac{\tilde{S}^2}{\tilde{l}} \right) \left(1 + \frac{3 + e^2}{\tilde{l}} - \frac{(3 + e^2)^2 + 2(1 + e^2)\tilde{S}^2}{\tilde{l}^2} \right). \quad (3.53)$$

In the limit as $\tilde{l} \rightarrow \infty$,

$$Q_{switch} = \tilde{l} + 3 + e^2 - \tilde{S}^2. \quad (3.54)$$

Equation (3.54) describes the locus of points at which $\tilde{L}_z = \tilde{S}\tilde{E}$ (which is effectively constant for large \tilde{l}); therefore, Q_{switch} does not describe a trajectory.

We have developed two formulae: one for the \tilde{L}_z^2 at the LSO (equation (3.14)) and the other for the X_{\pm}^2 of general circular and elliptical orbits (equation (3.48)). For each, there is an expression that describes where the plus and minus forms are equal. For \tilde{L}_z^2 , the boundary between the plus and minus forms is described by

$$R_p^5 - QR_p^4 + 3QR_p^3 + Q^2\tilde{S}^2 = 0, \quad (3.55)$$

where R_p represents the pericentre. And for X_{\pm}^2 , the abutment is described by

$$\tilde{l}^5 + \tilde{S}^2 Q^2 (1 - e^2)^2 + Q \tilde{l}^3 (3 - \tilde{l} + e^2) = 0. \quad (3.56)$$

As equations (3.55) and (3.56) describe the boundaries (where the plus and minus forms are equal) that pertain to different quantities (\tilde{L}_z and X_{\pm}^2) they will not in general coincide. If one substitutes $R_p = \tilde{l}/(1 + e)$ into equation (3.55) one obtains:

$$\tilde{l}^5 - Q(1 + e)\tilde{l}^4 + 3Q(1 + e)^2\tilde{l}^3 + Q^2\tilde{S}^2(1 + e)^5 = 0, \quad (3.57)$$

which equals equation (3.56) when $e = 0$, (i.e. for a circular orbit). If $\tilde{S} = 0$ (SBH case), then $X_{\pm}^2 = \tilde{L}_{\pm}^2$ and the two boundaries must be identical. If one substitutes $\tilde{l} = 6 + 2e$ into equation (3.56) and solves for Q , then the same expression as in equation (3.17) is obtained.

3.4 The Characteristics of the Carter Constant Equations and the Domain of the Orbital Parameters

3.4.1 Introduction

In describing an arbitrary orbit, it must be recognised that each parameter (\tilde{l} , e , and Q) has a domain. The value of e lies between 0, for a circular orbit, and 1 for a parabolic orbit. Although \tilde{l} has no upper limit, its minimum value is \tilde{l}_{LSO} ; while Q , which is non-negative, does have an upper limit that depends on the size of \tilde{l} .

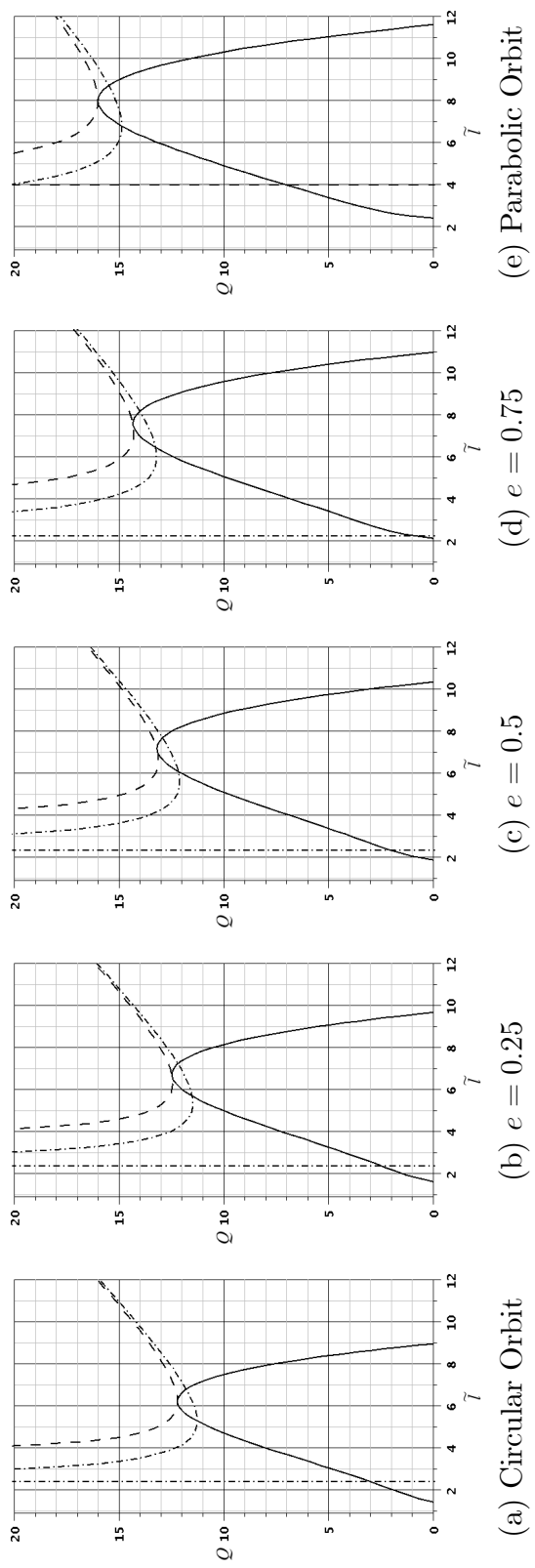


Figure 3-5: A sequence of $Q - \tilde{t}$ maps for various values of e for a KBH system with $\tilde{S} = 0.99$. The short-dashed lines represent Q_x (equation (3.63)), the long-dashed lines represent Q_{polar} (equation (3.69)), and the solid lines represent Q_{LSO} (equation (3.62)).

The complicated interrelationships between these parameters can be better understood if we derive a set of analytical formulae to describe the behaviour of Q with respect to \tilde{l} and e . In the sections that follow, we shall examine the LSO, abutment, and polar orbits. A representative plot of these curves is shown in figure 3-5 for $e = \{0.0, 0.25, 0.50, 0.75, 1.0\}$ and a KBH spin of $\tilde{S} = 0.99$.

3.4.2 Last Stable Orbit

In [29] a new analytical formula for the latus rectum of an elliptical equatorial LSO was developed. We can perform a similar treatment for inclined LSOs. But the polynomial that results is of ninth order in \tilde{l} , currently making the derivation of an analytical solution infeasible. The use of the companion matrix [39, 40, 29] simplifies the numerical calculation of the prograde and retrograde \tilde{l}_{LSO} .

We refer back to equations (3.25), (3.26), (3.30), and (3.31); because \tilde{E} will equal the maximum value of \tilde{V}_+ (closest to the event horizon) we can specify $r_3 = r_p$ as an additional condition [26, 33, 29]. Therefore the remaining root, r_4 , can be easily solved *viz.*

$$\frac{r_4 \tilde{l}^3}{(1+e)(1-e^2)} = \frac{Q \tilde{S}^2}{1 - \tilde{E}^2}, \quad (3.58)$$

to yield,

$$r_4 = \frac{Q \tilde{S}^2 (1+e)(1-e^2)}{(1 - \tilde{E}^2) \tilde{l}^3}. \quad (3.59)$$

Substituting the four roots (two of which are equal) into equation (3.43) yields

$$\frac{Q \tilde{S}^2 (1+e)(1-e^2)}{(1 - \tilde{E}^2) \tilde{l}^3} + 2 \frac{\tilde{l}}{1+e} + \frac{\tilde{l}}{1-e} = 2 (1 - \tilde{E}^2)^{-1}. \quad (3.60)$$

Substituting the expression for \tilde{E} (equation (3.44)) into equation (3.60) and cross multiplying, we obtain:

$$\tilde{l}^4 (1+e)^2 (1-e)^3 Z_{10} Z_{11} = 0 \quad (3.61)$$

where

$$Z_{10} = \left(-3\tilde{l} - 2\tilde{l}e + e^2\tilde{l}\right) X_{\pm}^2 + 4Q\tilde{S}^2 + 4Q\tilde{S}^2e - 2Q\tilde{l}e + Qe^2\tilde{l} - 3Q\tilde{l} + \tilde{l}^3$$

and

$$Z_{11} = (1 - e^2) \left(\tilde{l}X_{\pm}^2 + Q\tilde{l} - Q\tilde{S}^2\right) - \tilde{l}^3.$$

By setting $Z_{10} = 0$ and substituting the formula for X_{\pm}^2 (*viz.* equation (3.48)) one obtains a polynomial, $p(\tilde{l})$, in terms of \tilde{l} (to order 9), e , Q (to second order), and \tilde{S} (see equation (3.B7) in Appendix 3.B.3). The companion matrix of $p(\tilde{l})$ provides a powerful method to calculate the values of \tilde{l} for both a prograde and retrograde LSO by numerically evaluating the eigenvalues of the matrix. Optimised techniques for solving for eigenvalues are available [41, 42]. Such a numerical analysis was performed to obtain representative values of \tilde{l}_{LSO} . The corresponding values of \tilde{l}_{LSO} , which we derived from $Z_{11} = 0$ (*ceteris paribus*) were smaller and thus not physically reachable by a test-particle. This result demonstrates that $Z_{10} = 0$ is the appropriate solution.

Because $p(\tilde{l})$ is a quadratic in terms of Q , an alternative way to analyse the behaviour of orbits as they approach their LSO is available. One solves for Q , analytically, to obtain:

$$Q_{LSO} = \frac{1}{4} \left(Z_{12} - \tilde{S}^2 Z_{13} \sqrt{Z_{14}} \right) \left(\tilde{S}^4 Z_{15} \right)^{-1}, \quad (3.62)$$

where

$$\begin{aligned} Z_{12} &= \tilde{l}^4 (e+1) \left(\tilde{l}^2 - (2e^2 + e + 3)\tilde{l} + 2(e+1)(2e^2 - e + 3) \right) \tilde{S}^2 \\ &\quad - \tilde{l}^3 (e+1)^2 \left(2e^3 + e^2 + \tilde{l}(3-e) + 1 \right) \tilde{S}^4, \end{aligned}$$

$$Z_{13} = (3-e) \left((e+1)^2 \tilde{S}^2 - \tilde{l}(2e+2-\tilde{l}) \right),$$

$$Z_{14} = \tilde{l}^5 (e+1)^3 \left((e-1)^2 \tilde{S}^2 + \tilde{l}(\tilde{l} + 2e - 2) \right),$$

and

$$Z_{15} = (e+1)^2 \left((e-1)^2 (e+1)^3 \tilde{S}^2 - \tilde{l} \left(\tilde{l}^2 - (e+1)(e^2 - 2e + 3)\tilde{l} + (2e^2 - 4e + 3)(e+1)^2 \right) \right).$$

We now have, through equation (3.62), the means to plot the value of Q_{LSO} with respect to \tilde{l}_{LSO} . For a KBH, one may use \tilde{l}_{LSO} in the domain $[\tilde{l}_{LSO,prograde}, \tilde{l}_{LSO,retrograde}]$ as the independent variable.

3.4.3 The Abutment

The roots of equation (3.49) allow us to calculate the value of Q along the abutment (Q_X) in terms of the orbital values of \tilde{l} , e , and the KBH spin, \tilde{S} ; and we obtain, taking the minus sign of the quadratic solution:

$$Q_X = \frac{\tilde{l}^2}{2\tilde{S}^2(1-e^2)^2} \left(\tilde{l}(\tilde{l} - e^2 - 3) - \sqrt{\tilde{l}^2(\tilde{l} - e^2 - 3)^2 - 4\tilde{l}(1-e^2)^2\tilde{S}^2} \right). \quad (3.63)$$

Although equation (3.63) appears to have poles at $\tilde{S} = 0$ and $e = 1$, we can demonstrate that it reduces to a well behaved function at these values of \tilde{S} and e . We first factor out the term, $\tilde{l}(\tilde{l} - e^2 - 3)$, to obtain

$$Q_X = \frac{\tilde{l}^3(\tilde{l} - e^2 - 3)}{2(1-e^2)^2\tilde{S}^2} \left(1 - \sqrt{1 - \frac{4(1-e^2)^2\tilde{S}^2}{\tilde{l}(\tilde{l} - e^2 - 3)^2}} \right). \quad (3.64)$$

Equation (3.64) can be simplified by making a binomial expansion of its square root to yield,

$$Q_X = \frac{\tilde{l}^3 (\tilde{l} - e^2 - 3)}{2(1 - e^2)^2 \tilde{S}^2} \left\{ 1 - 1 + \frac{2(1 - e^2)^2 \tilde{S}^2}{\tilde{l} (\tilde{l} - e^2 - 3)^2} \right. \quad (3.65)$$

$$\left. + 2 \left[\frac{(1 - e^2)^2 \tilde{S}^2}{\tilde{l} (\tilde{l} - e^2 - 3)^2} \right]^2 + 4 \left[\frac{(1 - e^2)^2 \tilde{S}^2}{\tilde{l} (\tilde{l} - e^2 - 3)^2} \right]^3 + 10 \left[\frac{(1 - e^2)^2 \tilde{S}^2}{\tilde{l} (\tilde{l} - e^2 - 3)^2} \right]^4 \dots \right\}.$$

Equation (3.65), simplifies to a power series in terms of $(1 - e^2)^2 \tilde{S}^2$; therefore, only the first term will remain when $\tilde{S} = 0$ or $e = 1$. We now have a greatly simplified expression, which applies to elliptic orbits around an SBH and parabolic orbits about a KBH, i.e.

$$Q_X = \tilde{l}^2 (\tilde{l} - e^2 - 3)^{-1}$$

$$= \tilde{l}^2 (\tilde{l} - 4)^{-1}. \quad (3.66)$$

Further, as $\tilde{l} \rightarrow \infty$ in elliptical orbits,

$$\frac{4(1 - e^2)^2 \tilde{S}^2}{\tilde{l} (\tilde{l} - e^2 - 3)^2} \rightarrow 0, \quad (3.67)$$

therefore, a similar binomial treatment may be performed on equation (3.64) to yield $Q_X \cong \tilde{l} + e^2 + 3$ for large \tilde{l} . This result is consistent with the fact that as $\tilde{l} \rightarrow \infty$, the spacetime looks more Schwarzschild in nature. As in the case of equation (3.17), Q_X (equation (3.63)) also defines an upper limit on Q for specific values of \tilde{l} and e . The points above the Q_X curve are inaccessible, which can be shown by direct calculation.

This result confirms the choice of the minus sign in solving the quadratic equation (3.56) for Q_X . Recall that equation (3.48) applies to bound orbits in general and is not restricted to LSOs (as is the case for L_z^2 (see equation (3.14))). Therefore the value of Q_X can be evaluated for all values of $\tilde{l} \geq \tilde{l}_{LSO,prograde}$; and it will apply to both sets of

orbits governed by X_-^2 or X_+^2 .

3.4.4 Polar Orbit

We shall consider polar orbits in this paper, although orbits of arbitrary inclination are also important. The polar orbit (governed by X_-^2) is precisely defined by setting $\tilde{L}_z = 0$ from which we obtain $X_-^2 = \tilde{S}^2 \tilde{E}^2$; therefore, we can derive an analytical formula for Q of a polar orbit (Q_{polar}) of arbitrary \tilde{l} and e .

We have the formula for X_-^2 in terms of \tilde{l} , e , and Q (see equation (3.48)); because \tilde{E} can also be expressed in these terms (see equation (3.44)), $X_-^2 - \tilde{S}^2 \tilde{E}^2 = 0$ can be simplified and factored to yield:

$$A(B_1 Q - \tilde{l}^2 B_2) (C_1 Q - \tilde{l}^2 C_2) = 0 \quad (3.68)$$

where

$$A = \tilde{l}^3 - (2e^2 + 6)\tilde{l}^2 + (e^2 + 3)^2 \tilde{l} - 4\tilde{S}^2 (1 - e^2)^2,$$

$$B_1 = \tilde{l}^5 b_1 = \tilde{l}^5 \left\{ 1 - (3 + e^2)\tilde{l}^{-1} + 2\tilde{S}^2 (1 + e^2)\tilde{l}^{-2} - 2\tilde{S}^2 (1 - e^2)^2 \tilde{l}^{-3} + \tilde{S}^4 (1 - e^2)^2 \tilde{l}^{-4} + \tilde{S}^4 (1 - e^2)^3 \tilde{l}^{-5} \right\},$$

$$B_2 = \tilde{l}^4 b_2 = \tilde{l}^4 \left\{ 1 + 2\tilde{S}^2 (1 + e^2)\tilde{l}^{-2} - 4\tilde{S}^2 (1 - e^2)\tilde{l}^{-3} + \tilde{S}^4 (1 - e^2)^2 \tilde{l}^{-4} \right\},$$

$$C_1 = \tilde{l}^5 c_1 = \tilde{l}^5 \left\{ 1 - (3 + e^2)\tilde{l}^{-1} + 2\tilde{S}^2 (1 + e^2)\tilde{l}^{-2} + 2\tilde{S}^2 (1 - e^2)^2 \tilde{l}^{-3} - 3\tilde{S}^4 (1 - e^2)^2 \tilde{l}^{-4} + \tilde{S}^4 (1 - e^2)^3 \tilde{l}^{-5} \right\},$$

and

$$C_2 = \tilde{l}^4 c_2 = \tilde{l}^4 \left\{ 1 - 4\tilde{S}^2 \tilde{l}^{-1} + 2\tilde{S}^2 (3 - e^2) \tilde{l}^{-2} - 4\tilde{S}^2 (1 - e^2) \tilde{l}^{-3} + \tilde{S}^4 (1 - e^2)^2 \tilde{l}^{-4} \right\}.$$

The factor A offers no physically meaningful results. It does not provide a solution for Q ; and for $0 \leq \tilde{S} < 1.0$ and $0 \leq e \leq 1.0$, we find that $3 \leq \tilde{l} \leq 4$, which lies beyond the LSO. The factor, $B_1 Q - \tilde{l}^2 B_2 = 0$, yields the result

$$Q_{polar} = \tilde{l}^2 B_2 B_1^{-1}. \quad (3.69)$$

And the factor, $C_1 Q - \tilde{l}^2 C_2 = 0$, yields the result

$$Q_{polar} = \tilde{l}^2 C_2 C_1^{-1}. \quad (3.70)$$

We examine equations (3.69) and (3.70) to discover which one is physically significant. In the Schwarzschild limit ($\tilde{S} \rightarrow 0$) we find that they coincide. But let us consider the weak field limit ($\tilde{l} \rightarrow \infty$). Equation (3.69), $Q_{polar} = \tilde{l} b_2 b_1^{-1}$, can be expanded in powers of \tilde{l} . And the terms with powers of \tilde{l}^{-1} and lower approach zero as $\tilde{l} \rightarrow \infty$ to yield the asymptotic limit of equation (3.69):

$$Q_{polar} \cong \tilde{l} + 3 + e^2. \quad (3.71)$$

In a similar treatment of equation (3.70) one obtains:

$$\tilde{l} c_2 c_1^{-1} \cong \tilde{l} + 3 + e^2 - 4\tilde{S}^2, \quad (3.72)$$

which we can disregard as unphysical because it incorrectly implies that the spin of the KBH influences the trajectory of a test-particle at infinity. This situation differs from that described by equation (3.54), which does not describe a trajectory. Test calcula-

tions confirm that equation (3.69) is the appropriate choice and equation (3.70) can be disregarded since the values of \tilde{l}_{LSO} obtained by solving equation (3.70) are less than (or equal to) the results from equation (3.69) (*ceteris paribus*). Equation (3.69) applies to all bound orbits, hence Q_{polar} can be evaluated over a range $\tilde{l} \geq \tilde{l}_{LSO,prograde}$; but it applies only to orbits governed by X_-^2 . In the SBH case ($\tilde{S} = 0$), $B_1 = \tilde{l}^5 - (3 + e^2)\tilde{l}^4$ and $B_2 = \tilde{l}^4$. Therefore

$$Q_{polar} = \tilde{l}^2 \left(\tilde{l} - e^2 - 3 \right)^{-1}, \quad (3.73)$$

which has an asymptotic behaviour similar to that of Q_X .

3.4.5 Some Characteristics of the Carter Constant Formulae

3.4.5.1 The last stable orbit on the abutment

In figures (3-5) and (3-6) one observes that the functions for Q_X and Q_{LSO} intersect at a single tangential point, which represents the value of \tilde{l} of an LSO that lies at the abutment described by X_{\pm}^2 . The equation $Q_X - Q_{LSO} = 0$ (see equations (3.63) and (3.62)) can be solved to yield:

$$\tilde{l}_{LSO,abutment} = \frac{1}{12} \left(Z_{16}^{\frac{1}{3}} + \chi_1 + \chi_0 Z_{16}^{-\frac{1}{3}} \right), \quad (3.74)$$

where

$$Z_{16} = \left(216 (1 + e) (5 + e)^2 (1 - e)^2 \tilde{S}^2 + \chi_1 \chi_2 \chi_3 \right) + 12 \sqrt{3 Z_{17}},$$

$$\begin{aligned} Z_{17} &= (1 + e) (5 + e)^2 \\ &\times \left\{ 108 (1 + e) (5 + e)^2 (1 - e)^4 \tilde{S}^4 + \chi_1 \chi_2 \chi_3 (1 - e)^2 \tilde{S}^2 - (1 + e) (9 - e^2)^2 \chi_4^2 \right\}, \end{aligned}$$

$$\chi_0 = e^6 + 6e^5 - 9e^4 - 60e^3 + 111e^2 + 342e + 441,$$

$$\chi_1 = e^3 + 3e^2 + 3e + 33, \quad \chi_2 = e^3 + 3e^2 - 9e - 3,$$

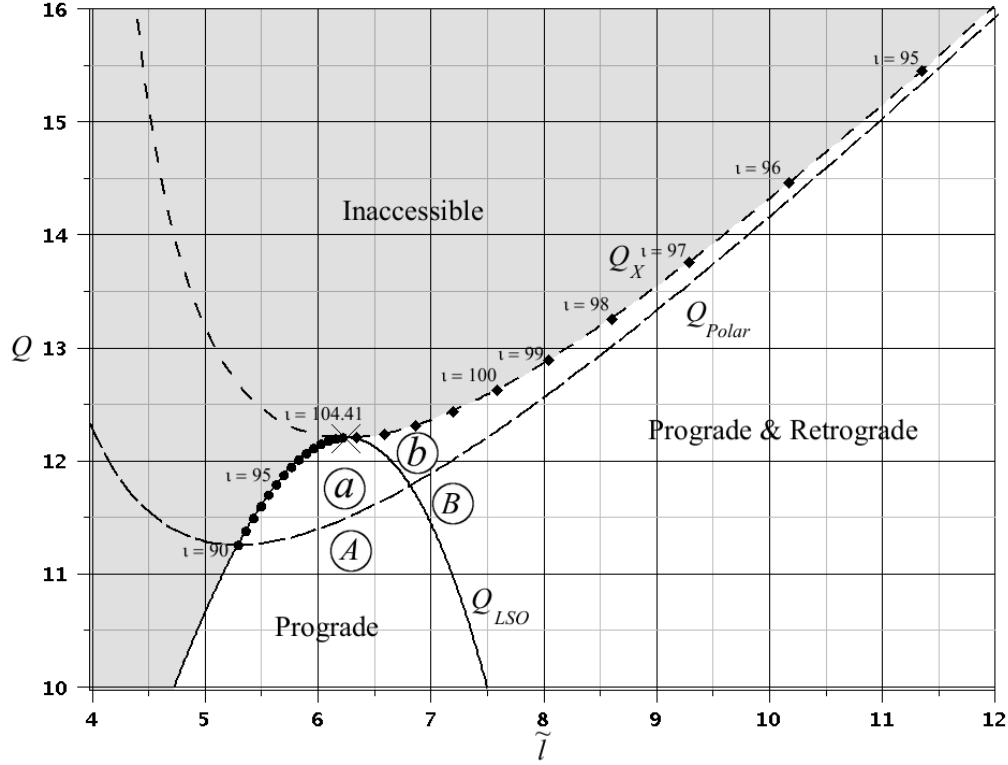


Figure 3-6: The three Q formulae derived in Section 3.4 define a map. In zone (A), only prograde orbits are found. And in zone (B), both prograde and retrograde orbits are found. Above the Q_{polar} curve (zones (a) and (b)) only retrograde orbits can exist. But in zone (a), the orbits are governed by X_-^2 ; while in zone (b), they are governed by either X_-^2 or X_+^2 . The points along Q_X and Q_{LSO} mark the values of ν . In this case the orbit is circular ($e = 0$) and the KBH spin is $\tilde{S} = 0.99$.

$$\chi_3 = e^3 + 3e^2 - 21e - 39, \quad \chi_4 = e^3 + 3e^2 - 5e + 9.$$

It is at this tangential point that the Q_{LSO} curve is split into two segments: the minus segment ($\tilde{l} < \tilde{l}_{LSO,abutment}$) that defines the values of \tilde{l}_{LSO} (and Q_{LSO}) associated with inclined LSOs that are governed by X_-^2 ; and the plus segment ($\tilde{l} > \tilde{l}_{LSO,abutment}$), which corresponds to inclined LSOs governed by X_+^2 . Consequently, the points beneath Q_{LSO} define only orbits governed by X_-^2 . Further, orbits with \tilde{l} and Q values that lie to the left of the minus segment of Q_{LSO} are undefined. Therefore the Q_{LSO} curve for $\tilde{l} < \tilde{l}_{LSO,abutment}$ and the Q_X curve for $\tilde{l} > \tilde{l}_{LSO,abutment}$ define a curve along which the upper limit of Q is specified.

Table 3.1: Parameters calculated for the tangential intersection of the Q_X and Q_{LSO} curves for an elliptical orbit about a KBH of spin $\tilde{S} = 0.5$ and $\tilde{S} = 0.99$. The \tilde{l} of the LSO at the maximum point of the Q_{LSO} curve is included for comparison.

| e | $\tilde{S} = 0.50$ | | | | $\tilde{S} = 0.99$ | | | |
|-----|--------------------|----------------|-----------------------------|------------------------|--------------------|----------------|-----------------------------|------------------------|
| | Q_{LSO} | ι (deg.) | $\tilde{l}_{LSO, abutment}$ | $\tilde{l}_{LSO, max}$ | Q_{LSO} | ι (deg.) | $\tilde{l}_{LSO, abutment}$ | $\tilde{l}_{LSO, max}$ |
| 0.0 | 12.054503 | 97.6 | 6.067459 | 6.067459 | 12.203171 | 104.4 | 6.245480 | 6.245480 |
| 0.1 | 12.102329 | 97.2 | 6.256148 | 6.268429 | 12.245340 | 103.8 | 6.407328 | 6.449754 |
| 0.2 | 12.237084 | 96.9 | 6.445623 | 6.467077 | 12.366092 | 103.3 | 6.570627 | 6.646723 |
| 0.3 | 12.449596 | 96.7 | 6.635958 | 6.663706 | 12.559674 | 103.0 | 6.735976 | 6.836993 |
| 0.4 | 12.734670 | 96.6 | 6.827228 | 6.858566 | 12.823381 | 102.8 | 6.903945 | 7.020995 |
| 0.5 | 13.090081 | 96.5 | 7.019514 | 7.051863 | 13.156912 | 102.7 | 7.075097 | 7.199015 |
| 0.6 | 13.515997 | 96.5 | 7.212909 | 7.243768 | 13.562022 | 102.7 | 7.250004 | 7.371204 |
| 0.7 | 14.014676 | 96.6 | 7.407517 | 7.434425 | 14.042359 | 102.9 | 7.429271 | 7.537586 |
| 0.8 | 14.590357 | 96.7 | 7.603465 | 7.623953 | 14.603445 | 103.1 | 7.613543 | 7.698050 |
| 0.9 | 15.249308 | 96.9 | 7.800900 | 7.812451 | 15.252772 | 103.5 | 7.803527 | 7.852335 |
| 1.0 | 16.000000 | 97.1 | 8.000000 | 8.000000 | 16.000000 | 103.9 | 8.000000 | 8.000000 |

Calculations of the value of $\tilde{l}_{LSO,abutment}$ (equation (3.74)) were performed for various eccentricities and two values of KBH spin ($\tilde{S} = 0.5$ and $\tilde{S} = 0.99$); they are listed in table 3.1. We have also numerically calculated the values of \tilde{l} for the maximal point of the Q_{LSO} curve and listed them for comparison. For both circular and parabolic orbits,

$$\tilde{l}_{LSO,abutment} = \tilde{l}_{LSO,max}, \quad (3.75)$$

regardless of the value of \tilde{S} . Otherwise,

$$\tilde{l}_{LSO,abutment} < \tilde{l}_{LSO,max}, \quad (3.76)$$

from which one may infer the curve that specifies the upper limit of Q is monotonically increasing with respect to \tilde{l} (with a point of inflection at $\tilde{l}_{LSO,abutment}$ for circular and parabolic orbits). The values of $\tilde{l}_{LSO,abutment}$ show that the upper limit of Q also increases monotonically with respect to e . Further, $\tilde{l}_{LSO,abutment} = 8.0$ for a parabolic orbit, which equals the \tilde{l}_{LSO} of a parabolic orbit about an SBH.

3.4.5.2 The last stable polar orbit

The polar curve applies to polar orbits, which are governed by X_-^2 ; therefore, only the intersection of the Q_{polar} curve with the minus segment of the Q_{LSO} curve ($\tilde{l} < \tilde{l}_{LSO,abutment}$) needs to be considered. It is at this point that the \tilde{l}_{LSO} of a polar orbit of arbitrary e is defined. It was found from numerical calculations of $\tilde{l}_{polar,LSO}$ (where the Q_{polar} curve intersects the minus segment of the Q_{LSO} curve) and \tilde{l} value at the minimal point of Q_{polar} that in the case of circular and parabolic orbits,

$$\tilde{l}_{polar,min} = \tilde{l}_{polar,LSO}; \quad (3.77)$$

otherwise,

$$\tilde{l}_{polar,min} < \tilde{l}_{polar,LSO}. \quad (3.78)$$

One may infer from this result that the value of Q_{polar} is monotonically increasing with respect to \tilde{l} (and has a point of inflection at $\tilde{l}_{polar, LSO}$ for circular and parabolic orbits).

3.4.5.3 The Schwarzschild limiting case

The analysis of these formulae in the case where $\tilde{S} \rightarrow 0$ is an important test. An examination of the analytical formulae for Q_{switch} (equation (3.51)), Q_X (equation (3.63)), and Q_{polar} (equation (3.69)), show that when $\tilde{S} = 0$, all three formulae equal

$$Q = \tilde{l}^2 (\tilde{l} - e^2 - 3)^{-1}. \quad (3.79)$$

In the Schwarzschild limit, we find that the abutment and the set of polar orbits approach one another, as required by the spherical symmetry of Schwarzschild spacetime.

3.5 The Analysis of the Carter Constant for an Evolving Orbit

3.5.1 Introduction

We shall now perform an analysis of the evolution of Q in Kerr spacetime in the domain, which is defined by the three Q curves we have derived (Q_{LSO} , Q_X , Q_{polar}) in equations (3.62), (3.63), and (3.69). The behaviour of Q_{switch} (equation (3.50)) will not be considered here, although it is important in guiding the choice of sign in $\pm\sqrt{X_-^2}$.

The three equations for Q_X , Q_{LSO} , and Q_{polar} define a map (see figure 3-6) from which one might infer the characteristics of a path followed by an inclined orbit as it evolves. These paths (Q_{path}) fall into two families: one governed by X_-^2 and the other by X_+^2 . We conjecture that paths in the same family never cross; therefore, if Q_{path} reaches Q_X , then it can do so only once. Let us concentrate on the behaviour of an evolving orbit at the abutment, which is where, Q_{path} , may change from one family to the other.

Therefore there are two modes to consider:

$$X_-^2 \Rightarrow X_+^2 \quad (3.80)$$

and

$$X_+^2 \Rightarrow X_-^2. \quad (3.81)$$

The mode represented by equation (3.80) corresponds to a rapid listing rate, where prograde orbits can cross Q_{polar} and intersect Q_X . The mode represented by equation (3.81) corresponds to orbits that: list at a slow rate, have constant ι , or exhibit decreasing ι over time. And a prograde orbit cannot reach Q_X ; even if it crosses Q_{polar} .

For this paper we will consider the evolution of a circular orbit ($e = 0$) because we wish to limit our initial analysis to the relationship between Q and \tilde{l} . Elliptical orbits will be treated in a forthcoming paper [38].

3.5.2 The Evolutionary Path in the $Q - \tilde{l}$ Plane

In figure 3-6 one may imagine a path, Q_{path} , that starts at a large value of \tilde{l} as both Q and \tilde{l} monotonically decrease with respect to time. If the curve reaches Q_X then it must intersect it tangentially (as the zone above the Q_X curve is inaccessible). It is at that point that the orbit ceases to be governed by X_{\mp}^2 and is governed by X_{\pm}^2 .

At the abutment, $\partial Q/\partial \tilde{l}$ and $\partial Q/\partial e$ can be calculated analytically (see Appendix 3.B.4) regardless of the model used to determine the radiation back reaction. Given an $\dot{\tilde{l}} = d\tilde{l}/dt$ and $\dot{e} = de/dt$ that have been derived according to some independent model, then according to a linear approximation one may define

$$\dot{Q} = \frac{\partial Q}{\partial \tilde{l}} \dot{\tilde{l}} + \frac{\partial Q}{\partial e} \dot{e}. \quad (3.82)$$

For a circular orbit ($e = 0$) it has been proven that $\dot{e} = 0$ [18]; therefore, the second term in equation (3.82) is zero.

Table 3.2: An estimate of $(M^2/m) \partial \tilde{l} / \partial t$, based on equation (3.83), for circular orbits. The values in parenthesis (which were originally calculated at $\iota \cong \pi/3$) are taken from Hughes [4] and have been adjusted to by dividing by $\sin(\iota)$.

| | $\tilde{l} = 7$ | | $\tilde{l} = 100$ | |
|--------------------|--------------------------|----------------------------|--------------------------|----------------------------|
| $\tilde{S} = 0.05$ | -1.1827×10^{-1} | (-1.2638×10^{-1}) | -1.2683×10^{-5} | (-1.4637×10^{-5}) |
| $\tilde{S} = 0.95$ | -1.3747×10^{-1} | (-5.2540×10^{-2}) | -1.2679×10^{-5} | (-1.4553×10^{-5}) |

3.5.2.1 A Preliminary Test at the Abutment

Because we can perform an analytical calculation of $\partial Q / \partial \tilde{l}$ at the abutment, we can estimate $\dot{\tilde{l}}$ viz. equation (3.82),

$$\frac{\partial \tilde{l}}{\partial t} = \dot{Q} \left(\frac{\partial Q}{\partial \tilde{l}} \right)^{-1}, \quad (3.83)$$

if the 2PN Q flux (see equation (A.3) in [22] (after equation (56) in [5])) is known, i.e.

$$\begin{aligned} \left(\frac{\partial Q}{\partial t} \right)_{2PN} &= -\sin(\iota) \frac{64 m^2}{5 M} (1 - e^2)^{3/2} \tilde{l}^{-7/2} \sqrt{Q} \\ &\times \left[g_9(e) - \tilde{l}^{-1} g_{11}(e) + \left(\pi g_{12}(e) - \cos(\iota) \tilde{S} g_{10}^b(e) \right) \tilde{l}^{-3/2} \right. \\ &\quad \left. - \left(g_{13}(e) - \tilde{S}^2 \left(g_{14}(e) - \frac{45}{8} \sin^2(\iota) \right) \right) \tilde{l}^{-2} \right], \end{aligned} \quad (3.84)$$

where the functions $g_9(e)$, $g_{10}^b(e)$, $g_{11}(e)$, $g_{12}(e)$, $g_{13}(e)$, and $g_{14}(e)$ are listed in Appendix 3.B.5 (the Carter constant, Q , has been normalised by dividing by $(mM)^2$). We performed test calculations on circular orbits of $\tilde{l} = \{7.0, 100.0\}$ with KBH spin $\tilde{S} = \{0.05, 0.95\}$, which correspond to those used by Hughes [4]. In table 3.2, we compare our results with those of Hughes to find that they are reasonably consistent, with some deviation for $\tilde{S} = 0.95$ and $\tilde{l} = 7.0$. We have adjusted the results in Hughes by dividing them by $\sin(\iota)$ (where $\iota \cong \pi/3$) so that they will correspond to our near-polar orbits; but this is only an approximation since ι appears in other terms in equation (3.84).

3.5.3 The Analysis of ι on the Abutment

The analysis of ι and its derivatives with respect to \tilde{l} and e will be treated in detail in a forthcoming paper [38]; but it is appropriate to present a short preliminary exploration here.

Unlike Q_{2PN} (which appears in equation (3.84)), Q_X contains no explicit variable ι , therefore, for circular orbits this property greatly simplifies the total derivative of Q_X with respect to \tilde{l} since $\partial Q_X / \partial \iota = 0$, i.e.

$$\begin{aligned} \frac{dQ_X}{d\tilde{l}} &= \frac{\partial Q_X}{\partial \tilde{l}} + \frac{\partial Q_X}{\partial \iota} \frac{\partial \iota}{\partial \tilde{l}} \\ &= \frac{\partial Q_X}{\partial \tilde{l}}. \end{aligned} \quad (3.85)$$

Therefore equation (3.85) demonstrates that $\partial \iota / \partial \tilde{l}$ is not constrained on the abutment in the same way as $\partial Q / \partial \tilde{l}$ (see section 3.5.2.1). Consider equations (3.63), (3.48), (3.44), and (3.42). They form a calculation sequence, which on the abutment creates a one to one mapping, $Q_X \rightarrow \iota$; otherwise, there are two possible values of ι for a given value of Q . Thus $\partial \iota / \partial \tilde{l}$ can be found either by numerical methods or analytically [38]. In the remainder of this section we shall investigate the behaviour of $\partial \iota / \partial \tilde{l}$ for orbits on the abutment.

3.5.3.1 Numerical Analysis of ι on the abutment

We can numerically estimate the change of ι with respect to \tilde{l} at the abutment by first finding the change in Q for an extrapolation of the evolving orbit's path (Q_{path}). Because both $Q_{path} = Q_X$ and $\partial Q_{path} / \partial \tilde{l} = \partial Q_X / \partial \tilde{l}$ at the point where Q_{path} intersects Q_X , the equations of the second-order extrapolation of Q_{path} at the abutment can be written as

$$Q_{path}(\tilde{l} - \delta\tilde{l}) = Q_X - \delta\tilde{l} \frac{\partial Q_X}{\partial \tilde{l}} + \frac{\delta\tilde{l}^2}{2} \frac{\partial^2 Q_{path}}{\partial \tilde{l}^2} \quad (3.86)$$

$$Q_{path}(\tilde{l} + \delta\tilde{l}) = Q_X + \delta\tilde{l} \frac{\partial Q_X}{\partial \tilde{l}} + \frac{\delta\tilde{l}^2}{2} \frac{\partial^2 Q_{path}}{\partial \tilde{l}^2}. \quad (3.87)$$

These equations are used to calculate ι_- (associated with $\tilde{l} - \delta\tilde{l}$) and ι_+ ($\tilde{l} + \delta\tilde{l}$), where $\delta\tilde{l}$ is the small amount (10^{-32}) by which we extrapolate from the value of \tilde{l} at which Q_X and Q_{path} intersect. Equations (3.86) and (3.87) include the second derivative of Q_{path} with respect to \tilde{l} , which warrants further analysis.

Because $\delta\tilde{l}$ is so small we used MATLAB, set to a precision of 256 digits, to perform the numerical analysis. From these extrapolated values of Q_{path} we obtain

$$\frac{\partial\iota}{\partial\tilde{l}} \cong (\iota_+ - \iota_-) (2\delta\tilde{l})^{-1}. \quad (3.88)$$

Since ι increases as \tilde{l} decreases (with respect to time), $\partial\iota/\partial\tilde{l} \leq 0$.

3.5.3.2 The first-order extrapolation

Consider a first-order linear approximation, in which we drop the second derivatives in equations (3.86) and (3.87). The derivation of the corresponding change in ι requires a sequence of calculations to be performed, which we will briefly outline.

1. Specify the spin (\tilde{S}) of the KBH.
2. Select the values of \tilde{l} and e for the point of intersection with the abutment. For this work, $e = 0$.
3. Calculate Q_X using equation (3.63) and $\partial Q_X/\partial\tilde{l}$ using equation (3.B8) (given in Appendix 3.B.4).
4. Calculate $\tilde{l}_{LSO,abutment}$ using equation (3.74). It must be smaller than the value of \tilde{l} specified in point (2) otherwise the test-particle would be placed beyond the LSO.
5. Calculate the values of $Q_{path}(\tilde{l} - \delta\tilde{l})$ and $Q_{path}(\tilde{l} + \delta\tilde{l})$ according to a prescribed estimate or extrapolation at \tilde{l} .
6. Calculate X_- and X_+ (equation (3.48)) from $Q_{path}(\tilde{l} + \delta\tilde{l})$ (We use $-\sqrt{X_+^2}$ and we must use $-\sqrt{X_-^2}$ if $Q_{path}(\tilde{l} \pm \delta\tilde{l}) > Q_{switch}$).

7. Calculate X_+ and X_- from $Q_{path}(\tilde{l} - \delta\tilde{l})$.
8. Using equation (3.44), calculate the orbital energies (\tilde{E}) for each of $Q_{path}(\tilde{l} - \delta\tilde{l})$ and $Q_{path}(\tilde{l} + \delta\tilde{l})$.
9. Now that the values of X_+ , X_- , \tilde{E} , \tilde{l} are known, the value of ι (ι_- and ι_+) can be calculated *viz.* equation (3.42). We use the expression, $\tilde{L}_z = X + \tilde{S}\tilde{E}$.
10. We can estimate $\partial\iota/\partial\tilde{l}$ *viz.* equation (3.88).

We have performed this sequence of first-order calculations for each mode (equations (3.80) and (3.81)) over a range of \tilde{S} and \tilde{l} values; a representative set is shown in table 3.3. The slow and fast modes yield $\partial\iota/\partial\tilde{l}$ values that are of opposite sign; and these results might suggest that the slow mode corresponds to orbits for which $\partial\iota/\partial t < 0$. But let us first assess the validity of the first-order approximation by testing it in the Schwarzschild limit. The results for small \tilde{S} (table 3.3) demonstrate that this approximation is incomplete since it produces a non-zero result for $\tilde{S} \gtrsim 0$, which is unphysical. On each side of the abutment, the value of Q_{path} is underestimated. This observation warrants the study of a more complete model that includes the higher derivatives of Q_{path} . Indeed, we have found that using $\partial Q_X/\partial\tilde{l}$ alone cannot offer a sufficiently accurate mathematical description of the orbital evolution at the abutment and warrants the development of second and higher derivatives of Q_{path} . One reasonably expects this numerical method to produce an accurate estimate of $\partial\iota/\partial\tilde{l}$; but the transition an orbit makes at the abutment from X_{\mp}^2 to X_{\pm}^2 makes its behaviour more complicated.

Table 3.3: The values of $\partial\iota/\partial\tilde{l}$ (in radians) obtained by a linear extrapolation by $\delta\tilde{l} = 10^{-32}$

| | $\tilde{l} = 6.25$ | $\tilde{l} = 7.0$ | $\tilde{l} = 10.0$ | $\tilde{l} = 100$ |
|---|--------------------------------|--------------------------------|--------------------------------|--------------------------------|
| $\tilde{S} = 0.99$ | | | | |
| ι (deg) | 104.3865 | 101.5796 | 96.1803 | 90.1719 |
| 1st-order (slow) | $+8.7969235019 \times 10^{-2}$ | $+6.3997248415 \times 10^{-2}$ | $+2.6730499968 \times 10^{-2}$ | $+2.6454077633 \times 10^{-4}$ |
| 1st-order (fast) | $-2.4667033336 \times 10^{-1}$ | $-1.7158228931 \times 10^{-1}$ | $-6.3094796456 \times 10^{-2}$ | $-3.5520692654 \times 10^{-4}$ |
| 2nd-order (slow) | $-7.9350549169 \times 10^{-2}$ | $-5.3792520450 \times 10^{-2}$ | $-1.8182148244 \times 10^{-2}$ | $-4.5333075104 \times 10^{-5}$ |
| $(\partial\iota/\partial\tilde{l})_{min}$ | $-7.9350549169 \times 10^{-2}$ | $-5.3792520450 \times 10^{-2}$ | $-1.8182148244 \times 10^{-2}$ | $-4.5333075104 \times 10^{-5}$ |
| $\tilde{S} = 0.5$ | | | | |
| ι (deg) | 97.2125 | 95.8133 | 93.1100 | 90.0868 |
| 1st-order (slow) | $+1.1326853682 \times 10^{-1}$ | $+8.3013385020 \times 10^{-2}$ | $+3.4263245153 \times 10^{-2}$ | $+2.8653789706 \times 10^{-4}$ |
| 1st-order (fast) | $-1.7629701738 \times 10^{-1}$ | $-1.3675258947 \times 10^{-1}$ | $-5.2506108860 \times 10^{-2}$ | $-3.3232275582 \times 10^{-4}$ |
| 2nd-order (slow) | $-3.9452655089 \times 10^{-2}$ | $-2.6869602227 \times 10^{-2}$ | $-9.1214318535 \times 10^{-3}$ | $-2.2892429382 \times 10^{-5}$ |
| $(\partial\iota/\partial\tilde{l})_{min}$ | $-3.9452655089 \times 10^{-2}$ | $-2.6869602227 \times 10^{-2}$ | $-9.1214318535 \times 10^{-3}$ | $-2.2892429382 \times 10^{-5}$ |
| $\tilde{S} = 0.1$ | | | | |
| ι (deg) | 91.4387 | 91.1602 | 90.6212 | 90.0174 |
| 1st-order (slow) | $+1.4004830192 \times 10^{-1}$ | $+1.0190058051 \times 10^{-1}$ | $+4.1058187759 \times 10^{-2}$ | $+3.0470614607 \times 10^{-4}$ |
| 1st-order (fast) | $-1.5573934281 \times 10^{-1}$ | $-1.1260500157 \times 10^{-1}$ | $-4.4698385942 \times 10^{-2}$ | $-3.1386271509 \times 10^{-4}$ |
| 2nd-order (slow) | $-7.8455204437 \times 10^{-3}$ | $-5.3522105306 \times 10^{-3}$ | $-1.8200990911 \times 10^{-3}$ | $-4.5782845088 \times 10^{-6}$ |
| $(\partial\iota/\partial\tilde{l})_{min}$ | $-7.8455204437 \times 10^{-3}$ | $-5.3522105306 \times 10^{-3}$ | $-1.8200990911 \times 10^{-3}$ | $-4.5782845088 \times 10^{-6}$ |

Table 3.3: (Continued.)

| | $\tilde{l} = 6.25$ | $\tilde{l} = 7.0$ | $\tilde{l} = 10.0$ | $\tilde{l} = 100$ |
|---|--------------------------------|--------------------------------|--------------------------------|---------------------------------|
| $\tilde{S} = 1.00 \times 10^{-3}$ | | | | |
| ι (deg) | 90.0144 | 90.0116 | 90.0062 | 90.0002 |
| 1st-order (slow) | $+1.4761389187 \times 10^{-1}$ | $+1.0708935531 \times 10^{-1}$ | $+4.2838945741 \times 10^{-2}$ | $+3.0923256836 \times 10^{-4}$ |
| 1st-order (fast) | $-1.4777076382 \times 10^{-1}$ | $-1.0719638097 \times 10^{-1}$ | $-4.2875344203 \times 10^{-2}$ | $-3.0932413388 \times 10^{-4}$ |
| 2nd-order (slow) | $-7.8435978256 \times 10^{-5}$ | $-5.3512828102 \times 10^{-5}$ | $-1.8199230792 \times 10^{-5}$ | $-4.5782761194 \times 10^{-8}$ |
| $(\partial \iota / \partial \tilde{l})_{min}$ | $-7.8435978256 \times 10^{-5}$ | $-5.3512828102 \times 10^{-5}$ | $-1.8199230792 \times 10^{-5}$ | $-4.5782761194 \times 10^{-8}$ |
| $\tilde{S} = 1.00 \times 10^{-6}$ | | | | |
| ι (deg) | 90.0000 | 90.0000 | 90.0000 | 90.0000 |
| 1st-order (slow) | $+1.4769222926 \times 10^{-1}$ | $+1.0714280363 \times 10^{-1}$ | $+4.2857124658 \times 10^{-2}$ | $+3.0927830473 \times 10^{-4}$ |
| 1st-order (fast) | $-1.4769238613 \times 10^{-1}$ | $-1.0714291066 \times 10^{-1}$ | $-4.2857161056 \times 10^{-2}$ | $-3.0927839630 \times 10^{-4}$ |
| 2nd-order (slow) | $-7.8435976327 \times 10^{-8}$ | $-5.3512827171 \times 10^{-8}$ | $-1.8199230615 \times 10^{-8}$ | $-4.5782761185 \times 10^{-11}$ |
| $(\partial \iota / \partial \tilde{l})_{min}$ | $-7.8435976331 \times 10^{-8}$ | $-5.3512827174 \times 10^{-8}$ | $-1.8199230616 \times 10^{-8}$ | $-4.5782761186 \times 10^{-11}$ |

3.5.3.3 The second-order extrapolation

Equations (3.86) and (3.87) provide a second-order approximation of Q_{path} in the vicinity of the point of tangential intersection between Q_X and Q_{path} . At this formative stage of our work with the abutment, we will use $\partial^2 Q_X / \partial \tilde{l}^2$ (see equation (3.B10) in Appendix 3.B.4) in place of $\partial^2 Q_{path} / \partial \tilde{l}^2$ in equations (3.86) and (3.87) as an approximation. We repeated the ten-point sequence of calculations for the slow mode (equation (3.81)), as outlined in section 3.5.3.2. The results of this numerical analysis are included in table 3.3. We observe that as $\tilde{S} \rightarrow 0$, $\partial \iota / \partial \tilde{l} \rightarrow 0$, as required. Further, the second-order $\partial \iota / \partial \tilde{l}$ results for the slow mode represent listing orbits (i.e. $\partial \iota / \partial \tilde{l} < 0$); therefore, the maximum list rate associated with paths that change from $X_+^2 \Rightarrow X_-^2$ (slow) at the abutment will have an upper limit that corresponds to the minimal value of $\partial \iota / \partial \tilde{l}$ for that mode.

3.5.3.4 The calculation of $\left(\partial \iota / \partial \tilde{l}\right)_{min}$

Let us consider the use of the Q_X curve itself to estimate the value of $\left(\partial \iota / \partial \tilde{l}\right)_{min}$ of an evolving orbit as it intersects the abutment. In this case,

$$Q_{path}(\tilde{l} - \delta \tilde{l}) = Q_X(\tilde{l} - \delta \tilde{l}) \quad (3.89)$$

$$Q_{path}(\tilde{l} + \delta \tilde{l}) = Q_X(\tilde{l} + \delta \tilde{l}), \quad (3.90)$$

where we have assumed that the path followed by the evolving orbit locally matches the Q_X curve (equations (3.89) and (3.90) that are used in point 5). This analysis yields the minimum value of $\left(\partial \iota / \partial \tilde{l}\right)_{min}$ at \tilde{l} for a KBH spin, \tilde{S} , as specified in point (1). For the slow mode, the rate of change of ι can be no smaller. If Q_{path} deviates from Q_X in its second and higher derivatives, then the actual value of $\partial \iota / \partial \tilde{l}$ will be greater than $\left(\partial \iota / \partial \tilde{l}\right)_{min}$.

Table 3.4: The coefficients and powers of the series that describes $\left(\partial\iota/\partial\tilde{l}\right)_{min}$.

| | Range | ϱ | κ_1 | κ_3 |
|-----------|------------------------------------|-------------------------------|-------------------------------|-------------------------------|
| $f_{2.5}$ | $10^9 \leq \tilde{l} \leq 10^{12}$ | $-2.500 \pm 3 \times 10^{-7}$ | $4.500 \pm 5 \times 10^{-13}$ | |
| $f_{3.5}$ | $10^7 \leq \tilde{l} \leq 10^{12}$ | $-3.500 \pm 7 \times 10^{-9}$ | $7.500 \pm 1 \times 10^{-7}$ | |
| $f_{4.5}$ | $10^5 \leq \tilde{l} \leq 10^{12}$ | $-4.500 \pm 2 \times 10^{-7}$ | $31.5 \pm 4 \times 10^{-9}$ | $8.75 \pm 1 \times 10^{-4}$ |
| $f_{5.5}$ | $10^2 \leq \tilde{l} \leq 10^{12}$ | $-5.500 \pm 2 \times 10^{-4}$ | $122.70 \pm 2 \times 10^{-8}$ | $-35.98 \pm 9 \times 10^{-4}$ |

3.5.3.5 Analysis

In table 3.3 the values of $\left(\partial\iota/\partial\tilde{l}\right)_{min}$ are in good agreement with the second-order calculations, although a difference is evident for $\tilde{S} = 10^{-6}$.

We calculated $\left(\partial\iota/\partial\tilde{l}\right)_{min}$ for various KBH spins ($10^{-18} \leq \tilde{S} \leq 0.99$) over a wide range of orbit sizes ($10^2 \leq \tilde{l} \leq 10^{12}$). It was noted that the results for very large orbits were described well by an equation of the form

$$\left(\frac{\partial\iota}{\partial\tilde{l}}\right)_{min} = -\kappa_1\tilde{S}\tilde{l}^e \quad (3.91)$$

and that κ_1 and e can be found by performing a least squares fit on $\left|\left(\partial\iota/\partial\tilde{l}\right)_{min}\right|$. For orbits closer to the LSO, we find that

$$\left(\frac{\partial\iota}{\partial\tilde{l}}\right)_{min} = -\left(\kappa_1\tilde{S} + \kappa_3\tilde{S}^3\right)\tilde{l}^e. \quad (3.92)$$

In figure 3-7, $\left|\left(\partial\iota/\partial\tilde{l}\right)_{min}\right|$ data for the range $10^9 \leq \tilde{l} \leq 10^{12}$ are shown on a log-log plot. By linear regression analysis, its asymptotic behaviour ($f_{2.5}$) can be found (see table 3.4). In successive steps each power of \tilde{l} in the series can be derived as the higher powers are subtracted from the original numerical data-set. A linear relationship between $\left(\partial\iota/\partial\tilde{l}\right)_{min}$ and \tilde{S} is found for $f_{2.5}$ and $f_{3.5}$; but for $f_{4.5}$ and $f_{5.5}$, which cover ranges of \tilde{l} closer to the LSO, an \tilde{S}^3 term appears. The correlation coefficients (r^2) of these regression analyses were better than 99.9999%.

Table 3.5: An estimate of $(M^2/m) \partial\iota/\partial t$, based on equation (3.94), for circular orbits. The values in parenthesis (which were originally calculated at $\iota \cong \pi/3$) are taken from Hughes [4] and have been adjusted by dividing by $\sin(\iota)$.

| | $\tilde{l} = 7$ | | $\tilde{l} = 100$ | |
|--------------------|--------------------------|----------------------------|---------------------------|-----------------------------|
| $\tilde{S} = 0.05$ | -9.4541×10^{-5} | (-1.2557×10^{-5}) | -2.9301×10^{-11} | $(-7.7291 \times 10^{-12})$ |
| $\tilde{S} = 0.95$ | -1.8144×10^{-3} | (-1.3941×10^{-4}) | -5.5681×10^{-10} | $(-1.3903 \times 10^{-10})$ |

One may find the specific mode that applies at the abutment by comparing the results in the first line of table 3.4 with the weak field radiation-reaction post-Newtonian results available in the literature. Consider the quotient of the formulae presented in equation (3.9) of Hughes [4] where $\iota \cong \pi/2$.

$$\frac{\dot{i}_{weak}}{\dot{R}_{weak}} = \frac{\partial\iota}{\partial\tilde{l}} = -\frac{61}{48}\tilde{S}\tilde{l}^{-\frac{5}{2}}. \quad (3.93)$$

An identical first-order result can also be derived from equation (4.3) in Ganz [7]. Equation (3.93) is of the same form as equation (3.91). Because $-61/48 > -4.5$ in the weak field radiation-reaction regime, one may consider $X_+^2 \Rightarrow X_-^2$ to be the pertinent mode. Therefore $\left(\partial\iota/\partial\tilde{l}\right)_{min}$ describes the lower limit of $\partial\iota/\partial\tilde{l}$ for all $\tilde{l} > \tilde{l}_{LSO, abutment}$. By numerical analysis, we found

$$\begin{aligned} \left(\frac{\partial\iota}{\partial\tilde{l}}\right)_{min} &\cong -\left(122.7\tilde{S} - 36\tilde{S}^3\right)\tilde{l}^{-11/2} - \left(63/2\tilde{S} + 35/4\tilde{S}^3\right)\tilde{l}^{-9/2} \\ &\quad -15/2\tilde{S}\tilde{l}^{-7/2} - 9/2\tilde{S}\tilde{l}^{-5/2}. \end{aligned} \quad (3.94)$$

In table 3.5, we compare the results of equation (3.94) with those of Hughes [4]; and although they differ, it is confirmed that the listing of an inclined orbit in a KBH system proceeds by the slow method. As before (table 3.2) we adjust the results in [4] by dividing them by $\sin(\pi/3)$ so that they will correspond approximately to our near-polar orbits. Although we use equation (3.42) to calculate the value of ι in this work, and this differs from the formula used in [21, 5], we recognise that they are sufficiently similar for us to

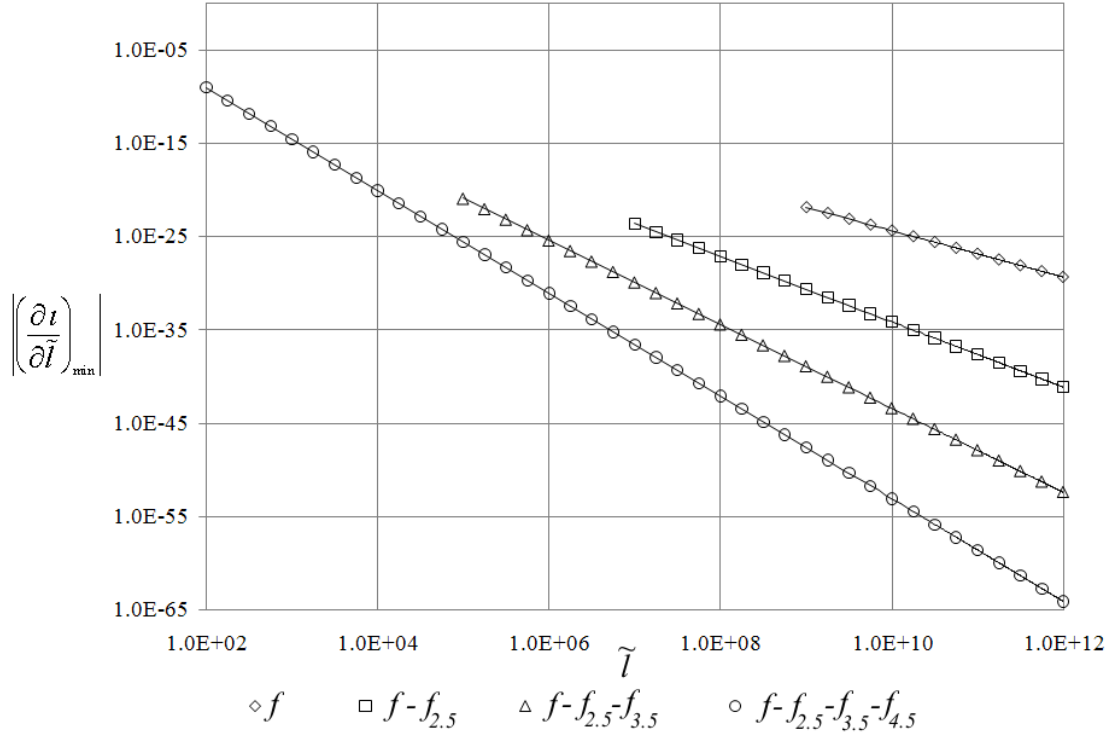


Figure 3-7: The values of $\left| \left(\frac{\partial \iota}{\partial \tilde{l}} \right)_{min} \right|$ plotted for various values of \tilde{S} for circular orbits, where $\tilde{S} = 0.99$ and $10^2 \leq \tilde{l} \leq 10^{12}$.

make a general inference about the relative sizes of $\partial \iota / \partial t$ in [4] and those calculated here.

Figure 3-8 shows the contours of constant Q on an $\tilde{l} - \iota$ plane for circular orbits ($e = 0$) about a KBH of spin $\tilde{S} = 0.99$. One of the important features of $d\iota/d\tilde{l}$ on the abutment is the suggestion of a coordinate singularity ($d\iota/d\tilde{l} \rightarrow \infty$); but this is for the specialized case in which the orbit evolves with a constant value of Q . It has been confirmed that $\partial Q / \partial \tilde{l} > 0$ on the abutment (see section 3.5.2.1); hence, such a singularity for the $d\iota/d\tilde{l}$ of an evolving orbit is not physically manifested. The arrows labelled (a), (b), (c), and (d) show some important examples of how $\partial \iota / \partial \tilde{l}$ can vary at the abutment. One observes that $\partial \iota / \partial \tilde{l}$ is not uniquely fixed by $\partial Q / \partial \tilde{l}$. Nevertheless, figure 3-8 provides an important picture of the behaviour of ι as the orbit tangentially intersects the abutment; and it warrants further study.

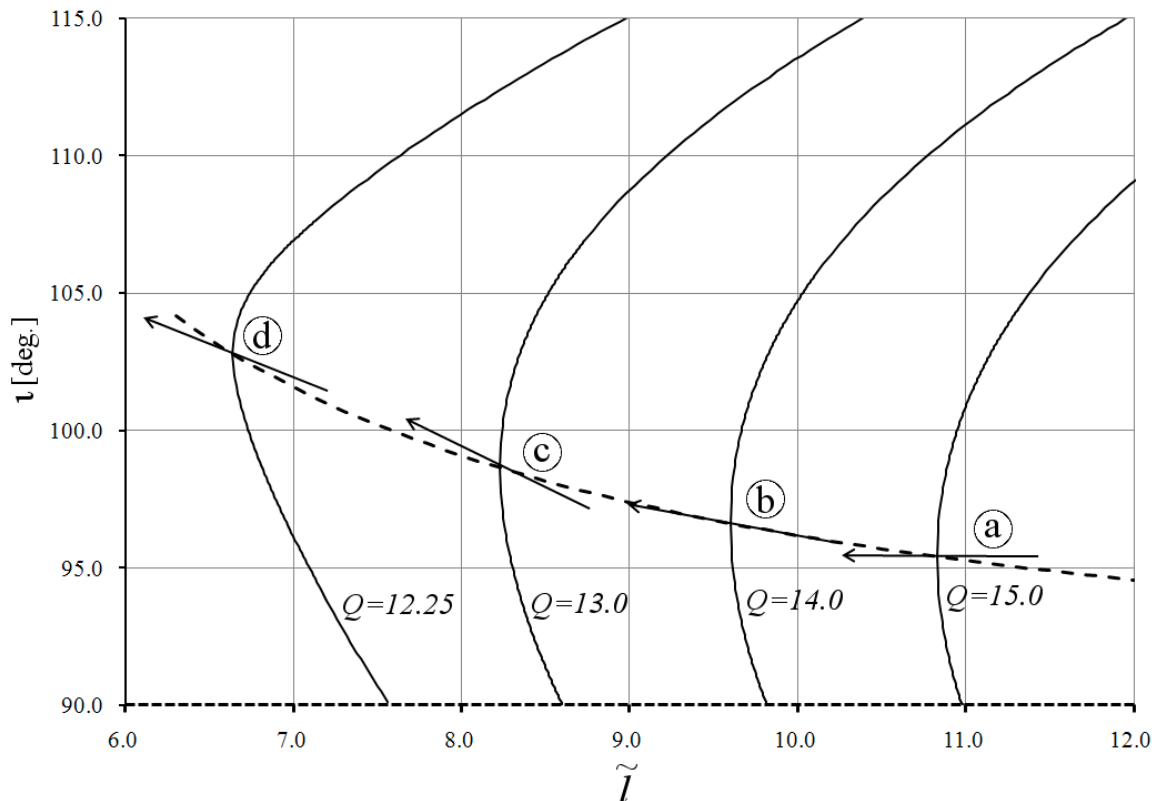


Figure 3-8: Contours of constant Q in the $\tilde{l} - \iota$ plane for a circular ($e = 0$) orbit about a KBH with spin $\tilde{S} = 0.99$. Polar orbits are indicated by the short-dashed line on the \tilde{l} -axis. The long-dashed curve corresponds to the abutment. Four curves (solid lines) of constant $Q = \{12.25, 13.0, 14.0, 15.0\}$ are shown over a range of orbital inclination angles ($90^\circ \leq \iota \leq 115^\circ$). The segment of each curve that lies below the abutment is governed by X_-^2 ; above the abutment, the segment is governed by X_+^2 . At the points of intersection between the abutment and the curves of constant Q , $\partial\iota/\partial\tilde{l} = \infty$, which suggests a singularity. The four arrows represent four tangential intersections on the abutment: (a) corresponds to the case where ι is constant; (b) corresponds to the evolution of the orbit along the abutment; (c) represents the fast mode, and (d) the slow mode. Note: the four cases cannot occur together; they are shown on a single plot for illustrative purposes.

3.6 Conclusions

In our study of inclined elliptical orbits about a Kerr black hole (KBH), we found that the minus form of X_{\pm}^2 ($X = \tilde{L}_z - \tilde{S}\tilde{E}$) is shifted away from the polar orbit position to encompass near-polar retrograde orbits. The abutment (which is a set of orbits that lie at the junction between the minus and plus forms of X_{\pm}^2) is shifted the greatest near to the LSO of the KBH and asymptotically becomes more polar with increasing latus rectum (\tilde{l}).

We developed a set of analytical formulae that characterise the behaviour of the Carter constant (Q) at the last stable orbit (LSO), abutment, and polar orbit. Further, the curves that describe Q for an LSO and Q at the abutment (between the minus and plus forms of X_{\pm}^2) intersect at a single tangential point, for which we derived an analytical formula. From these equations one can define the domain of Q for an evolving orbit (Q_{path}). The two families of curves defined by Q_{path} are governed by either X_+^2 or X_-^2 , and the curves within each family never cross. Therefore, at the abutment, Q_{path} can either change from $X_-^2 \Rightarrow X_+^2$ or from $X_+^2 \Rightarrow X_-^2$. This result aids in the investigation of the listing of an orbit at the abutment.

We have used the abutment as an analytical and numerical laboratory for the study of the evolution of Q for inclined circular orbits. The first derivative of Q_X with respect to \tilde{l} ($\partial Q_X / \partial \tilde{l}$) allows us to test the consistency of 2PN Q fluxes with estimated values of $\partial \tilde{l} / \partial t$. Further, by converting Q to the angle of orbital inclination (ι), it was possible to calculate the minimum rate of change of ι with respect to \tilde{l} , $\left(\partial \iota / \partial \tilde{l} \right)_{min}$, independently of a radiation back reaction model. Comparison with published weak-field post-Newtonian results show that the $X_+^2 \Rightarrow X_-^2$ mode applies, and this mode must apply to the entire range of orbit size, $\tilde{l} \geq \tilde{l}_{LSO, abutment}$.

Although Q_X and $\partial Q_X / \partial \tilde{l}$ are important, the higher derivatives also display critical behaviour. The second derivatives of Q_{path} warrant more study as it will improve our understanding to the effect of the radiation back reaction on the listing behaviour of the

orbit. The analysis of elliptical orbits at the abutment will introduce new elements to the listing behaviour, which arise from the first derivative of Q_X and the second and higher derivatives of Q_{path} , both with respect to e . Such a result might be valuable in our understanding of current and future radiation back reaction models.

Appendix 3.A Terms

Table 3.A.1: Orbital Parameters

| Parameter | Symbol | Normalised Symbol* |
|---|------------|---|
| Test-Particle Mass | m | - |
| Mass of MBH (typically $10^7 M_\odot$) | M | - |
| Orbital Radius | r | $R = rM^{-1}$ |
| Semi-Major Axis | a | $A = aM^{-1}$ |
| Latus Rectum | l | $\tilde{l} = lM^{-1}$ |
| Proper Time | τ | $\tilde{\tau} = \tau M^{-1}$ |
| Orbital Energy | E | $\tilde{E} = Em^{-1}$ |
| Effective Potential Energy | V | $\tilde{V} = Vm^{-1}$ |
| Spin Angular Momentum (KBH) | J | $\tilde{S} = \mathbf{J} M^{-2}$ |
| Orbital Angular Momentum (z component) | L_z | $\tilde{L}_z = L_z (mM)^{-1}$ |
| Orbital Angular Momentum (θ component) | L_θ | $\tilde{L}_\theta = L_\theta (mM)^{-1}$ |
| | Σ | $\tilde{\Sigma} = \Sigma M^{-2}$ |
| | | $= R^2 + \tilde{S}^2 \cos^2(\theta)$ |
| | Δ | $\tilde{\Delta} = \Delta M^{-2}$ |
| | | $= R^2 - 2R + \tilde{S}^2$ |
| Governs prograde, polar, and retrograde orbits up to the abutment | X_-^2 | $= \left(\tilde{L}_z - \tilde{S}\tilde{E} \right)^2$ |
| Governs the retrograde orbits beyond the abutment | X_+^2 | |

*We set the speed of light and gravitational constant to unity (i.e. $c = 1$ and $G = 1$); therefore, mass-energy is in units of time (seconds).

Appendix 3.B Ancillary Equations

3.B.1 The Kerr metric and its Inverse

$$g_{\alpha\beta} \Big|_{Kerr} = \begin{bmatrix} -\frac{\Delta - M^2 \tilde{S}^2 \sin^2(\theta)}{\rho^2} & 0 & 0 & -2M \frac{M^2 \tilde{S} R \sin^2(\theta)}{\rho^2} \\ 0 & \frac{\rho^2}{\Delta} & 0 & 0 \\ 0 & 0 & \rho^2 & 0 \\ -2M \frac{M^2 \tilde{S} R \sin^2(\theta)}{\rho^2} & 0 & 0 & \frac{M^4 (R^2 + \tilde{S}^2)^2 - M^2 \tilde{S}^2 \Delta \sin^2(\theta)}{\rho^2} \sin^2(\theta) \end{bmatrix}, \quad (3.B1)$$

The inverse Kerr metric expressed in the Boyer-Lindquist coordinate system. To simplify the presentation of the metric, we define the parameter:

$$\Sigma = \rho^2 = M^2 \left(R^2 + \tilde{S}^2 \cos^2(\theta) \right).$$

The inverse Kerr metric is:

$$g^{\delta\gamma} \Big|_{Kerr} = (\Sigma)^{-1} \begin{bmatrix} -\frac{\Sigma(R^2 + \tilde{S}^2) + 2\tilde{S}^2 R - 2\cos^2(\theta)\tilde{S}^2 R}{(R^2 - 2R + \tilde{S}^2)} & 0 & 0 & -2\frac{\tilde{S}R}{M(R^2 - 2R + \tilde{S}^2)} \\ 0 & \Delta & 0 & 0 \\ 0 & 0 & 1 & 0 \\ -2\frac{\tilde{S}R}{M(R^2 - 2R + \tilde{S}^2)} & 0 & 0 & \frac{R^2 - 2R + \tilde{S}^2 \cos^2(\theta)}{(R^2 - 2R + \tilde{S}^2)\sin^2(\theta)} \end{bmatrix}. \quad (3.B2)$$

For equatorial orbits, $\theta = \frac{\pi}{2}$, therefore, the inverse Kerr metric simplifies to the form:

$$g^{\delta\gamma} \Big|_{Kerr} = \begin{bmatrix} -\frac{R^4 + R^2\tilde{S}^2 + 2\tilde{S}^2 R}{(R^2 - 2R + \tilde{S}^2)R^2} & 0 & 0 & -2\frac{\tilde{S}}{M(R^2 - 2R + \tilde{S}^2)R} \\ 0 & \frac{R^2 - 2R + \tilde{S}^2}{R^2} & 0 & 0 \\ 0 & 0 & \frac{1}{M^2 R^2} & 0 \\ -2\frac{\tilde{S}}{M(R^2 - 2R + \tilde{S}^2)R} & 0 & 0 & \frac{R^2 - 2R}{(R^2 - 2R + \tilde{S}^2)M^2 R^2} \end{bmatrix}. \quad (3.B3)$$

The determinant of the Kerr metric was calculated to be, $Det = -\Sigma^2 \sin^2(\theta)$.

3.B.2 Effective Potentials

The effective potentials [1, 34, 30, 43] that appear in equations (3.18), (3.19), (3.20), and (3.21):

$$\tilde{V}_R(R) = T^2 - \tilde{\Delta} \left[R^2 + \left(\tilde{L}_z - \tilde{S}\tilde{E} \right)^2 + Q \right] \quad (3.B4)$$

$$\tilde{V}_\theta(\theta) = Q - \cos^2(\theta) \left[\tilde{S}^2 (1 - \tilde{E}^2) + \frac{\tilde{L}_z^2}{\sin^2(\theta)} \right] \quad (3.B5)$$

$$\tilde{V}_\phi = - \left(\tilde{S}\tilde{E} - \frac{\tilde{L}_z}{\sin^2(\theta)} \right) + \frac{\tilde{S}T}{\tilde{\Delta}}$$

$$\tilde{V}_t = -\tilde{S} \left(\tilde{S}\tilde{E} \sin^2(\theta) - \tilde{L}_z \right) + \frac{(R^2 + \tilde{S}^2) T}{\tilde{\Delta}}$$

with

$$T = \tilde{E} (R^2 + \tilde{S}^2) - \tilde{L}_z \tilde{S}.$$

The Carter constant (Q) is normalised,

$$\begin{aligned} Q &= \frac{1}{(mM)^2} \left[\frac{\cos^2(\theta) L_z^2}{\sin^2(\theta)} + L_\theta^2 + \cos^2(\theta) S^2 (m^2 - E^2) \right] \\ &= \frac{\cos^2(\theta) \tilde{L}_z^2}{\sin^2(\theta)} + \tilde{L}_\theta^2 + \cos^2(\theta) \tilde{S}^2 (1 - \tilde{E}^2). \end{aligned} \quad (3.B6)$$

3.B.3 Ninth Order Polynomial in \tilde{l} for calculating \tilde{l}_{LSO}

$$\begin{aligned} p(\tilde{l}) &= \tilde{l}^9 - 4(3+e)\tilde{l}^8 \\ &\quad - \left(-36 - 2\tilde{S}^2 e^2 + 6\tilde{S}^2 - 24e + 4\tilde{S}^2 e - 4e^2 \right) \tilde{l}^7 \\ &\quad + 4\tilde{S}^2 (e+1) (-e^2 + 2Q - 7) \tilde{l}^6 \\ &\quad - \tilde{S}^2 (e+1) \left(-\tilde{S}^2 e^3 + 5\tilde{S}^2 e^2 - 3\tilde{S}^2 e - 9\tilde{S}^2 + 16Qe^2 + 8Qe + 24Q \right) \tilde{l}^5 \\ &\quad + 8Q\tilde{S}^2 (e+1)^2 \left(4e^2 + \tilde{S}^2 e - 2e - 3\tilde{S}^2 + 6 \right) \tilde{l}^4 \\ &\quad + 8Q\tilde{S}^4 (e+1)^2 (-2e^3 - e^2 + 2Q - 1) \tilde{l}^3 - 16\tilde{S}^4 Q^2 (e^2 - 2e + 3) (e+1)^3 \tilde{l}^2 \\ &\quad + 16\tilde{S}^4 Q^2 (2e^2 - 4e + 3) (e+1)^4 \tilde{l} - 16\tilde{S}^6 Q^2 (e-1)^2 (e+1)^5 \\ &= 0 \end{aligned} \quad (3.B7)$$

3.B.4 The First and Second Derivatives of Q_X

Given:

$$\begin{aligned}\xi_1 &= \tilde{l}(\tilde{l} - e^2 - 3), \\ \xi_2 &= 4\tilde{l}\tilde{S}^2(1 - e^2)^2 \\ \xi_3 &= 2\tilde{l} - e^2 - 3.\end{aligned}$$

From equation (3.63) the equation for Q_X is

$$Q_X = \frac{2\tilde{l}^3}{\xi_2} \left(\xi_1 - \sqrt{\xi_1^2 - \xi_2} \right).$$

We obtain the following first and second derivatives of Q_X with respect to \tilde{l} and with respect to e :

$$\frac{\partial Q_X}{\partial \tilde{l}} = \frac{2\tilde{l}^3}{\xi_2} \left(\left(\tilde{l}\xi_3 - \frac{1}{2} \frac{(2\tilde{l}\xi_1\xi_3 - \xi_2)}{\sqrt{\xi_1^2 - \xi_2}} \right) + 2 \left(\xi_1 - \sqrt{\xi_1^2 - \xi_2} \right) \right), \quad (3.B8)$$

$$\begin{aligned}\frac{\partial Q_X}{\partial e} &= \frac{4e\tilde{l}^3}{\xi_2(1 - e^2)} \left[\left(-\tilde{l}(1 - e^2) + \frac{(\tilde{l}(1 - e^2)\xi_1 - \xi_2)}{\sqrt{\xi_1^2 - \xi_2}} \right) \right. \\ &\quad \left. + 2 \left(\xi_1 - \sqrt{\xi_1^2 - \xi_2} \right) \right], \quad (3.B9)\end{aligned}$$

$$\begin{aligned}\frac{\partial^2 Q_X}{\partial \tilde{l}^2} &= \frac{2\tilde{l}}{\xi_2} \left[2\tilde{l}^2 + \frac{1}{4} \frac{(2\tilde{l}\xi_1\xi_3 - \xi_2)^2}{(\xi_1^2 - \xi_2)^{3/2}} - \tilde{l}^2 \frac{(6\xi_1 + (3 + e^2)^2)}{\sqrt{\xi_1^2 - \xi_2}} \right. \\ &\quad \left. + 4 \left(\tilde{l}\xi_3 - \frac{1}{2} \frac{(2\tilde{l}\xi_1\xi_3 - \xi_2)}{\sqrt{\xi_1^2 - \xi_2}} \right) + 2 \left(\xi_1 - \sqrt{\xi_1^2 - \xi_2} \right) \right], \quad (3.B10)\end{aligned}$$

$$\begin{aligned}
\frac{\partial^2 Q_X}{\partial e^2} = & \frac{4\tilde{l}^3}{\xi_2(1-e^2)^2} \left[-\tilde{l}(1-e^2)^2 + 2e^2 \left(\frac{(\tilde{l}(1-e^2)\xi_1 - \xi_2)^2}{(\xi_1^2 - \xi_2)^{3/2}} \right) \right. \\
& + (1-e^2)^2 \left(\frac{(l^2(\tilde{l} - 3(1+e^2)) + 4\tilde{l}\tilde{S}^2(3e^2 - 1))}{\sqrt{\xi_1^2 - \xi_2}} \right) \\
& + 8e^2 \left(-\tilde{l}(1-e^2) + \left(\frac{(\tilde{l}(1-e^2)\xi_1 - \xi_2)}{\sqrt{\xi_1^2 - \xi_2}} \right) \right) \\
& \left. + 2(5e^2 + 1) \left(\xi_1 - \sqrt{\xi_1^2 - \xi_2} \right) \right]. \tag{3.B11}
\end{aligned}$$

3.B.5 The 2PN flux for Q

According to equation (A.3) in [22] (after equation (56) in [5]):

$$\begin{aligned}
\left(\frac{\partial Q}{\partial t} \right)_{2PN} = & -\sin(\iota) \frac{64 m^2}{5 M} (1-e^2)^{3/2} \tilde{l}^{-7/2} \sqrt{Q} \\
& \times \left[g_9(e) - \tilde{l}^{-1} g_{11}(e) + \left(\pi g_{12}(e) - \cos(\iota) \tilde{S} g_{10}^b(e) \right) \tilde{l}^{-3/2} \right. \\
& \left. - \left(g_{13}(e) - \tilde{S}^2 \left(g_{14}(e) - \frac{45}{8} \sin^2(\iota) \right) \right) \tilde{l}^{-2} \right], \tag{3.B12}
\end{aligned}$$

where

$$\begin{aligned}
g_9 = 1 + \frac{7}{8}e^2, \quad g_{10}^b = \frac{61}{8} + \frac{91}{4}e^2 + \frac{461}{64}e^4, \quad g_{11} = \frac{1247}{336} + \frac{425}{336}e^2, \\
g_{12} = 4 + \frac{97}{8}e^2, \quad g_{13} = \frac{44711}{9072} + \frac{302893}{6048}e^2, \quad g_{14} = \frac{33}{16} + \frac{95}{16}e^2.
\end{aligned}$$

The Carter constant has been normalised by dividing by $(mM)^2$.

3.B.6 Tables associated with figures 3-1, 3-2, and 3-3

Table 3.B.1: Numerical values of R_{LSO} estimated from figure 3-1 for a circular LSO around an SBH. There is no circular LSO for $Q > 12$.

| Q | Label | R_{LSO} (Prograde) | Label | R_{LSO} (Retrograde) |
|-----------|-------------|----------------------|-------------|------------------------|
| 0.000000 | <i>a</i> | 6.000 | <i>A</i> | 6.000 |
| 5.000000 | <i>b</i> | 6.000 | <i>B</i> | 6.000 |
| 10.000000 | <i>c</i> | 6.000 | <i>C</i> | 6.000 |
| 12.000000 | <i>d, e</i> | 6.000 | <i>D, E</i> | 6.000 |
| 13.000000 | <i>f</i> | | <i>F</i> | |
| 16.000000 | <i>g</i> | | <i>G</i> | |

Table 3.B.2: Numerical values of R_{LSO} estimated from figure 3-2 for a circular LSO around a KBH of spin $\tilde{S} = 0.50$. There is no circular LSO for $Q > 12.0545$.

| Q | Label | R_{LSO} (Governed by X_-^2) | Label | R_{LSO} (Governed by X_+^2) |
|-----------|----------|----------------------------------|----------|----------------------------------|
| 0.000000 | <i>a</i> | 4.233 | <i>A</i> | 7.555 |
| 5.000000 | <i>b</i> | 4.709 | <i>B</i> | 7.227 |
| 10.000000 | <i>c</i> | 5.366 | <i>C</i> | 5.366 |
| 11.828365 | <i>d</i> | 5.842 | <i>D</i> | 6.287 |
| 12.054503 | <i>e</i> | 6.067 | <i>E</i> | 6.068 |
| 13.000000 | <i>f</i> | | <i>F</i> | |
| 16.000000 | <i>g</i> | | <i>G</i> | |

Table 3.B.3: Numerical values of R_{LSO} estimated from figure 3-3 for a circular orbit around a KBH of spin $\tilde{S} = 0.99$. There is no circular LSO for $Q > 12.203171$.

| Q | Label | R_{LSO} (Governed by X_-^2) | Label | R_{LSO} (Governed by X_+^2) |
|-----------|----------|----------------------------------|----------|----------------------------------|
| 0.000000 | <i>a</i> | 1.455 | <i>A</i> | 8.972 |
| 5.000000 | <i>b</i> | 3.074 | <i>B</i> | 8.403 |
| 10.000000 | <i>c</i> | 4.730 | <i>C</i> | 7.501 |
| 11.252920 | <i>d</i> | 5.280 | <i>D</i> | 7.091 |
| 12.203171 | <i>e</i> | 6.245 | <i>E</i> | 6.245 |
| 13.000000 | <i>f</i> | | <i>F</i> | |
| 16.000000 | <i>g</i> | | <i>G</i> | |

Appendix 3.C An Explicit Treatment of $d\theta/d\tau$ in the Effective Potential

For the sake of completeness, we shall demonstrate a method for calculating a polynomial that describes $d\theta/d\tau$.

Recall that:

$$\Delta = M^2 \left(R^2 - 2R + \tilde{S}^2 \right) \quad (3.C1)$$

and

$$\Sigma = \rho^2 = M^2 \left(R^2 + \tilde{S}^2 \cos^2(\theta) \right). \quad (3.C2)$$

Therefore one may consider a normalised form of these equations:

$$\tilde{\Delta} = \frac{\Delta}{M^2} = \left(R^2 - 2R + \tilde{S}^2 \right) \quad (3.C3)$$

and

$$\tilde{\Sigma} = \frac{\rho^2}{M^2} = \left(R^2 + \tilde{S}^2 \cos^2(\theta) \right). \quad (3.C4)$$

Note:

$$\begin{aligned} \frac{\rho^2}{\Delta} &= \frac{\Sigma}{\Delta} \\ &= \frac{\tilde{\Sigma}}{\tilde{\Delta}}. \end{aligned} \quad (3.C5)$$

In working with the quantity, $dr/d\tau$, in [29] it did not matter about the division of the radial distance by the black hole mass, M , since the proper time, τ , would also have been normalised in the same way i.e.,

$$\begin{aligned} \frac{dr}{d\tau} &= \frac{d \left(M \left(\frac{r}{M} \right) \right)}{d \left(M \left(\frac{\tau}{M} \right) \right)} \\ &= \frac{dR}{d\tilde{\tau}}. \end{aligned} \quad (3.C6)$$

Indeed, one ought to consider the normalisation of the proper time with respect to black hole mass. Although one could escape difficulties when only considering $dr/d\tau$, it is mandatory that the normalised proper time be explicitly considered when evaluating the quantity, $d\theta/d\tau$. The polar angle, θ , is already dimensionless, and as such cannot be normalised. Therefore

$$\begin{aligned}\frac{d\theta}{d\tau} &= \frac{d\theta}{d\left(M\left(\frac{\tau}{M}\right)\right)} \\ &= \frac{1}{M} \frac{d\theta}{d\tilde{\tau}}.\end{aligned}\tag{3.C7}$$

We may rewrite the 4-momentum in terms of $d\theta/d\tilde{\tau}$ in addition to $dR/d\tilde{\tau}$, where $X = \tilde{L}_z - \tilde{S}\tilde{E}$.

$$P_\gamma = \left[-m\tilde{E}, m\frac{\rho^2}{\Delta} \left(\frac{dR}{d\tilde{\tau}} \right), m\frac{\rho^2}{M} \left(\frac{d\theta}{d\tilde{\tau}} \right), mM \left(X + \tilde{S}\tilde{E} \right) \right].\tag{3.C8}$$

By evaluating $\vec{P} \cdot \vec{P}$ and substituting the known relation for $dR/d\tilde{\tau}$ one obtains,

$$\begin{aligned}&\tilde{\Sigma}^2 \sin^2(\theta) \left(\left(\frac{dR}{d\tilde{\tau}} \right)^2 + \tilde{\Delta} \left(\frac{d\theta}{d\tilde{\tau}} \right)^2 \right) \\ &= -\sin^2(\theta) \left(1 - \tilde{E}^2 \right) R^4 + 2 \sin^2(\theta) R^3 \\ &\quad - \left(X^2 + \tilde{S}^2 + 2X\tilde{E}\tilde{S} - \cos^4(\theta) \tilde{S}^2 \left(1 - \tilde{E}^2 \right) \right) R^2 \\ &\quad + 2 \left(X^2 + \tilde{S}^2 \cos^2(\theta) + 2X \cos^2(\theta) \tilde{E}\tilde{S} - \cos^4(\theta) \tilde{S}^2 \left(1 - \tilde{E}^2 \right) \right) R \\ &\quad - \left(\left(X^2 + \tilde{S}^2 + 2X\tilde{E}\tilde{S} \right) \cos^2(\theta) - \cos^4(\theta) \left(1 - \tilde{E}^2 \right) \tilde{S}^2 \right) \tilde{S}^2.\end{aligned}\tag{3.C9}$$

We know from our previous work that

$$\begin{aligned}\tilde{\Sigma}^2 \left(\frac{dR}{d\tilde{\tau}} \right)^2 &= - \left(1 - \tilde{E}^2 \right) R^4 + 2 R^3 \\ &\quad - \left(X^2 + \tilde{S}^2 + 2\tilde{S}\tilde{E}X + Q \right) R^2 + 2 \left(X^2 + Q \right) R - Q\tilde{S}^2\end{aligned}\tag{3.C10}$$

and we can substitute this expression into equation (3.C9) to simplify it thus:

$$\begin{aligned}
& \tilde{\Sigma}^2 \sin^2(\theta) \left(\tilde{\Delta} \left(\frac{d\theta}{d\tilde{\tau}} \right)^2 \right) \\
= & 0 \times R^4 + 0 \times R^3 \\
& - \left(\left(X^2 + \tilde{S}^2 + 2 X \tilde{E} \tilde{S} \right) \cos^2(\theta) - \cos^4(\theta) \tilde{S}^2 \left(1 - \tilde{E}^2 \right) - \sin^2(\theta) Q \right) R^2 \\
& + 2 \left(\left(X^2 + \tilde{S}^2 + 2 X \tilde{E} \tilde{S} \right) \cos^2(\theta) - \cos^4(\theta) \tilde{S}^2 \left(1 - \tilde{E}^2 \right) - \sin^2(\theta) Q \right) R \\
& - \left(\left(X^2 + \tilde{S}^2 + 2 X \tilde{E} \tilde{S} \right) \cos^2(\theta) - \cos^4(\theta) \tilde{S}^2 \left(1 - \tilde{E}^2 \right) - \sin^2(\theta) Q \right) \tilde{S}^2,
\end{aligned} \tag{3.C11}$$

which factors to

$$\begin{aligned}
& \tilde{\Sigma}^2 \sin^2(\theta) \left(\tilde{\Delta} \left(\frac{d\theta}{d\tilde{\tau}} \right)^2 \right) \\
= & \tilde{\Delta} \left(\sin^2(\theta) Q - \left(X^2 + \tilde{S}^2 + 2 X \tilde{E} \tilde{S} \right) \cos^2(\theta) + \cos^4(\theta) \tilde{S}^2 \left(1 - \tilde{E}^2 \right) \right)
\end{aligned} \tag{3.C12}$$

and simplifies to

$$\begin{aligned}
\tilde{\Sigma}^2 \left(\frac{d\theta}{d\tilde{\tau}} \right)^2 &= \frac{1}{\sin^2(\theta)} \left(\sin^2(\theta) Q - \left(X^2 + \tilde{S}^2 + 2 X \tilde{E} \tilde{S} \right) \cos^2(\theta) + \cos^4(\theta) \tilde{S}^2 \left(1 - \tilde{E}^2 \right) \right) \\
&= Q - \tilde{L}_z^2 \left(\frac{\cos^2(\theta)}{\sin^2(\theta)} \right) - \tilde{S}^2 \left(1 - \tilde{E}^2 \right) \cos^2(\theta).
\end{aligned} \tag{3.C13}$$

One can equate:

$$mM\tilde{L}_\theta = m \frac{\rho^2}{M} \left(\frac{d\theta}{d\tilde{\tau}} \right) \tag{3.C14}$$

and thus obtain:

$$\tilde{L}_\theta = \tilde{\Sigma} \frac{d\theta}{d\tilde{\tau}}, \tag{3.C15}$$

which *viz.* equation (3.C11) confirms the relationship for the Carter constant. Further, we note that $\tilde{L}_\theta^2 = Q$ at the orbital nodes and $\tilde{L}_\theta = 0$ at the zenith or nadir of the orbit. It is in these respects that the Carter constant possesses a physical meaning for a KBH.

3.4 References

- [1] B. Carter. Global Structure of the Kerr Family of Gravitational Fields. *Physical Review*, 174:1559–1571, 1968.
- [2] B. Carter. Black Hole Equilibrium States. In C. Dewitt and B. S. Dewitt, editors, *Black Holes (Les Astres Occlus)*, pages 57–214, 1973.
- [3] H. Goldstein, C. Poole, and J. Safko. *Classical Mechanics*. Pearson Education, 2005.
- [4] S. A. Hughes. Evolution of Circular, Nonequatorial Orbits of Kerr Black Holes due to Gravitational-Wave Emission. *Phys. Rev. D*, 61(8):084004, 2000.
- [5] J. R. Gair and K. Glampedakis. Improved Approximate Inspirals of Test Bodies into Kerr Black Holes. *Phys. Rev. D*, 73(6):064037, 2006.
- [6] S. D. Mohanty and R. K. Nayak. Tomographic Approach to Resolving the Distribution of LISA Galactic Binaries. *Phys. Rev. D*, 73(8):083006, 2006.
- [7] K. Ganz, W. Hikida, H. Nakano, N. Sago, and T. Tanaka. Adiabatic Evolution of Three ‘Constants’ of Motion for Greatly Inclined Orbits in Kerr Spacetime. *Progress of Theoretical Physics*, 117:1041–1066, 2007.
- [8] P. C. Peters and J. Mathews. Gravitational Radiation from Point Masses in a Keplerian Orbit. *Phys. Rev.*, 131(1):435–440, 1963.
- [9] P. C. Peters. Gravitational Radiation and the Motion of Two Point Masses. *Phys. Rev.*, 136(4B):B1224–B1232, 1964.
- [10] K. S. Thorne. *300 Years of Gravitation*, chapter Gravitational Radiation. Cambridge University Press, 1987.
- [11] L. Barack and C. Cutler. Lisa Capture Sources: Approximate waveforms, signal-to-noise ratios, and parameter estimation accuracy. *Phys. Rev. D*, 69:082005, 2004.

- [12] W. H. Press and S. A. Teukolsky. On the Evolution of the Secularly Unstable, Viscous Maclaurian Spheroids. *Astrophys. J.*, 181:513–518, 1973.
- [13] S. A. Teukolsky. Perturbations of a Rotating Black Hole. I. Fundamental Equations for Gravitational, Electromagnetic, and Neutrino-Field Perturbations. *Astrophys. J.*, 185:635–648, 1973.
- [14] W. H. Press and S. A. Teukolsky. Perturbations of a Rotating Black Hole. II. Dynamical Stability of the Kerr Metric. *Astrophys. J.*, 185:649–674, 1973.
- [15] A. Ori. Radiative Evolution of the Carter Constant for Generic Orbits Around a Kerr Black Hole. *Phys. Rev. D*, 55(6):3444–3456, 1997.
- [16] A. Ori. Radiative Evolution of Orbits Around a Kerr Black Hole. *Physics Letters A*, 202(5-6):347–351, 1995.
- [17] F. D. Ryan. Effect of Gravitational Radiation Reaction on Nonequatorial Orbits Around a Kerr Black Hole. *Phys. Rev. D*, 53:3064–3069, 1996.
- [18] D. Kennefick and A. Ori. Radiation-Reaction-Induced Evolution of Circular Orbits of Particles Around Kerr Black Holes. *Phys. Rev. D*, 53(8):4319–4326, 1996.
- [19] S. A. Hughes. Evolution of Circular, Nonequatorial Orbits of Kerr Black Holes due to Gravitational-Wave Emission. II. Inspiral trajectories and gravitational waveforms. *Phys. Rev. D*, 64(6):064004, 2001.
- [20] K. Glampedakis and D. Kennefick. Zoom and Whirl: Eccentric equatorial orbits around spinning black holes and their evolution under gravitational radiation reaction. *Phys. Rev. D*, 66(4):044002, 2002.
- [21] K. Glampedakis, S. A. Hughes, and D. Kennefick. Approximating the Inspiral of Test Bodies into Kerr Black Holes. *Phys. Rev. D*, 66(6):064005, 2002.

- [22] E. Barausse, S. A. Hughes, and L. Rezzolla. Circular and Noncircular Nearly Horizon-Skimming Orbits in Kerr Spacetimes. *Phys. Rev. D*, 76(4):044007, 2007.
- [23] F. D. Ryan. Effect of Gravitational Radiation Reaction on Circular Orbits Around a Spinning Black Hole. *Phys. Rev. D*, 52:3159, 1995.
- [24] J. M. Bardeen. Timelike and Null Geodesics in the Kerr Metric. In C. Dewitt and B. S. Dewitt, editors, *Black Holes (Les Astres Occlus)*, pages 215–239, 1973.
- [25] S. L. Shapiro and S. A. Teukolsky. *Black Holes, White Dwarfs, and Neutron Stars: The physics of compact objects*. Wiley-Interscience, New York,, 1983.
- [26] S. Chandrasekhar. *The Mathematical Theory of Black Holes*. Oxford University Press, 1983.
- [27] B. F. Schutz. *A First Course in General Relativity*. Cambridge University Press, 17 edition, 2005.
- [28] A. Ori and K. S. Thorne. Transition from Inspiral to Plunge for a Compact Body in a Circular Equatorial Orbit Around a Massive, Spinning Black Hole. *Phys. Rev. D*, 62(12):124022, 2000.
- [29] P. G. Komorowski, S. R. Valluri, and M. Houde. A Study of Elliptical Last Stable Orbits About a Massive Kerr Black Hole. *Class. Quantum Grav.*, 26(8):085001, 2009.
- [30] W. Schmidt. Celestial Mechanics in Kerr Spacetime. *Class. Quantum Grav.*, 19(10):2743–2764, 2002.
- [31] P. A. Sundararajan. Transition from Adiabatic Inspiral to Geodesic Plunge for a Compact Object Around a Massive Kerr Black Hole: Generic orbits. *Phys. Rev. D*, 77(12):124050, 2008.

- [32] S. Drasco and S. A. Hughes. Gravitational Wave Snapshots of Generic Extreme Mass Ratio Inspirals. *Phys. Rev. D*, 73(2):024027, 2006.
- [33] C Cutler, D. Kennefick, and E Poisson. Gravitational Radiation Reaction for Bound Motion Around a Schwarzschild Black Hole. *Phys. Rev. D*, 50(6):3816–3835, 1994.
- [34] J. M. Bardeen, W. H. Press, and S. A. Teukolsky. Rotating Black Holes: Locally nonrotating frames, energy extraction, and scalar synchrotron radiation. *Astrophys. J.*, 178:347, 1972.
- [35] E. Stoghianidis and D. Tsoubelis. Polar Orbits in the Kerr Space-time. *General Relativity and Gravitation*, 19(12):1235–1249, 1987.
- [36] T. Alexander and M. Livio. Tidal Scattering of Stars on Supermassive Black Holes in Galactic Centers. *The Astrophysical Journal*, 560(2):L143–L146, 2001.
- [37] T. Bogdanović, M. Eracleous, S. Mahadevan, S. Sigurdsson, and P. Laguna. Tidal Disruption of a Star by a Black Hole: Observational Signature. *The Astrophysical Journal*, 610(2):707–721, 2004.
- [38] P. G. Komorowski, S. R. Valluri, and M. Houde. The Carter Constant for Inclined Orbits About a Massive Kerr Black Hole: II. near-circular, near-polar orbits. *ArXiv e-prints*, arXiv:1101.0996v1 [gr-qc], 2011.
- [39] G. H. Golub and C. F. van Loan. *Matrix Computations*. Baltimore : Johns Hopkins University Press, 1996. (Johns Hopkins studies in the mathematical sciences), 1996.
- [40] A. Edelman and H. Murakami. Polynomial Roots from Companion Matrix Eigenvalues. *Mathematics of Computation*, 64(210):763–776, 1995.
- [41] D. C. Sorensen and C. C. Yang. A Truncated RQ Iteration for Large Scale Eigenvalue Calculations. *Siam Journal on Matrix Analysis and Applications*, 19(4):1045–1073, 1998.

- [42] C. Yang. Solving Large-Scale Eigenvalue Problems in SciDAC Applications. *Journal of Physics Conference Series*, 16:425–434, 2005.
- [43] S. Babak, H. Fang, J. R. Gair, K. Glampedakis, and S. A. Hughes. “Kludge” Gravitational Waveforms for a Test-body Orbiting a Kerr Black Hole. *Phys. Rev. D*, 75(2):024005–024030, 2007.

Chapter 4

**The Carter Constant for Inclined
Elliptical Orbits About a Massive
Kerr Black Hole: near-polar,
near-circular orbits**

Abstract

In an extreme mass ratio binary black hole system, a non-equatorial orbit will list (i.e. increase its angle of inclination, ι) as it evolves in Kerr spacetime. The abutment, a set of evolving near-polar retrograde orbits for which the instantaneous Carter constant (Q) is at its maximum value (Q_X), for given values of latus rectum (\tilde{l}) and eccentricity (e), has been introduced as a device by which the consistency of dQ/dt with corresponding evolution equations for $d\tilde{l}/dt$ and de/dt might be tested, and as a means of elucidating second-order effects on the listing rate of the orbital angle of inclination, $\partial\iota/\partial t$ (independently of a specific radiation back-reaction model). Our present work expands upon these two uses.

An analytical expression for ι in terms of \tilde{l} , e , and Kerr black hole spin ($\tilde{S} = |\mathbf{J}|/M^2$) was derived for elliptical orbits on the abutment. From this expression, we verified the numerical calculations of $\partial\iota/\partial\tilde{l}$, which were made previously for hypothetical circular orbits that evolve along the abutment. Further, we also obtained an expression for $\partial\iota/\partial e$ on the abutment. True orbital evolution in Kerr spacetime does not follow a path confined to the abutment. And second-order effects also present themselves in calculating $d\iota/dt$. It was found that for elliptical orbits, $\partial\iota/\partial\tilde{l}$ can be successfully modelled by incorporating a reduction in $\partial^2 Q_X/\partial\tilde{l}^2$, while no such change is required for $\partial^2 Q_X/\partial e^2$. The resulting expression for $d\iota/dt$ was consistent with corresponding formulae in the literature.

A derivation of dQ/dt , based only on published formulae for $d\tilde{l}/dt$ and de/dt , was performed for elliptical orbits on the abutment. The resulting expression for dQ/dt closely matched published results. We believe the abutment is a potentially useful tool for improving the accuracy of evolution equations to higher orders of e and \tilde{l}^{-1} .

4.1 Introduction

An extreme mass ratio binary black hole system (EMRI) is composed of a primary object, which can be a Kerr black hole of mass $M \sim 10^6 - 10^7$ solar masses with a spin $\tilde{S} = |\mathbf{J}|/M^2$ (where \mathbf{J} is the spin angular momentum), and an orbiting secondary object of mass $m \sim 1 - 10$ solar masses. Theoretical models to describe the orbital evolution of the secondary object in various situations have been derived and presented in the literature: circular orbits in the equatorial plane of the primary object [1–5], elliptical orbits in the equatorial plane [6–12], and an extensive body of research on circular or elliptical orbits inclined with respect to the equatorial plane [13–30]. Such models are used to generate hypothetical gravitational waveforms (GW), which provide templates for use in the detection of gravitation wave signals by pattern recognition (Punturo et al. [31]). The detection of GW radiation by the Earth-based Laser Interferometer Gravitational Wave Observatory (LIGO) or the Laser Interferometer Space Antenna (LISA) depends fundamentally on the availability of correct templates [12, 32, 33]. Because the part played by a theoretician is a fiduciary one, the introduction of tools with which the evolution equations can be tested is most beneficial. The abutment is one such tool.

The concept of the abutment, a boundary that defines a set of near-polar retrograde orbits, was introduced by Komorowski et al. [34] (we shall review the abutment in detail in section 4.2.2.1); in that work two uses of the abutment emerged. First, it suggested a means of testing the consistency of the evolution of the Carter constant of circular orbits (dQ/dt) with respect to that of the latus rectum ($d\tilde{l}/dt$). And second, it permitted a numerical analysis of the rate of change of the orbital angle of inclination, ι , with respect to \tilde{l} ($(\partial\iota/\partial\tilde{l})_{\min}$) for circular orbits constrained to evolve along the abutment. In this work we shall extend these uses to orbits of non-zero eccentricity ($0 \leq e \leq 1$) by testing the consistency of expressions for dQ/dt with expressions for $d\tilde{l}/dt$ and de/dt , and we shall perform an analytical treatment of ι , and the list rate of the same. Further, a physically realistic orbital evolution follows the abutment (Q_X) in only one case, the

evolution of an orbit in a Schwarzschild black hole (SBH) system ($\tilde{S} = 0$). We shall now consider the general case of an evolving orbit that intersects the abutment, Q_X , tangentially at a single point (contact of the first order (see §99 in [35])) as it follows a path defined by Q_{path} . Further, by performing our analysis on elliptical orbits, the abutment becomes a two dimensional surface that defines the maximum value of Q for given values of e and latus rectum, $\tilde{l} = l/M$. Therefore one must view the abutment as a set of contiguous points rather than a path to be followed by an evolving orbit; and it is at these points that the derivatives, $\partial Q_X/\partial \tilde{l}$ and $\partial Q_X/\partial e$, fix the corresponding slopes of Q_{path} . But as reported in [34], second-order effects must be included when working with ι at the abutment.

In section 4.2 we shall analytically derive the formula for ι for elliptical orbits on the abutment, and thus confirm the result for $\left(\partial \iota/\partial \tilde{l}\right)_{\min}$ [34], which was derived numerically for circular orbits. In addition, we shall analytically derive $\partial \iota/\partial e$ for elliptical orbits that evolve on the abutment. In section 4.3 we shall include the effect of the second derivative of Q_{path} by introducing reductive ansätze for circular and elliptical orbits, and thus create a more physically realistic model for an evolving orbit at the abutment.

Because our abutment model is independent of any specific radiation back-reaction model, we now have a laboratory that allows us to perform tests of established listing formulae. In section 4.4, we shall demonstrate the usefulness of the abutment in testing the consistency of dQ/dt equations with respect to $d\tilde{l}/dt$ and de/dt evolution equations, and in calculating $d\iota/dt$ for elliptical orbits of small eccentricity (i.e. near-circular). In section 4.5 we shall conclude our work and recommend directions that warrant further study.

We define ι to be the maximum polar angle reached by the secondary object in its orbit (see equation (42) in [34]). This definition differs from that used by others (Gair and Glampedakis [26] and Glampedakis, Hughes, and Kennefick [22]); but when performing our analysis to the leading order in \tilde{S} , there is no significant difference.

4.2 An Analytical Formula for the Angle of Inclination of an Elliptical Orbit on the Abutment

4.2.1 Introduction

The listing of an inclined elliptical orbit of eccentricity (e) can be described by $\partial\iota/\partial\tilde{l}$ and $\partial\iota/\partial e$, where ι is the angle of inclination of the orbit and \tilde{l} is its latus rectum normalised with respect to the mass (M) of the Kerr black hole (KBH). A set of essential analytical formulae for the orbital constants of motion has been derived in [34]: the Carter constant at the abutment (Q_X), the orbital energy (\tilde{E}), and the quantity, $X = \tilde{L}_z - \tilde{S}\tilde{E}$, as well as an analytical formula for ι in terms of these constants of motion. Numerical analysis yielded an equation for $\left(\frac{\partial\iota}{\partial\tilde{l}}\right)_{\min}$ for circular orbits:

$$\begin{aligned} \left(\frac{\partial\iota}{\partial\tilde{l}}\right)_{\min} &\cong -\left(122.7\tilde{S} - 36\tilde{S}^3\right)\tilde{l}^{-11/2} - \left(63/2\tilde{S} + 35/4\tilde{S}^3\right)\tilde{l}^{-9/2} \\ &\quad - 15/2\tilde{S}\tilde{l}^{-7/2} - 9/2\tilde{S}\tilde{l}^{-5/2}. \end{aligned} \quad (4.1)$$

Observe that equation (4.1) is a series expansion in terms of $\tilde{l}^{-\frac{1}{2}}$. Further, the series coefficients are themselves series expansions of odd powers of \tilde{S} . These are important properties, which we shall confirm and investigate. Equation (4.1) is not sufficient for understanding the effect of radiation back-reaction on the listing of near-polar orbits; therefore, it is necessary to develop an analytical formula for ι on the abutment so that a more thorough treatment can be made. We shall review the analytical formulae reported in [34] for elliptical orbits, and develop appropriate expansions of those formulae in terms of \tilde{S} . The Maclaurin series expansions summarised in Appendix 4.A.1 are essential for this work.

To verify equation (4.1) analytically, we shall derive the result to order 3 in \tilde{S} (i.e.

$O(\tilde{S}^3)$). But the numerical analysis in [34] stopped at $O(\tilde{l}^{-11/2})$ because of numerical limitations. For completeness, we shall determine the power of \tilde{l} at which the coefficient is $O(\tilde{S}^5)$, and we shall stop our analysis at the term prior to that one. For this particular purpose, it is advantageous and sufficient to work with circular orbits ($e = 0$).

4.2.2 Review of Analytical Formulae

4.2.2.1 The abutment, Q_X .

The analytical formula for X_{\pm}^2 (where $X = \tilde{L}_z - \tilde{S}\tilde{E}$) for elliptical and inclined orbits about a KBH was found to be [34]:

$$X_{\pm}^2 = \frac{Z_5 + Z_6 Q \pm 2\tilde{S} \sqrt{Z_7 Z_8 Z_9}}{\tilde{l} \left(\tilde{l} (3 - \tilde{l} + e^2)^2 - 4\tilde{S}^2 (1 - e^2)^2 \right)}, \quad (4.2)$$

where

$$Z_5 = \tilde{l}^3 \left\{ (\tilde{l} + 3e^2 + 1) \tilde{S}^2 - \tilde{l} (3 - \tilde{l} + e^2) \right\}, \quad (4.3)$$

$$Z_6 = -2 (1 - e^2)^2 \tilde{S}^4 + 2\tilde{l} (2e^4 + (2 - \tilde{l})e^2 + 4 - \tilde{l}) \tilde{S}^2 - \tilde{l}^2 (3 - \tilde{l} + e^2)^2, \quad (4.4)$$

$$Z_7 = \tilde{S}^2 (1 + e)^2 + \tilde{l} (\tilde{l} - 2(1 + e)), \quad (4.5)$$

$$Z_8 = \tilde{S}^2 (1 - e)^2 + \tilde{l} (\tilde{l} - 2(1 - e)), \quad (4.6)$$

and

$$Z_9 = \left(\tilde{l}^5 + \tilde{S}^2 Q^2 (1 - e^2)^2 + Q \tilde{l}^3 (3 - \tilde{l} + e^2) \right). \quad (4.7)$$

The abutment corresponds to the set of orbits for which $Z_9 = 0$ [34], i.e.

$$\tilde{l}^5 + \tilde{S}^2 Q^2 (1 - e^2)^2 + Q \tilde{l}^3 (3 - \tilde{l} + e^2) = 0. \quad (4.8)$$

The solution of equation (4.8) is:

$$Q_X = \frac{\tilde{l}^2}{2\tilde{S}^2(1-e^2)^2} \left(\tilde{l}(\tilde{l}-e^2-3) - \sqrt{\tilde{l}^2(\tilde{l}-e^2-3)^2 - 4\tilde{l}(1-e^2)^2\tilde{S}^2} \right). \quad (4.9)$$

By performing an expansion in terms of \tilde{S}^2 (*viz.* equation (4.A2)) one obtains:

$$Q_X \cong \frac{\tilde{l}^2}{(\tilde{l}-e^2-3)} + \frac{\tilde{l}(1-e^2)^2\tilde{S}^2}{(\tilde{l}-e^2-3)^3} + 2\frac{(1-e^2)^4\tilde{S}^4}{(\tilde{l}-e^2-3)^5} + 5\frac{(1-e^2)^6\tilde{S}^6}{\tilde{l}(\tilde{l}-e^2-3)^7} \dots \quad (4.10)$$

Therefore $Q_X = O(\tilde{S}^0)$ and the j^{th} term of $Q_X = O(\tilde{S}^{2j})$. The expansion of Q_X in terms of \tilde{l} can be derived from equation (4.10) once it has been determined to which power of \tilde{S} one wishes to work. This result, and its derivatives with respect to \tilde{l} and e , are presented in Appendix 4.A.5 for use in our analysis in section 4.4.1.

We return to equation (4.2). The terms under the square root can be excluded since $Z_9 = 0$. Substitution of Q_X (truncated to $O(\tilde{S}^4)$) into the remaining part of the equation yields:

$$\begin{aligned} X_{\pm}^2 &= \frac{Z_5 + Z_6 Q_X}{\tilde{l} \left(\tilde{l} (3 - \tilde{l} + e^2)^2 - 4\tilde{S}^2 (1 - e^2)^2 \right)}, \quad (4.11) \\ &\cong \left(\tilde{l}^3 (2e - 2 + \tilde{l}) (\tilde{l} - 2e - 2) (\tilde{l} - e^2 - 3)^4 \tilde{S}^2 \right. \\ &\quad - 2(1 - e^2)^2 \tilde{l}^2 (\tilde{l} - 2) (\tilde{l} - e^2 - 3)^3 \tilde{S}^4 \\ &\quad - 2(1 - e^2)^4 \tilde{l} (\tilde{l}^2 - 4\tilde{l} - 3e^4 + 2e^2 + 1) \tilde{S}^6 \\ &\quad \left. - 4(1 - e^2)^6 \tilde{S}^8 \right) \\ &\times \frac{1}{(\tilde{l} - e^2 - 3)^7 \tilde{l}^2 - 4(\tilde{l} - e^2 - 3)^5 \tilde{l} (1 - e^2)^2 \tilde{S}^2}, \end{aligned}$$

which is (*viz.* equation (4.A1)),

$$\begin{aligned}
X_{\pm}^2 &\cong \tilde{S}^2 \left(\frac{\tilde{l} (\tilde{l}^2 - 4\tilde{l} - 4e^2 + 4)}{(\tilde{l} - e^2 - 3)^3} \right. \\
&\quad + 2 \frac{(2 - 10e^2 + e^2\tilde{l} - 3\tilde{l} + \tilde{l}^2) (1 - e^2)^2 \tilde{S}^2}{(\tilde{l} - e^2 - 3)^5} \\
&\quad \left. + \frac{(6\tilde{l}^2 + (8e^2 - 16)\tilde{l} + 9 - 74e^2 + e^4) (1 - e^2)^4 \tilde{S}^4}{\tilde{l} (\tilde{l} - e^2 - 3)^7} \right). \tag{4.12}
\end{aligned}$$

From equation (4.12) one finds that $X_{\pm}^2 = O(\tilde{S}^2, \tilde{l}^0)$. Further analysis (*viz.* equation (4.A2)) yields the result:

$$\begin{aligned}
X &= \pm \tilde{S} \sqrt{\frac{\tilde{l} (\tilde{l}^2 - 4\tilde{l} - 4e^2 + 4)}{(\tilde{l} - e^2 - 3)^3}} \\
&\quad \times \left(1 + \frac{(1 - e^2)^2 \tilde{S}^2}{(\tilde{l} - e^2 - 3)^2 \tilde{l} (\tilde{l}^2 - 4\tilde{l} - 4e^2 + 4)} P_1 \right. \\
&\quad \left. + \frac{1}{2} \frac{(1 - e^2)^4 \tilde{S}^4}{(\tilde{l} - e^2 - 3)^4 \tilde{l}^2 (\tilde{l}^2 - 4\tilde{l} - 4e^2 + 4)^2} P_2 \right) \tag{4.13}
\end{aligned}$$

where

$$\begin{aligned}
P_1 &= \tilde{l}^2 - (3 - e^2)\tilde{l} + 2 - 10e^2 \\
P_2 &= 5\tilde{l}^4 - (34 - 6e^2)\tilde{l}^3 + (84 - 104e^2)\tilde{l}^2 \\
&\quad - (88 - 328e^2 + 16e^4)\tilde{l} + 32 - 292e^2 + 200e^4 - 4e^6.
\end{aligned}$$

4.2.2.2 Orbital energy, \tilde{E}

The formula for orbital energy, \tilde{E} , for inclined elliptical orbits (see equation (44) in [34]) is presented here in a form that more clearly shows that $\tilde{E} = O(\tilde{S}^0)$.

$$\tilde{E} = \sqrt{1 - (1 - e^2) \frac{\tilde{l}^3 - Q(\tilde{l} - \tilde{S}^2)(1 - e^2) - \tilde{l}X^2(1 - e^2)}{\tilde{l}^4}}, \quad (4.14)$$

Further, substitution of $Q_X(\tilde{S})$ and $X_{\pm}^2(\tilde{S})$ into equation (4.14) and the expansion of the same (*viz.* equation (4.A2)) yields:

$$\begin{aligned} \tilde{E} &= \sqrt{\frac{\tilde{l}^2 - 4\tilde{l} - 4e^2 + 4}{\tilde{l}(\tilde{l} - e^2 - 3)}} \\ &\times \left(1 + \frac{(1 - e^2)^2 \tilde{S}^2}{\tilde{l}(\tilde{l} - e^2 - 3)^2 (\tilde{l}^2 - 4\tilde{l} - 4e^2 + 4)} P_3 \right. \\ &\quad \left. + \frac{1}{2} \frac{(1 - e^2)^4 \tilde{S}^4}{\tilde{l}^2 (\tilde{l} - e^2 - 3)^4 (\tilde{l}^2 - 4\tilde{l} - 4e^2 + 4)^2} P_4 \right) \end{aligned} \quad (4.15)$$

where

$$P_3 = (e^2 + 1)\tilde{l} - 6e^2 - 2$$

$$P_4 = \tilde{l}^4 - 4(1 - e^2)\tilde{l}^3 - 52e^2\tilde{l}^2 + (16 + 152e^2 - 8e^4)\tilde{l} - 16 - 132e^2 + 88e^4 - 4e^6.$$

The term $\tilde{S}^2 (1 - \tilde{E}^2)$ will be used in our analysis; and it is calculated *viz.* equation (4.15) to yield:

$$\begin{aligned} \tilde{S}^2 (1 - \tilde{E}^2) = & \frac{(1 - e^2) (\tilde{l} - 4) \tilde{S}^2}{\tilde{l} (\tilde{l} - e^2 - 3)} - 2 \frac{(1 - e^2)^2 (e^2 \tilde{l} + \tilde{l} - 6 e^2 - 2) \tilde{S}^4}{\tilde{l}^2 (\tilde{l} - e^2 - 3)^3} \\ & - \frac{(1 - e^2)^4 (-3 - 30 e^2 + 4 e^2 \tilde{l} + \tilde{l}^2 + e^4) \tilde{S}^6}{\tilde{l}^3 (\tilde{l} - e^2 - 3)^5}, \end{aligned} \quad (4.16)$$

which can be expressed to second-order in \tilde{S} as,

$$\tilde{S}^2 (1 - \tilde{E}^2) = \frac{(1 - e^2) (\tilde{l} - 4) \tilde{S}^2}{\tilde{l} (\tilde{l} - e^2 - 3)}. \quad (4.17)$$

4.2.2.3 Orbital angle of inclination, ι

The exact formula for ι was derived in Boyer-Lindquist coordinates (BL coordinates) and found to be:

$$\sin^2(\iota) = \frac{Q + \tilde{L}_z^2 + \tilde{S}^2 (1 - \tilde{E}^2) - \sqrt{(Q + \tilde{L}_z^2 + \tilde{S}^2 (1 - \tilde{E}^2))^2 - 4 Q \tilde{S}^2 (1 - \tilde{E}^2)}}{2 \tilde{S}^2 (1 - \tilde{E}^2)}, \quad (4.18)$$

which suggests an approximate expansion in the cases of small \tilde{S} or for $\tilde{l} \rightarrow \infty$ (for which $\tilde{E} \rightarrow 1$) [34]. In particular, near-equatorial orbits can also be approximated by such an expansion since $Q \gtrsim 0$. But we are studying near-polar orbits, for which $Q > 12$; so it is advantageous to exploit the fact that $\tilde{L}_z \cong 0$ and convert equation (4.18) to an

alternative form:

$$\cos^2(\iota) = -\frac{Q + \tilde{L}_z^2 - \tilde{S}^2(1 - \tilde{E}^2) - \sqrt{\left(Q + \tilde{L}_z^2 - \tilde{S}^2(1 - \tilde{E}^2)\right)^2 + 4\tilde{L}_z^2\tilde{S}^2(1 - \tilde{E}^2)}}{2\tilde{S}^2(1 - \tilde{E}^2)}. \quad (4.19)$$

This equation can also be expanded as a series (not strictly in powers of \tilde{S}^2) to obtain:

$$\begin{aligned} \cos^2(\iota) \cong & \frac{\tilde{L}_z^2}{Q + \tilde{L}_z^2 - \tilde{S}^2(1 - \tilde{E}^2)} - \frac{\tilde{L}_z^4(1 - \tilde{E}^2)\tilde{S}^2}{\left(Q + \tilde{L}_z^2 - \tilde{S}^2(1 - \tilde{E}^2)\right)^3} \\ & + \frac{2\tilde{L}_z^6(1 - \tilde{E}^2)^2\tilde{S}^4}{\left(Q + \tilde{L}_z^2 - \tilde{S}^2(1 - \tilde{E}^2)\right)^5} \end{aligned} \quad (4.20)$$

It is essential to establish the lowest order of \tilde{S} for each term of equation (4.20); the results in equations (4.10), (4.12), and (4.15) will help.

It was found that $X_{\pm} = -\sqrt{X_{\pm}^2}$ in the vicinity of the abutment (see section 3.5 in Komorowski et al. [34]), therefore,

$$\tilde{L}_z = -\sqrt{X_{\pm}^2} + \tilde{S}\tilde{E}. \quad (4.21)$$

Each of the expressions in equations (4.13) and (4.15), when expanded as a power series in \tilde{l}^{-1} , will have a leading factor of \tilde{S} and *unity*, respectively. In evaluating equation (4.21), the leading terms subtract out; therefore, we find that $\tilde{L}_z^2 = O(\tilde{S}^2, \tilde{l}^{-2})$. The inverse dependence of \tilde{L}_z^2 on \tilde{l} is consistent with the physical meaning of \tilde{L}_z for orbits on the abutment. Further, equation (4.10) indicates that $Q_X = O(\tilde{S}^0, \tilde{l})$; therefore, the first term in equation (4.20) is $O(\tilde{S}^2)$, and the second term, $O(\tilde{S}^6)$, with each term containing higher order terms of \tilde{S} in increments of 4.

Taking the square root of both sides of equation (4.20) yields,

$$\cos(\iota) = \underbrace{O(\tilde{S})}_{1^{st} \text{ term}} + \underbrace{O(\tilde{S}^5)}_{2^{nd} \text{ term}} + \underbrace{O(\tilde{S}^9)}_{3^{rd} \text{ term}} \quad (4.22)$$

with higher order terms of odd power of \tilde{S} . The second term in equation (4.20) will contribute to equation (4.22) a factor $O(\tilde{S}^5)$; therefore, to derive an analytical formula for $(\partial\iota/\partial\tilde{l})_{\min}$ valid to $O(\tilde{S}^3)$ (see equation (4.1)) it is sufficient to use the first term of equation (4.20). If we choose to work in stronger gravitational fields, for which terms of greater order in \tilde{S} are required, then the second and possibly higher order terms in equation (4.20) would be used. But we wish to work with terms that contain \tilde{S} and \tilde{S}^3 , to the exclusion of those with \tilde{S}^5 , so we shall restrict our analysis to the first term:

$$\begin{aligned} \cos^2(\iota) &\cong \frac{\tilde{L}_z^2}{Q + \tilde{L}_z^2 - \tilde{S}^2(1 - \tilde{E}^2)} \\ &= \frac{\tilde{L}_z^2}{Q \left(1 + \frac{\tilde{L}_z^2}{Q} - \frac{\tilde{S}^2(1 - \tilde{E}^2)}{Q}\right)}. \end{aligned} \quad (4.23)$$

This equation can be simplified *viz.* equations (4.A1) and (4.A2) to yield:

$$\cos(\iota) \cong \frac{\tilde{L}_z}{\sqrt{Q}} \left[1 - \frac{1}{2} \frac{\tilde{L}_z^2}{Q} + \frac{1}{2} \frac{\tilde{S}^2(1 - \tilde{E}^2)}{Q} \right]. \quad (4.24)$$

Given $x = \cos(\iota)$, one may calculate ι to $O(\tilde{S}^5)$ *viz.* equation (4.A3):

$$\iota = \frac{\pi}{2} - x - \frac{1}{6}x^3 - \frac{3}{40}x^5. \quad (4.25)$$

4.2.3 Analytical Formula for $\iota(e, \tilde{l})$ on the Abutment

We shall now evaluate equation (4.24) analytically by working with the constituent terms as series expansions in \tilde{S} , the coefficients of which are in terms of e and \tilde{l} . The result to third order in \tilde{S} is our target, while the \tilde{S}^5 term will be treated superficially. An aperçu of the method by which the expression in equation (4.24) is treated appears in Appendix 4.B.

4.2.3.1 First-order in \tilde{S}

To perform our calculation of ι to $O(\tilde{S})$ (see Appendix 4.B.1) it is sufficient to use:

$$\iota^{(1)} = \frac{\pi}{2} - \frac{\tilde{L}_z^{(1)}}{\sqrt{Q_X}} \quad (4.26)$$

where

$$\frac{\tilde{L}_z^{(1)}}{\sqrt{Q_X}} = -\tilde{S}(e^2 + 3) \left(\frac{1}{\tilde{l}^{3/2}} + \frac{(1+e^2)}{\tilde{l}^{5/2}} + \frac{(3+2e^2+e^4)}{\tilde{l}^{7/2}} + \frac{(9+5e^2+5e^4+e^6)}{\tilde{l}^{9/2}} \right), \quad (4.27)$$

and the number in parenthesis indicates the order in \tilde{S} of the term below it.

4.2.3.2 Third-order in \tilde{S}

Our third-order equations are more complicated. Consider the third-order equation for ι :

$$\iota^{(3)} = \frac{\pi}{2} - x - \frac{1}{6}x^3 \quad (4.28)$$

where

$$x = \frac{\tilde{L}_z^{(3)}}{\sqrt{Q_X}} \left(1 - \frac{1}{2} \left(\frac{\tilde{L}_z^{(3)}}{\sqrt{Q_X}} \right)^2 + \frac{1}{2} \frac{\tilde{S}^2 (1 - \tilde{E}^2)}{Q_X} \right) \quad (4.29)$$

in which

$$\frac{\overset{(3)}{\tilde{L}_z}}{\sqrt{Q_X}} = \frac{\overset{(1)}{\tilde{L}_z}}{\sqrt{Q_X}} - \tilde{S}^3 (1 - e^2)^2 \left(\frac{1}{\tilde{l}^{7/2}} + \frac{1}{2} \frac{11 + 5e^2}{\tilde{l}^{9/2}} \right) \quad (4.30)$$

and

$$\frac{\overset{(2)}{\tilde{S}^2 (1 - \tilde{E}^2)}}{Q_X} = (1 - e^2) \left(\frac{1}{\tilde{l}^2} - \frac{4}{\tilde{l}^3} \right) \tilde{S}^2 \quad (4.31)$$

(see Appendix 4.B.2). We evaluate equation (4.28) to obtain the final result, of $O(\tilde{S}^3)$:

$$\begin{aligned} \overset{(3)}{\iota} &= \left[\tilde{S}^3 (-8 - 13e^2 - 2e^4 + 5/3 e^6) + (e^2 + 3) (9 + 5e^2 + 5e^4 + e^6) \tilde{S} \right] \tilde{l}^{-9/2} \\ &+ \left[1/2 (1 - e^2) (5 - e^2) \tilde{S}^3 + (e^2 + 3) (3 + 2e^2 + e^4) \tilde{S} \right] \tilde{l}^{-7/2} \\ &+ \tilde{S} (3 + e^2) (1 + e^2) \tilde{l}^{-5/2} + \tilde{S} (3 + e^2) \tilde{l}^{-3/2} + \frac{\pi}{2}. \end{aligned} \quad (4.32)$$

4.2.3.3 Fifth-order in \tilde{S}

In Komorowski et al. [34] the numerical analysis proceeded as far as was practical given the difficulties that arose from round-off error. In particular, the relative contributions of the terms of higher order in $\tilde{l}^{-1/2}$ were small compared to those of lower order.

We now have a method to calculate the terms in the series that represents ι analytically; but such an approach is not without its own difficulties. Therefore we have resolved to limit our result to terms of maximum order \tilde{S}^3 , which requires us to know the greatest power of \tilde{l} for which the coefficient contains \tilde{S}^5 . It is sufficient to perform these calculations for circular orbits ($e = 0$) for which the expressions used will be greatly simplified. An outline of these calculations can be found in Appendix 4.B.3. The result is $\tilde{l}^{-11/2}$.

4.2.4 Derivatives of $\iota(e, \tilde{l})$ on the Abutment

By taking the partial derivative of ι with respect to \tilde{l} (equation (4.32)) one obtains:

$$\begin{aligned} \left(\frac{\partial \iota}{\partial \tilde{l}}\right)_{min} &= -\frac{3}{2} \left[3 (e^2 + 3) (9 + 5e^2 + 5e^4 + e^6) \tilde{S} - (24 + 39e^2 + 6e^4 - 5e^6) \tilde{S}^3 \right] \tilde{l}^{-11/2} \\ &\quad - \frac{7}{2} \left[(e^2 + 3) (3 + 2e^2 + e^4) \tilde{S} + \frac{1}{2} (1 - e^2) (5 - e^2) \tilde{S}^3 \right] \tilde{l}^{-9/2} \\ &\quad - \frac{5}{2} (3 + e^2) (1 + e^2) \tilde{S} \tilde{l}^{-7/2} - \frac{3}{2} (3 + e^2) \tilde{S} \tilde{l}^{-5/2}. \end{aligned} \quad (4.33)$$

The partial derivative of ι with respect to e can also be derived:

$$\begin{aligned} \left(\frac{\partial \iota}{\partial e}\right)_{min} &= 2e \left(4 (6 + 10e^2 + 6e^4 + e^6) \tilde{S} - (13 - 5e^4 + 4e^2) \tilde{S}^3 \right) \tilde{l}^{-9/2} \\ &\quad + 2e \left((9 + 10e^2 + 3e^4) \tilde{S} - (3 - e^2) \tilde{S}^3 \right) \tilde{l}^{-7/2} \\ &\quad + 4e (2 + e^2) \tilde{S} \tilde{l}^{-5/2} + 2e \tilde{S} \tilde{l}^{-3/2}. \end{aligned} \quad (4.34)$$

The formula in equation (4.33), when evaluated at $e = 0$, matches the numerical result in equation (4.1) for all of the terms with the exception of $-122.7 \tilde{S} \tilde{l}^{-11/2}$, which differs slightly from the analytical result of $-243/2 \tilde{S} \tilde{l}^{-11/2}$.

4.2.5 Directional Derivatives in the $\tilde{l} - e$ Plane

Consider the constant of motion Q and the corresponding quantity ι in the $\tilde{l} - e$ plane; by using the concept of the directional derivative for two variables, one may represent dQ/dt by the equation:

$$\frac{dQ}{dt} = \frac{\partial Q}{\partial \tilde{l}} \frac{d\tilde{l}}{dt} + \frac{\partial Q}{\partial e} \frac{de}{dt}, \quad (4.35)$$

and in a similar manner we may define,

$$\frac{d\iota}{dt} = \frac{\partial \iota}{\partial \tilde{l}} \frac{d\tilde{l}}{dt} + \frac{\partial \iota}{\partial e} \frac{de}{dt}, \quad (4.36)$$

where the terms $d\tilde{l}/dt$ and de/dt denote the evolution of \tilde{l} and e to arbitrary order. We have the benefit of knowing the analytical expressions $\partial Q/\partial\tilde{l}$ (see equation (4.A18)) and $\partial Q/\partial e$ (see equation (4.A19)) at the abutment, which we can derive to the required order.

Further, the weak-field approximations of $d\tilde{l}/dt$ and de/dt are well known [6, 7, 10, 28]:

$$\frac{d\tilde{l}}{dt} = -\frac{64}{5} \left(\frac{m}{M^2}\right) \tilde{l}^{-3} (1 - e^2)^{\frac{3}{2}} \left(1 + \frac{7}{8}e^2\right) \quad (4.37)$$

and

$$\frac{de}{dt} = -e \frac{304}{15} \left(\frac{m}{M^2}\right) \tilde{l}^{-4} (1 - e^2)^{\frac{3}{2}} \left(1 + \frac{121}{304}e^2\right). \quad (4.38)$$

Therefore equations (4.37) and (4.38) can be used to derive the formulae for dQ/dt and $d\iota/dt$ at the abutment. Further, one may calculate the quotient,

$$\frac{\partial e}{\partial\tilde{l}} = \frac{de}{dt} \frac{dt}{d\tilde{l}}, \quad (4.39)$$

using equations (4.38) and (4.37), or evolution equations to higher order if required.

A weak-field solution for $d\iota/dt$ in terms of \tilde{l} and e has been derived and reported in the literature (see equation (15a) in [16]):

$$\frac{d\iota}{dt} = \frac{m\tilde{S}}{M^2} \tilde{l}^{-\frac{11}{2}} (1 - e^2)^{\frac{3}{2}} \sin(\iota) \left(\frac{244}{15} + \frac{252}{5}e^2 + \frac{19}{2}e^4 - \cos(2\psi_0) \left(8e^2 + \frac{26}{5}e^4 \right) \right), \quad (4.40)$$

where the term $\cos(2\psi_0)$, in which ψ_0 represents the orientation of the elliptical orbit in the orbital plane, typically averages to zero with the possible exception where the orbit has a large value of $e < 1$ [16]. More recently, a solution for $d\iota/dt$ to higher order in \tilde{l}^{-1} (we present the weak-field portion here) was derived by Flanagan and Hinderer [29]:

$$\frac{d\iota}{dt} = \frac{m\tilde{S}}{M^2} \tilde{l}^{-\frac{11}{2}} (1 - e^2)^{\frac{3}{2}} \sin(\iota) \left(\frac{266}{15} + \frac{184}{5}e^2 + \frac{151}{20}e^4 + \cos(2\iota) \left(\frac{22}{15} - \frac{62}{5}e^2 - \frac{39}{20}e^4 \right) \right), \quad (4.41)$$

in which they confirmed a weak-field correspondence to equation (4.40). In addition to

the $\sin(\iota)$ contribution found in both equation (4.40) and (4.41), there is a $\cos(2\iota)$ term in the latter expression.

The trigonometric quantities $\sin(\iota)$ and $\cos(\iota)$ do not occur in our expressions for ι and its derivatives at the abutment. But such trigonometric terms are found, usually in a product with \tilde{S} , in the general evolution equations (i.e. $d\tilde{l}/dt$, de/dt , dQ/dt , and $d\iota/dt$) published in the literature [23, 28, 30]. Let us use equation (4.32) to derive approximations of $\sin(\iota)$ and $\cos(\iota)$ that are suitable for working in the leading order of \tilde{S} . Using equations (4.A4) and (4.A5) in Appendix 4.A.1 and the trigonometric identities in Appendix 4.A.2 we find:

$$\sin(\iota) \cong 1 - \frac{1}{2}\tilde{S}^2(3 + e^2)^2\tilde{l}^{-3}, \quad (4.42)$$

and

$$\cos(\iota) \cong -\tilde{S}(3 + e^2)\tilde{l}^{-3/2}. \quad (4.43)$$

Further, we may use

$$\cos(2\iota) \cong -1 + 2\tilde{S}^2(3 + e^2)^2\tilde{l}^{-3}, \quad (4.44)$$

to corroborate the conclusion that equation (4.41) is the same as (4.40) in the weak-field regime. These trigonometric approximations are valid on the abutment; if it is necessary to perform a differentiation of a trigonometric term (as in equation (4.A26)), the differentiation must be performed before making the approximation. Such limitations notwithstanding, the trigonometric approximations are of value to us investigators since they afford us a systematic method for their treatment.

4.3 Correction of $\partial\iota/\partial\tilde{l}$ and $\partial\iota/\partial e$ for Second-order Effects

4.3.1 Introduction

For circular orbits, Komorowski et al. [34] found that the numerical estimate of $\left(\partial\iota/\partial\tilde{l}\right)_{\min}$ in the weak-field regime deviates from the $\partial\iota/\partial\tilde{l}$ results reported in the literature (see Flanagan and Hinderer [29] and Hughes [20]). Consider the quotient of the formulae presented in equation (3.9) of Hughes [20] where $\iota \cong \pi/2$:

$$\frac{i_{weak}}{\dot{R}_{weak}} = \frac{\partial\iota}{\partial\tilde{l}} = -\frac{61}{48}\tilde{S}\tilde{l}^{-\frac{5}{2}}. \quad (4.45)$$

Because $-61/48 > -4.5$ in the weak-field regime, $X_+^2 \Rightarrow X_-^2$ is the pertinent mode; and the best information one can obtain from $\left(\partial\iota/\partial\tilde{l}\right)_{\min}$ is the specification of the lower limit of $\partial\iota/\partial\tilde{l}$ for all $\tilde{l} > \tilde{l}_{LSO,abutment}$. Therefore the second-order (i.e. $\partial^2 Q_{path}/\partial\tilde{l}^2$) behaviour at the point of tangential intersection of Q_X and Q_{path} must be considered. In section 4.2 the numerical results have been verified by analytical derivation of the formula for $\left(\partial\iota/\partial\tilde{l}\right)_{\min}$ to $O(\tilde{S}^3)$. It remains for us to extend this analysis to include second-order effects on elliptical orbits; to this end, we shall discuss how to incorporate second-order effects into Q_X , and the resultant change to the formula for X_{\pm}^2 (see equation (4.2)). Equation (4.26) is sufficient in treating X_{\pm}^2 , and then ultimately ι , to the leading order in \tilde{S} .

4.3.2 Second-order Effects in Q_{path}

4.3.2.1 Circular orbits

Let us begin our treatment in the $Q - \tilde{l}$ plane with $e = 0$ and held constant. The form of Q_X is represented by the series in equation (4.10); and because Q_{path} intersects Q_X

tangentially at a single point (\tilde{l}_o) (contact of the first order), we surmise:

$$Q_{path} \Big|_{\tilde{l}=\tilde{l}_o} = Q_X \Big|_{\tilde{l}=\tilde{l}_o} \quad (4.46)$$

and

$$\frac{\partial Q_{path}}{\partial \tilde{l}} \Big|_{\tilde{l}=\tilde{l}_o} = \frac{\partial Q_X}{\partial \tilde{l}} \Big|_{\tilde{l}=\tilde{l}_o}. \quad (4.47)$$

But the abutment can only offer an upper bound on the second derivative of Q_{path} , i.e.

$$\frac{\partial^2 Q_{path}}{\partial \tilde{l}^2} \Big|_{\tilde{l}=\tilde{l}_o} \leq \frac{\partial^2 Q_X}{\partial \tilde{l}^2} \Big|_{\tilde{l}=\tilde{l}_o}. \quad (4.48)$$

To perform an analytical treatment of the second derivative of Q_{path} , we define an ansatz:

$$Q_{path} = Q_X - \frac{\lambda^2}{2} f(\tilde{l}_o) \quad (4.49)$$

where

$$f(\tilde{l}_o) = (\tilde{l}_o)^p (\tilde{S})^q \left(\sum_{k=0}^n a_k (\tilde{l}_o)^{-k} \right), \quad (4.50)$$

$$a_0 > 0,$$

and

$$\lambda = \tilde{l} - \tilde{l}_o, \quad (4.51)$$

where p and q shall be determined by requiring that the weak-field solution be of the form, $\tilde{S}\tilde{l}^{-\frac{5}{2}}$ (see equations (4.33) and (4.45)). The adjustment represented by equation (4.49) is based on the Taylor expansion of a function; the function $f(\tilde{l}_o)$ represents a second derivative of a primitive, $\wp(e, \tilde{l})$, with respect to \tilde{l} , which is evaluated at \tilde{l}_o . One must not embrangle the concept of the abutment and Taylor series; equation (4.49) is not intended to be a Taylor series representation of Q_{path} . We have taken the analytical formula for Q_X and incorporated a term, which is designed to adjust the second derivative of Q_{path}

so that it makes contact with Q_X tangentially at a prescribed point, \tilde{l}_o . If $\tilde{l} = \tilde{l}_o$, then the adjustment to Q_{path} and $\partial Q_{path}/\partial \tilde{l}$ is zero; and the value of $\partial^2 Q_{path}/\partial \tilde{l}^2$ is reduced by $f(\tilde{l}_o)$. Equation (4.49) can be applied to the analytical development of $\partial \iota/\partial \tilde{l}$. We shall call this reduction of the second derivative the reductive ansatz circular.

Let us consider how the reductive ansatz affects equation (4.2), with attention given to equations (4.7) and (4.8). Evaluate

$$\begin{aligned} Z_9(Q_{path}) &= Z_9(Q_X - \Phi) \\ &= \left[\tilde{l}^5 + \tilde{S}^2 (1 - e^2)^2 Q_X^2 - (\tilde{l} - 3 - e^2) \tilde{l}^3 Q_X \right] \\ &\quad + \Phi \left(2\tilde{S}^2 (1 - e^2)^2 Q_X + \Phi \tilde{S}^2 (1 - e^2)^2 + (\tilde{l} - 3 - e^2) \tilde{l}^3 \right) \end{aligned} \quad (4.52)$$

where

$$\Phi = \frac{\lambda^2}{2} f(\tilde{l}_o),$$

for which the quantity in square brackets in equation (4.52) is equal to zero (*viz.* equation (4.8)) for all values of $\tilde{l} > \tilde{l}_{LSO, abutment}$; therefore, the use of this reductive ansatz has assured us of an effective means to simplify the expressions. The terms that remain share a common factor, λ^2 , which will appear as $\pm\lambda$ when taken outside of the square root in equation (4.2). We shall limit our analysis to $O(\tilde{S})$ (the \tilde{S}^2 terms will affect terms of higher order in \tilde{l}^{-1} in the series in equations (4.33) and (4.34)); therefore, the product of Z_7 (equation (4.5)), Z_8 (equation (4.6)), and Z_9 (equation(4.52)) simplifies to:

$$\begin{aligned} Z_{\sqrt{\bullet}} &= Z_7 Z_8 Z_9 \\ &= \Phi \tilde{l}^5 \left(\tilde{l} - 2(1 + e) \right) \left(\tilde{l} - 2(1 - e) \right) \left(\tilde{l} - 3 - e^2 \right), \end{aligned} \quad (4.53)$$

where we evaluate $Z_{\sqrt{\bullet}}$ at the point of intersection on the abutment by setting $\tilde{l}_o = \tilde{l}$ (i.e. $\lambda = 0$). We take the square root of $Z_{\sqrt{\bullet}}$, and a term, $\pm\lambda\sqrt{2}/2$, emerges. The choice of sign is determined by the mode at the abutment.

There are two modes at the abutment: the fast mode

$$X_-^2 \Rightarrow X_+^2, \quad (4.54)$$

and the slow mode

$$X_+^2 \Rightarrow X_-^2. \quad (4.55)$$

In section 5 of [34] it was established that orbits that evolve on a path towards the

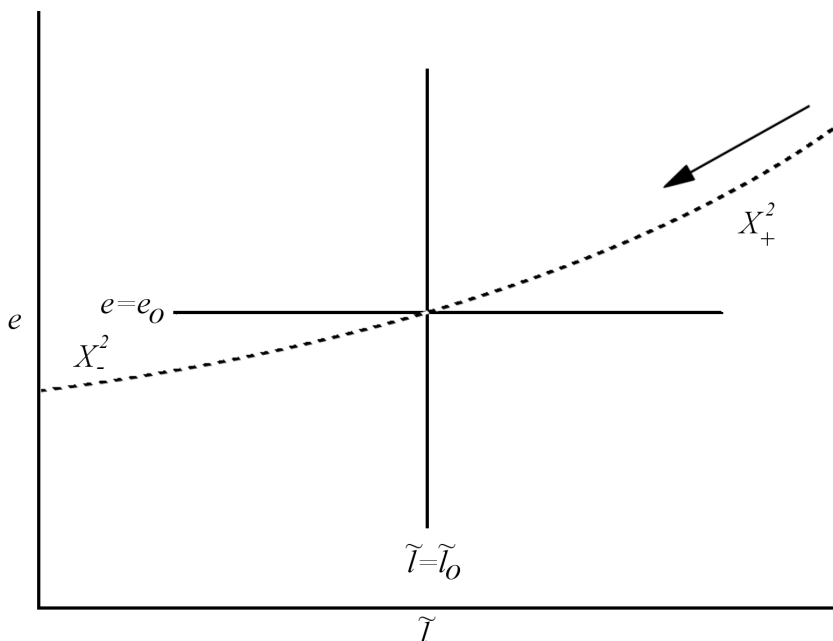


Figure 4-1: A schematic presentation of the $\tilde{l} - e$ plane in which Q_{path} is depicted making contact of the first order at a point (\tilde{l}_o, e_o) on the Q_X surface. The direction in which the orbit evolves is shown by the arrow.

abutment (during which $\tilde{l} > \tilde{l}_o$ and $\lambda > 0$) are governed by X_+^2 (see equation (4.2)) and after making contact with the abutment at $\tilde{l} = \tilde{l}_o$ the orbits are then governed by X_-^2 (for which $\tilde{l} < \tilde{l}_o$ and $\lambda < 0$) (see figure 4-1). Thus by choosing the positive sign for $\pm\lambda$ the equation remains consistent with the dominance of the slow mode.

An examination of equations (4.3), (4.4), and (4.10) reveals that

$$Z_5 + Z_6 Q_X = O\left(\tilde{S}^2, \tilde{l}^4\right), \quad (4.56)$$

from which one may infer

$$2\tilde{S}\sqrt{Z_{\sqrt{\bullet}}} = O\left(\tilde{S}^2\right) \quad (4.57)$$

\Rightarrow

$$\sqrt{2}\lambda\tilde{S} \times \tilde{S}^{q/2} = O\left(\tilde{S}^2\right); \quad (4.58)$$

therefore, $q = 2$ in the reductive ansatz (see equation (4.50)). The value of p can be derived by considering the order of \tilde{L}_z in \tilde{l} . We find (*viz.* equation (4.21)) that $\tilde{L}_z = O\left(\tilde{l}^{-1}\right)$, which must not be changed by the reductive ansätze. And the leading term, \tilde{S} , in the expression for X (see equation (4.13)) must remain. Given the order of \tilde{l} in equation (4.56), one must work with the next lower order, i.e.,

$$2\tilde{S}\sqrt{Z_{\sqrt{\bullet}}} = O\left(\tilde{l}^3\right) \quad (4.59)$$

\Rightarrow

$$\pm \frac{\sqrt{2}}{2} \lambda \tilde{l}^{p/2} \tilde{l}^4 = O\left(\tilde{l}^3\right). \quad (4.60)$$

Given $\lambda = O\left(\tilde{l}\right)$, we conclude that $p = -4$. We have found the values of p and q in our reductive ansätze, which ensure that the second-order effect does not change the form of $\partial\iota/\partial\tilde{l}$ in the weak-field regime.

4.3.2.2 Elliptical orbits

The general formulation of the reductive ansatz elliptical can be derived by starting with Taylor series for two variables (see Appendix 4.A.3). Because we concern ourselves with second-order effects, we shall use the following operator:

$$\frac{1}{2!} \left(\lambda \frac{\partial}{\partial \tilde{l}} + \epsilon \frac{\partial}{\partial e} \right)^2 \quad (4.61)$$

where $\lambda = (\tilde{l} - \tilde{l}_o)$ and $\epsilon = (e - e_o)$, and where the ordered pair (e_o, \tilde{l}_o) specifies the location of the contact of first order between Q_{path} and Q_X . One may define the reductive

ansatz elliptical, i.e.

$$\begin{aligned}
 Q_{path} &= Q_X - \frac{1}{2} \left[\left(\lambda \frac{\partial}{\partial \tilde{l}} + \epsilon \frac{\partial}{\partial e} \right)^2 \wp(e, \tilde{l}) \right]_{\substack{e=e_o \\ \tilde{l}=\tilde{l}_o}} \\
 &= Q_X - \frac{\lambda^2}{2} \left[\frac{\partial^2}{\partial \tilde{l}^2} \wp(e, \tilde{l}) \right]_{\substack{e=e_o \\ \tilde{l}=\tilde{l}_o}} - \lambda \epsilon \left[\frac{\partial^2}{\partial \tilde{l} \partial e} \wp(e, \tilde{l}) \right]_{\substack{e=e_o \\ \tilde{l}=\tilde{l}_o}} - \frac{\epsilon^2}{2} \left[\frac{\partial^2}{\partial e^2} \wp(e, \tilde{l}) \right]_{\substack{e=e_o \\ \tilde{l}=\tilde{l}_o}} \quad (4.62)
 \end{aligned}$$

where we conjecture the existence of a primitive function, $\wp(e, \tilde{l})$.

The expression for Q_{path} is best regarded as a parameterized curve, and to make such a treatment in equation (4.62), one may factor out the λ , to obtain

$$\begin{aligned}
 Q_{path} &= Q_X - \frac{\lambda^2}{2} \left\{ \left[\frac{\partial^2}{\partial \tilde{l}^2} \wp(e, \tilde{l}) \right]_{\substack{e=e_o \\ \tilde{l}=\tilde{l}_o}} + 2 \left(\frac{\epsilon}{\lambda} \right) \left[\frac{\partial^2}{\partial \tilde{l} \partial e} \wp(e, \tilde{l}) \right]_{\substack{e=e_o \\ \tilde{l}=\tilde{l}_o}} + \left(\frac{\epsilon}{\lambda} \right)^2 \left[\frac{\partial^2}{\partial e^2} \wp(e, \tilde{l}) \right]_{\substack{e=e_o \\ \tilde{l}=\tilde{l}_o}} \right\} \\
 &= Q_X - \frac{\lambda^2}{2} g(e_o, \tilde{l}_o), \quad (4.63)
 \end{aligned}$$

for which we have the benefit of knowing the limiting form of ϵ/λ ($= de/d\tilde{l}$) to arbitrary order in \tilde{l}^{-1} . Thus it is possible to parameterize Q_{path} in terms of λ . We can use the expression,

$$g(e_o, \tilde{l}_o) = \tilde{S}^2 \sum_{i=0}^n \frac{a_i(e_o)}{\tilde{l}_o^{i+4}}; \quad (4.64)$$

and this will form the basis of the reductive ansatz elliptical.

4.3.3 Application of the Reductive Ansätze to the Analytical Derivation of $\partial \iota / \partial \tilde{l}$ and $\partial \iota / \partial e$

The reductive ansätze (equations (4.49-4.51) and (equation (4.63))) constitute a reduction of the second derivative of Q_X to more realistically model the behaviour of Q_{path} at the abutment and the methodical treatment of this reduction in the analytical calculation of $\partial \iota / \partial \tilde{l}$ and $\partial \iota / \partial e$.

The procedure outlined in Appendix 4.A.4 yields the following formula for $\partial\iota/\partial\tilde{l}$:

$$\frac{\partial\iota}{\partial\tilde{l}} = \frac{\partial \left[\iota \left(e, \tilde{l}, \lambda, \tilde{S} \right) \right]_{\lambda=0}}{\partial\tilde{l}} + \left[\frac{\partial \left[\iota \left(e, \tilde{l}, \lambda, \tilde{S} \right) \right]}{\partial\lambda} \frac{\partial\lambda}{\partial\tilde{l}} \right]_{\lambda=0}, \quad (4.65)$$

where

$$\frac{\partial\lambda}{\partial\tilde{l}} = 1 \text{ and } \lambda \Big|_{\tilde{l}=\tilde{l}_o} = 0;$$

but the result for $\partial\iota/\partial e$ is simpler,

$$\begin{aligned} \frac{\partial\iota}{\partial e} &= \frac{\partial \left[\iota \left(e, \tilde{l}, \lambda, \tilde{S} \right) \right]_{\lambda=0}}{\partial e} \\ &= \left(\frac{\partial\iota}{\partial e} \right)_{\min}. \end{aligned} \quad (4.66)$$

Equation (4.66) and the first term in equation (4.65) yields the formulae that describe the evolution of ι for a Q_{path} along the abutment (i.e. $(\partial\iota/\partial e)_{\min}$ and $(\partial\iota/\partial\tilde{l})_{\min}$). The second term of equation (4.65) incorporates second-order effects, and thus describes the physically more realistic situation in which Q_{path} intersects the abutment tangentially at a single point. Because one takes the first derivative with respect to λ , the second and higher powers of λ will vanish when setting $\lambda = 0$. But as we shall presently see, the second-order effects of the reductive ansätze remain.

We choose to work with the symbols e and \tilde{l} rather than e_o and \tilde{l}_o , given that e and \tilde{l} can be used to represent an arbitrary point on the abutment (see Appendix 4.A.4). The reductive ansatz circular (see equations (4.49-4.51)) is applied at the abutment with $p = -4$, $q = 2$, and $n = 2$ (while retaining the two terms of leading order in \tilde{S} at the conclusion of the calculation) with

$$\frac{\partial\iota}{\partial\tilde{l}} = -\tilde{S} \left\{ \frac{15}{2} + \frac{3}{2}A_0(0) - \frac{1}{4}A_1(0) \right\} \tilde{l}^{-7/2} - \tilde{S} \left\{ \frac{9}{2} - A_0(0) \right\} \tilde{l}^{-5/2} \quad (4.67)$$

where

$$A_0(e) = +\frac{\sqrt{2}}{2}\sqrt{a_0(e)}, \text{ and } A_1(e) = \frac{a_1(e)}{A_0(e)}.$$

To apply this method to elliptical orbits, we will be required to use $g(e, \tilde{l})$. To calculate that function, the common primitive $\wp(e, \tilde{l})$ is needed.

4.3.4 Analytical Derivation of the Common Primitive, $\wp(e, \tilde{l})$

Now that the values of the parameters, $p = -4$ and $q = 2$, have been found, it is possible to derive the formula for $\wp(e, \tilde{l})$. Consider the reductive ansatz circular:

$$f(\tilde{l}) = \tilde{S}^2 \sum_{i=0}^n \frac{a_i}{\tilde{l}^{i+4}}. \quad (4.68)$$

We conjecture a more general form of $f(\tilde{l})$ that includes e :

$$f(e, \tilde{l}) = \tilde{S}^2 \sum_{i=0}^n \frac{a_i(1 + b_i e^2)}{\tilde{l}^{i+4}}. \quad (4.69)$$

Performing the first integration over \tilde{l} yields:

$$\begin{aligned} F(e, \tilde{l}) &= \int f(e, \tilde{l}) d\tilde{l} \\ &= -\tilde{S}^2 \left[\sum_{i=0}^n \left(\frac{1}{i+3} \frac{a_i(1 + b_i e^2)}{\tilde{l}^{i+3}} \right) - \varkappa(e) \right]. \end{aligned} \quad (4.70)$$

The second integration over \tilde{l} yields an expression for the common primitive:

$$\begin{aligned} \wp(e, \tilde{l}) &= \int F(e, \tilde{l}) d\tilde{l} \\ &= \tilde{S}^2 \left[\sum_{i=0}^n \left(\frac{1}{(i+2)(i+3)} \frac{a_i(1 + b_i e^2)}{\tilde{l}^{i+2}} \right) + \varkappa(e) \tilde{l} + \zeta(e) \right]. \end{aligned} \quad (4.71)$$

The constants of integration, $\varkappa(e) \tilde{l}$ and $\zeta(e)$, can each be set to zero since we require

$\lim_{\tilde{l} \rightarrow \infty} \wp(e, \tilde{l}) = 0$. Now that the formula for $\wp(e, \tilde{l})$ is known, it is possible to obtain $g(e, \tilde{l})$, which is required by the reductive ansatz elliptical.

4.4 The Treatment of dQ/dt and $d\iota/dt$ on the Abutment

4.4.1 The dQ/dt Evolution Equations

Komorowski et al. [34] investigated the consistency of dQ/dt with the evolution equation $d\tilde{l}/dt$, for circular orbits at the abutment ($\iota \gtrsim \pi/2$) by performing a preliminary numerical analysis for values of $\tilde{l} = \{7.0, 100.0\}$ and KBH spin $\tilde{S} = \{0.05, 0.95\}$ (see section 5.2.1 of [34]). The published values of $d\tilde{l}/dt$ [20] that were used were calculated for $\iota \simeq \pi/3$, and the difference of this value of ι contributed to some inaccuracy in the analysis. In this work, the derivation of analytical formulae for ι and its derivatives as well as the use of the directional derivative to determine dQ/dt now allow one to perform a more complete treatment for elliptical orbits.

Let us consider the directional derivative in equation (4.35) as a means of deriving dQ/dt at the abutment. We have demonstrated that the second-order effects are not seen when calculating the first derivatives of Q_{path} (i.e. $\partial Q_{path}/\partial \tilde{l}$ and $\partial Q_{path}/\partial e$, see equations (4.46) and (4.63)); therefore, we may use $\partial Q_X/\partial \tilde{l}$ (equation (4.A18)) and $\partial Q_X/\partial e$ (equation (4.A19)) when working with equation (4.35).

The form of dQ/dt (equation (A.3) in [27] (after equation (56) in [26])), which was used in [34] to test dQ/dt will be revisited in this work (see equation (4.A21) in Appendix

4.A.6):

$$\begin{aligned}
\left(\frac{dQ}{dt}\right)_{2PN} &= - \left(1 - \frac{1}{2} \frac{\tilde{S}^2 (3 + e^2)^2}{\tilde{l}^3}\right) \frac{64 m^2}{5 M} (1 - e^2)^{3/2} \frac{\sqrt{Q}}{\tilde{l}^{7/2}} \\
&\times \left[g_9(e) - \frac{g_{11}(e)}{\tilde{l}} + \pi \frac{g_{12}(e)}{\tilde{l}^{3/2}} \right. \\
&\quad \left. - \frac{\left(g_{13}(e) - \tilde{S}^2 \left(g_{14}(e) - \frac{45}{8}\right)\right)}{\tilde{l}^2} \right. \\
&\quad \left. + \tilde{S}^2 \frac{g_{10}^b(e) (3 + e^2)}{\tilde{l}^3} + \frac{45 \tilde{S}^4 (3 + e^2)^2}{8 \tilde{l}^5} \right]. \tag{4.72}
\end{aligned}$$

But it is preferable that the formula for dQ/dt (and for du/dt) that we test be accompanied, in the same work, by their associated expressions for $d\tilde{l}/dt$ and de/dt ; and fortunately a paper by Ganz et al. [28] provides such information, which we shall use in our analysis. In particular, we will use equation (4.3) in [28], the evolution equation for \tilde{l} ,

$$\begin{aligned}
\frac{d\tilde{l}}{dt} &= -\frac{64}{5} \left(\frac{m}{M^2}\right) \tilde{l}^{-3} (1 - e^2)^{\frac{3}{2}} \\
&\times \left[g_9 - \frac{f_1}{\tilde{l}} + \pi \frac{g_{12}}{\tilde{l}^{3/2}} + \frac{f_3 - f_4 \tilde{S}^2}{\tilde{l}^2} - \pi \frac{f_7}{\tilde{l}^{5/2}} \right. \\
&\quad \left. + \frac{f_2 (3 + e^2) \tilde{S}^2}{\tilde{l}^3} - \frac{f_6 (3 + e^2) \tilde{S}^2}{\tilde{l}^4} + \frac{f_5 (3 + e^2)^2 \tilde{S}^4}{\tilde{l}^5} \right], \tag{4.73}
\end{aligned}$$

which is (excluding the common factor, \tilde{l}^{-3}) to $O(\tilde{l}^{-5/2})$ in [28]; and the evolution equation for e ,

$$\begin{aligned}
\frac{de}{dt} &= -\frac{304}{15} \left(\frac{m}{M^2}\right) \tilde{l}^{-4} (1 - e^2)^{\frac{3}{2}} \\
&\times \left[h_1 - \frac{h_2}{\tilde{l}} + \pi \frac{h_4}{\tilde{l}^{3/2}} - \frac{h_5 + h_6 \tilde{S}^2}{\tilde{l}^2} - \pi \frac{h_9}{\tilde{l}^{5/2}} \right. \\
&\quad \left. + \frac{h_3 (3 + e^2) \tilde{S}^2}{\tilde{l}^3} - \frac{h_8 (3 + e^2) \tilde{S}^2}{\tilde{l}^4} + \frac{h_7 (3 + e^2)^2 \tilde{S}^4}{\tilde{l}^5} \right], \tag{4.74}
\end{aligned}$$

which is (excluding the common factor, \tilde{l}^{-4}) also to $O(\tilde{l}^{-5/2})$ in [28].

The evolution equation of Q ,

$$\begin{aligned} \frac{dQ}{dt} = & -\frac{64}{5} \left(\frac{m}{M^2} \right) \tilde{l}^{-3} (1 - e^2)^{\frac{3}{2}} \left(1 - \frac{\tilde{S}^2 (3 + e^2)^2}{\tilde{l}^3} \right) \times [g_9 \\ & - \frac{d_1}{\tilde{l}^1} + \pi \frac{g_{12}}{\tilde{l}^{3/2}} - \frac{d_3 - d_4 \tilde{S}^2}{\tilde{l}^2} - \pi \frac{d_7}{\tilde{l}^{5/2}} \\ & + \frac{\tilde{S}^2 (3 + e^2) d_2}{\tilde{l}^3} - \frac{\tilde{S}^2 (3 + e^2) d_6}{\tilde{l}^4} + \frac{\tilde{S}^4 (3 + e^2)^2 d_5}{\tilde{l}^5}] , \end{aligned} \quad (4.75)$$

which corresponds to equation (4.1) in [28], was of $O(\tilde{l}^{-5/2})$ (excluding the common factor, \tilde{l}^{-3}). These formulae (equations (4.73), (4.74), and (4.75)) have been converted from the variables used in [28] to our variables (see Appendices 4.A.6 and 4.A.7). Because some of the original coefficients contained $\cos(\iota)$, which we have replaced with the approximation in equation (4.43), there are new terms, which correspond to \tilde{l}^{-3} , \tilde{l}^{-4} , and \tilde{l}^{-5} , in each of equations (4.73), (4.74), and (4.75). The original expressions did not include terms with these powers of \tilde{l} , so we cannot use the new terms to extend the accuracy of our analysis beyond that of the original expressions in Ganz et al. [28].

Table 4.1: The coefficients of $-5/64 M^2/m \tilde{l}^3 dQ/dt$ up to \tilde{l}^{-3} . The first column contains the ideal results at the abutment. The second column contains the results of Ganz et al. [28], and the third column contains the results of Barausse, Hughes, and Rezzolla [27]. The trigonometric functions in both of these sets were evaluated on the abutment using the approximations in equations (4.43) and (4.42).

| | Directional Derivative at the Abutment (see equation (4.35)) | (equation 4.1 in [28]) (see equation (4.75)) | (equation (A3) in [27]) (see equation (4.72)) |
|--------------------|--|---|---|
| \tilde{l}^0 | $1 + \frac{7}{8}e^2$ | $1 + \frac{7}{8}e^2$ | $1 + \frac{7}{8}e^2$ |
| \tilde{l}^{-1} | $-\left(\frac{743}{336} - \frac{23}{42}e^2 - \frac{121}{96}e^4\right)$ | $-\left(\frac{743}{336} - \frac{23}{42}e^2\right)$ | $-\left(\frac{743}{336} - \frac{23}{42}e^2 - \frac{7}{16}e^4\right)$ |
| $\tilde{l}^{-3/2}$ | $\pi\left(4 + \frac{97}{8}e^2\right)$ | $\pi\left(4 + \frac{97}{8}e^2\right)$ | $\pi\left(4 + \frac{97}{8}e^2\right)$ |
| \tilde{l}^{-2} | $-\left[\frac{129293}{18144} + \frac{84035}{1728}e^2 - \frac{629}{672}e^4 + \tilde{S}^2\left(\frac{329}{96} + \frac{929}{96}e^2\right)\right]$ | $-\left[\frac{129293}{18144} + \frac{84035}{1728}e^2 + \tilde{S}^2\left(\frac{329}{96} + \frac{929}{96}e^2\right)\right]$ | $-\left[\frac{129293}{18144} + \frac{84035}{1728}e^2 - \frac{575}{336}e^4 + \tilde{S}^2\left(\frac{342}{96} - \frac{570}{96}e^2\right)\right] \S$ |
| $\tilde{l}^{-5/2}$ | $-\pi\left(\frac{4159}{672} + \frac{21229}{1344}e^2 - \frac{41783}{1344}e^4\right)$ | $-\pi\left(\frac{4159}{672} + \frac{21229}{1344}e^2\right)$ | $\pi\left(\frac{4032}{672} + \frac{27132}{1344}e^2 + \frac{8148}{1344}e^4\right)$ |
| \tilde{l}^{-3} | $-\left[\frac{3819}{112} + \frac{770993}{12096}e^2 + \frac{333937}{2304}e^4 - \tilde{S}^2\left(\frac{250}{8} + \frac{2495}{64}e^2\right)\right]$ | $-\left[0 - \tilde{S}^2\left(\frac{183}{8} + \frac{4856}{64}e^2\right)\right]$ | $-$ |

We assume that the evolution of the orbit, $d\tilde{l}/dt$ and de/dt , is described by equations (4.A23) and (4.A24) (from Ganz et al. [28]). The result of evaluating equation (4.35) is compiled in table 4.1 (first column). The second column contains the result dQ/dt , derived by Ganz et al. (see equation (4.A22)), evaluated on the abutment. Similarly, the third column contains the formula for dQ/dt based on equation (A.3) in [27], also evaluated on the abutment.

The results are in good agreement with the exception of the coefficients for the e^4 terms, which is to be expected since most of the original expressions drawn from the literature were accurate to $O(e^2)$. The coefficient corresponding to the \tilde{l}^{-5} term in the third column in table 4.1 (marked with §) differs from the other two results, but for that term, the original equation in Barausse, Hughes, and Rezzolla [27] differed from that of Ganz et al. [28].

Because the expressions for $\partial Q_X/\partial\tilde{l}$ and $\partial Q_X/\partial e$ can be derived to arbitrary order in \tilde{l}^{-1} , and the coefficients for each power are exact finite series in e^2 , it is worthwhile to consider using the abutment or improving the order of e of the evolution equations in the weaker field regime. Since the abutment extends down to the last stable orbit (LSO), one might also explore the development and testing of evolution equations in the strong-field regime, given that on the abutment the trigonometric contributions of $\sin(\iota)$ and $\cos(\iota)$ can be expressed as functions of e , \tilde{l} , and \tilde{S} . But one must be mindful of the assumptions made at the outset of this exercise, in particular, the assumption that the secondary object can be approximated as a test-particle of infinitesimal mass, and the use of adiabatically evolving orbits.

4.4.2 The Second-order Calculation of $d\nu/dt$ for the Leading Order of \tilde{S} (weak-field regime)

Now that $\wp(e, \tilde{l})$ is known we can calculate $g(e, \tilde{l})$; but let us first derive $de/d\tilde{l}$. From equation (4.73):

$$\frac{d\tilde{l}}{dt} = -\frac{64}{5} \left(\frac{m}{M^2}\right) \tilde{l}^{-3} (1 - e^2)^{\frac{3}{2}} \left(g_9 - \frac{f_1}{\tilde{l}}\right), \quad (4.76)$$

and equation (4.74):

$$\frac{de}{dt} = -\frac{304}{15} \left(\frac{m}{M^2}\right) \tilde{l}^{-4} (1 - e^2)^{\frac{3}{2}} \left(h_1 - \frac{h_2}{\tilde{l}}\right), \quad (4.77)$$

from which we find the following:

$$\frac{de}{d\tilde{l}} = \frac{19}{12} e \left(\frac{1 - \frac{145}{304} e^2}{\tilde{l}} + \frac{\frac{3215}{3192} - \frac{33373}{102144} e^2}{\tilde{l}^2} \right). \quad (4.78)$$

From equation (4.63), one derives:

$$g(e, \tilde{l}) = \tilde{S}^2 \left[\frac{a_0(e)}{\tilde{l}^4} + \frac{a_1(e)}{\tilde{l}^5} \right], \quad (4.79)$$

where

$$a_0(e) = a_0(0) \left(1 - \frac{119}{432} b_0 e^2 \right)$$

and

$$a_1(e) = a_1(0) \left(1 + \left(\frac{3215}{72576} b_0 - \frac{143}{864} b_1 \right) e^2 \right),$$

which can be used to calculate $\partial\nu/\partial\tilde{l}$ under the reductive ansatz elliptical,

$$\begin{aligned} \frac{\partial\nu}{\partial\tilde{l}} &= -\tilde{S} \left\{ \frac{5}{2} (3 + e^2) (1 + e^2) + \frac{1}{2} (3 + e^2) A_0(e) - \frac{1}{4} A_1(e) \right\} \tilde{l}^{-7/2} \\ &\quad - \tilde{S} \left\{ \frac{3}{2} (3 + e^2) - A_0(e) \right\} \tilde{l}^{-5/2}, \end{aligned} \quad (4.80)$$

where

$$A_0(e) = A_0(0) \left(1 - \frac{1}{2} \frac{119}{432} b_0 e^2 \right)$$

and

$$A_1(e) = \frac{a_1(e)}{A_0(e)}.$$

Now that we have developed a formula for $\partial\iota/\partial\tilde{l}$ (equation (4.80)) that incorporates the reductive ansatz elliptical, and we have found that $\partial\iota/\partial e$ (equation(4.34)) is unaffected by the reductive ansatz elliptical, the expression for $d\iota/dt$ can be obtained from equation (4.36) to the leading order in \tilde{S} with coefficients of $O(e^2)$:

$$\frac{d\iota}{dt} = \tilde{S} \frac{m}{M^2} \tilde{l}^{-4} (1 - e^2)^{\frac{3}{2}} \left(\frac{U_1}{\tilde{l}^{3/2}} - \frac{U_3}{\tilde{l}^{5/2}} \right), \quad (4.81)$$

where

$$\begin{aligned} U_1 &= \frac{32}{15} (9 - 2A_0(e)) + \frac{4}{15} (-109 + 42A_0(e)) e^2 \\ U_3 &= \frac{2}{105} (1647 - 2494A_0(e) + 168A_1(e)) \\ &\quad + \frac{1}{105} (682 - 2978A_0(e) + 147A_1(e)) e^2. \end{aligned}$$

Equation (4.A27) can be expanded and expressed to leading order in \tilde{S} to yield:

$$\frac{d\iota}{dt} = \frac{244}{15} \tilde{S} \frac{m}{M^2} \tilde{l}^{-4} (1 - e^2)^{\frac{3}{2}} \left(\frac{u_1}{\tilde{l}^{3/2}} - \frac{u_3}{\tilde{l}^{5/2}} \right). \quad (4.82)$$

By equating the terms in equations (4.81) and (4.82) (i.e. $U_1 = 244u_1/15$ and $U_3 = 244u_3/15$) one first solves for $A_0(0)$ and $A_1(0)$, for a circular orbit, by setting $e = 0$:

$$A_0(0) = \frac{155}{48}$$

and

$$A_1(0) = \frac{279289}{4032}.$$

By substituting these values into equation (4.81), we obtain,

$$\begin{aligned} \frac{dt}{dt} = & \frac{244}{15} \tilde{S} \frac{m}{M^2} \tilde{l}^{-4} (1 - e^2)^{\frac{3}{2}} \\ & \times \left[\frac{\left(1 + \left(\frac{18445}{52704} b_0 - \frac{213}{488}\right) e^2\right)}{\tilde{l}^{3/2}} \right. \\ & \left. - \frac{\left(\frac{10461}{1708} + \left(\frac{79869}{54656} - \frac{39938327}{17708544} b_1 + \frac{5621763839}{1487517696} b_0\right) e^2\right)}{\tilde{l}^{5/2}} \right]. \end{aligned} \quad (4.83)$$

When evaluated at $e = 0$, the expression in equation (4.83) matches the results reported in the literature (equations (4.40), (4.41), and (4.82)) for near-polar orbits. For near-circular orbits, values of b_0 and b_1 can be found for which the coefficients of the $\tilde{l}^{-3/2}$ and $\tilde{l}^{-5/2}$ terms in equation (4.83) match its theoretical counterpart in equation (4.82).

4.4.3 The Independence of the Abutment of Radiation Back-reaction Models

Let us clarify the meaning of our statement that the abutment model is independent of any specific radiation back-reaction model. The expression for the abutment, Q_X (equation (4.9)), is determined by the characteristics of the Kerr spacetime of the primary object, in which the secondary object (i.e. test-particle) orbits. The analytical expressions for $d\tilde{l}/dt$ and de/dt describe the effects of radiation back-reaction on the values of \tilde{l} and e of the orbit, and they serve as inputs to our abutment model in two ways: first, through the quotient $\epsilon/\lambda \cong \partial e/\partial \tilde{l}$ (equation (4.63)); and second, through the directional derivatives in equations (4.35) and (4.36).

The mechanics of the abutment remain consistent, the details of the radiation back-reaction model notwithstanding. The results of either directional derivative are outputs of the abutment model that describe the effect of the radiation back-reaction on the listing of the test-particle orbit.

4.5 Conclusions

In this work we derived an analytical formula for the value of orbital inclination, ι , of an elliptical orbit on the abutment. By performing the partial derivative of ι with respect to \tilde{l} , we were able to confirm the numerical result for $\partial\iota/\partial\tilde{l}$ reported in Komorowski et al. [34] for circular orbits, and we were able to extend the formula to include $\partial\iota/\partial\tilde{l}$ for elliptical orbits. A result for $\partial\iota/\partial e$ was also obtained for elliptical orbits.

Evolving orbits in Kerr spacetime are not constrained to follow the abutment. Instead, the value of the Carter constant (Q) will follow Q_{path} , which intersects the abutment tangentially at an arbitrary point of contact of the first order. For circular orbits, we modelled the second-order behaviour reported in [34] by introducing a bounded function $f(e, \tilde{l})$ (also in terms of \tilde{S}) to reduce the value of $\partial^2 Q_{path}/\partial\tilde{l}^2$ while leaving Q_{path} and $\partial Q_{path}/\partial\tilde{l}$ equal to their corresponding values (Q_X and $\partial Q_X/\partial\tilde{l}$) on the abutment. This approach was then applied to elliptical orbits, and a new bounded function $g(e, \tilde{l})$, which depends upon $de/d\tilde{l}$, was also applied to $\partial^2 Q_{path}/\partial\tilde{l}^2$. It was discovered that the value of $\partial^2 Q_{path}/\partial e^2$ remained unchanged. An expression was thus generated for $d\iota/dt$, which was consistent with published results, using a method that itself is independent of any specific radiation back-reaction model.

The consistency of published evolution equations, dQ/dt , $d\tilde{l}/dt$, and de/dt , was tested by using $d\tilde{l}/dt$ and de/dt to generate an expression for dQ/dt at the abutment. In general, the calculation of dQ/dt is more difficult to perform than that of $d\tilde{l}/dt$ and de/dt [18]; hence, the abutment provides a useful mechanism for testing the validity of radiation back-reaction models. This method also promises to be a powerful tool for extending the accuracy of evolution equations to greater order in e and \tilde{l}^{-1} . Further work might entail the development of a more precise mathematical treatment of the ansätze in relation to the underlying physical concepts of the radiation back-reaction process and its effect on the listing behaviour of orbits near the abutment.

Appendix 4.A Ancillary Equations

4.A.1 Maclaurin Series Expansions of Various Functions

These results are widely available, see for example: §97 in [35], page 111 in [36], and page 231 in [37], or calculate them directly to the precision one requires

$$\frac{1}{1+x} \cong 1 - x + x^2 - x^3 + x^4 + O(x^5) \quad (4.A1)$$

$$\sqrt{1+x} \cong 1 + \frac{1}{2}x - \frac{1}{8}x^2 + \frac{1}{16}x^3 - \frac{5}{128}x^4 + O(x^5) \quad (4.A2)$$

$$\arccos(x) \cong \frac{\pi}{2} - x - \frac{1}{6}x^3 - \frac{3}{40}x^5 + O(x^7) \quad (4.A3)$$

$$\cos(x) = 1 - \frac{1}{2}x^2 + \frac{1}{24}x^4 + O(x^6) \quad (4.A4)$$

$$\sin(x) = x - \frac{1}{6}x^3 + \frac{1}{120}x^5 + O(x^7). \quad (4.A5)$$

4.A.2 Selected Trigonometric Identities

The value of $\iota \gtrsim \pi/2$, therefore, the following two trigonometric identities are essential for our analytical treatment of the evolution equations

$$\sin\left(\frac{\pi}{2} + x\right) = \cos(x) \quad (4.A6)$$

$$\cos\left(\frac{\pi}{2} + x\right) = -\sin(x) \quad (4.A7)$$

$$\cos(\pi + x) = -\cos(x). \quad (4.A8)$$

4.A.3 Taylor Series for two Variables

Refer to Chapter 6 in [37] for a more detailed treatment. Let us consider a locally continuous function with two independent variables, $f(x, y)$. We may use an operator

$$\left(h \frac{\partial}{\partial x} + k \frac{\partial}{\partial y} \right) \quad (4.A9)$$

to construct a Taylor series of n terms

$$\begin{aligned} f(x_o + h, y_o + k) &= f(x_o, y_o) \\ &+ \left[\left(h \frac{\partial}{\partial x} + k \frac{\partial}{\partial y} \right) f(x, y) \right]_{\substack{x=x_o \\ y=y_o}} + \frac{1}{2!} \left[\left(h \frac{\partial}{\partial x} + k \frac{\partial}{\partial y} \right)^2 f(x, y) \right]_{\substack{x=x_o \\ y=y_o}} \\ &\dots + \frac{1}{n!} \left[\left(h \frac{\partial}{\partial x} + k \frac{\partial}{\partial y} \right)^n f(x, y) \right]_{\substack{x=x_o \\ y=y_o}} \end{aligned} \quad (4.A10)$$

if the $(n + 1)^{th}$ partial derivatives are continuous. In this paper, we are concerned only with the second derivative.

4.A.4 Treatment of the Taylor Series Under Partial Differentiation

Given the term:

$$A = hf(x_o)g(x), \quad (4.A11)$$

where $h = (x - x_o)$. We can calculate the partial derivative of A with respect to x ,

$$\begin{aligned} \frac{\partial A}{\partial x} &= \frac{\partial}{\partial x} (hf(x_o)g(x)) \\ &= f(x_o) \frac{\partial}{\partial x} (hg(x)) \\ &= f(x_o) \left(h \frac{\partial}{\partial x} g(x) + g(x) \frac{\partial}{\partial x} h \right), \end{aligned} \quad (4.A12)$$

and thus demonstrate

$$\left. \frac{\partial A}{\partial x} \right|_{x=x_o} = f(x_o)g(x_o). \quad (4.A13)$$

Consider a more complicated case where we have a function $F(x, h, y, k)$, where $h =$

$(x - x_o)$ and $k = (y - y_o)$. Calculate

$$\left. \frac{\partial F}{\partial x} \right|_{x=x_o} \quad \text{and} \quad \left. \frac{\partial F}{\partial y} \right|_{y=y_o}. \quad (4.A14)$$

If we hold y constant and set $k = 0$, then

$$\frac{dF}{dx} = \frac{\partial F}{\partial x} + \frac{\partial F}{\partial h} \frac{\partial h}{\partial x}. \quad (4.A15)$$

If we hold x constant and set $h = 0$, then

$$\frac{dF}{dy} = \frac{\partial F}{\partial y} + \frac{\partial F}{\partial k} \frac{\partial k}{\partial y}. \quad (4.A16)$$

These results will be of use in applying the second-order effects to Q_{path} as it makes contact with the abutment, Q_X .

4.A.5 Treatment of Q_X as a Series in \tilde{l}

The expansion of Q_X in terms of \tilde{S} (equation (4.10)) can be expressed as a series in \tilde{l} :

$$Q_X = \tilde{l} + \sum_{i=0}^{\infty} \left[\frac{(3 + e^2)^{i+1}}{\tilde{l}^i} + \frac{i(i-1)(3 + e^2)^{i-2}(1 - e^2)}{2\tilde{l}^i} \tilde{S}^2 \right]. \quad (4.A17)$$

From equation (4.A17) one can obtain $\partial Q_X / \partial \tilde{l}$ and $\partial Q_X / \partial e$ directly:

$$\frac{\partial Q_X}{\partial \tilde{l}} = 1 - \sum_{i=0}^{\infty} \left[\frac{i(3 + e^2)^{i+1}}{\tilde{l}^{i+1}} + \frac{i^2(i-1)(3 + e^2)^{i-2}(1 - e^2)}{2\tilde{l}^{i+1}} \tilde{S}^2 \right], \quad (4.A18)$$

and

$$\begin{aligned} \frac{\partial Q_X}{\partial e} = & 2e \sum_{i=0}^{\infty} \left[\frac{(i+1)(3 + e^2)^i}{\tilde{l}^i} - \frac{i(i-1)(3 + e^2)^{i-2}}{2\tilde{l}^i} \tilde{S}^2 \right. \\ & \left. + \frac{i(i-1)(i-2)(3 + e^2)^{i-3}(1 - e^2)}{2\tilde{l}^i} \tilde{S}^2 \right]. \end{aligned} \quad (4.A19)$$

The $\sqrt{Q_X}$ will also be required for the treatment of dQ/dt , (see Appendix 4.A.6)

$$\begin{aligned}\sqrt{Q_X} &= \sqrt{\tilde{l}} + \frac{1}{2} \frac{3+1e^2}{\sqrt{\tilde{l}}} + \frac{3}{8} \frac{(3+e^2)^2}{\tilde{l}^{3/2}} + \frac{1}{2} \frac{\left((1-e^2)\tilde{S}^2 + \frac{5}{8}(3+e^2)^3\right)}{\tilde{l}^{5/2}} \\ &\quad + \frac{5}{128} \frac{(3+e^2)\left(32(1-e^2)\tilde{S}^2 + 7(3+e^2)^3\right)}{\tilde{l}^{7/2}} \\ &\quad + \frac{7}{256} \frac{(3+e^2)^2\left(80(1-e^2)\tilde{S}^2 + 9(3+e^2)^3\right)}{\tilde{l}^{9/2}} + \dots\end{aligned}\quad (4.A20)$$

4.A.6 The 2PN Flux for Q

An expression for dQ/dt was derived from equation (A.3) in [27] (after equation (56) in [26]) by substituting $\sin(\iota)$ and $\cos(\iota)$ for their approximations on the abutment (see equations (4.42) and (4.43))

$$\begin{aligned}\left(\frac{dQ}{dt}\right)_{2PN} &= - \left(1 - \frac{1}{2} \frac{\tilde{S}^2(3+e^2)^2}{\tilde{l}^3}\right) \frac{64}{5} \frac{m^2}{M} (1-e^2)^{3/2} \frac{\sqrt{Q}}{\tilde{l}^{7/2}} \\ &\quad \times \left[g_9(e) - \frac{g_{11}(e)}{\tilde{l}} + \pi \frac{g_{12}(e)}{\tilde{l}^{3/2}} - \frac{\left(g_{13}(e) - \tilde{S}^2(g_{14}(e) - \frac{45}{8})\right)}{\tilde{l}^2} \right. \\ &\quad \left. + \tilde{S}^2 \frac{g_{10}^b(e)(3+e^2)}{\tilde{l}^3} + \frac{45}{8} \frac{\tilde{S}^4(3+e^2)^2}{\tilde{l}^5} \right],\end{aligned}\quad (4.A21)$$

where

$$\begin{aligned}g_9 &= 1 + \frac{7}{8}e^2, & g_{10}^b &= \frac{61}{8} + \frac{91}{4}e^2 + \frac{461}{64}e^4, & g_{11} &= \frac{1247}{336} + \frac{425}{336}e^2, \\ g_{12} &= 4 + \frac{97}{8}e^2, & g_{13} &= \frac{44711}{9072} + \frac{302893}{6048}e^2, & g_{14} &= \frac{33}{16} + \frac{95}{16}e^2.\end{aligned}$$

An alternative expression for dQ/dt was presented by Ganz et al. (equation (4.1) in [28]) in which we have converted their variable, $Y \simeq \cos(\iota)$, to $-\tilde{S}(3+e^2)\tilde{l}^{-3/2}$ *viz.*

equation (4.43):

$$\begin{aligned} \frac{dQ}{dt} = & -\frac{64}{5} \left(\frac{m}{M^2} \right) \tilde{l}^{-3} (1 - e^2)^{\frac{3}{2}} \left(1 - \frac{\tilde{S}^2 (3 + e^2)^2}{\tilde{l}^3} \right) \\ & \times \left[g_9 - \frac{d_1}{\tilde{l}^1} + \pi \frac{g_{12}}{\tilde{l}^{3/2}} - \frac{d_3 - d_4 \tilde{S}^2}{\tilde{l}^2} - \pi \frac{d_7}{\tilde{l}^{5/2}} \right. \\ & \left. + \frac{\tilde{S}^2 (3 + e^2) d_2}{\tilde{l}^3} - \frac{\tilde{S}^2 (3 + e^2) d_6}{\tilde{l}^4} + \frac{\tilde{S}^4 (3 + e^2)^2 d_5}{\tilde{l}^5} \right] \end{aligned} \quad (4.A22)$$

where

$$\begin{aligned} d_1 = \frac{743}{336} - \frac{23}{42} e^2, \quad d_2 = \frac{85}{8} + \frac{211}{8} e^2, \quad d_3 = \frac{129193}{18144} + \frac{84035}{1728} e^2, \\ d_4 = \frac{329}{96} + \frac{929}{96} e^2, \quad d_5 = \frac{53}{8} + \frac{163}{8} e^2, \quad d_6 = \frac{2553}{224} - \frac{553}{192} e^2, \quad d_7 = \frac{4159}{672} + \frac{21229}{1344} e^2. \end{aligned}$$

4.A.7 Evolution Equations for \tilde{l} , e , and ι

The evolution equations for \tilde{l} , e , and ι are reported by Ganz et al. (see equation (4.3) in [28]) to $O(\tilde{l}^{-5/2})$. We reproduce them here after having converted their original variable, $v = \sqrt{\frac{M}{\iota}}$, to $\tilde{l}^{-1/2}$, and by using $dv = -1/2\tilde{l}^{-3/2}d\tilde{l}$

$$\begin{aligned} \frac{d\tilde{l}}{dt} = & -\frac{64}{5} \left(\frac{m}{M^2} \right) \tilde{l}^{-3} (1 - e^2)^{\frac{3}{2}} \\ & \times \left[g_9 - \frac{f_1}{\tilde{l}} + \pi \frac{g_{12}}{\tilde{l}^{3/2}} + \frac{f_3 - f_4 \tilde{S}^2}{\tilde{l}^2} - \pi \frac{f_7}{\tilde{l}^{5/2}} \right. \\ & \left. + \frac{f_2 (3 + e^2) \tilde{S}^2}{\tilde{l}^3} - \frac{f_6 (3 + e^2) \tilde{S}^2}{\tilde{l}^4} + \frac{f_5 (3 + e^2)^2 \tilde{S}^4}{\tilde{l}^5} \right] \end{aligned} \quad (4.A23)$$

where

$$\begin{aligned} f_1 = \frac{743}{336} + \frac{55}{21} e^2, \quad f_2 = \frac{133}{12} + \frac{379}{24} e^2, \quad f_3 = \frac{34103}{18144} - \frac{526955}{12096} e^2, \\ f_4 = \frac{329}{96} + \frac{929}{96} e^2, \quad f_5 = \frac{815}{96} + \frac{477}{32} e^2, \quad f_6 = \frac{1451}{56} + \frac{1043}{96} e^2, \\ f_7 = \frac{4159}{672} + \frac{48809}{1344} e^2; \end{aligned}$$

$$\begin{aligned}
\frac{de}{dt} = & -e \frac{304}{15} \left(\frac{m}{M^2} \right) \tilde{l}^{-4} (1 - e^2)^{\frac{3}{2}} \\
& \times \left[h_1 - \frac{h_2}{\tilde{l}} + \pi \frac{h_4}{\tilde{l}^{3/2}} - \frac{h_5 + h_6 \tilde{S}^2}{\tilde{l}^2} - \pi \frac{h_9}{\tilde{l}^{5/2}} \right. \\
& \left. + \frac{h_3(3 + e^2) \tilde{S}^2}{\tilde{l}^3} - \frac{h_8(3 + e^2) \tilde{S}^2}{\tilde{l}^4} + \frac{h_7(3 + e^2)^2 \tilde{S}^4}{\tilde{l}^5} \right] \quad (4.A24)
\end{aligned}$$

where

$$\begin{aligned}
h_1 = 1 + \frac{121}{304} e^2, \quad h_2 = \frac{6849}{2128} + \frac{4509}{2128} e^2, \quad h_3 = \frac{879}{76} + \frac{515}{76} e^2, \\
h_4 = \frac{985}{152} + \frac{5969}{608} e^2, \quad h_5 = \frac{286397}{38304} + \frac{2064415}{51072} e^2, \quad h_6 = \frac{3179}{608} + \frac{8925}{1216} e^2, \\
h_7 = \frac{5869}{608} + \frac{10747}{1216} e^2, \quad h_8 = \frac{1903}{304} - \frac{22373}{8512} e^2, \quad h_9 = \frac{87947}{4256} - \frac{4072433}{68096} e^2; \\
1 - Y^2 \simeq \sin^2(\iota); \quad (4.A25)
\end{aligned}$$

$$\begin{aligned}
\frac{dY}{dt} &= \frac{d \cos(\iota)}{dt} \times \frac{dt}{dt} \\
&= -\sin(\iota) \times \frac{d\iota}{dt}; \quad (4.A26)
\end{aligned}$$

and

$$\begin{aligned}
\frac{dt}{dt} = & \frac{244}{15} \left(\frac{m}{M^2} \right) \tilde{l}^{-4} (1 - e^2)^{\frac{3}{2}} \left(1 - \frac{1}{2} \tilde{S}^2 (3 + e^2)^2 \tilde{l}^{-3} \right) \\
& \times \left[\frac{u_1 \tilde{S}}{\tilde{l}^{3/2}} - \frac{u_3 \tilde{S}}{\tilde{l}^{5/2}} + \frac{u_2 (3 + e^2) \tilde{S}^3}{\tilde{l}^{7/2}} \right] \\
= & \frac{244}{15} \left(\frac{m}{M^2} \right) \tilde{l}^{-4} (1 - e^2)^{\frac{3}{2}} \\
& \times \left[\frac{u_1 \tilde{S}}{\tilde{l}^{3/2}} - \frac{u_3 \tilde{S}}{\tilde{l}^{5/2}} + \frac{u_2 (3 + e^2) \tilde{S}^3}{\tilde{l}^{7/2}} \right. \\
& \left. - \frac{1}{2} \frac{u_1 (3 + e^2)^2 \tilde{S}^3}{\tilde{l}^{9/2}} + \frac{1}{2} \frac{u_3 (3 + e^2)^2 \tilde{S}^3}{\tilde{l}^{11/2}} - \frac{1}{2} \frac{u_2 (3 + e^2)^3 \tilde{S}^5}{\tilde{l}^{13/2}} \right] \quad (4.A27)
\end{aligned}$$

where

$$u_1 = 1 + \frac{189}{61}e^2, \quad u_2 = \frac{13}{244} + \frac{277}{244}e^2, \quad u_3 = \frac{10461}{1708} + \frac{83723}{3416}e^2.$$

Appendix 4.B Series Expansions of Critical Values in Terms of \tilde{S} and \tilde{l}

Our conversion of the quantities X (equation (4.13)), \tilde{E} (equation (4.15)), and Q_X (equation (4.10)) to expansion series in \tilde{S} helped to simplify our analysis by avoiding the use of the much more complicated series expansions in terms of \tilde{l} . Equation (4.24) can be converted to a series:

$$\frac{\tilde{L}_z^{(2n+1)}}{\sqrt{Q_X}} = \sum_{i=0}^n c_{2i+1} \tilde{S}^{2i+1}. \quad (4.B1)$$

By choosing the order of \tilde{S} (the value of $2n + 1$) in which to work, it becomes easier to derive suitable series approximations of these quantities, and their mathematical combinations, in terms of \tilde{l} . Since the equations derived during the full analytical treatment are Brobdingnagian, and thus preclude detailed presentation in this paper, we shall offer the essential highlights of our analysis.

4.B.1 First-order Calculations

We require the series expansion of the quotient, which appears in equation (4.26),

$$\frac{\tilde{L}_z^{(1)}}{\sqrt{Q_X}}, \quad (4.B2)$$

to be expressed in terms of \tilde{l} . To obtain this result we perform a careful manipulation of \tilde{L}_z (in terms of X and \tilde{E} , *viz.* equation (4.21)) and Q_X (as a series expansion in \tilde{S}) using the Maclaurin series in Appendix 4.A.1 (i.e. equations (4.A1) and (4.A2)). The coefficient of \tilde{S}^1 (i.e. c_1) is converted to an expansion in \tilde{l} by use of the same Maclaurin

series expansions. We find c_1 to be:

$$c_1 = \frac{\psi_1 - \psi_2}{\sqrt{\frac{\tilde{l}^2}{\tilde{l} - e^2 - 3}}} \quad (4.B3)$$

where

$$\psi_1 = \sqrt{\frac{\tilde{l} \left(\tilde{l}^2 - 4 \left(\tilde{l} + e^2 - 1 \right) \right)}{\left(\tilde{l} - e^2 - 3 \right)^3}}$$

$$\psi_2 = \sqrt{\frac{\tilde{l}^2 - 4 \left(\tilde{l} + e^2 - 1 \right)}{\tilde{l} \left(\tilde{l} - e^2 - 3 \right)}}.$$

From equation (4.B3), one obtains the result:

$$c_1 = - (e^2 + 3) \left(\frac{1}{\tilde{l}^{3/2}} + \frac{(1 + e^2)}{\tilde{l}^{5/2}} + \frac{(3 + 2e^2 + e^4)}{\tilde{l}^{7/2}} + \frac{(9 + 5e^2 + 5e^4 + e^6)}{\tilde{l}^{9/2}} \right), \quad (4.B4)$$

which appears in equation (4.27).

4.B.2 Third-order Calculations

The third-order calculations require two additional factors:

$$\frac{\tilde{L}_z^{(3)}}{\sqrt{Q_X}} \text{ and } \frac{\tilde{S}^2 (1 - \tilde{E}^2)^{(2)}}{Q_X}, \quad (4.B5)$$

which are used to evaluate $x = \cos(\iota)$ using equation (4.29). The first factor can be derived by converting the coefficient of \tilde{S}^3 ,

$$c_3 = -\frac{1}{2} \frac{(1 - e^2)^2 \left(\left(\tilde{l}^2 - 2\tilde{l} + 2\tilde{l}e^2 - 16e^2 \right) \psi_1 + (-4 + \tilde{l}) \left(\tilde{l} - 2 - 2e^2 \right) \psi_2 \right)}{\sqrt{\frac{\tilde{l}^2}{\tilde{l} - e^2 - 3}} \tilde{l} \left(\tilde{l} - e^2 - 3 \right) \left(\tilde{l}^2 - 4\tilde{l} + 4e^2 - 4 \right)}, \quad (4.B6)$$

in equation (4.B1), to a series expansion in \tilde{l} (see equation (4.30)) and adding the result to the first order term:

$$c_3 = -\tilde{S}^3 (1 - e^2)^2 \left(\frac{1}{\tilde{l}^{7/2}} + \frac{1}{2} \frac{11 + 5e^2}{\tilde{l}^{9/2}} \right) \quad (4.B7)$$

(see equation (4.30)). The second factor in equation (4.B5) is also obtained by working in expansions of \tilde{S} , which proceeds by a simpler derivation (see equation (4.31)). The orbital inclination, ι , is then obtained by using equation (4.28).

4.B.3 Fifth-order Calculations

The second term in equation (4.20) can provide the power of \tilde{l} at which the a coefficient with an \tilde{S}^5 term appears in the series expansion of ι , by working in the leading terms of \tilde{l} . Such a simple analysis yields the result $\tilde{l}^{-11/2}$.

The calculation of ι to the fifth order in \tilde{S} , by using the first term in equation (4.20) is complicated, but demanded by the exercise of due diligence. The analysis can be greatly simplified by setting $e = 0$. The terms required are:

$$\tilde{S}^2 \left(1 - \tilde{E}^2 \right)^{(4)} = \frac{(\tilde{l} - 4) \tilde{S}^2}{\tilde{l}^3} + \frac{(\tilde{l} - 4) \tilde{S}^4}{\tilde{l}^4 (\tilde{l} - 3)^2}, \quad (4.B8)$$

and

$$\frac{\tilde{L}_z^{(5)}}{\sqrt{Q}} = \frac{\tilde{L}_z^{(3)}}{\sqrt{Q}} - \left(\frac{9}{2} \tilde{l}^{-13/2} + \frac{527}{8} \tilde{l}^{-15/2} + \frac{463}{8} \tilde{l}^{-17/2} + \frac{31771}{8} \tilde{l}^{-19/2} \right) \tilde{S}^5, \quad (4.B9)$$

the second of which is derived from c_5 in the series in equation (4.B1).

Consider equation (4.23):

$$\cos^2(\iota) = \frac{\tilde{L}_z^2}{Q(1 + K)}, \quad (4.B10)$$

where

$$K = \left[\frac{\tilde{L}^{(5)}}{\sqrt{Q}} \right]^2 - \tilde{S}^2 \left(1 - \tilde{E}^2 \right).$$

By using the expansion series approximations in equations (4.A1), (4.A2), and (4.A3), one obtains:

$$\begin{aligned} \tilde{l}^{(5)} &= \frac{\pi}{2} - x - \frac{1}{6}x^3 - \frac{3}{40}x^5 \\ &= O\left(\tilde{l}^{-11/2}\right), \end{aligned} \tag{4.B11}$$

where

$$x = \frac{\tilde{L}^{(5)}}{\sqrt{Q}} \left(1 - \frac{1}{2}KK - \frac{1}{8}KK^2 \right)$$

and

$$KK = K - K^2.$$

Therefore one finds that $\left(\partial\tilde{l}/\partial\tilde{l}\right)_{\min} = O\left(\tilde{l}^{-13/2}\right)$.

4.3 References

- [1] J. M. Bardeen. Timelike and Null Geodesics in the Kerr Metric. In C. Dewitt and B. S. Dewitt, editors, *Black Holes (Les Astres Occlus)*, pages 215–239, 1973.
- [2] E. Poisson. Gravitational Radiation from a Particle in Circular Orbit Around a Black hole. I. Analytical results for the nonrotating case. *Phys. Rev. D*, 47:1497–1510, 1993.
- [3] C. Cutler, L. S. Finn, E. Poisson, and G. J. Sussman. Gravitational Radiation from a Particle in Circular Orbit Around a Black Hole. II. Numerical results for the nonrotating case. *Phys. Rev. D*, 47:1511–1518, 1993.
- [4] F. D. Ryan. Effect of Gravitational Radiation Reaction on Circular Orbits Around a Spinning Black Hole. *Phys. Rev. D*, 52:3159, 1995.
- [5] A. Ori and K. S. Thorne. Transition from Inspiral to Plunge for a Compact Body in a Circular Equatorial Orbit Around a Massive, Spinning Black Hole. *Phys. Rev. D*, 62(12):124022, 2000.
- [6] P. C. Peters and J. Mathews. Gravitational Radiation from Point Masses in a Keplerian Orbit. *Phys. Rev.*, 131(1):435–440, 1963.
- [7] P. C. Peters. Gravitational Radiation and the Motion of Two Point Masses. *Phys. Rev.*, 136(4B):B1224–B1232, 1964.
- [8] V. A. Brumberg. *Essential Relativistic Celestial Mechanics*. IOP Publishing Bristol, UK, 1991.
- [9] W. Junker and G. Schaefer. Binary Systems - Higher Order Gravitational Radiation Damping and Wave Emission. *Mon. Not. R. astr. Soc.*, 254:146–164, 1992.
- [10] C Cutler, D. Kennefick, and E Poisson. Gravitational Radiation Reaction for Bound Motion Around a Schwarzschild Black Hole. *Phys. Rev. D*, 50(6):3816–3835, 1994.

- [11] K. Glampedakis and D. Kennefick. Zoom and Whirl: Eccentric equatorial orbits around spinning black holes and their evolution under gravitational radiation reaction. *Phys. Rev. D*, 66(4):044002, 2002.
- [12] S. A. Hughes, S. Drasco, É. É. Flanagan, and J. Franklin. Gravitational Radiation Reaction and Inspiral Waveforms in the Adiabatic Limit. *Physical Review Letters*, 94(22):221101, 2005.
- [13] S. A. Teukolsky. Perturbations of a Rotating Black Hole. I. Fundamental Equations for Gravitational, Electromagnetic, and Neutrino-Field Perturbations. *Astrophys. J.*, 185:635–648, 1973.
- [14] W. H. Press and S. A. Teukolsky. Perturbations of a Rotating Black Hole. II. Dynamical Stability of the Kerr Metric. *Astrophys. J.*, 185:649–674, 1973.
- [15] A. Ori. Radiative Evolution of Orbits Around a Kerr Black Hole. *Physics Letters A*, 202(5-6):347–351, 1995.
- [16] F. D. Ryan. Effect of Gravitational Radiation Reaction on Nonequatorial Orbits Around a Kerr Black Hole. *Phys. Rev. D*, 53:3064–3069, 1996.
- [17] D. Kennefick and A. Ori. Radiation-Reaction-Induced Evolution of Circular Orbits of Particles Around Kerr Black Holes. *Phys. Rev. D*, 53(8):4319–4326, 1996.
- [18] A. Ori. Radiative Evolution of the Carter Constant for Generic Orbits Around a Kerr Black Hole. *Phys. Rev. D*, 55(6):3444–3456, 1997.
- [19] F. de Felice and G. Preti. On the Meaning of the Separation Constant in the Kerr Metric. *Class. Quantum Grav.*, 16:2929–2935, 1999.
- [20] S. A. Hughes. Evolution of Circular, Nonequatorial Orbits of Kerr Black Holes due to Gravitational-Wave Emission. *Phys. Rev. D*, 61(8):084004, 2000.

- [21] S. A. Hughes. Evolution of Circular, Nonequatorial Orbits of Kerr Black Holes due to Gravitational-Wave Emission. II. Inspirational trajectories and gravitational waveforms. *Phys. Rev. D*, 64(6):064004, 2001.
- [22] K. Glampedakis, S. A. Hughes, and D. Kennefick. Approximating the Inspiral of Test Bodies into Kerr Black Holes. *Phys. Rev. D*, 66(6):064005, 2002.
- [23] L. Barack and C. Cutler. Lisa Capture Sources: Approximate waveforms, signal-to-noise ratios, and parameter estimation accuracy. *Phys. Rev. D*, 69:082005, 2004.
- [24] N. Sago, T. Tanaka, W. Hikida, and H. Nakano. Adiabatic Radiation Reaction to Orbits in Kerr Spacetime. *Progress of Theoretical Physics*, 114(2):509–514, 2005.
- [25] N. Sago, T. Tanaka, W. Hikida, K. Ganz, and H. Nakano. Adiabatic Evolution of Orbital Parameters in Kerr Spacetime. *Progress of Theoretical Physics*, 115(5):873–907, 2006.
- [26] J. R. Gair and K. Glampedakis. Improved Approximate Inspirals of Test Bodies into Kerr Black Holes. *Phys. Rev. D*, 73(6):064037, 2006.
- [27] E. Barausse, S. A. Hughes, and L. Rezzolla. Circular and Noncircular Nearly Horizon-Skimming Orbits in Kerr Spacetimes. *Phys. Rev. D*, 76(4):044007, 2007.
- [28] K. Ganz, W. Hikida, H. Nakano, N. Sago, and T. Tanaka. Adiabatic Evolution of Three ‘Constants’ of Motion for Greatly Inclined Orbits in Kerr Spacetime. *Progress of Theoretical Physics*, 117:1041–1066, 2007.
- [29] É. É. Flanagan and T. Hinderer. Evolution of the Carter Constant for Inspirals into a Black Hole: Effect of the black hole quadrupole. *Phys. Rev. D*, 75(12):124007, 2007.
- [30] S. Babak, H. Fang, J. R. Gair, K. Glampedakis, and S. A. Hughes. “Kludge” Gravitational Waveforms for a Test-body Orbiting a Kerr Black Hole. *Phys. Rev. D*, 75(2):024005–024030, 2007.

- [31] M. Punturo et al. The Third Generation of Gravitational Wave Observatories and their Science Reach. *Class. Quantum Grav.*, 27:084007, 2010.
- [32] C. Cutler and M. Vallisneri. LISA Detections of Massive Black Hole Inspirals: parameter extraction errors due to inaccurate template waveforms. *Phys. Rev. D*, 76:104018, 2007.
- [33] M. E. Normandin, A Vajda, and S. R. Valluri. Gravitational Wave Signal Templates, Pattern Recognition, and Reciprocal Eulerian Gamma Functions. *Theor. Comput. Sci.*, 409(2):241–254, 2008.
- [34] P. G. Komorowski, S. R. Valluri, and M. Houde. The Carter Constant for Inclined Orbits About a Massive Kerr Black Hole: I. circular orbits. *Class. Quantum Grav.*, 27(22):225023, 2010.
- [35] J. W. Mellor. *Higher Mathematics for Students of Chemistry and Physics*. Dover Publications Inc. Mineola, New York, 4th edition, 1955.
- [36] M. R. Spiegel. *Mathematical Handbook of Formulas and Tables*. McGraw-Hill, 1968.
- [37] M. R. Spiegel. *Theory and Problems of Advanced Calculus*. McGraw-Hill, 1963.

Chapter 5

Summary and Future Work

5.1 Summary

An extreme mass-ratio binary black hole system was modelled as a massive Kerr black hole (KBH) about which a test-particle of infinitesimal mass, $m \rightarrow 0$, travels in an elliptical orbit. In the general case, this system has four constants of motion: m , the test-particle mass; E , the orbital energy, L_z , its z -component of orbital angular momentum; and Q , the Carter constant. The spin angular momentum of the KBH, $\mathbf{s} = J/M$ (where M is the KBH mass), is a property of the associated Kerr spacetime.

If the orbit is bound and on an inclined plane with respect to the equatorial plane of the KBH then the value of Q is positive. In this thesis, E was normalised by dividing by m ; while L_z and Q were normalised by dividing by mM and $(mM)^2$, respectively. Henceforth, three constants of motion are discussed: \tilde{E} , \tilde{L}_z , and Q . The KBH spin, \mathbf{s} is normalised by dividing by M to give \tilde{S} .

Consider a test-particle orbiting in the equatorial plane of a KBH; its elliptical path may be characterised by the latus rectum (\tilde{l}) and eccentricity (e). Further, \tilde{E} and \tilde{L}_z may be expressed using these terms, although, not in an explicit form. If the orbit is inclined with respect to the equatorial plane of the KBH, then one may introduce the angle of inclination (ι) which can be expressed in terms of Q , \tilde{E} , \tilde{L}_z , and \tilde{S} .

The test-particle makes its final plunge into the event horizon of the KBH when it reaches its last stable orbit (LSO). The first objective, to determine the latus rectum of the LSO (\tilde{l}_{LSO}) for an equatorial orbit, required the use of a new constant ($X^2 = (\tilde{L}_z - \tilde{S}\tilde{E})^2$). Hence, an expression for \tilde{l}_{LSO} in terms of \tilde{l} , e , and \tilde{S} , could be derived for the prograde and the retrograde orbits. The original purpose of this exercise was to facilitate the treatment of the orbit's radial oscillation frequency as it approached the LSO; and by so doing, explore more realistic treatments of the post-Newtonian (PN) approximations near the LSO. This line of investigation was not perused in this thesis work.

The second objective, to derive a generalisation of the expression for \tilde{l}_{LSO} for inclined orbits, followed an approach similar to that taken for the equatorial orbit case. The result was an ninth order polynomial in \tilde{l} ($p(\tilde{l}, Q)$), which though interesting, was not feasible to solve explicitly. Fortunately, $p(\tilde{l}, Q)$ was a second-order polynomial in Q , which led to an analytical solution for the value of Q at the LSO.

For a Schwarzschild black hole, the prograde and retrograde expressions for \tilde{L}_z are symmetrical in an $R - \tilde{L}_z$ plot. But a fascinating asymmetry emerges, which is more pronounced for higher values of \tilde{S} , for a KBH. This discovery guided the treatment of Q for inclined orbits in general. The value of Q is greater than zero for both prograde and retrograde orbits; and in either of the equatorial cases Q is equal to zero; therefore, an intermediate orbit may be found (described by \tilde{l} and e) at which the value of Q is a maximum. The analytical expression for X^2 was composed of two roots: positive and negative. The positive case corresponds only to retrograde orbits; but the negative case corresponds to all prograde orbits, polar orbits, and retrograde orbits up to the point where the positive and negative solutions are equal. It is at this point of equality that the abutment is found. Because $dQ/d\tilde{l}$ is known analytically on the abutment, a new technique to test the consistency of the evolution equation of Q (dQ/dt) with respect to the those for \tilde{l} and e is available without imposing a radiation back-reaction model. This technique was used to test two sets of evolution equations (2PN and 2.5PN order) [1, 2], with excellent results. Although no direct study of PN approximations was undertaken, a

new method to test the validity of PN approximations, which were derived and published by other physicists, was found.

Investigations of $d\iota/d\tilde{l}$ for orbits of constant e on the abutment were performed, and an approximate expression for $d\iota/d\tilde{l}$ was found for circular orbits by numerical means. The derivative, $d^2Q/d\tilde{l}^2$ is not fixed at the abutment, therefore, a second-order influence on the value of $d\iota/d\tilde{l}$ is present. No such effect was found when calculating dQ/dt .

Additional analytical work was performed to derive expressions for $d\iota/d\tilde{l}$ and $d\iota/de$ for slightly elliptical orbits at the abutment. By so doing, it was possible to model the second-order effects by applying two ansätze in which the second derivatives of Q with respect to \tilde{l} and e were adjusted in a methodical manner. Although the second-order effects remain to be quantified, it was possible to corroborate the validity of the $d\iota/dt$ evolution equation at the abutment with those available in the literature [3–8, 2, 1, 9, 10].

5.2 Future work

The post-Newtonian (PN) evolution equations, which were accurate to 2.5PN order, were analysed on the abutment to the leading order in \tilde{S} . Because concern has been expressed about the convergence of PN approximations of higher order [11], future investigations of PN evolution equations of 3PN and 4PN order ought to be undertaken. The Teukolsky formalism [12–14] promises to provide more accurate mathematical models to describe orbital evolution and GW emission in strong gravitational fields [2]; but the treatment of stronger gravitational effects requires expressions for $dQ/d\tilde{l}$ and dQ/de to be treated to higher order in \tilde{S} (e.g. \tilde{S}^3) on the abutment. Such an analytical treatment would be challenging; but a combination of numerical and analytical techniques would offer an effective approach.

Although no exploration of the second-order effects on $d\iota/d\tilde{l}$ was made in this thesis, an investigation of models to describe and explain this second-order effect, based upon existing radiation back-reaction models, are worthwhile. In this work, the detailed

consideration of radiation back-reaction mechanisms has been avoided. But eventually, the abutment may prove to be a powerful tool in the development and testing of improved radiation back-reaction models. Work on these projects in the future is warranted since the PN approximation and Teukolsky formalism provide those who investigate the evolution of extreme mass-ratio binary black hole systems with mathematical predictions of orbital evolution; yet the corroborating observations of this type of system are minimal.

5.3 References

- [1] K. Ganz, W. Hikida, H. Nakano, N. Sago, and T. Tanaka. Adiabatic Evolution of Three ‘Constants’ of Motion for Greatly Inclined Orbits in Kerr Spacetime. *Progress of Theoretical Physics*, 117:1041–1066, 2007.
- [2] E. Barausse, S. A. Hughes, and L. Rezzolla. Circular and Noncircular Nearly Horizon-Skimming Orbits in Kerr Spacetimes. *Phys. Rev. D*, 76(4):044007, 2007.
- [3] F. D. Ryan. Effect of Gravitational Radiation Reaction on Nonequatorial Orbits Around a Kerr Black Hole. *Phys. Rev. D*, 53:3064–3069, 1996.
- [4] S. A. Hughes. Evolution of Circular, Nonequatorial Orbits of Kerr Black Holes due to Gravitational-Wave Emission. *Phys. Rev. D*, 61(8):084004, 2000.
- [5] S. A. Hughes. Evolution of Circular, Nonequatorial Orbits of Kerr Black Holes due to Gravitational-Wave Emission. II. Inspirational trajectories and gravitational waveforms. *Phys. Rev. D*, 64(6):064004, 2001.
- [6] K. Glampedakis, S. A. Hughes, and D. Kennefick. Approximating the Inspiral of Test Bodies into Kerr Black Holes. *Phys. Rev. D*, 66(6):064005, 2002.
- [7] N. Sago, T. Tanaka, W. Hikida, K. Ganz, and H. Nakano. Adiabatic Evolution of Orbital Parameters in Kerr Spacetime. *Progress of Theoretical Physics*, 115(5): 873–907, 2006.
- [8] J. R. Gair and K. Glampedakis. Improved Approximate Inspirals of Test Bodies into Kerr Black Holes. *Phys. Rev. D*, 73(6):064037, 2006.
- [9] É. É. Flanagan and T. Hinderer. Evolution of the Carter Constant for Inspirals into a Black Hole: Effect of the black hole quadrupole. *Phys. Rev. D*, 75(12):124007, 2007.

- [10] S. Babak, H. Fang, J. R. Gair, K. Glampedakis, and S. A. Hughes. “Kludge” Gravitational Waveforms for a Test-body Orbiting a Kerr Black Hole. *Phys. Rev. D*, 75(2):024005–024030, 2007.
- [11] T. Damour. *300 Years of Gravitation*, chapter The Problem of Motion in Newtonian and Einsteinian Gravity. Cambridge University Press, 1978.
- [12] W. H. Press and S. A. Teukolsky. On the Evolution of the Secularly Unstable, Viscous Maclaurian Spheroids. *Astrophys. J.*, 181:513–518, 1973.
- [13] S. A. Teukolsky. Perturbations of a Rotating Black Hole. I. Fundamental Equations for Gravitational, Electromagnetic, and Neutrino-Field Perturbations. *Astrophys. J.*, 185:635–648, 1973.
- [14] W. H. Press and S. A. Teukolsky. Perturbations of a Rotating Black Hole. II. Dynamical Stability of the Kerr Metric. *Astrophys. J.*, 185:649–674, 1973.

Curriculum Vitae

Peter George Komorowski

Education

- | | | |
|---------------|---------|--|
| (in progress) | Ph.D. | Physics Department of Physics and Astronomy The University of Western Ontario London, Ontario, Canada |
| 1992 | Ph.D | Major: Materials Science Minor: Process Metallurgy Department of Metallurgy and Materials Science The University of Toronto Toronto, Ontario, Canada |
| 1987 | M.A.Sc. | Materials Science Department of Metallurgy and Materials Science The University of Toronto Toronto, Ontario, Canada |
| 1982 | B.A.Sc. | Engineering Science Applied Science and Engineering The University of Toronto Toronto, Ontario, Canada |

Scientific Work Experience

- | | |
|-----------|---|
| 1994 | Research Scientist (Level 1) (Six months) Natural Resources Canada CANMET Devon, Alberta, Canada |
| 1992-1994 | Visiting Scientist NSERC: Visiting Fellowships in Canadian Government Laboratories Program Natural Resources Canada CANMET Devon, Alberta, Canada |

Submitted Article

1. **P. G. Komorowski**, S. R. Valluri, and M. Houde. The Carter Constant for Inclined Orbits About a Massive Kerr Black Hole: II. near-circular, near-polar orbits. *ArXiv e-prints*, arXiv:1101.0996v1 [gr-qc], (40pp), 2011. (Submitted to *Class. Quantum Grav.*)

Journal Publications

1. **P. G. Komorowski**, S. R. Valluri, and M. Houde. The Carter Constant for Inclined Orbits about a Massive Kerr Black Hole: I. Circular orbits. *Class. Quantum Grav.*, 27(22), 085001 (28pp), 2010.
2. **P. G. Komorowski**, S. R. Valluri, and M. Houde. A Study of Elliptical Last Stable Orbits About a Massive Kerr Black Hole. *Class. Quantum Grav.*, 26(8), 225023 (36pp), 2009.
3. J. Szynekarczuk, **P. G. Komorowski**, and J. C. Donini. Redox Reactions of Hydro-sulfide Ions on the Platinum-Electrode .2. An Impedance Spectroscopy Study and Identification of the Polysulfide Intermediates. *Electrochimica Acta*, 40(4):487-494, 1995.
4. J. Szynekarczuk, **P. G. Komorowski** and J. C. Donini. Redox Reactions of Hydro-sulfide Ions on the Platinum-Electrode .1. The Presence of Intermediate Polysulfide Ions and Sulfur Layers. *Electrochimica Acta*, 39(15):2285-2289, 1994.
5. **P. G. Komorowski**, S. A. Argyropoulos, J. D. Canaday, *et al.* The Analysis of Protonically Exchanged Beta"-Alumina Powder. *Solid State Ionics*, 60(4):343-345, 1993.
6. **P. G. Komorowski**, S. A. Argyropoulos, J. Graydon, *et al.* The Effect of Absorbed Water on Hydronium NASICON and HYCERAM. *Solid State Ionics*, 60(4):335-341, 1993.
7. S. F. Chehab, J. D. Canaday, *et al.* (including **P. G. Komorowski**). Impedance Measurements of Platinum-Electrodes on a Solid Protonic Conductor. *Solid State Ionics*, 59(1-2):125-132, 1993.
8. **P. G. Komorowski** and C. B. Alcock. Impedance Analysis of Solid Electrolytes by a Voltage-Pulsing Technique. *Solid State Ionics*, 58(3-4):293-301, 1992.
9. **P. G. Komorowski**, S. A. Argyropoulos, J. D. Canaday, *et al.* The Study of Hydronium NASICON Conductivity with Deuterium. *Solid State Ionics*, 50(3-4):253-258, 1992.

10. **P. G. Komorowski**, S. A. Argyropoulos, R. G. V. Hancock, *et al.* Characterization of Protonically Exchanged NASICON. *Solid State Ionics*, 48(3-4):295-301, 1991.

Conference Proceedings

1. **P. G. Komorowski**, S. A. Argyropoulos, and J. D. Canaday. Intelligent Processing of Data for Materials Processing. In *Artificial Intelligence in Materials Processing*, pages 245-256, 1992. International Symposium on Artificial Intelligence in Materials Processing, at the 31st Annual Conference of Metallurgists of CIM, Edmonton, Canada, 1992. S. A. Argyropoulos and G. Carayannis, editors
2. C. B. Alcock and **P. G. Komorowski**. Millisecond Impedance Spectroscopy of Stabilized Zirconia. *CIM Bulletin*, 80(902):100, 1987.